Streptomyces coelicolor BIOFILM GROWTH KINETICS AND OXYGEN MASS TRANSFER WITHIN A MEMBRANE GRADOSTAT BIOREACTOR

by

DEBBIE DE JAGER

Thesis submitted in the requirements for the degree

Magister Technologiae: Chemical Engineering

in the Faculty of

Engineering

at the

CAPE PENINSULA UNIVERSITY OF TECHNOLOGY

(Cape Town Campus)

Supervisor: Ass. Prof. Marshall Sheldon

Co-supervisor: Dr. Wade Edwards

Cape Town

August 2009

DECLARATION

I, Debbie de Jager, declare that the contents of this thesis represent my own unaided work, and that the thesis has not previously been submitted for academic examination towards any qualification. Furthermore, it represents my own opinions and not necessarily those of the Cape Peninsula University of Technology. Opinions expressed in this thesis and the conclusions arrived at, are those of the author, and are not necessarily to be attributed to the National Research Foundation.

DJager — March 2010

Signed **Date**

ABSTRACT

The main purpose of this study was to quantify the growth and oxygen mass transfer kinetic parameters of the filamentous bacterium *Streptomyces coelicolor*, immobilised on the external surface of a ceramic membrane in a continuously operated pressurised Membrane Gradostat Bioreactor (MGR).

One of the most important and critical parameters required when studying biofilms, are the growth kinetics, as they can be utilised to model both the mass transfer and biological reactions occurring within the biofilm. Single fibre MGR's (SFMGR) were operated using a pneumatic system to supply humidified pressurised air to the extra capillary space (ECS) and pressurised growth medium to the lumen of the ceramic membrane. Two growth media; a complex growth medium, ISP2, and a defined growth medium, were tested and supplied to the lumen of the ceramic membrane in the dead-end mode.

Utilising the Monod single-substrate growth kinetic model, the average glucose consumption rate, (r_B), was determined to be approximately 92.27 g/m^3.hr; the Monod saturation constant, (K_m), 29605.65 g/m^3; the maximum substrate consumption rate, (r_m), 434.7 g/m^3.hr, and the yield coefficient 0.603 g biofilm/g glucose for ISP2 complex growth medium.

The growth curve obtained for *Streptomyces coelicolor* A3(2) showed the presence of two growth cycles (biphasic growth), with no evident intermediate lag phase. The first growth cycle identified between ±66 and 162 hr, had a specific growth rate in the range of ±0.033 to 0.073 hr^{-1}, while the second growth cycle identified between ±162 and 354 h had a specific growth rate in the range ±0.013 to 0.019 hr^{-1}.

In vertically orientated pressurised membrane gradostat bioreactors (MGR's) mass transport of oxygen occurs via both diffusion and convection depending on the location of the biofilm immobilised on the surface of the membrane with regards to the air inlet. An important design parameter in aerobic biological systems is the rate of oxygen diffusion. Profile 1.0 software and Taylor's expansion series were utilised to calculate the oxygen mass transfer parameters from the oxygen profiles obtained using Clark-type oxygen microsensors and Profix 3.0 data acquisition software.

Using Profile 1.0 software the substrate saturation constants were in the range of 2.45 to 4.25 g/m^3; the oxygen diffusion coefficient in the range of 8.15×10^{-6} to 1.75×10^{-5} m^2/hr and dissolved oxygen flux through the biofilm in the range of 0.13 to 0.29 $g/m^2.hr$ for the continuously operated pressurised MGR system. Both the average oxygen penetration depth and penetration ratio decreased with time, with the penetration ratio decreasing from 1.6 to 0.26.

The mathematical model developed to model oxygen mass transport within a biofilm grown in a pressurised MGR system, combines both diffusive and convective mass transport terms.

DEDICATION

For my mother Mrs MM De Jager for her endless support and belief in me. Thank you.

ACKNOWLEDGEMENTS

I wish to thank:

- The NRF (National Research Foundation of South Africa) and DAAD (Deutscher Akademischer Austausch Dienst/German Academic Exchange Service) for their financial support, without whom this research project would not have been possible.
- My supervisor Ass. Prof. Marshall Sheldon for her patience, knowledge and guidance.
- My co-supervisor Dr. Wade Edwards for his assistance and guidance.
- Synexa Lifes Sciences where I was able to complete most of the research and I was treated like one of their own.
- All my colleagues at Synexa Life Sciences for their support.
- Dr. Karabo Obed Ntwampe for challenging me and inspiring me to continue with my studies.
- Mr. Buntu Godongwana for his support and assistance especially with the mathematics.
- Mrs. Chantal Williams, laboratory assistant at CPUT (Cape Peninsula University of Technology), for her assistance in the laboratory.
- My fellow students in the CPUT laboratory for their support.
- My family for travelling this journey with me.
- The Lord above for giving me the strength to keep on going.

TABLE OF CONTENTS

LIST OF FIGURES

LIST OF TABLES

LIST OF SYMBOLS

∇	Gradient operator (dimensionless)
a, b, c	Experimental coefficients for Taylor's expansion method (dimensionless)
a_1, a_2, a_3	Experimental coefficients (dimensionless)
A_{bs}	Absorbance (dimensionless)
a_{tm}	Atmospheric level solubility of oxygen in the relevant liquid at the relevant temperature (µmol O_2/L)
b	Subscript indicating on the biofilm-side
Bl	Blank (dimensionless)
C_1	Spore concentration of the undiluted spore stock solution (spores/ml)
C_2	Standard spore concentration (spores/ml)
C_{actino}	Actinorhodin concentration (mg/ml)
C_{O_2}	Oxygen concentration (g/m^3)
$C_{O_2(0)}$	Initial oxygen concentration (g/m^3)
$C_{O_2(air)}$	Oxygen concentration in the air (g/m^3)
$C_{O_2(b)}$	Oxygen concentration in the biofilm (g/m^3)
$C_{O_2(bulk)}$	Oxygen concentration in the bulk (g/m^3)
$C_{O_2(f)}$	Final oxygen concentration (g/m^3)
$C_{O_2(s)}$	Oxygen concentration at the biofilm surface (g/m^3)
C_{sub}	Substrate concentration (g/m^3)
d	Grouping parameter (dimensionless)
$D_{a,f}$	Oxygen diffusion coefficient in the aerial mycelia (m^2/hr)
D_{AB}	Substrate diffusivity (m^2/hr)
D_f	Oxygen diffusivity coefficient in the biofilm (m^2/hr)
d_h	Hydraulic radius (m)
D_m	Molecular diffusivity of the growth limiting nutrient or oxygen (m^2/hr)
D_w	Oxygen diffusivity coefficient in water (m^2/hr)
E	Extinction coefficient (L/mol.cm or L/g.cm)
f	Fraction retentate (dimensionless)

G	Grouping parameter (dimensionless)
J	Substrate flux (g/m^2.hr)
J_f	Flux of substrate across the biofilm surface (m^3/m^2.hr)
J_{fo2}	Oxygen flux through the biofilm (g/m^2.hr)
J_w	Substrate flux across the water-biofilm interface (g/m^2.hr)
k	First-order rate constant (hr^{-1})
K	Linear growth rate (hr^{-1})
k_1	External mass transfer coefficient (m/s)
K_m	Monod saturation constant (g/m^3)
k_m	Membrane initial hydraulic permeability (m/Pa.s)
K_s	Substrate saturation constant (g/m^3)
L	Ratio between the specific growth rate at the start of the deceleration phase and the specific growth rate during the exponential phase (dimensionless)
l	Pathlength (cm)
L_b	Glass bioreactor length (m)
L_f	Average biofilm thickness (m)
L_m	Effective membrane length (m)
m_s	Maintenance coefficient (hr^{-1})
n	Exponent placeholder (dimensionless)
N_s	Nutrient flux to the biofilm surface (g/m^2.hr)
p_0	Inlet hydrostatic pressure (Pa)
p_1	Outlet hydrostatic pressure (Pa)
Q	Growth medium flow rate (m^3/s)
q	Specific rate of substrate uptake (g/m^3.hr)
r	Radial co-ordiante (m)
R_2	Pitch (m)
R_3	Glass manifold inner radius (m)
r_A	Rate of substrate production or consumption (g/m^3.hr)
r_B	Biological reaction/consumption rate (g/m^3.hr)
Re	Reynold's number (dimensionless)
R_L	Membrane inner radius (m)
r_m	Maximum substrate consumption rate (g/m^3.hr)

R_x	Membrane outer radius (m)
S	Partial pressure signal (pA)
S_0	Zero oxygen partial pressure reading (pA)
S_a	Atmospheric partial pressure reading (pA)
Sc	Schmidt number (dimensionless)
$(S_{cal})_i$	ith Theoretical substrate concentration (g/m^3)
$(S_{exp})_i$	ith Experimental substrate concentration (g/m^3)
Sh	Sherwood number (dimensionless)
S_w	Mass of substrate consumed (g)
t	Time (hr)
t_a	Time at which the growth switches from the exponential phase to the deceleration phase (hr)
$\bar{u}$	Velocity vector (m/s)
u	Axial velocity (m/s)
v	Radial velocity (m/s)
V	Volume (ml)
V_1	Volume undilted spore stock solution (ml)
V_2	Final volume diluted spore stock solution (ml)
v_f	Fluid velocity (m/s)
V_{max}	Maximum rate of reaction (g/m^3.hr)
w	Subscript indicating on the water side of the water-biofilm interface
x	Distance from the bottom of the biofilm (m)
X	Microbial biomass (g)
X_0	Initial biomass (g)
X_A	Biomass at the start of the decelaration phase (g)
X_f	Final biomass (g)
X_m	Maximum biomass obtained (g)
X_ρ	Biofilm density (g/m^3)
x_s	Distance of the biofilm surface from the bottom (m)
$Y_{X/S}$	Growth yield coefficient (g biomass/g substrate)
z	Axial co-ordinate (m)

Greek letters

β	Experimental coefficient (m^{-1})
μ	Specific growth rate constant (hr^{-1})
μ_1	Fluid viscosity (Pa.s)
$\mu_{experimental}$	Experimental specific growth rate (hr^{-1})
μ_g	Growth medium viscosity (Pa.s)
μ_{max}	Maximum specific growth rate (hr^{-1})
$\mu_{predicted}$	Theoretical specific growth rate (hr^{-1})
ρ	Fluid density (kg/m^3)
ρ_g	Growth medium density (kg/m^3)

LIST OF ABBREVIATIONS

CA	Cellulose Acetate
CDA	Ca-Dependent Antibiotic
CT	Capillary Tube
CWF	Clear Water Flux Testing
DC	Direct Current
dMBR	Diffusive Membrane Bioreactor
DNS	Dinitrosalicylic acid
DO	Dissolved Oxygen
ECS	Extracapillary Space
eMBR	Extractive Membrane Bioreactor
Eq.	Equation
Exp.	Experiment
FC	Pleated Filter Cartridge
FS	*Plate-and-frame/Flat Sheet*
G6P	Glucose-6-Phosphate
HF	Hollow Fibre
ID	Inner Diameter
iMBR	Submerged or immersed Membrane Bioreactor
ISP2	International *Streptomyces* Project, medium 2
M	Molar
MAB	Membrane-Aerated Bioreactor
MBR	Membrane Bioreactor
MF	Micro Filtration
MFMGR	Multi-Fibre Membrane Gradostat Reactor
MGR	Membrane Gradostat Bioreactor
MM1	Minimal medium 1
MT	(Multi)tubular
M_w	Molecular weight
NF	Nano Filtration
OD	Outer Diameter
OD_{450}	Optical Density at 450 nm
ODE	Ordinary Differential Equations Solver
P. chrysosporium	*Phanerochaete chrysosporium*
PAN	Polyacrylonitrile
PE	Polyethylene

PES	Polyethylsulphone
PID	Proportional-Integral-Derivative
PP	Polypropylene
PSO	Polysulfone
PV	Process Value
PVDF	Polyvinylidene difluoride
R^2	Correlation coefficient between modelled and experimental data
Re	Reynold's number
RO	Reverse Osmosis
RSSE	Residual Sum of Square Estimates
S. coelicolor A3(2)	*Streptomyces coelicolor* A3(2)
S. lividans	*Streptomyces lividans*
Sc	Schmidt number
SEM	Scanning-Electron Microscopy
SFMGR	*Single Fibre Membrane Gradostat Reactor*
Sh	Sherwood number
sMBR	Sidestream Membrane Bioreactor
SOP	Standard Operating Procedure
SSD	Sum of Square Differences
SSF	Solid State Fermentation
SV	Set Value
SW	Spiral wound
TMP	Transmembrane Pressure
UF	Ultra Filtration
YEME	Yeast Extract Malt Extract

GLOSSARY

Terms/Concepts	Definition/Explanation
Gradostat	Describes a bioreactor system in which gas and liquid flow are both uni-directional (the gradients of the gas and liquid moves from a high to a low concentration) and bi-directional (the gradients are running in cpposite directions, from outside-in and inside-out, respectively). Contact occurs between the different growth phases in the immobilised biofilm and spatial nutrient concentration gradients exist within the biofilm.
Immobilise	The process by which a micro organism or its reproductive cells are attached to a surface.
Membrane Bioreactor (MBR)	A reactor vessel utilising micro organisms grown on the outside surface of a permeable membrane that allows essential nutrients to pass through but retains the microbial cells. Membrane bioreactors (MBRs) combine biological processes with membrane technology.
Membrane Gradostat Bioreactor (MGR)	Is an MBR in which a biofilm has been immobilised on a membrane, with the gas and liquid flow both uni-directional and bi-directional, and spatial nutrient concentration gradients exist within the biofilm.
Secondary metabolite	Is an extracellular compound produced by a micro organism in response to nutrient limitations. This compound is not needed for the growth or maintenance of cellular functions.

OUTPUTS FROM THIS STUDY

- **Publications**

Godongwana, B., **De Jager, D.**, Sheldon, M.S. & Edwards, W. 2009. The effect of *Streptomyces coelicolor* on the hydrodynamics of a vertically orientated capillary membrane gradostat reactor. *Journal of Membrane Science,* 333:79-87.

De Jager, D., Sheldon, M.S. & Edwards, W. 2009. Modelling growth kinetics of *Streptomyces coelicolor* A3(2) in a pressurised membrane gradostat reactor (MGR). *Enzyme and Microbial Technology,* 45:449-456.

- **Presentations**

Godongwana, B., **De Jager, D.**, Sheldon, M.S. & Edwards, W. 2009. The effect of *Streptomyces coelicolor* on the hydrodynamics of a vertically orientated capillary membrane gradostat reactor. WISA-MTC'09, Stellenbosch, South Africa, 13 - 15 May 2009.

- **Posters**

De Jager, D., Sheldon, M.S. & Edwards, W. 2009. Modelling growth kinetics of *Streptomyces coelicolor* A3(2) in a pressurised membrane gradostat reactor (MGR). WISA-MTC'09, Stellenbosch, South Africa, 13 - 15 May 2009.

- **Awards**

Awarded for best poster presentation (runner-up) at the International Water Institute of Southern Africa Membrane Technology Conference (WISA-MTC'09); Stellenbosch, South Africa, 13 – 15 May 2009.

CHAPTER 1

INTRODUCTION

CHAPTER ONE
INTRODUCTION

1.1 Background

Membrane technology is utilised in many environmental, water treatment, chemical, petrochemical, petroleum, pharmaceutical, medical, beverage, dairy, food, paper, and textile applications (Stanojević *et al.*, 2003). Much research has been performed on the optimisation of membrane bioreactor (MBR) systems, such as the membrane gradostat bioreactor (MGR), for the cultivation of micro organisms identified for their potential applications in diverse industries (Godongwana *et al.*, 2007).

To better understand the behaviour of an MBR, and to be able to predict the effect of operating parameters/variables on the system performance, validated mathematical models are required (Pavasant *et al.*, 1997). The models must therefore describe not only the microbial growth kinetics but also the transport phenomena within the substrate bed and the mass and energy exchanges between the bed and subsystems of the MBR, such as the membrane wall and the extracellular space gases (Mitchell *et al.*, 2003).

The modelling of microbial growth kinetics plays an important role in the design and optimisation of MGR systems, such as the one patented by Leukes *et al.* (1999) as a possible system for the continuous production of secondary metabolites. Therefore, studying and quantifying the growth kinetics within a continuous MGR is important as this can be utilised in the development of an efficient nutrient gradient within the biofilm, as well as to model the mass transfer of the bioprocess (Sheldon *et al.*, 2008).

The main problem of oxygen supply in aerobic biological systems, such as MBR's and MGR's is oxygen's nominal solubility in water (Hibiya *et al.*, 2003). Inadequate oxygen transfer results in reduced microbial activity (Thibault *et al.*, 2000), which in turn can result in decreased production of low volume high value secondary metabolites. The production of secondary metabolites, such as actinorhodin by *Streptomyces coelicolor*, is strongly affected by the dissolved oxygen (DO) concentration (Ozergin-Ulgen *et al.* 1998). In order to determine the effect of oxygen limitation on the production of secondary metabolites, oxygen profiles within the biofilm can be measured utilising microsensors (Frederick *et al.*, 1991). Microsensors were introduced through the work of Revsbech (1989), who constructed reliable oxygen microsensors, to be utilised in the profiling of oxygen distribution in sediments and biofilms. The mathematical modeling of the oxygen concentration profiles recorded with the oxygen microsensors, allowed the determination of oxygen kinetic

parameters (Frederick *et al.*, 1991). The oxygen profiles obtained within biofilms not only added to increased understanding with regards to biological processes on a microscale, but also increased the information available regarding physical processes, such as diffusion and convection (Kuenen *et al.*, 1986).

To date, limited information is available with regards to the microbial growth kinetics and dissolved oxygen distribution within biofilms of bacteria immobilised on the external surface of single fibre ceramic membrane MGR's, operated under continuously pressurised air and nutrient supply.

1.2 Problem statement

Inadequate oxygen transfer in immobilised MBR systems results in decreased microbial activity within biofilms (Thibault *et al.*, 2000) resulting in reduced production of low volume high value secondary metabolites. The limiting step in most aerobic systems is the transfer of oxygen from the gas phase to the reaction zone in the immobilised micro organism.

1.3 Research questions

- How does the growth kinetics of *Streptomyces coelicolor* in a continuously operated single fibre membrane gradostat reactor compare to batch and fed-batch cultures?
- How does the biofilm thickness and position within the MBR, with regards to the oxygen supply, influence the oxygen mass transfer within the biofilm?
- Does the presence of oxygen depleted zones within the biofilm have an effect on the production of secondary metabolites, such as actinorhodin?
- How do the oxygen mass transfer kinetics for batch liquid systems compare to continuous MGR systems?
- What relationship exists between the biomass, oxygen penetration depth and ratio within a biofilm?

1.4 Aim and objectives

The main purpose for performing the following research project was to quantify the growth and oxygen mass transfer kinetics, including the diffusive and convective parameters, using *Streptomyces coelicolor* cultures, immobilised on the external surface of a ceramic membrane in a continuously operated pressurised Membrane Gradostat Bioreactor (MGR) utilised for the production of the secondary metabolite, actinorhodin.

The objectives of this study were:

- Compare *Streptomyces coelicolor* A3(2) growth in both a complex growth medium, International *Streptomyces* Project, medium 2 (ISP2) and defined growth medium.

- Quantify the substrate consumption kinetic parameters of *S. coelicolor* using a complex (ISP2) and defined growth medium.
- Quantify and compare the product formation in biofilms of *S. coelicolor*, using a complex growth medium in both single fibre membrane gradostat reactor's (SFMGR) and multifibre gradostat reactor's (MFMGR).
- Design a reactor that allows for *in-situ* oxygen measurements in order to determine the oxygen penetration depth and ratio and evaluate the existence of anaerobic zones.
- Quantify the oxygen mass transfer parameters, consumption, diffusive and convective mass transfer rates.

1.5 Significance

It is known that a higher production of secondary metabolites can be accomplished utilising immobilised systems than in batch liquid cultures. Adequate oxygen transfer results in improved DO concentration within the system. With the aid of oxygen microsensors, the oxygen penetration depth and ratio will be determined. This study will determine whether a comparison exists between the oxygen mass transfer kinetics of batch liquid systems and continuous pressurised membrane systems; as well as determine whether oxygen depleted zones exist within biofilms cultured in MGR systems and the effect this will have on secondary metabolite production.

On completion of this study there will be a better understanding of growth kinetics of *Streptomyces coelicolor* A3(2) in a pressurised MGR, as well as of oxygen mass transfer kinetics within microbial cultures in an MGR. The information obtained will contribute to a better understanding of reactor design and secondary metabolite production optimisation. A bioreactor will have been constructed that allows for *in-situ* oxygen measurements. The relationship between the biomass, oxygen penetration depth and ratio within a biofilm will be better understood. The oxygen profiles obtained will provide increased understanding of both the biological (microscale) and physical (diffusion and convection) processes within an MGR system. More data will be available with regards to oxygen distribution within gradostat systems, thereby increasing the limited amount of information that is currently available. Both the growth kinetics and oxygen mass transfer of *Streptomyces* and more specifically this micro organism within this type of continuous reactor has not been reported previously.

1.6 Delineation

This research will be limited to growth and substrate kinetics, as well as oxygen mass transfer kinetics within a pressurised MGR. The following areas will not be covered during this study:

- Product purification.
- Microbial metabolic activity.
- Different single substrate limiting models.

CHAPTER 2

LITERATURE REVIEW

CHAPTER TWO
LITERATURE REVIEW

2.1 Introduction

This literature review is divided into three main sections, namely:

- Membranes and membrane processes.
- Biofilms, growth and substrate kinetics.
- Dissolved oxygen (DO) mass transfer within aerobic immobilised biofilms.

2.2 Membrane technology

2.2.1 Membranes

A membrane is generally defined as being a selective barrier. The membrane utilised in a bioreactor can provide either a barrier to certain components, while being permeable to others, prevent certain components from contacting a catalyst, or contain reactive sites and be a catalyst itself (Fogler, 1999). A membrane has the ability to control mass transfer between two bulk phases in a membrane process. The movement of a phase across the membrane is due to the presence of one or more driving forces that can be a gradient in concentration, pressure, temperature or electrical potential (Stanojević *et al.*, 2003).

In immobilised membrane bioreactors (MBR's), membranes allow the transport of nutrients to the cells immobilised on their external surface, while providing transport pathways for the metabolic products produced by the immobilised cells from the cells to a product collection bottle (Curcio *et al.*, 2005). Membranes provide high surface area for cell adhesion and culture for anchorage-dependent cells and allow a sufficient exchange of nutrients and metabolites to maintain cell viability and function *in vitro* (Curcio *et al.*, 2005). The large surface area of a membrane to the small volume allows for high operational capacities (Stamatialis *et al.*, 2008).

New applications continue to emerge, such as membranes for the development of microsensors (Gavalas *et al.*, 2003) and molecularly imprinted polymeric membranes for the separation of molecules (Yoshikawa, 2002; Han *et al.*, 2003). Recently introduced applications of membrane processes include MBR's, membrane chromatography and membrane contactors (Charcosset, 2006).

2.2.1.1 Membrane materials

Membrane materials are divided into two groups, namely organic (eg. polymeric) and inorganic (eg. ceramic). Metallic membrane filters also exist; however they have no applications relating to MBR technology (Judd, 2006). Membranes can be formed from various organic polymers, the most common polymers utilised for the duty of membrane separation being polyvinylidene difluoride (PVDF), polyethersulphone (PES), polyethylene (PE) and polypropylene (PP) (Judd, 2006). Inorganic membranes, such as ceramic membranes, are more rigid and therefore more mechanically stable and can be both chemically and steam sterilised (Ntwampe *et al.*, 2007). Sheldon and Small (2005) tested the immobilisation of *Phanerochaete chrysosporium* on both organic and inorganic membranes. From results obtained the highest attachment and immobilisation of spores was observed on organic (polysulphone) capillary membranes. However, for operation purposes the organic (ceramic) capillary membrane was more suitable. Ceramic systems are very expensive, but very effective for micro filtration (MF) (Wagner, 2001). These membranes are suitable for use in the industrial production of secondary metabolites due to the fact that microbial stress in the immobilised biofilm will be high as a direct consequence of the thicker biofilm (Sheldon & Small, 2005; Ntwampe *et al.*, 2007).

2.2.1.2 Membrane processes

Membrane processes are categorised according to the pore size, molecular cut-off and pressure at which the membranes operate. These categories are inter-related, because as the pore size or the molecular cut-off is decreased the pressure applied to the membrane increases (Van der Roest *et al.*, 2002).

Membrane separation processes can be broadly categorised into four groups, based on the pore size of the membranes. These categories, arranged from smallest to largest pore size are reverse osmosis (RO), nanofiltration (NF), ultrafiltration (UF) and microfiltration (MF) (Mallia & Till, 2001; Judd, 2006). See Table 2.1 (Wagner, 2001) for comparison of the four membrane processes. The coarsest membrane, associated with MF, is capable of rejecting particulate matter, while the most selective membrane, associated with RO can reject singly charged ions, like sodium (Na^+) and chloride (Cl^-) (Judd, 2006). All RO, NF and UF membranes are asymmetric (Wagner, 2001). Asymmetric refers to the graded porosity of the membrane substructure and indicates that the membranes have an inside coating, called a skin layer and combine the high selectivity of a dense membrane with a high permeation rate of a thin membrane. The membrane itself provides the structural support for the skin layer. The graded porosity

Table 2. 1: Comparison of the four membrane processes (Wagner, 2001)

	Reverse osmosis	Nanofiltration	Ultrafiltration	Microfiltration
Membrane	Asymetrical	Asymetrical	Asymetrical	Symmetrical, Asymetrical
Thickness	150 µm	150 µm	150 to 250 µm	10 to 150 µm
Thin film	1µm	1µm	1µm	
Pore size	<0.002 µm	<0.002 µm	0.2 to 0.02 µm	4 to 0.02 µm
Rejection of	High and low molecular weight components, Sodium chloride, glucose, amino acids	High molecular weight components, mono-, di- and oligosaccharides, polyvalent negative ions	Macromolecules, proteins, polysaccharides vira	Particles, clay, bacteria
Membrane material(s)	Celulose acetate, Thin film	Celulose acetate, Thin film	Ceramic, PSO, PVDF, celulose acetate, Thin film	Ceramic, PP, PSO, PVDF
Membrane module	Tubular, spiral wound, plate-and-frame	Tubular, spiral wound, plate-and-frame	Tubular, hollow fibre, spiral wound, plate-and-frame	Tubular, hollow fibre
Operating pressure	15 to150 bar	5 to 35 bar	1 to10 bar	< 2 bar

is most dense directly below the skin layer, but the porosity increases as one moves away from this layer (Wagner, 2001; Ntwampe *et al.*, 2007).

UF and MF are membrane separation processes that filter material on the basis of size (Van der Roest *et al.*, 2002) to recover macromolecules and retain suspended colloids and particles (Charcosset, 2006). An application of UF in downstream processing is for product concentration, in other words, the removal of buffer or solvent. An application of MF is virus removal from cell cultures (Charcosset, 2006). In RO separation occurs due to differing solubility and diffusion rates of solvents and solutes, while in NF separation occurs through a combination of charge rejection, solubility-diffusion and sieving through the membrane micropores (< 2 µm) (Judd, 2006). MF and UF membrane separation processes are generally utilised in MBR concepts (Van der Roest *et al.*, 2002).

2.2.1.3 Membrane system configurations

Membrane systems take advantage of the inherent properties of high selectivity, high surface area per unit volume of reactor space (i.e. high packing density) and their potential for controlling the level of contact and/or mixing between two phases (Charcosset, 2006). The configuration (its geometry and the way the membrane has been mounted and orientated with respect to flow) of the membrane is important in determining the overall performance of the process (Judd, 2006). Six principal configurations are utilised in membrane processes, namely plate-and-frame/flat sheet (FS), hollow fibre (HF), tubular (MT), capillary tube (CT), pleated filter cartridge (FC) as well as spiral wound (SW) (Judd, 2006).

Cross-flow and dead-end operation are two standard modes of operation in conventional pressure-driven membrane processes (Judd, 2006). In cross-flow the fluid being filtered flows parallel to the membrane surface, and permeates through the membrane due to the existence of a pressure difference across the membrane (Charcosset, 2006). No retentate stream is found in dead-end operation (Judd, 2006), therefore this mode of operation is often applied in MF as the feed is forced through the membrane. The permeate and retentate refers to the parts of the feed that, respectively, does and does not pass through the membrane (Seader & Henley, 2006). In industrial applications however, cross-flow operation is preferred over dead-end operation as less fouling occurs. With cross-flow operations flux decline is lower and there is a variety of different cross-flow modes such as co-current, counter-current and cross-flow with perfect permeate mixing (Stanojević *et al.*, 2003).

2.2.2 Membrane bioreactors (MBR's)

MBR's combine a biological process with membrane separation (Van der Roest *et al.*, 2002). Therefore, as cited by Sheldon and Small (2005) when culturing micro organisms for the production of complex biological molecules, MBR's can be used. MBR's are divided into three categories: (1) where the micro organism is immobilised within the membrane matrix itself (i.e. immobilised MBR) and can be fed from the extracapillary space (ECS) to the lumen or vice versa; (2) where biocatalysts such as enzymes, micro organisms and antibodies immobilised on a membrane are suspended in solution and compartmentalised in a reaction vessel (i.e. immersed MBR) (Charcosset, 2006); or (3) the bioreactor and membrane modules are separate from each other (i.e. sidestream MBR).

The immobilised MBR, like the membrane gradostat bioreactor (MGR) can be divided into three compartments: the shell side, the biofilm and the tube side. Most of the microbial reaction occurs in the biofilm that grows on the external surface of a membrane (Pavasant *et al.*, 1997). Immobilised MBR's retain the cells on the membranes in a low shear environment with a continuous nutrient supply, as well as the continuous removal of metabolic products. These immobilised systems ensure that cells can be maintained in a state of low or non-proliferation for extended time periods, while still producing the products desired (Belfort, 1989; Solomon & Petersen, 2002; Nwampe, 2005; Ntwampe & Sheldon, 2006; Ntwampe *et al.*, 2007; Sheldon *et al.*, 2008).

Immersed MBR's (iMBR's) and sidestream MBR's (sMBR's) are used as conventional biomass rejection MBR's. iMBR's require less energy than sMBR's since membrane modules in a pumped sidestream cross-flow utilises more energy due to the high pressures and volumetric flows (Judd, 2006).

2.2.2.1 Applications of membrane bioreactors

MBR's were introduced over 30 years ago, with their main industrial application being wastewater treatment (Voight *et al.*, 2001; Xu *et al.*, 2003; Hai *et al.*, 2006). Only limited success has been achieved with MBR's in the biotechnology field. The main difficulties using MBR's on an industrial level are the rate-limiting aspects and scale-up difficulties (Charcosset, 2006). MBR's have been utilised for the production of amino acids, antibiotics, anti-inflammatories, anticancer drugs, vitamins (Charcosset, 2006) and secondary metabolites (Leukes, 1999; Burton, 2001; Ntwampe, 2005; Ntwampe *et al.*,

2007; Ntwampe & Sheldon, 2006; Sheldon *et al.*, 2008). MBR's with immobilised whole cells provide an environment for increased cell densities, thus producing higher product titre. In immobilised whole cell MBR's the cells are retained through a membrane barrier that is perfused with a steady continuous flow of growth medium and supplied with oxygen, while product and wastes are removed. Many configurations have been tested, including flat sheet (FS) and rotating bioreactors. However, the HF configuration was the most interesting. In the HF configuration the cells were either grown within the ECS or within the lumen of the membrane (Charcosset, 2006). The utilisation of membrane technology in the treatment of wastewater may be more appropriate and superior to existing treatment processes. However, there are situations where membrane technology can only be used to assist existing treatment processes (Mallia & Till, 2001). A promising MBR application is the production of high value-low volume extra-cellular, complex biological molecules (i.e. secondary metabolites) like enzymes (Leukes, 1999; Burton, 2001; Solomon & Petersen, 2002; Govender *et al.*, 2003; Ntwampe, 2005; Charcosset, 2006; González Diaz *et al.*, 2006), antibiotics, anti-inflammatories, anticancer drugs and vitamins (Charcosset, 2006), through the immobilisation and culture of various micro organisms (Belfort, 1989; Beeton *et al.*, 1993; Yang *et al.*, 2006), such as fungi and bacteria (Venkatadri & Irvine, 1993; Leukes, 1999; Solomon & Petersen, 2002; Ntwampe, 2005; Hai *et al.*, 2006; Ntwampe & Sheldon, 2006; Sheldon *et al*, 2008), have been reported in literature.

The advantages of MBR's with a shell and tube reactor configuration are the presence of a large surface area of biofilm per unit volume of bioreactor and the ability to operate at high flow rates over the biofilm surface, thus enhancing substrate transfer into the biofilm (Casey *et al.*, 1999).

2.2.3 The membrane gradostat bioreactor (MGR)

The term gradostat is utilised to describe an MBR system in which the liquid nutrient gradient and the gas gradient are both uni-directional and bi-directional. Contact between these gradients occurs between the primary and stationary growth phases of the biomass (Leukes *et al.*, 1999). As shown in Figure 2.1, the term uni-directional indicates that the gradient of the parameter moves from a high to a low concentration, while the term bi-directional indicates the gradients are running in opposite directions.

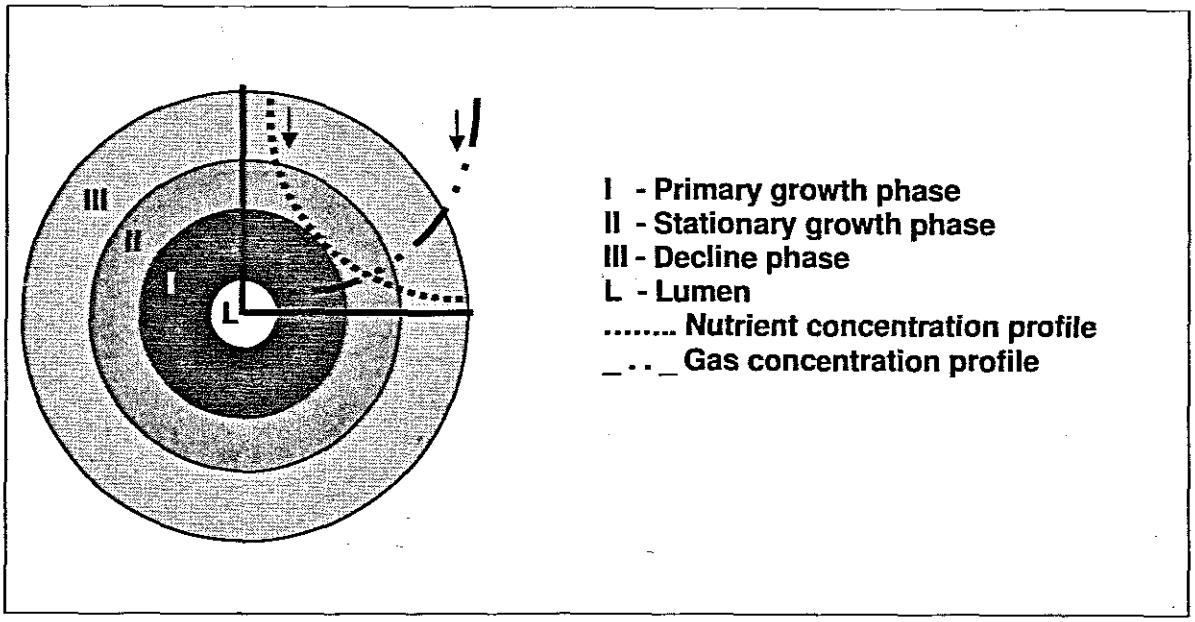

Figure 2.1: A schematic representation of the theoretical gradostat concept (Leukes, 1999)

The term membrane gradostat bioreactor (MGR) describes a biofilm reactor that indicates a good potential to be used in an industrial application, which utilises a synthetic capillary ultrafiltration membrane (Jacobs & Leukes, 1996; Jacobs & Sanderson, 1997). The MGR conceptualised and patented by Leukes *et al.* (1999) was designed for the continuous production of extra-cellular secondary metabolites. The MGR consists of a porous substratum (i.e. membrane) that has a biofilm immobilised onto the external surface of an UF capillary membrane via reverse filtration (Govender *et al.*, 2004). A synthetic nutrient solution flows through the membrane lumen towards the ECS. The nutrient flow rate is sufficiently low for a nutrient gradient to be established across the biofilm. The MGR system mimics the natural environment of the micro organism, where substrate distribution gradients are established across the biofilm (Leukes, 1999; Leukes *et al.*, 1999; Govender *et al.*, 2003; Sheldon & Small, 2005; Ntwampe & Sheldon, 2006; Ntwampe *et al.*, 2008). This allows growth to occur in the nutrient rich zone, forcing the older biofilm into the nutrient poor zone where secondary metabolism is induced due to nutrient limitations (Solomon & Petersen, 2002; Govender *et al.*, 2003). The liquid nutrient gradient moves from a high nutrient concentration inside the lumen of the membrane through the biofilm towards the outside where a low nutrient concentration is present; while the air gradient moves from a high oxygen concentration outside the biofilm growing on the surface of the membrane through the biofilm towards the lumen of the membrane, where a low or none existent oxygen concentration is present, hence the term bi-directional.

In an MGR system, when nutrients are abundantly available, the biofilm closest to the membrane will grow rapidly. Biofilm situated further away from the membrane surface is exposed to lower nutrient concentrations, due to its location from the nutrient supply. Therefore, the biofilm exhibits slower growth and even growth cessation. When the biofilm becomes thick enough for substrate limitation to occur, the overall growth would be constant and controlled by the rate at which the limiting nutrient is being supplied to the MGR system (Sheldon *et al.*, 2008).

As cited by Ntwampe *et al.* (2008), the most important external factors influencing the production and activity of secondary metabolites produced by a micro organism such as *P. chrysosporium* immobilised in an MGR are temperature, pH and dissolved oxygen (DO) concentration (Fenn *et al.*, 1981; Fenn & Kirk, 1981; Jeffries *et al.*, 1981; Leisola *et al.*, 1984). When compared to submerged batch culture systems, the MGR has shown to have higher production of secondary metabolites per reactor volume (Ntwampe *et al.*, 2008).

Microbial stratification is created within the biofilm due to the counter-diffusion of oxygen and nutrients (Ahmadi Motlagh *et al.*, 2006). The region of the biofilm closest to the membrane surface experiences the highest concentrations of growth medium; in thick biofilms this region is likely to contain anaerobic zones. By contrast the outer regions of the biofilm in contact with the air/oxygen are rich in DO and are likely to contain aerobic zones (Ahmadi Motlagh *et al.*, 2006). As the biofilm becomes thicker over time the oxygen and substrates from the growth medium have to diffuse over greater distances and biofilm performance declines (Ahmadi Motlagh *et al.*, 2006). In MGR's potentially limiting reaction substrates are supplied from opposite sides of the biofilm increasing the complexity of performance analysis (Casey *et al.*, 2000).

2.2.3.1 Capillary membrane structure and micro organism immobilisation in MGR's

Capillary membranes, such as polysulfone membranes and ceramic membranes fall into the category of integrally skinned asymmetric membranes. Integrally skinned indicates that the skin layer of the membrane is an integrated part of the membrane substructure. Sheldon and Small (2005) tested the immobilisation of *P. chrysosporium* on an internally skinned capillary polysulphone, two tubular aluminium oxide ceramic membranes with an average pore size of 0.2 and 3 µm, respectively, and one capillary titanium oxide ceramic membrane with an average pore size of 3 µm in separate MGR's. From the

results obtained the highest attachment and immobilisation of spores was observed on the capillary membranes with less on the tubular ceramic membranes. However, it was further concluded that the more suitable membrane material for spore immobilisation and biofilm development were the capillary polysulphone membranes. However, for day-to-day operation the ceramic membranes proved to be more rigid, mechanically stable and were reuseable after cleaning with chemicals and steam (Sheldon & Small, 2005).

Figure 2.2(a-c) shows how the spores of the white rot fungi *P. chrysosporium* inoculated onto a polysulphone membrane germinated into hyphae within the microvoids of the membrane. The hyphae within the microvoids are believed to anchor the fungus (Sheldon & Small, 2005). Figure 2.3 shows a biofilm of *P. chrysosporium* immobilsed on the extremal surface of a tubular ceramic membrane. The SEM indicates that unlike with the polysulphone membrane no hyphae grew into the microvoids, therefore the biofilm was only immobilised on the surface and not within the membrane matrix (Sheldon & Small, 2005).

According to Govender *et al.* (2004) spore immobilisation via reverse filtration promotes uniform growth and better surface coverage. When utilising reverse filtration in a non-pressurised system, spore immobilisation is dependent on the differential pressure across the membrane and the fluid flow pattern within the membrane. The spatial distribution of spores on the external membrane surface and within the microvoids in the membrane wall is influenced by the immobilisation method utilised. The resultant lateral and radial biofilm development on the external surface of the membrane is dependent on the spore immobilisation method utilised (Govender *et al.*, 2004).

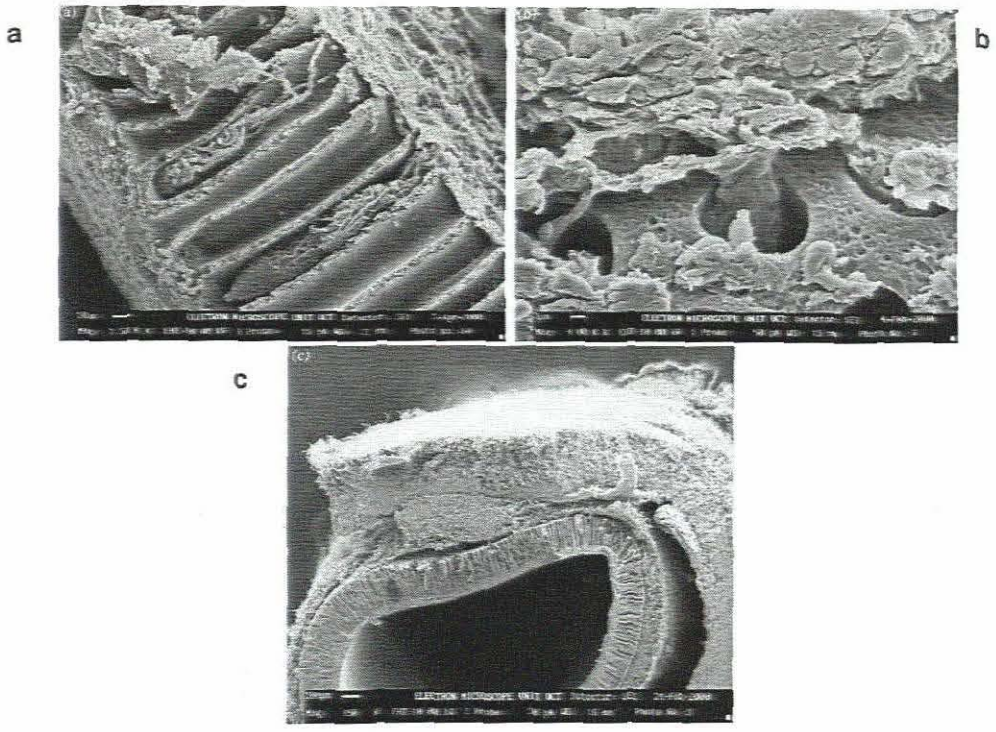

Figure 2.2: (a) SEM of a cross section of the polysulphone membrane with biofilm growth showing cords within the microvoids (magnification 1500×); (b) SEM of a cross section of the polysulphone membrane with biofilm growth showing cords from the microvoids and spreading across the surface (magnification 4000×); (c) SEM of a cross section of the polysulphone membrane showing biofilm thickness (magnification 150×) (Sheldon & Small, 2005)

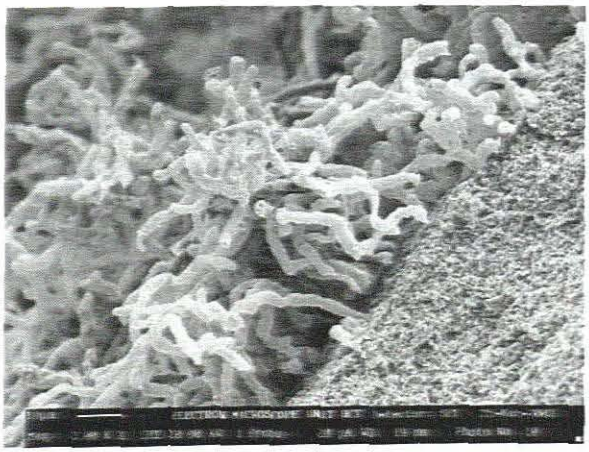

Figure 2.3: SEM of *Phareochaete chrysosporium* biofilm growth on 0.2 m tubular ceramic membrane (magnification 3000×) (Sheldon & Small, 2005)

2.3 Biofilms, growth and substrate kinetics

Bacteria differentiate from an independent free-living growth mode to an interdependent surface-attached existence when exposed to certain environmental signals. These surface-attached microbial communities are known as biofilms, which are capable of developing into elaborate three-dimensional structures in flowing systems with nutrients readily available (Davey *et al.*, 2003). Biofilms of immobilised micro organisms arrange their morphology according to the conditions at which they are cultured. Thus, the internal mass transfer rates and microbial activity is affected by biofilm morphology. Biofilms grown at a low flow velocity have a low density and high effective diffusivity, but are not able to resist higher shear stress (Beyenal & Lewandowski, 2002; Ntwampe *et al.*, 2008)

2.3.1 Streptomyces bacteria

Streptomycetes are mycelial bacteria resembling filamentous fungi in their apical growth (Flärdh, 2003). They are found as a microbes in soil (Kim & Kim, 2004), and are the most important source of antibiotics for medical, veterinary and agricultural use. Members of the genus *Streptomyces* grow as a mycelium of branching hyphal filaments and reproduce by sending up aerial branches that turn into chains of spores (Chater, 2006). Streptomycetes are mycelial prokaryotes, that grow by hyphal extension and branching, to form a matted substrate mycelium. Little information is available regarding the mechanisms of apical growth and inherent poleward transport processes in mycelial prokaryotes, unlike fungi that have been extensively studied (Flärdh, 2003). *Streptomyces* species have a tendency to form cell pellets in culture fluids and biofilms on surfaces during growth (Melzoch *et al.*, 1997).

Streptomyces species produce commercially important medicinal products utilised therapeutically as anti-infective (i.e. antibiotics, antifungal and antiparasitic), anticancer or immunosuppressant agents (Champness, 2000). A special feature of this bacterium is the production of extracellular molecules, such as proteins, antibiotics and signal molecules at the time when the main growth period is ending. The reproductive phase corresponds to the secretion of antibiotics, which protect the colony against invading bacteria during aerial growth (Chater, 2006). The production of secondary metabolites by the Gram positive mycelial Streptomycetes normally coincides with or slightly precedes the development of aerial hyphae in surface attached cultures. In liquid-grown cultures

the production of secondary metabolites is generally confined to the stationary phase and occurs in response to nutrient limitation (Bibb, 2005).

The strain *Streptomyces coelicolor* A3(2) is the most effectively studied Streptomycete. After the first coherent map of various genes on the *S. coelicolor* chromosome was published in 1967 by David Hopwood (Hopwood *et al.*, 1995; Bibb, 1996; Bentley *et al.*, 2002; Thompson *et al.*, 2002; Kim & Kim, 2004; Chater, 2006), it became the model species internationally for understanding the growth, metabolism and secondary metabolite production by filamentous bacteria. This included work on the genetics and molecular biology of antibiotic-producing Streptomycetes

2.3.1.1 *Streptomyces coelicolor* A3(2)

Four antibiotics are produced by *Streptomyces coelicolor* A3(2) namely methylenomycin, Ca-dependent antibiotic (CDA), undercylprodigiosin (anti-tumour agent and immunosuppressant) and actinorhodin. Depending on the pH, red tripyrolle undercylprodigiosin and the blue polyketide antibiotic, actinorhodin, are produced (Champness & Chater, 1994; Okamoto *et al.*, 2003). Actinorhodin and undercylprodigiosin are pigmented antibiotics facilitating the visual observation of product synthesis (Ates *et al.*, 1997). The pH indicator antibiotic, actinorhodin, is produced by *S. coelicolor* A3(2) when the micro organism is subjected to various nutrient limitations, such as ammonium, nitrate, phosphate or trace elements (Bystrykh *et al.*, 1996) and the micro organism has a low growth rate or enters the stationary growth phase (Champness & Chater, 1994).

Actinorhodin turns red at a pH below 8.5 and blue at pH above 8.5 (Zhang *et al.*, 2006). At growth medium pH values of 4.5 to 5.5 significant amounts of actinorhodin occur. However, it is located almost exclusively intracellularly. At growth medium pH values of 6.0 to 7.5 a different blue pigment is produced both intracellularly and extracellularly. *S. coelicolor* A3(2) is therefore capable of producing large amounts of two actinorhodin-related pigments. The main intracellular pigment is actinorhodin, while the compound responsible for the blue colour of the permeate and mycelium is its lactone derivative γ-actinorhodin (Bystrykh *et al.*, 1996). According to Bystrykh *et al.* (1997) γ-actinorhodin is most probably synthesised as an end product of the actinorhodin pathway during its export from the cell.

The general response of *S. coelicolor* A3(2) to a depletion of glucose is the abolishment of blue pigment synthesis; and to growth limitation by nitrogen (either ammonium or nitrate), phosphate, or trace elements is the synthesis of blue pigment (Bystrykh *et al.*, 1996). The final pH of the growth medium, rather than specific nutrient limitation, has been identified as the determining factor in which blue pigment will be produced. Bystrykh *et al.* (1996) reported that when grown at a neutral pH, the major exported product of the actinorhodin biosynthetic pathway by *S. coelicolor* A3(2) is γ-actinorhodin.

Grown in complex growth medium *S. coelicolor* A3(2) exhibits a transient growth pause before entering into the stationary phase and actinorhodin production commences. A similar pause is seen in *Streptomyces hygroscopius* when grown in a complex growth medium (Champness & Chater, 1994). In chemically defined media, S. *coelicolor* grows as mycelial strands and pellets that are composed of densely interwoven hyphae (Elibol, 2001).

2.3.1.2 Secondary metabolite (actinorhodin) production

Nutrition plays a pivotal role in the production and yield of secondary metabolites. A limiting supply of an essential nutrient effectively restricts the organism's growth, because the choice of limiting nutrient can have both specific metabolic and regulatory effects. High product yields are achieved by designing a proper production medium. A relationship normally exists between the growth medium composition and the biosynthesis of antibiotics (Elibol, 2004). The onset of secondary metabolism is triggered by one of two methods, either by limiting the nutrients to the organism, in other words starving the organism, or via reduced growth opportunities (Doull & Vining, 1990; Bruheim *et al.*, 2002).

The extent of secondary metabolism is influenced by carbon catabolic, nitrogen metabolic and phosphate regulation (Martin & Demain, 1980). Doull and Vining (1990) found that actinorhodin production by *S. coelicolor* was insensitive to the carbon source concentration, but was triggered by nitrogen depletion, phosphate depletion or a decline in growth rate. Phosphate limitation was found to be epistatic to that of nitrogen when ammonium is the nitrate source (Hobbs *et al.*, 1990; Coisne *et al.*, 1999). Secondary metabolites are normally produced during the slow growth rates or stationary phase when one of the essential nutrients has been exhausted (Shapiro, 1989). While studying carbon catabolic repression Ates *et al.* (1997) found an increased actinorhodin production in fed-batch cultures when the glucose concentration was kept below the

critical level. Catabolite repression occurs when enzyme synthesis is prevented due to the rapid utilisation of carbon sources (Aunstrup *et al.*, 1979).

Actinorhodin, one of the four antibiotics produced by *S. coelicolor* A3(2) is a red/blue *acid/base indicator pigment with weak antibiotic properties.* Actinorhodin is a member of a group of chemically related antibiotics called isochromanoquinines. Synthesis is via the polyketide pathway, an important biosynthetic route for the synthesis of antibiotics (Rudd & Hopwood, 1979; Abbas & Edwards, 1990). The only carbon precursor required for actinorhodin synthesis is acetyl CoA (Bruheim *et al.*, 2002). Aromatic polyketides are a large family of structurally diverse natural products with a large range of biological activities such as antibiotic, anticancer, antiparasitic and immunosuppressant properties (Naeimpoor & Mavituna, 2000).

In chemostat cultures the highest actinorhodin production rates occurred under nitrogen or carbon limited-growth conditions, with the lowest production rates occurring under sulfate or magnesium-limited growth conditions (Melzoch *et al.*, 1997). Therefore, actinorhodin production is repressed by ammonium ions but this repression is relieved when the carbon source is present at particular growth-limiting concentrations (Melzoch *et al.*, 1997).

Hobbs *et al.* (1990) reported that actinorhodin production was inhibited by phosphate concentrations greater than 24 mM as cited by Melzoch *et al.* (1997). According to Bystrykh *et al.* (1996) the nature of the growth-limiting nutrient plays an important role in the production of the extracellular pigment. The resultant stationary phase due to a depletion of the nitrogen source (either ammonium or nitrate), phosphate or trace elements caused actinorhodin production (Melzoch *et al.*, 1997).

According to Ozergin-Ulgen and Mavituna (1994) actinorhodin production in the complex *growth medium* YEME described by Hopwood *et al.* (1985) was 50 times as much when compared to the defined growth medium described by Hobbs *et al.* (1989). However, according to Brystrykh *et al.* (1996) this excreted pigment is not actinorhodin but its lactone derivative γ-actinorhodin (Coisne *et al.*, 1999). Actinorhodin is navy blue in the defined growth medium and dark purple in the complex growth medium (Ozergin-Ulgen & Mavituna, 1994).

The biosynthesis of actinorhodin is a multi-functional process which mainly occurs after the active growth phase or during the stationary phase in batch cultures. Many factors have been implicated in the synthesis of actinorhodin. However, phosphate or nitrogen depletion normally results in production, with phosphate control being epistatic to that of actinorhodin (Doull & Vining, 1990; Coisne *et al.,* 1999). The pH of the culture medium was important as the excretion of actinorhodin seemed to occur at pH values above 6.7 (Coisne *et al.,* 1999).

Actinorhodin production starts when the cells in the biofilm enter the exponential growth phase, therefore cell growth and actinorhodin production occur simultaneously. However, in defined media (Hobbs *et al.,* 1989) the accumulation of actinorhodin continues after growth has stopped. Therefore, the growth of *S. coelicolor* and actinorhodin production does not follow the normal secondary metabolite production seen in defined media (Elibol, 2001). Ozergin-Ulgen and Mavituna (1994) also reported that *S. coelicolor* produced the secondary metabolite, actinorhodin, during its growth phase.

2.3.1.3 The effect of growth medium composition on secondary metabolite production

The role of the medium is normally considered in terms of the nutrients and precursors it provides to the culture. A good medium provides the correct osmotic balance between the cell's cytoplasm and the external environment (Elibol & Mavituna, 1998).

According to Elibol (2002) the optimum glucose concentration for *S. coelicolor* A3(2) was 12.25 g/L for a 2 L batch bioreactor operated with the defined medium described by Hobbs *et al.,* (1989) at an airflow rate of 2 L/min and an agitation speed of 300 rpm (Elibol, 2002). Under these conditions an actinorhodin concentration of 60 mg/L was obtained, with a biomass concentration of 1.9 g/L; a maximum volumetric oxygen uptake rate of 180 mgO_2/L.hr and a glucose consumption rate of 0.110 g glucose/L.hr.

Nitrogen-limited medium resulted in low yields of actinorhodin, while the presence of ammonium as a nitrogen source, which is a superior nitrogen source to nitrate, resulted in an actinorhodin yield three times higher in a fed-batch culture of *Streptomyces lividans* (Bruheim *et al.,* 2002). Nitrogen limitation had a much greater physiological impact than phosphate limitation. According to Bruheim *et al.* (2002) phosphate limitation may allow

some increase in the cell mass, while nitrogen limitation inhibited protein synthesis. Phosphate limitation resulted in a higher specific production rate of actinorhodin, while nitrogen limitation resulted in the conversion of carbon into α-ketoglutaric acid instead of actinorhodin in fed-batch cultures of *S. lividans* (Bruheim *et al.*, 2002). An increase in biomass concentration is normally accompanied by a decrease in the residual glucose concentration (Elibol, 2001). Iron limitation enhanced the intracellular production and export of the pigmented antibiotic, actinorhodin. The effect was most pronounced when the bacterium was grown with nitrate instead of ammonium as the nitrogen source (Coisne *et al.*, 1999). Glucose is a carbon substrate used to form cell material, metabolic products and in the maintenance of cells (Elibol & Mavituna, 1999a).

Table 2.2 is a summary of data collected from various articles with reference to operating *S. coelicolor* at an optimum using different culture methods.

2.3.2 Sloughing

Casey *et al.* (2002) observed sloughing of the biofilm off the membrane when the accumulation rate of the biofilm was at its highest. This membrane aerated biofilm reactor (MABR) system was operated with the oxygen in the lumen of the membrane and the liquid growth medium in contact with the external surface of the membrane. Within a membrane-aerated bioreactor (MAB) Ahmadi Motlagh *et al.* (2006) concluded that the mixing conditions within the bioreactor were responsible for the occurrence of sloughing.

Table 2.2: Various operating conditions for *S. coelicolor*

Strain	Culture	Airflow rate	Dissolved oxygen	Volumetric mass transfer coefficient ($k_L a$)	Volumetric oxygen uptake rate ($q_{O_2} x$)	Maximum specific growth rate (μ_{max})	Biomass concentration	Actinorhodin concentration	Glucose concentration	References
Streptomyces coelicolor A3(2)	Batch culture	2 to 6 L/min	90 – 100 %			0.03 h^{-1}				Ozergin-Ulgen & Mavituna, 1993
Streptomyces coelicolor A3(2)	Batch culture	2 L/min	< 40 %			0.017 h^{-1}	2 g/L	28.5 mg/L	120 g/L	Ates *et al.*, 1997
Streptomyces coelicolor A3(2)	Fed-batch culture	2 L/min				0.022 h^{-1}	3.4 g/L	37.4 mg/L	264 g/L	Ates *et al.*, 1997
Streptomyces coelicolor A3(2)	Batch defined media	2 to 8 L/min	40 %	40 to 100 hr^{-1}	5 to 6 mmolO_2/L.hr			38.2 mg/L		Ozergin-Ulgen & Mavituna, 1998
Streptomyces coelicolor A3(2)	Batch complex media	2 to 8 L/min		18 to 70 hr^{-1}				47 to 52 mg/L		Ozergin-Ulgen & Mavituna, 1998
Streptomyces coelicolor A3(2)	Batch culture	2 L/min		0.0038 hr^{-1}	98 mgO_2/L.hr					Elibol & Mavituna, 1999a
Streptomyces coelicolor A3(2)	Fermentation (No PFC)	2 L/min	0.47 Mm/dm^3		7 mmol/L.hr		5.7 g/L	45 mg/L		Elibol, 2001
Streptomyces coelicolor A3(2)	Fermentation (PFC)	2 L/min	0.96 Mm/dm^3	122 to 175 hr^{-1}	4.9 mmol/L.hr		2.9 g/L	90 mg/L		Elibol, 2001
Streptomyces coelicolor A3(2)	Fermentation	2 L/min			180 mgO_2/L.hr		1.9 g/L	60 mg/L	0.110 g glucose/L.hr	Elibol, 2001

Rasmussen and Lewandowski (1998) experienced sloughing when biofilms were grown at lower flow velocities (0.62 to 1.53 cm/sec) and the biofilms had fluffy characteristics. Biofilms grown at higher flow velocities (1.53 to 2.60 cm/sec) were more rigid and thus less susceptible to sloughing. Increasing the flow velocity causes physiological responses by the biofilm, and may have resulted in the sloughing of the entire biofilm in extreme cases (Beyenal & Lewandowski, 2002).

2.3.3 Microbial growth kinetics

The modelling of microbial growth kinetics plays an important role in the design and optimisation of bioreactor systems (Mitchell *et al.*, 2003). Growth kinetics have been identified as one of the critical parameters when studying biofilms, as they can be utilised to model mass transfer and biological reactions (Ntwampe & Sheldon, 2006). Microbial growth kinetics can be described using one of two methods: (1) either using simple empirical equations; or (2) mechanistic models that try to describe intraparticle diffusion processes related to growth (Mitchell *et al.*, 2004).

2.3.3.1 Basic kinetic equations

Various empirical kinetic profiles have been described in solid state fermentation (SSF) systems including linear, exponential, logistic and fast acceleration/slow deceleration. Figure 2.4 shows the typical shapes these curves have. The empirical equations describing these curves in Figure 2.4 are shown in Table 2.3. These empirical equations do not include the effect that the nutrient concentration has on the microbial growth (Mitchell *et al.*, 2004).

The growth kinetics of micro organisms are frequently described by the logistic empirical equation (Equations 2.3a and b) (Mitchell *et al.*, 2004; Van de Lagemaat & Pyle, 2005). However, this empirical model does not provide insight into what controls the microbial growth (Ikasari & Mitchell, 2000). The logistic equation is often used due to its mathematical simplicity; in a single equation an adequate approximation of the entire growth curve is given, including both the lag phase and cessation of growth. The other kinetic equations such as the exponential (Equations 2.2a and b) and two-phase (Equations 2.4a and b) equations require that the growth curve be separated into various phases, with a different equation describing each phase (Mitchell *et al.*, 2004).

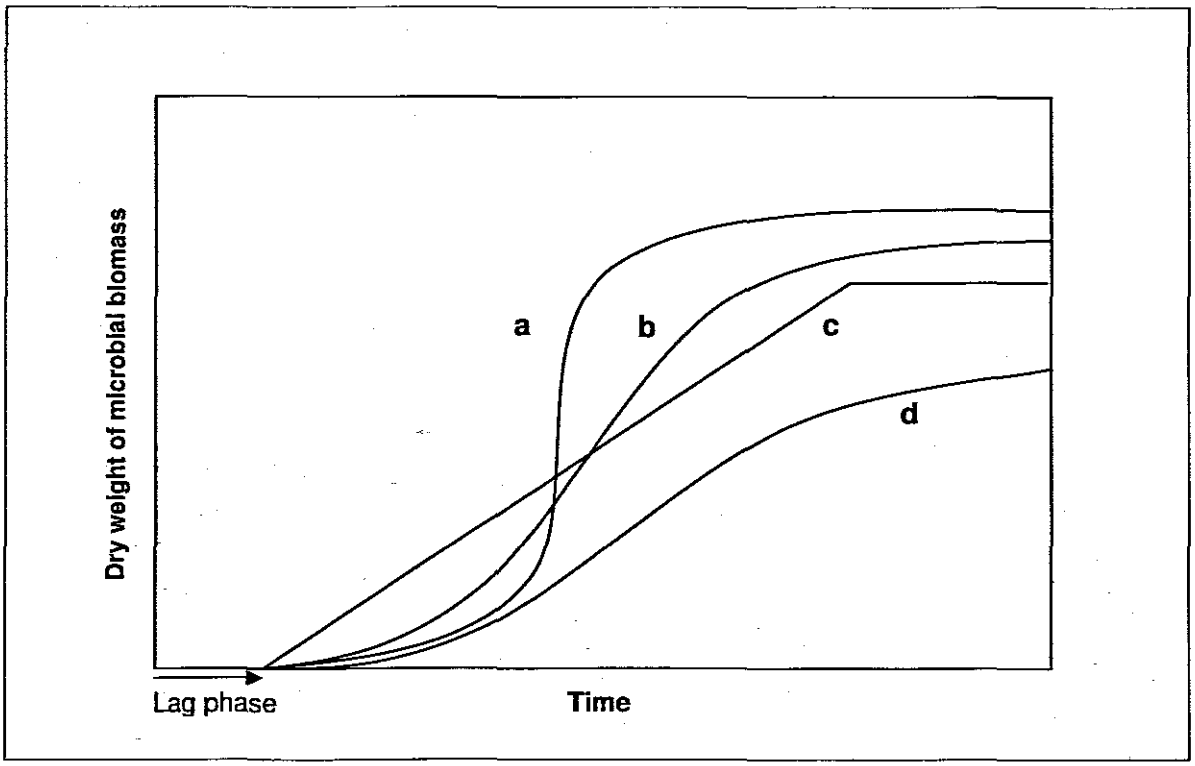

Figure 2.4: Various empirical kinetic profiles describing solid state fermentation systems: (a) exponential, (b) logistic, (c) linear, (d) fast acceleration/slow deceleration (Mitchell *et al.*, 2004)

The logistic equation is an autonomous biomass rate equation allowing for the serial rather than simultaneous evaluation of all model parameters (Elibol & Mavituna, 1999a). The other kinetic equations such as the exponential and two-phase equations require that the growth curve be separated into various phases, with a different equation describing each phase (Mitchell *et al.*, 2004).

Non-symmetrical growth profiles can be described by the power-law, as shown in Equation 2.6a; a modification of the logistic model, in which n takes on values either greater or less than 1 (Ikasari & Mitchell, 2000).

Table 2.3: Differential and Integrated forms of the empirical kinetic growth equations

Name	Differential form	Eq.	Integral form	Eq.	References
Linear	$\frac{dX}{dt} = K$	2.1a	$X = Kt + X_0$	2.1b	Ikasari & Mitchell, 2000; Mitchell *et al.*, 2004
Exponential	$\frac{dX}{dt} = \mu X$	2.2a	$X = X_0 e^{\mu t}$	2.2b	Mitchell *et al.*, 2004
Logistic	$\frac{dX}{dt} = \mu X\left(1 - \frac{X}{X_m}\right)^n, n = 1$	2.3a	$X = \frac{X_m}{1 + \left((X_m / X_0) - 1\right)e^{-\mu t}}$	2.3b	Mitchell *et al.*, 2004
Two phase	Fast acceleration				
	$\frac{dX}{dt} = \mu X, t < t_a$	2.4a	$X = X_0 e^{\mu t}, t < t_a$	2.4b	Mitchell *et al.*, 2004
	Slow deceleration				
	$\frac{dX}{dt} = \left[\mu L e^{-k(t-t_a)}\right]X, t \geq t_a$	2.5a	$X = X_A \exp\left[\frac{\mu L}{k}\left(1 - e^{-k(t-t_a)}\right)\right], t \geq t_a$	2.5b	Mitchell *et al.*, 2004
Power-law	$\frac{dX}{dt} = \mu X\left(1 - \frac{X}{X_m}\right)^n, n < \text{or} > 1$	2.6a			Ikasari & Mitchell, 2000

The two-phase model (fast acceleration/slow deceleration) represents an exponential phase followed by a deceleration phase. Ikasari and Mitchell (2000) suggested that an exponential phase followed by a sudden deceleration phase might be associated with the meeting of hyphae from different expanding microcolonies. According to Mitchell *et al.* (2004) the specific growth rate during the deceleration phase is represented by the quantity in the square brackets in Equation 2.5a. The parameter L in the slow decelaration phase of the two-phase model (Equations 2.5a and b) represents the ratio between the specific growth rate at the start of the deceleration phase and the specific growth rate during the exponential phase.

2.3.3.2 Modelling of growth kinetics for process optimisation

When seeking the optimum conditions for a particular process one has to identify the input variables that have the greatest influence on the experimental process (Elibol, 2002). Kinetic models allow bioengineers to design, predict and thus control the behaviour of a microbial process (Elibol & Mavituna, 1999a).

According to Sinclair and Kristiansen (1987) as cited by Elibol and Mavituna (1999a), mathematical models describing a microbial process can be expressed using two different mechanisms: (1) a structured model, where the basic aspects of cell structure, function and composition are taken into account; or (2) an unstructured model, where *only cell mass is utilised to describe the biological system.*

The aim of bioreactor kinetic growth models is to describe the overall performance of the bioreactor. Therefore, the growth models must describe not only the microbial growth kinetics but also the transport phenomena within the substrate bed and the mass and energy exchanges between the subsystems of the bioreactor, such as the biofilm and the ECS gases (Mitchell *et al.*, 2003). The model must essentially describe how the microbial growth is affected by environmental conditions within the bioreactor as a function of time as well as how the environment is affected by the microbial growth.

Bioreactor kinetic growth models consist of two sub-models (see Figure 2.5): firstly the kinetic sub-model and secondly the balance/transport sub-model. The kinetic sub-model describes how environmental variables affect the growth rate of the micro organism, while the second balance/transport sub-model describes the mass and heat transfer within and between the various phases within the bioreactor (Mitchell *et al.*, 2003; Mitchell *et al.*, 2004).

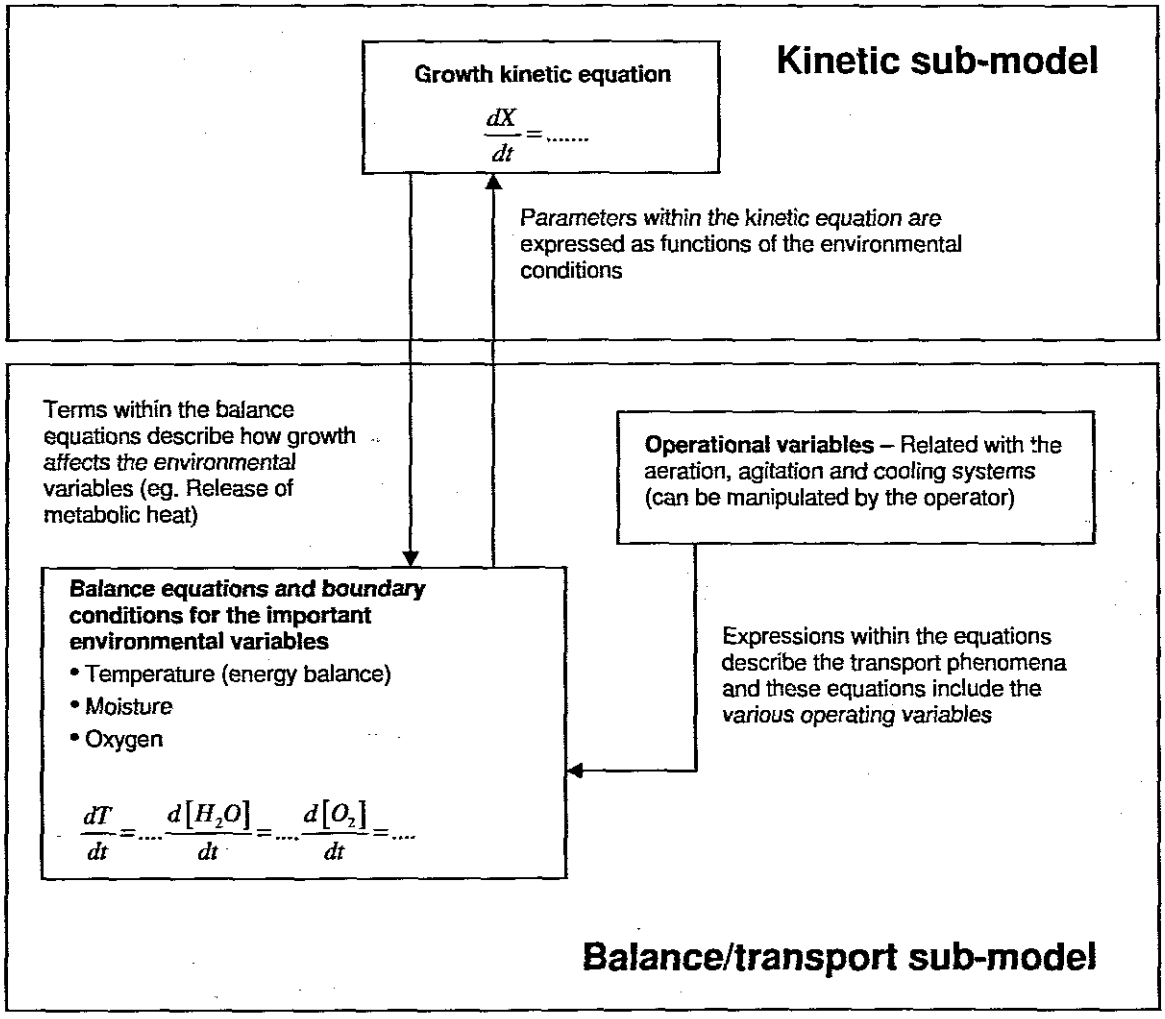

Figure 2.5: The structure of bioreactor models, showing the two sub-models (Mitchell *et al.*, 2003; Mitchell *et al.*, 2004)

2.3.3.3 Modelling growth kinetics for a filamentous micro organism

The growth kinetics of filamentous micro organisms, whether bacteria or fungi, is frequently described by the logistic empirical equation (Equation 2.3a). However, this empirical model does not provide insight into what controls the microbial growth (Ooijkaas *et al.*, 2000). Growth kinetic equations are typically complex as they account for the temperature and oxygen gradients present within the substrate bed. However, attempting to include the concentration gradients of the nutrients within the substrate particles would lead to extremely complex models as these models would describe the heterogeneity at the micro scale for each location at the macro scale. Microscopic models attempt to describe growth mechanisms, while macroscopic models describe the changes in total biomass with time (Ikasari & Mitchell, 2000).

For the logistic equation shown by Equation 2.3a, n is equivalent to 1, the model is symmetrical around the inflection point. Therefore, the acceleration and deceleration rates are the same (Ikasari & Mitchell, 2000). Using a membrane culture system Mitchell *et al.* (1991) investigated the fungal growth of *Rhizopus oligosporus* and observed that the growth profile consisted of a brief period of rapid acceleration, followed by an extended period of slow deceleration. Therefore, to describe the growth of a fungal micro organism, a two-phase growth model utilising the exponential growth model to represent the fast acceleration phase and an equation to represent the slow deceleration phase was developed. This two-phase model complements, rather than replaces, the logistic model (Ikasari & Mitchell, 2000).

Non-symmetrical growth profiles can be described by the power-law (Equation 2.6a), a modification of the logistic model, in which n takes on values either greater or less than 1. Mitchell *et al.* (1991) showed that the power-law model provided a better fit to the experimental data profile obtained than the logistic model. However, some deviation from the experimental data was still observed especially during the early growth (Ikasari & Mitchell, 2000).

The fermentation kinetics of the extracellular antibiotic, actinorhodin, produced by *S. coelicolor* was studied in a batch fermentation system by Elibol and Mavituna (1999a). The fermentation batch bioreactor used in this study was operated with Hobbs *et al.* (1989) growth medium. The logistic equation, that is substrate independent, was used as the empirical equation to describe the microbial growth. By using the logistic equation, an autonomous biomass rate equation, it was possible to evaluate the model parameters serially rather than simultaneously, without requiring simultaneous parameter estimation or computer techniques (Elibol & Mavituna, 1999a).

For micro organisms showing fungal growth, the growth rate should not be described as depending on the substrate concentration, because the growth of a micro organism depends on the substrate concentration within its local environment and not on the average substrate concentration within the biofilm (Ikasari & Mitchell, 2000). A limited understanding of the kinetic model for actinorhodin production exists due to the unstable, complex heterogeneous nature of *S. coelicolor* (Elibol & Mavituna, 1999a).

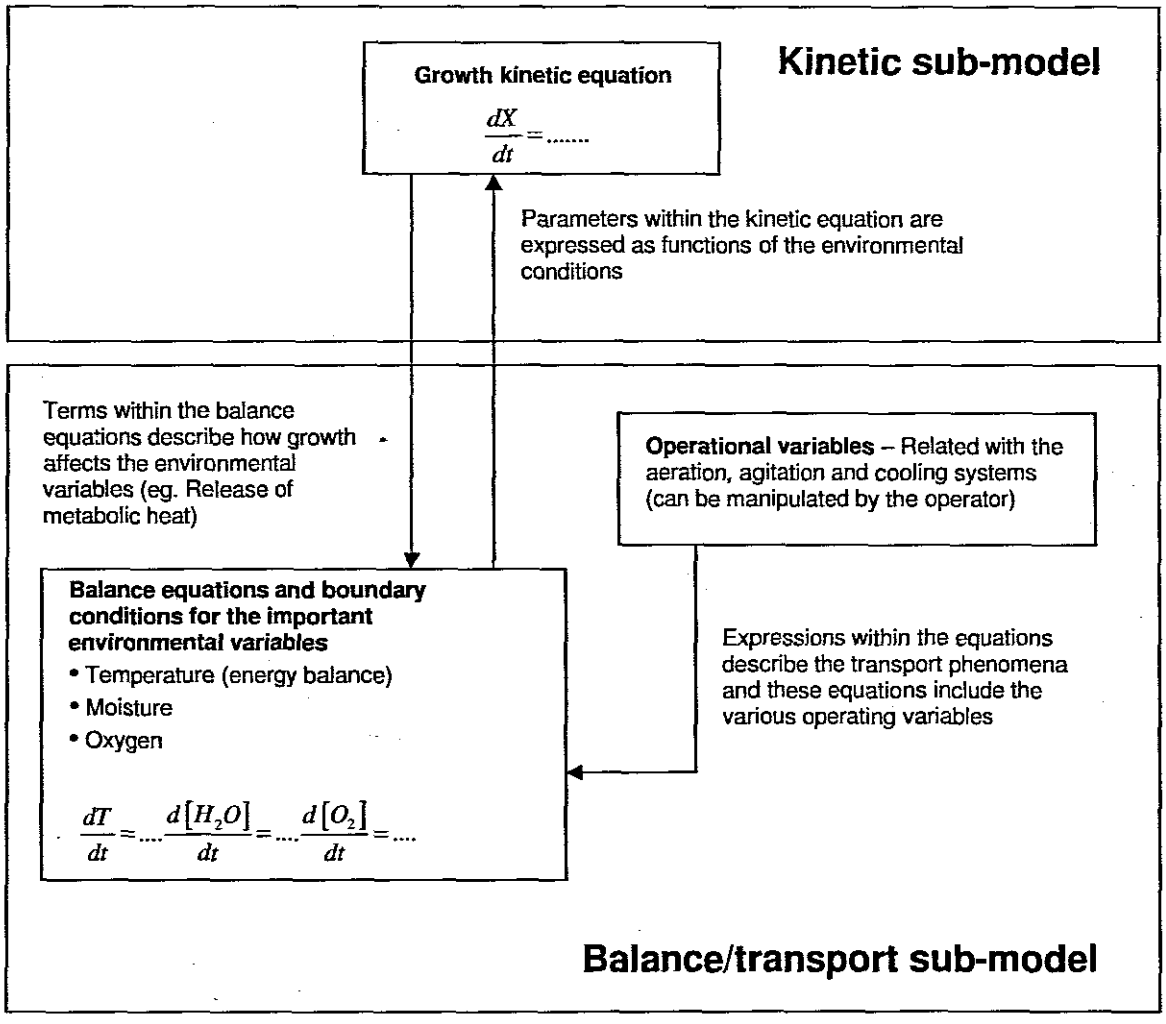

Figure 2.5: The structure of bioreactor models, showing the two sub-models (Mitchell et al., 2003; Mitchell et al., 2004)

2.3.3.3 Modelling growth kinetics for a filamentous micro organism

The growth kinetics of filamentous micro organisms, whether bacteria or fungi, is frequently described by the logistic empirical equation (Equation 2.3a). However, this empirical model does not provide insight into what controls the microbial growth (Ooijkaas *et al.*, 2000). Growth kinetic equations are typically complex as they account for the temperature and oxygen gradients present within the substrate bed. However, attempting to include the concentration gradients of the nutrients within the substrate particles would lead to extremely complex models as these models would describe the heterogeneity at the micro scale for each location at the macro scale. Microscopic models attempt to describe growth mechanisms, while macroscopic models describe the changes in total biomass with time (Ikasari & Mitchell, 2000).

For the logistic equation shown by Equation 2.3a, n is equivalent to 1, the model is symmetrical around the inflection point. Therefore, the acceleration and deceleration rates are the same (Ikasari & Mitchell, 2000). Using a membrane culture system Mitchell *et al.* (1991) investigated the fungal growth of *Rhizopus oligosporus* and observed that the growth profile consisted of a brief period of rapid acceleration, followed by an extended period of slow deceleration. Therefore, to describe the growth of a fungal micro organism, a two-phase growth model utilising the exponential growth model to represent the fast acceleration phase and an equation to represent the slow deceleration phase was developed. This two-phase model complements, rather than replaces, the logistic model (Ikasari & Mitchell, 2000).

Non-symmetrical growth profiles can be described by the power-law (Equation 2.6a), a modification of the logistic model, in which n takes on values either greater or less than 1. Mitchell *et al.* (1991) showed that the power-law model provided a better fit to the experimental data profile obtained than the logistic model. However, some deviation from the experimental data was still observed especially during the early growth (Ikasari & Mitchell, 2000).

The fermentation kinetics of the extracellular antibiotic, actinorhodin, produced by *S. coelicolor* was studied in a batch fermentation system by Elibol and Mavituna (1999a). *The fermentation batch bioreactor used in this study was operated with Hobbs et al.* (1989) growth medium. The logistic equation, that is substrate independent, was used as the empirical equation to describe the microbial growth. By using the logistic equation, an autonomous biomass rate equation, it was possible to evaluate the model parameters serially rather than simultaneously, without requiring simultaneous parameter estimation or computer techniques (Elibol & Mavituna, 1999a).

For micro organisms showing fungal growth, the growth rate should not be described as depending on the substrate concentration, because the growth of a micro organism depends on the substrate concentration within its local environment and not on the average substrate concentration within the biofilm (Ikasari & Mitchell, 2000). A limited understanding of the kinetic model for actinorhodin production exists due to the unstable, complex heterogeneous nature of *S. coelicolor* (Elibol & Mavituna, 1999a).

2.3.3.4 Biphasic growth

Biphasic growth occurs when two growth phases separated by a short intermediate lag phase is visible. The short intermediate lag phase occurs due to depletion of a substrate necessary for growth within the growth medium. The phenomenon of biphasic growth occurs when a micro organism exhibits two growth phases while, consuming only one substrate source, for example only one carbon source (Kodama *et al.* 1969; Meunier & Choder, 1999; Sheldon *et al.*, 2008).

Anaerobic biphasic growth, consisting of two logarithmic phases separated by an intermediate phase where the growth rate was very low, was observed by Kodama *et al.* (1969). The anaerobic biphasic growth was observed in the Gram-negative rod-shaped bacterium *Pseudomonas stutzeri* (Van Niel strain) grown under anaerobic conditions with nitrate limitation.

Biphasic growth was also observed by Meunier and Choder (1999) in a well separated colony of the budding yeast *Saccharomyces cerevisiae*, which showed a rapid growth phase proceeded by a sharp transition to a slower growth phase. During the slower growth phase the cells in the centre of the colony gradually entered stationary growth so that towards the end of this growth phase most of the growth occured at the periphery of the colony (Meunier & Choder, 1999).

Ntwampe and Sheldon (2006) reported a primary and secondary growth phase for the white rot fungus *Phanerochaete chrysosporium* (BKMF-1767) immobilised on a vertically orientated polysulphone capillary membrane. Sheldon *et al.* (2008) demonstrated biphasic growth in a continuously operated MGR system used for the continuous production of secondary metabolites by an immobilised biofilm, of the white rot fungus *P. chrysosporium* (BKMF-1767).

P. chrysosporium was immobilised on a polysulphone membrane in a flow-cell MGR operated with a peristaltic pump system. It was concluded that the short intermediate lag phase occurred due to ammonium depletion and not due to glucose depletion (Sheldon *et al.*, 2008). Two exponential growth phases were identified with specific growth rates in the range of 0.07 to 0.1 hr^{-1} for the first growth cycle and in the range of 0.015 to 0.05 hr^{-1} for the second growth cycle.

Karandikara *et al.* (1997) studied the life cycle of *Streptomyces coelicolor* on solid medium from a physiological perspective. In this study a biphasic growth pattern was identified, with a continuous transition from an initial exponential growth cycle into a slower growth cycle of biomass accretion. The change from the initial exponential growth cycle to the slower growth cycle coincided with the depletion of nitrate in the growth medium (Karandikara *et al.*, 1997).

2.3.3.5 Diauxic growth

The phenomenon of diauxic growth, according to Monod (1942), Shuler and Kargi (2002) and Adour *et al.* (2005) occurs when two growth phases are observed due to the sequential use of two different substrates, for example two carbon sources. According to Shuler and Kargi (2002) this is normally observed when the one substrate source for carbon, such as glucose, becomes depleted and the cells adapt their metabolic activities in order to be able to utilise a second substrate source for carbon, such as arginine, as cited by Sheldon *et al.* (2008). When substrates are present in non-growth limiting concentrations the substrate that supports the highest growth rate is utilised preferentially from the mixture and diauxic growth is often observed due to sequential utilisation. However, according to Harder and Dijkhuizen (1982) when the substrates are present in growth limiting concentrations, simultaneous utilisation appears to occur.

De Orduña *et al.* (2000) observed a diauxic growth pattern after careful analysis of batch growth in both culture flasks and bioreactors, of *S. coelicolor* A3(2) in minimal medium 1 (MM1). MM1 was a modified version of the defined growth medium described by Hobbs *et al.* (1989). The glutamic acid present in MM1, which was the sole carbon and nitrogen source, was degraded prior to maltose during the first phase of the diauxic growth. The shift from glutamic acid to maltose after glutamic acid depletion occurred with corresponding cessation of biomass formation.

Diauxic growth of *Penicillium camembertii* was observed during batch culture in a synthetic medium containing glucose and arginine by Adour *et al.* (2005) and Amrane *et al.* (2005). During the first phase of the diauxic growth glucose and arginine were utilised as carbon and nitrogen sources, respectively. After glucose depletion, arginine was used as both the carbon and nitrogen source during the second phase.

2.3.4 Substrate utilisation kinetics

Quantitative characterisation of the activity of an enzyme or microbe on a particular substrate is an essential requirement for the detailed understanding of the dynamics of any process (Goudar & Devlin, 2001). The quantification process of substrate utilisation involves estimating several parameters in the kinetic models using experimental data. A simple unstructured kinetic model is used to describe the interaction between the substrate and the enzyme or microbe (Gouder & Devlin, 2001). Substrate utilisation by a micro organism normally results in the removal of a chemical, increase in microbial biomass and the subsequent biodegradation of the chemical. Several microbial growth and substrate kinetic models exist. These include Monod's, Andrew's, Bungay's weighted model, general substrate inhibition models (GSIM) and the sum kinetic models (Okpokwasili & Nweke, 2006).

Substrate depletion by enzymes and non-growing bacterial suspensions are generally described by the Michaelis-Menten equation, while the Monod equation generally describes growth associated substrate consumption (Goudar & Devlin, 2001). The Monod equation defines the relationship between the growth rate and the concentration of the growth limiting nutrient.

In continuous cultures the limiting nutrient is the substrate controlling or limiting micro organism growth, while in batch systems the limiting nutrient refers to the substrate that limits the extent of culture growth (Bazin, 1982).

2.3.4.1 The Monod single-substrate-limited model

The growth limiting substrate concept was introduced by the Monod model. The Monod empirical model, shown in Table 2.4 (Equation 2.7a), has been the dominating model used in substrate growth kinetics. In the Monod model the parameters μ_{max} and K_m relate the growth rate to the concentration of a single growth-limiting substrate. An important feature of the model is that the growth rate is zero when there is no substrate and when in excess the growth rate tends to the upper limit (Owens & Legan, 1987; Lobry *et al.*, 1992; Okpokwasili & Nweke, 2006).

$$\mu = \frac{\mu_{max} C_s}{K_m + C_s} \qquad \textbf{2.7a}$$

Where μ represents the specific growth rate (hr^{-1}); μ_{max} represents the maximum specific growth rate (hr^{-1}); C_s represents the substrate concentration (g/m^3) and K_m the Monod saturation constant (g/m^3), which is equivalent to the substrate concentration at half μ_{max} (Owens & Legan, 1987; Lobry *et al.*, 1992; Okpokwasili & Nweke, 2006).

The Monod equation is the most commonly applied unstructured, non-segregated model of microbial growth, describing substrate-limited growth only when the growth is slow and population density low. When derived from the Michaelis-Menton hypothesis, the Monod equation can be expressed as in Equation 2.8 (Shuler & Kargi, 2002).

$$r_B = \frac{r_m C_s}{K_m + C_s} \qquad \textbf{2.8}$$

Where r_B is the biological consumption rate ($g/m^3.hr$) and r_m is the maximum substrate consumption rate ($g/m^3.hr$) (Shuler & Kargi, 2002).

2.3.4.2 Other single-substrate-limited growth models

The Tessier, Moser and Contois equations (Beyenal *et al.*, 2003) are all examples of alternative single-substrate-limited growth kinetic models as shown in Table 2.4.

The Moser equation, the most general form of these equations, is a modified form of the Monod equation, which according to Blanch (1981) admits a range of interesting dynamic behaviour. The Moser equation has three constants (μ_{max}, K_s, n) and is equivalent to the Monod equation when $n = 1$, while the Tessier equation only has two constants (μ_{max}, K_s) (Blanch, 1981). A saturation constant proportional to cell concentration in the Contois equation describes substrate-limited growth at high cell densities. According to the Contois equation, with decreasing substrate concentrations the specific growth rate decreases and eventually becomes inversely proportional to the medium cell concentration (Shuler & Kargi, 2002).

Table 2.4: Single-substrate limited growth kinetic models

Name	Kinetic expression	Dimensionless expression	Differential form	Integral form	References
Monod	$\mu = \frac{\mu_{max} C_s}{K_s + C_s}$	$\frac{\mu}{\mu_{max}} = \frac{C_s / K_s}{1 + C_s / K_s}$	$\frac{dC_s}{dt} = -\frac{1}{Y_{xs}} \frac{\mu_{max} C_s}{K_s + C_s} X$	$\frac{K_s Y_{X/S} + X_o + Y_{X/S} C_s}{X_o + Y_{X/S} C_s} \ln\left[1 + \frac{Y_{X/S}}{X_o}\left(C_{s(o)} - C_s\right)\right] - \frac{C_s Y_{X/S}}{X_o + Y_{X/S} C_s} \ln\left[\frac{C_s}{C_{s(o)}}\right] = \mu_{max} t$	Blanch, 1981; Owens & Legan, 1987; Goudar & Devlin, 2001; Shuler & Kargi, 2002; Beyenal *et al.*, 2003
Eq.	2.7a	2.7b	2.7c	2.7d	
Tessier	$\mu = \mu_{max}\left(1 - e^{-C_s / K_s}\right)$				Blanch, 1981; Shuler & Kargi, 2002; Beyenal *et al.*, 2003
Eq.	2.9				
Moser	$\mu = \mu_{max} \frac{C_s^n}{C_s^n + K_s}$				Blanch, 1981; Shuler & Kargi, 2002; Beyenal *et al.*, 2003
Eq	2.10				
Contois	$\mu = \mu_{max} \frac{C_s^n}{C_s^n + K_s X}$		$\frac{dC_s}{dt} = -\frac{1}{Y_{XS}} \frac{\mu_{max} C_s}{K_s X + C_s} X$	$\ln\left[1 + \frac{Y_{X/S}}{X_o}\left(C_{s(o)} - C_s\right)\right] - K_s Y_{X/S} \ln\left[\frac{C_s}{C_{s(o)}}\right] = \mu_{max} t$	Goudar & Devlin, 2001; Shuler & Kargi, 2002; Beyenal *et al.*, 2003
Eq.	2.11a	2.11b		2.11c	

2.3.4.3 Linear kinetic parameter estimation methods

The Lineweaver-Burke (Equation 2.12), Eadie-Hofstee (Equation 2.13) and Langmuir (Equation 2.14) methods are linearisation techniques in which the hyperbolic relationship between the rate of the reaction and the substrate concentration is arranged linearly in order to determine the substrate saturation constant (K_s) (Shuler & Kargi, 2002). According to Owens and Legan (1987) the direct linear plot of Eisenthal and Cornish-Bowden appears to be the best method for analyzing μ versus C_s. In the Monod equation the substrate saturation constant (K_s) is the concentration of the growth rate-limiting nutrient that supports half the maximum specific growth rate (Owens & Legan, 1987).

$$\frac{1}{\mu}=\frac{1}{\mu_{\max}}+\frac{K_s}{\mu_{\max}C_s} \qquad \textbf{2.12}$$

$$\frac{\mu}{C_s}=\frac{\mu_{\max}}{K_s}-\frac{\mu}{K_s} \qquad \textbf{2.13}$$

$$\frac{C_s}{\mu}=\frac{K_s}{\mu_{\max}}+\frac{C_s}{\mu_{\max}} \qquad \textbf{2.14}$$

The Lineweaver-Burke plot of $\frac{1}{\mu}$ against $\frac{1}{C_s}$ is linear with the intercept $\frac{1}{\mu_{max}}$ and slope $\frac{K_s}{\mu_{\max}}$. The Eadie-Hofstee plot of μ against $\frac{\mu}{C_s}$ is linear with slope $-\frac{1}{K_s}$ and intercept $\frac{\mu_{\max}}{K_s}$ and the Langmuir plot of C_s against $\frac{C_s}{\mu}$ is linear with intercept $-K_s$ (Owens & Legan, 1987).

Ntwampe and Sheldon (2006) and Sheldon *et al.* (2008) utilised the Monod equation derived from the Michaelis-Menton hypothesis (shown in Equation 2.8) for determining the substrate consumption parameters for the white rot fungus *Phanerochaete chrysosporium*, immobilised in an MGR system. Addition of the experimentally determined daily substrate consumed over time resulted in an accumulative substrate consumption curve that was plotted against time. This accumulative substrate consumption curve was best described by a third-order polynomial, shown by Equation 2.15.

$$C_s=a_1t^3+a_2t^2+a_3t+a_4 \qquad \textbf{2.15}$$

The derivative of Equation 2.15 is equivalent to the substrate consumption rate (r_B), described by Equation 2.16.

$$\frac{dC_s}{dt} = 3a_1t^2 + 2a_2t + a_3 = r_B = \frac{r_m C_s}{K_m + C_s} \qquad \textbf{2.16}$$

Equation 2.17 represents the relationship between the inverse of the first-order derivative and the inverse of the Monod equation.

$$\left(\frac{dC_s}{dt}\right)^{-1} = \frac{1}{3a_1t^2 + 2a_2t + a_3} = \left(\frac{K_m}{r_m}\right)\frac{1}{C_s} + \frac{1}{r_m} \qquad \textbf{2.17}$$

According to Ntwampe (2005) for the MGR system the Lineweaver-Burke linearisation method gave the best fit with correlation coefficients (R^2) of 0.9 and higher. Both Ntwampe (2005) and Sheldon *et al.* (2008) used the Lineweaver-Burke method to linearise the rate limiting nutrient data, by rearranging Equation 2.16 into Equation 2.17 in order to evaluate the kinetic constants. According to Shuler and Kargi (2002), from the plot of $\left(\frac{dC_s}{dt}\right)^{-1}$ against $\left(\frac{1}{C_s}\right)$ the Monod saturation constant (K_m) can be calculated for different time intervals by dividing the slope $\left(\frac{K_m}{r_m}\right)$ by the intercept $\left(\frac{1}{r_m}\right)$.

The most accurate method to determine the Monod saturation constant (K_m) is to assay the concentrations of the growth rate-limiting nutrients in steady-state continuous cultures. Knowledge of the substrate saturation constant is required for the modelling of microbial cultures. In the Monod equation when the specific growth rate is set equal to half the maximum specific growth rate, the substrate saturation constant equals the concentration of the growth rate-limiting nutrient (Owens & Legan, 1987).

2.3.4.4 Non-linear kinetic parameter estimation methods

It is important to note most kinetic models, as well as their integrated forms are non-linear, making kinetic parameter estimation difficult. Some models can be linearised, but the linearisation of non-linear expressions is limited as it transforms the error associated with the dependent variable, resulting in inaccurate estimates of the kinetic parameters (Goudar &

Devlin, 2001; Okpokwasili & Nweke, 2006). Therefore, linearisation techniques are only used to determine the initial estimates ofkinetic constraints.

Parameter estimates obtained from the linearised form of a non-linear equation are inaccurate and the non-linear least squares regression method is more accurate for kinetic parameter estimation (Goudar & Devlin, 2001). Application of the non-linear least squares regression method is complicated. Due to the iterative nature of non-linear least squares regression, initial estimates of kinetic parameters are required (Goudar & Devlin, 2001). The kinetic parameter estimates obtained from the linearised kinetic expressions can be utilised as the initial estimates for the non-linear least squares regression (Okpokwasili & Nweke, 2006).

Two non-linear regression methods are: (1) minimising the sum of square differences (SSD), shown in Equation 2.18 (Beyenal *et al.*, 2003); and (2) minimising the residual sum of square estimates (RSSE), shown in Equation 2.19 (Goudar &Devlin, 1987).

$$SSD = \sum_{i=1}^{N} \left(\mu_{experimental} - \mu_{predicted} \right)^2 \qquad \textbf{2.18}$$

$$Minimse\ RSSE = \sum_{i=1}^{N} \left[\left(S_{exp} \right)_i - \left(S_{cal} \right)_i \right]^2 \qquad \textbf{2.19}$$

In the non-linear regression analysis to determine the biokinetic parameters of *Pseudomonas aeruginosa* Beyenal *et al.* (2003) minimised the sum of square differences (SSD) between the experimental and theoretical (i.e. predicted) data for specific growth rates. Schmidt *et al.* (1987) utilised the non-linear regression method to compare the kinetics of *p*-Nitrophenol degradation by *Pseudomonas sp.* cultured in Erlenmeyer flasks when *p*-Nitrophenol was utilised as the sole substrate and when it was utilised simultaneously with other substrates. By minimising the least squares of the differences between the data and the model curve, the best fit was obtained from the model giving the lowest residual sum of squares (Schmidt *et al.*, 1987). Goudar and Devlin (2001) calculated initial estimates of the kinetic parameters from the linearised form of the Michaelis-Menton equation for previously published data from three different experiments including the pyruvate kinase reaction, 2-chiorophenol biodegradation and glucose uptake by *Penicillium chrysogenum.* The non-linear kinetic parameters were estimated by minimising the residual sum of squares (Goudar & Devlin, 2001).

2.3.4.5 Specific growth rate

The specific growth rate, μ, for any value of $X(t)$ is described by Equation 2.20 (Viniegra-Gonzalez *et al.*, 1992; Shuler & Kargi, 2002).

$$\mu = \frac{1}{X}\frac{dX}{dt} \qquad \textbf{2.20}$$

Utilising the logisitic equation (Equation 2.3a) the empirical maximum specific growth rate, μ_{max}, can be found by plotting $\ln\left(\frac{X(t)}{[X_m - X(t)]}\right)$ of the experimental data versus time. *Where $X(t)$ is the total biomass (g) at time (t) and X_m is the maximum biomass (g)* obtained (Van de Lagemaat & Pyle, 2005).

Shahab *et al.* (1996) determined a specific growth rate of 0.048 hr^{-1} for *S. coelicolor* grown in a continuous culture, as cited by Naeimpoor and Mavituna (2000). Utilising linear *programming, Naeimpoor and Mavituna (2000) analysed the specific growth rate of S. coelicolor* grown in chemostat cultures under various nutrient limitations. The experimental growth rate was determined to be 0.06 hr^{-1}, the maximum theoretical growth rate was 0.093 hr^{-1} for nitrogen limitation, 0.071 hr^{-1} for phosphate limitation and 0.065 hr^{-1} for both sulphur and potassium limitations.

2.3.4.6 Yield and maintenance coefficients

The yield coefficient (Equation 2.21) describes the relationship between the biomass generated and the amount of substrate consumed to produce the biomass. A yield coefficient is defined based on the consumption of a substrate (Shuler & Kargi, 2002).

$$Y_{X/S} = \frac{\Delta X_w}{\Delta S_w} \qquad \textbf{2.21}$$

Where $Y_{X/S}$ is the growth yield coefficient (g biomass/g substrate); X_w is the mass of biofilm generated (g) and S_w is the mass of substrate consumed (g) (Shuler & Kargi, 2002; Ntwampe & Sheldon, 2006).

When glucose was the carbon source, the yield coefficient for the following micro organisms: *Enterobacter aerogenes, Candida utilis, Penicillium chrysogenum, Pseudomonas fluorescens, Rhodopseudomonas spheroids* and *Saccharomyces cerevisae* was calculated

to be 0.40, 0.51, 0.43, 0.38, 0.45 and 0.5 g biomass/g glucose, respectively (Shuler & Kargi, 2002).

The maintenance coefficient (Equation 2.22) describes the specific rate of substrate uptake for biomass maintenance when biomass production is negligible (Shuler & Kargi, 2002; Ntwampe & Sheldon, 2006).

$$m_s = \frac{dS/dt}{X_\rho} \qquad \textbf{2.22}$$

Where m_s is the maintenance coefficient (hr^{-1}) and X_ρ is the biofilm density (g/m^3) (Shuler & Kargi, 2002).

In Equation 2.23 Monod related the yield coefficient $\left(Y_{X/S}\right)$ to both the specific growth rate (μ) and the specific rate of substrate uptake (q) for biomass maintenance (Okpokwasili & Nweke, 2006).

$$\frac{ds}{dt} \equiv Y_{X/S} q \qquad \textbf{2.23}$$

2.4 Introduction to oxygen in aerobic biofilms

Aeration is a critical factor in aerobic bioreactors as both growth and production of aerobic micro organisms are seriously affected by the dissolved oxygen (DO) concentration (Elibol, 2002). In many microbial processes the microbial oxygen demand exceeds the oxygen transfer capabilities of the system. The oxygen transfer rate (OTR) has therefore become the rate limiting factor in these processes (Ozergin-Ulgen & Mavituna, 1998).

The cells present in an aerobic biofilm utilise oxygen for cell maintenance, respiratory oxidation for further growth and for the oxidation of substrates into metabolic products (Ozergin-Ulgen & Mavituna, 1998). Due to the low solubility of oxygen in aqueous media, the poor mass transfer capability of most industrial bioreactors and the highly viscous nature of dense mycelia cultures, oxygen transfer from the gas phase to the liquid bulk interface and the biofilm are of critical importance (Elibol, 2001).

According to Thibault *et al.* (2000) inadequate oxygen supply results in a reduction of microbial activity and low oxygen concentrations negatively affect the production of the secondary metabolites (Hibiya *et al.*, 2003). Improved oxygen supply to aerobic cultures are thus necessary in order to minimise oxygen limitation, via the manipulation of microbial metabolism through genetic engineering and possibly the use of oxygen carriers such as perfluoro-carbons (Tremper *et al.*, 1985; Cho *et al.*, 1988; Elibol, 2001; Gotoh, *et al.*, 2001; Takeshi *et al.*, 2001; Ntwampe, 2009); haemoglobin (Magnolo *et al.*, 1991); and hydrocarbons (MacLean, 1977; Ho *et al.*, 1990; Elibol, 2002).

2.4.1 Oxygen distribution in biofilms

Measuring oxygen profiles in biofilms increases the understanding of biological processes and physical processes such as diffusion and convection (Kuenen *et al.*, 1986). The spatial distribution of oxygen within biofilms is therefore important for the optimal operation of bioreactors (Hibiya *et al.*, 2003). Using the oxygen distribution in the biofilms, the kinetic parameters and the effective diffusion coefficient can be calculated (Hibiya *et al.*, 2003). The kinetic parameters and coefficients are affected by the internal features of biofilms, which change according to the age, thickness, density, porosity and tortuousity of the biofilm (Hibiya *et al.*, 2003).

Pseudo-steady state within a biofilm occurs when the measured oxygen concentration profile does not change over long periods of time at the same location within the biofilm (Lewandowski & Beyenal, 2003b; Yurt *et al.*, 2003). It can then be assumed that oxygen transfer is one-dimensional if the oxygen concentration profiles measured along the length of the biofilm do not differ significantly. Therefore, mass transfer is not considered to be one

dimensional in heterogeneous biofilms as these biofilms are not structurally uniform (Yurt *et al.*, 2003).

2.4.1.1 Oxygen mass transfer at the bulk-biofilm interface

Mass transport is defined as "the tendency of a component in a mixture to travel from a region of high concentration to one of low concentration". Diffusional mass transport obeys the second law of thermodynamics, this means that a system will spontaneously move toward the uniform distribution of components and thus a state of equilibrium. Therefore, any gradient within a system, be it concentration, density, temperature or pressure, the system will spontaneously move toward the uniform distribution of its components (Lewandowski & Beyenal, 2003a).

Mass transfer of oxygen, in an immobilised biofilm system follows three steps (Zhang & Bishop, 1994; Beyenal & Lewandowski, 2002):

1. Transport from the bulk medium to the biofilm surface.
2. Diffusive and convective mass transfer across the biofilm surface.
3. Consumption within the biofilm.

The oxygen transport rate within the biofilm is determined by linking the convective mass transfer rate to the diffusive mass transfer rate across the biofilm surface (Beyenal & Lewandowski, 2002). Measured oxygen concentration profiles within immobilised biofilms can be used to quantify mass transfer parameters within the biofilms (Lewandowski & Beyenal, 2003b).

No oxygen consumption occurs in the bulk medium and the flux of oxygen across the biofilm surface needs to be conserved. Therefore, the rate of internal $\left(D_f\left(\frac{dC_{O_2}}{dx}\right)\right)$ and external (J_f) *oxygen mass transfer needs to be equal at the biofilm surface, as described by* Equation 2.24 (Beyenal & Lewandowski, 2002; Hibiya *et al.*, 2003; Lewandowski & Beyenal, 2003b).

$$J_f = D_w\beta\left(C_{air} - C_s\right) = D_f\left(\frac{dC_{O_2}}{dx}\right)_{f,x_s} \qquad \textbf{2.24}$$

The oxygen diffusivity coefficient in the biofilm (D_f), and the oxygen diffusivity coefficient in water (D_w) at the incubation temperature need to therefore be determined to solve Equation 2.24 (Ntwampe *et al.*, 2008). According to Fick's law, the transport of substrates

across a membrane and biofilm depends on the substrate diffusivity across the membrane and biofilm, as well as the thickness of the biofilm (Stamatialis *et al.*, 2008).

Wasche *et al.* (2002) determined the mass transfer at the bulk-biofilm interface using the results obtained from microsensor measurements. From the oxygen concentration profiles, the linear region with a constant gradient was assumed to be inside the biofilm. The nearly vertical part of the oxygen concentration profile belonged to the completely mixed bulk phase. The thickness of the concentration boundary layer was defined as the distance of the profile between linear parts. This method differs from the inflection point method utilised by Lewandowski and Beyenal (2003b) and is known as the applied method. When compared, the applied method yielded a smaller concentration boundary layer thickness. Both methods do however show the same relationship between concentration boundary layer thickness and growth conditions (Wasche *et al.*, 2002).

2.4.1.2 Oxygen flux through the biofilm

The maximum rate of oxygen flux through the biofilm in the absence of diffusion limitations is given by Equation 2.25, as described by Hibiya *et al.* (2003) and Lewandowski and Beyenal (2003b):

$$J_{f_{O_2}} = D_f\left(\frac{dC_{O_2}}{dX}\right) \qquad \textbf{2.25}$$

At the biofilm-water interface flux continuity is continuously preserved, hence $\left(J_{f_{O_2}} = J_w\right)$ (Hibiya *et al.*, 2003) the internal diffusion coefficient inside the biofilm is given by Equation 2.25. Equation 2.25 indicates that the flux of oxygen through the biofilm is equivalent to the oxygen mass transfer across the bulk liquid interface which in turn is equivalent to the diffusive and convective mass transfer and consumption within the biofilm itself. Equation 2.26 is a simplified version of Equation 2.25.

$$D_f = J_{f_{O_2}}\left(\frac{X_f - X_o}{C_{O_2(o)} - C_{O_2(f)}}\right) \qquad \textbf{2.26}$$

2.4.2 Introduction to microsensors

In order to be able to determine the effect of oxygen limitation on the production of secondary metabolites, oxygen profiles within the biofilm can be measured utilising microsensors (Frederick *et al.*, 1991). Microsensors were introduced through the work of Revsbech (1989), who constructed reliable oxygen microsensors, to be utilised in the profiling of oxygen

distribution sediments and biofilms. The mathematical modelling of the oxygen concentration profiles recorded with the oxygen microsensors, allowed the determination of oxygen kinetic parameters (Frederick *et al.*, 1991). The oxygen profiles obtained within biofilms not only added to increased understanding with regards to biological processes on a microscale, but also increased the information available regarding physical processes, such as diffusion and convection (Kuenen *et al.*, 1986).

Microsensors are the most useful equipment for the direct measurement of the chemical composition within biofilms, due to the fragility of biofilms. Although the technique employed with microsensors are invasive, their influence is small, and from the observations made both fluxes and transport phenomena can be derived. Of late, microsensor technology has improved considerably and can now be utilised directly inside bioreactors. When used in combination with molecular techniques, such as fluorescence *in situ* hybridisation, microsensors can elucidate the microbial ecology of biofilms (Berg *et al.*, 1998). Microsensors allow local microenvironments to be probed and the quantification of local chemistries at the microscale level with high spatial resolution. Utilising microsensors the concentration profiles of dissolved substances within the space occupied by the biofilm, as well as in the bulk solution near the biofilm surface can be measured.. Biofilm thicknesses rarely exceed a few hundred micrometers and microsensors are indispensable when it comes to measurements within the space occupied by the biofilm (Lewandowski & Beyenal, 2003b).

2.4.2.1 Oxygen profiles

The DO microsensor is an amperometric microsensor that measures the current resulting from the transfer of electrons between members of redox couples. Amperometric microsensors can be used to measure the concentration of dissolved gases, ions, organic and inorganic molecules. Oxygen microsensors have a high sensitivity and are among the most reliable microsensors used in biofilm research. An advantage of a Clark-type (polarographic) oxygen microsensor is its insensitivity to electric fields (Horn, 2000).

When quantifying the shape of the oxygen profiles obtained, it is important to find the exact position of the biofilm surface. Conceptually the biofilm surface is at the inflection point of the oxygen concentration profile. Lewandowski and Beyenal (2003a) who utilised the inflection point method combined an oxygen microsensor and an optical density microprobe to create a combined microsensor, to aid in the identification of the biofilm surface. From the oxygen profile obtained with this combined microsensor, it was concluded that the biofilm surface is at the beginning of the linear part of the oxygen profile within the mass transport boundary layer (Lewandowski & Beyenal, 2003a).

The data recorded from below the biofilm surface contains information regarding the biofilm reaction rate and substrate diffusivity through the biofilm, which is utilised to calculate the kinetic parameters of oxygen consumption. The data recorded from above the biofilm surface contains information regarding the mass transport rate to the biofilm, which is utilised to calculate the oxygen flux to the biofilm (as shown in Equation 2.27) (Lewandowski & Beyenal, 2003b).

$$\left(\frac{dC_{O_2(b)}}{dx}\right)_{b,x_s} = \frac{J_{w,x_s}}{D_f} \qquad \textbf{2.27}$$

Equation 2.28 is an empirical exponential equation describing the shape of oxygen profile above the biofilm surface (Lewandowski *et al.*, 1994; Lewandowski & Beyenal, 2003b).

$$\frac{C_{O_2(b)} - C_{O_2(s)}}{C_{O_2(bulk)} - C_{O_2(s)}} = 1 - \exp[-\beta(x - x_s)] \qquad \textbf{2.28}$$

Where $C_{O_2(b)}$ describes the oxygen concentration in the biofilm (g/m^3); $C_{O_2(s)}$ the oxygen concentration at the biofilm surface (g/m^3); $C_{O_2(bulk)}$ the oxygen concentration in the bulk water (g/m^3); β the experimental coefficient (m^{-1}); x the distance from the bottom of the biofilm (m); and x_s the distance of the biofilm surface from the bottom (m). The function $(x - x_s)$, is the distance measured from the biofilm surface toward the bulk liquid phase (Rasmussen & Lewandowski, 1998; Lewandowski & Beyenal, 2003b; Ntwampe *et al.*, 2008).

The experimental coefficient (β) can be determined from the experimental data by linearising Equation 2.28. The value for β is determined by finding the slope of $(x - x_s)$ versus $Ln\dfrac{\left[1-\left(C_{O_2(b)} - C_{O_2(s)}\right)\right]}{\left(C_{O_2(bulk)} - C_{O_2(s)}\right)}$ (Lewandowski, 1994; Lewandowski & Beyenal, 2003b; Ntwampe *et al.*, 2008).

The computational procedures available for determining the mass transfer parameters from substrate concentration profiles, require that it be assumed that biofilms are homogeneous (uniform), and not heterogeneous. It is possible for the researcher to minimise the effect of biofilm heterogeneity by selecting the location of the microsensor measurements (De Beer & Schramn, 1999; Lewandowski & Beyenal, 2001; Lewandowski & Beyenal, 2003b).

becoming loosely packed. Mass transfer is not only dependent on substrate loading and hydrodynamic conditions, but also on time (Horn & Hempel, 1998).

2.4.2.3 Oxygen penetration ratio

The oxygen penetration ratio is calculated by dividing the oxygen penetration depth into the biofilm by the biofilm thickness. With the aid of oxygen microsensors the oxygen penetration depth and ratio can be determined. Oxygen penetration depth increases with increasing biofilm thickness, while the oxygen penetration ratio decreases gradually with increasing biofilm thickness (Ntwampe *et al.*, 2008. According to Hibiya *et al.* (2003) a thick anaerobic zone exists at the bottom of thick biofilms, indicating the possibility of microbial denitrification.

Oxygen distributions within biofilms are influenced by both the thickness and density of the biofilm. The density of biofilms change in the depth direction. Thin biofilms have a dense homogeneous structure. A lower substrate penetration depth is expected due to the high density of the biofilm structure, resulting in a small diffusion coefficient. Thicker biofilms show a heterogeneous structure with large pores (Hibiya *et al.*, 2003).

2.4.3 Mathematical modelling of oxygen mass transfer within a biofilm

In biofilms at pseudo-steady state Equation 2.29 is often used to describe substrate concentration profiles (Lewandowski & Beyenal, 2003b). Equation 2.29 can be expanded into Equation 2.30. This equation equates the biofilm activity with the internal mass transport, assuming constant effective diffusivity and constant biofilm density (Beyenal & Lewandowski, 2002).

$$D_f \frac{d^2 C_{O_2(b)}}{dx^2} = \frac{V_{\max} C_{O_2(s)}}{\left(K_m - C_{O_2(b)}\right)} \qquad 2.29$$

Where D_f is the oxygen diffusivity coefficient in the biofilm (m^2/hr); $C_{O_2(b)}$ is the oxygen concentration in the biofilm (g/m^3); x is the distance from the bottom of the biofilm (m); $V_{\max}$ is the maximum rate of reaction ($g/m^3.hr$); $C_{O_2(s)}$ is the oxygen concentration at the biofilm surface (g/m^3) and K_m is the Monod half rate constant (g/m^3) (Lewandowski & Beyenal, 2003b).

$$D_f \frac{d^2 C_{O_2}}{dx^2} = \frac{\mu_{\max} C_{O_2(s)} X_\rho}{Y_{X/S}\left(K_m - C_{O_2(b)}\right)} \qquad 2.30$$

Where μ_{max} is the maximum specific growth rate (hr^{-1}); X_ρ is the biofilm density (g/m^3) and $Y_{X/S}$ is the yield coefficient (g biomass/g substrate) (Beyenal & Lewandowski, 2002). Therefore,

$$V_{max} = \frac{\mu_{max} X_\rho}{Y_{X/S}} \qquad \textbf{2.31}$$

The kinetic parameters D_f, V_{max} and K_m can be estimated by Taylor's expansion of the function shown by Equation 2.29. The function describes the concentration profile around the point $x = x_s$ positioned at the biofilm surface. The oxygen concentration in the vicinity of this point is described by Equation 2.32 (Lewandowski & Beyenal, 2003b).

$$C_{O_2(b)} = C_{O_2(s)} + \left(\frac{dC_{O_2(b)}}{dx}\right)_{x_s} \times (x - x_s) + \frac{1}{2!}\left(\frac{d^2C_{O_2(b)}}{dx^2}\right)_{x_s} \times (x - x_s)^2 + \frac{1}{3!}\left(\frac{d^3C_{O_2(b)}}{dx^3}\right)_{x_s} \times (x - x_s)^3 + \ldots$$

$$\ldots + \frac{1}{n!}\left(\frac{d^nC_{O_2(b)}}{dx^n}\right)_{x_s} \times (x - x_s)^n \qquad \textbf{2.32}$$

The first derivative $\left(\frac{dC_{O_2(b)}}{dx}\right)$ can be estimated by observing that the substrate flux across the biofilm surface must be continuous, as shown in Equation 2.33.

$$J = J_{w,x_s} = J_{b,x_s} \qquad \textbf{2.33}$$

On the biofilm side (indicated by subscript b):

$$J_{b,x_s} = D_f \left(\frac{dC_{O_2(b)}}{dx}\right)_{b,x_s} \qquad \textbf{2.34}$$

On the water side of the water-biofilm interface (indicated by subscript w);

$$J_{w,x_s} = D_f \left(\frac{dC_{O_2(b)}}{dx}\right)_{w,x_s} \qquad \textbf{2.35}$$

Therefore, according to Lewandowski and Beyenal (2003b) $\left(\frac{dC_{O_2(b)}}{dx}\right)$ can be estimated from the flux of substrate across the biofilm surface from the water side and the diffusion coefficient within the biofilm (shown in Equation 2.27).

The first order derivative can be estimated using Equation 2.27, while the second- and third-order derivatives can be estimated from Equations 2.36 and 2.37, respectively (Lewandowaki & Beyenal, 2003b, Ntwampe *et al.*, 2008):

$$\frac{d^2C_{O_2(b)}}{dx^2} = \frac{V_{max}}{D_f} - \frac{V_{max}K_m}{D_f}\frac{1}{K_m + C_{O_2(b)}} \quad \textbf{2.36}$$

$$\frac{d^3C_{O_2(b)}}{dx^3} = \frac{V_{max}K_m}{D_f}\frac{1}{\left(K_m + C_{O_2(b)}\right)^2} \times \frac{dC_{O_2(b)}}{dx} \quad \textbf{2.37}$$

Utilising the least squares method, the best fit of experimental data to a third-order polynomial (Equation 2.38) can be obtained.

$$C_{O_2(b)} = C_{O_2(s)} + a\left(x - x_s\right) + b\left(x - x_s\right)^2 + c\left(x - x_s\right)^3 \quad \textbf{2.38}$$

From Equation 2.38, Equations 2.39 to 2.41 proved to be valid (Lewandowski & Beyenal, 2003b, Ntwampe *et al.*, 2008)

$$a = \frac{J_{w,x_s}}{D_f} \quad \textbf{2.39}$$

$$b = \frac{1}{2}\frac{V_{max}}{D_f}\frac{C_{O_2(s)}}{K_m + C_{O_2(s)}} \quad \textbf{2.40}$$

$$c = \frac{1}{6}\frac{J_{w,x_s}}{D_f}\frac{V_{max}K_m}{D_f\left(K_m + C_{O_2(s)}\right)^2} \quad \textbf{2.41}$$

From oxygen concentration profiles utilising the Monod kinetic growth model, the oxygen flux, diffusion coefficient and maximum reaction rate can be estimated at any location within a biofilm (Lewandowski & Beyenal, 2003b). According to Ntwampe *et al.* (2008) this method can be utilised to determine the oxygen mass transfer parameters of *P.chrysosporium*

biofilms grown in continuous vertical single capillary MGR's. These parameters include, the Monod saturation constants used to model the experimental profiles; the oxygen uptake rate within the biofilm; the oxygen diffusion coefficient; and the DO flux (Ntwampe *et al.*, 2008).

2.4.3.1 Convective mass transfer

The rate of substrate transport to the biofilm is quantified by linking the convective external mass transfer rate to the diffusive mass transport rate across the biofilm surface. The flux of substrates across the biofilm surface must be conserved, as there is no substrate consumption within the bulk solution surrounding the biofilm surface. Therefore, the rates of the convective external mass transfer $\left(k_1\left(C_{O_2(bulk)}-C_{O_2(s)}\right)\right)$ and the diffusive internal mass transfer $\left(D_f\left(\frac{dC_{O_2(b)}}{dx}\right)\right)\Big|_{x=L_f}$ must be equal at the biofilm surface (Beyenal & Lewandowski, 2002).

$$N_s = k_1\left(C_{O_2(bulk)}-C_{O_2(s)}\right) = D_f\frac{dC_{O_2(b)}}{dx}\Big|_{x=L_f} \qquad \textbf{2.42}$$

Where k_1 is the external mass transfer coefficient (m/s) and L_f is the average biofilm thickness (m) (Beyenal & Lewandowski, 2002).

In order to solve the Equations 2.30 and 2.42, the external mass transfer coefficient, k_1, and the effective diffusivity in the biofilm, D_f, need to be determined. Horn and Hempel (1997) recommended calculating the Sherwood number (Sh) for biofilms using Equation 2.43.

$$Sh = 2Re^{0.5}Sc^{0.5}\left(\frac{d_h}{L_b}\right)(1+0.0021Re) \qquad \textbf{2.43}$$

Where Re is the Reynolds number (dimensionless), Sc is the Schmidt number (dimensionless), d_h is the hydraulic radius (m) and L_b is the length of the reactor (m) (Beyenal & Lewandowski, 2002).

$$Re = \frac{v_f d_h \rho}{\mu_1} \qquad \textbf{2.44}$$

Where v_f is the flow fluid velocity (m/s), d_h is the hydraulic radius (m), ρ the fluid density (kg/m^3) and μ_1 the fluid viscosity (Pa.s). A Reynold's number smaller than 2100 but larger than 500 indicates laminar flow conditions, while a Reynold's number larger than 2100 indicates turbulent flow conditions (Beyenal & Lewandowski, 2002).

$$Sc = \left(\frac{\rho}{\mu_1 D_m} \right) \qquad \textbf{2.45}$$

Where D_m is the molecular diffusivity of the growth limiting nutrient or oxygen (m^2/hr) (Beyenal & Lewandowski, 2002).

After calculating the Sherwood number, (Sh) (dimensionless), the external mass transfer coefficient can be calculated using Equation 2.46 (Beyenal & Lewandowski, 2002).

$$k_1 = Sh \left(\frac{D_m}{d_h} \right) \qquad \textbf{2.46}$$

2.4.3.2 Convective and diffusive oxygen mass transfer in a heterogeneous biofilm

Biofilms are generally heterogeneous in structure, which facilitates mass transport of substrates by convection as well as diffusion into the biofilm pores, even when the flow over the biofilm is laminar (Rasmussen & Lewandowski, 1998). It has been shown that the biofilm closest to the surface of the membrane presents the largest resistance to mass transfer. This is of particular importance in membrane attached biofilms as one of the limiting substrates must be transported through the denser biofilm layer. Horn and Hempel (1994) proved the existence of density gradients within biofilms (Casey *et al.*, 2000). According to Rasmussen and Lewandowski (1997) convective mass transport is active near the biofilm/liquid interface and in the upper layers of heterogeneous biofilms. This convective mass transport is independent of biofilm thickness and flow velocity. The diffusion coefficient of biofilms is lower than that of water. The diffusion coefficient of water at 21 °C is 2.0 x 10^{-9} m^2/s (Hibiya *et al.*, 2003).

2.4.3.3 Development of a combined mathematical model describing convective and diffusive substrate mass transfer within an immobilised MBR

According to Bird *et al.* (2002) and Eberl *et al.* (2006) Equation 2.47 represents the vector form of the convective-diffusion equation for substrate mass transfer.

$$\frac{\partial C_{sub}}{\partial t} + \bar{u}\nabla C_{sub} = D_{AB}\nabla^2 C_{sub} + r_A \qquad \textbf{2.47}$$

Where C_{sub} represents the local substrate concentration (g/m^3); t represents the time (hr); $\bar{u}$ represents the axial velocity vector; ∇ represents the gradient operator; D_{AB} represents the substrate diffusivity (m^2/s) which was assumed to be constant and r_A represents the rate of substrate production or consumption $(-r_A)$ (g/m^3.hr). The substrate production or consumption, r_A, is a function of the local growth rate, biofilm density, and time.

The left hand side of Equation 2.47 represents bulk transport (convective) and the right hand side excluding r_A represents diffusive transport within the biofilm. Equation 2.47 can be rearranged so that both methods of substrate mass transport are on the right hand side of the equation, as shown in Equations 2.48 and 2.49.

$$\frac{\partial C_{sub}}{\partial t} = D_{AB}\nabla^2 C_{sub} - \bar{u}\nabla C_{sub} + r_A \qquad \textbf{2.48}$$

$$\frac{\partial C_{sub}}{\partial t} = diffusion - convection + reaction \qquad \textbf{2.49}$$

$$\frac{DC_{sub}}{Dt} = D_{AB}\nabla^2 C_{sub} + r_A \qquad \textbf{2.50}$$

Equation 2.50 is an alternative compacted form of Equation 2.47, with $\frac{DC_{sub}}{Dt}$ representing $\frac{\partial C_{sub}}{\partial t} + \bar{u}\nabla C_{sub}$.

Equation 2.51 represents the two dimensional expanded form of Equation 2.47.

$$\frac{\partial C_{sub}}{\partial t} + u\frac{\partial C_{sub}}{\partial z} + v\frac{\partial C_{sub}}{\partial r} = \frac{D_{AB}}{r}\left[\frac{\partial C_{sub}}{\partial r} + r\frac{\partial^2 C_{sub}}{\partial r^2} + r\frac{\partial^2 C_{sub}}{\partial z^2}\right] + r_A \qquad \textbf{2.51}$$

For pseudo-steady state $\frac{\partial C_{sub}}{\partial t}=0$, therefore in cylindrical co-ordinates Equation 2.52 was postulated:

$$u\frac{\partial C_{sub}}{\partial z}+v\frac{\partial C_{sub}}{\partial r}=\frac{D_{AB}}{r}\left[\frac{\partial C_{sub}}{\partial r}+r\frac{\partial^2 C_{sub}}{\partial r^2}+r\frac{\partial^2 C_{sub}}{\partial z^2}\right]+r_A \qquad \textbf{2.52}$$

The convective (i.e. left hand side) and diffusive (i.e. right hand side) terms were then separated as shown in Equation 2.53.

$$u\frac{\partial C_{sub}}{\partial z}-\frac{D_{AB}}{r}\frac{\partial^2 C_{sub}}{\partial z^2}=\frac{D_{AB}}{r}\left[\frac{\partial C_{sub}}{\partial r}+r\frac{\partial^2 C_{sub}}{\partial r^2}\right]-v\frac{\partial C_{sub}}{dr}+r_A \qquad \textbf{2.53}$$

The mathematical model describing substrate mass transfer in a pressurised continuously operated MGR was further developed in section 8.6 of Chapter 8.

2.4.4 Dissolved oxygen transfer in immobilised membrane bioreactors (MBR's)

Many papers dedicated to hollow fibre bioreactors assume that the transport of low molecular weight nutrients, such as oxygen, occurs by diffusion (Dionne *et al.*, 1996; Qin & Cabral, 1998; Hay *et al.*, 2000; McClelland *et al.*, 2003). The removal of the convective contribution to mass transfer decreases the complexity of transport analysis. Convective contributions to mass transfer are generally neglected due to pressure shear stress decreasing cell viability. Convective mass transfer regulates the mass transfer of macromolecular species and proteins. It is thus important from an engineering view point to evaluate both diffusive and convective contributions to mass transfer. Very little data is available with regards to the concomitant action of both transport mechanisms within MBR's (Curcio *et al.*, 2005).

2.4.4.1 Dissolved oxygen transfer in membrane gradostat bioreactors (MGR's)

In pressurised vertical MGR systems (as described in section 3.3.4) oxygen for the immobilised biofilm is continuously supplied to the extracapillary space (ECS) in the shell of the reactor. The MGR's are positioned vertically to enhance the radial distribution of substrates across the biofilm, which according to Leukes *et al.* (1999) is a requirement for an effective MGR system. Controlling the oxygen partial pressure in the ECS controls the oxygen penetration depth into the biofilm. The existence of the DO concentration gradient across the membrane and the biofilm creates an ideal environment for the culturing of aerobic micro organisms (Casey *et al.*, 1999). According to Stamatialis *et al.* (2008) oxygen

mass transfer through a biofilm from the ECS when under pressure, can occur by both diffusive and convective transport, as observed in dialysis membranes.

Limited information exists regarding the *in-situ* mass transfer of oxygen in biofilms immobilised on the external surface of a capillary membrane in a pressurised vertical MGR system. If there is no flow of air over the surface of the biofilm it can be assumed that oxygen mass transfer is by diffusion only and that convective mass transfer is negligible (Yurt *et al.*, 2003). The type of model to be used to determine the DO mass transport parameters in immobilised biofilms depends on whether the DO transport into the biofilm is by convection or diffusion (Ntwampe *et al.*, 2008). Therefore, to effectively design and operate an MGR it is important to have an accurate quantitative description of both the diffusive and convective transport of the substrate across the biofilm (Stamatialis *et al.*, 2008).

DO mass transfer is an essential component for microbial activity in biofilms of aerobic micro organisms. According to Ntwampe *et al.* (2008) in biofilms of *P. chrysosporium* immobilised on the external surface of ultrafiltration capillary membranes in an MGR system, the DO penetration depth decreased with increasing biofilm thickness. This resulted in the formation of anaerobic zones within the biofilm. The DO spatial distribution was quantified using a Clark-type microsensor. Ntwampe *et al.* (2008) refuted the hypotheses that DO mass transfer parameters obtained in submerged pellets, allowed to equilibrate with air, can be used to estimate and model DO mass transfer parameters, for the same micro organism, in a non-pressurised MGR system.

2.4.4.2 Diffusive mass transfer within MGR's

Diffusional mass transport obeys the second law of thermodynamics, which implies that a system will spontaneously move toward the uniform distribution of components and thus a state of equilibrium (Lewandowski & Beyenal, 2003a). Oxygen transport through the biofilm from the ECS can occur by diffusion only as described by Ntwampe *et al.* (2008), since the biofilm was placed in direct contact with the gas phase and diffusion requires contact between either a gas or a liquid. The method of Lewandowski (1994) was then utilised to determine the mass transfer parameters (Hibiya *et al.*, 2003).

The mass transfer equation for oxygen distribution in a biofilm is described in Equation 2.54 (Hibiya *et al.*, 2003).

$$\frac{dC_{O_2}}{dt} = D_f \frac{d^2C_{O_2}}{dx^2} - \frac{kXC_{O_2}}{K_m + C_{O_2}} \qquad \textbf{2.54}$$

A steady supply of air is fed into the MGR, therefore it was assumed that the oxygen concentration available did not change over time, hence $\frac{dC_{O_2}}{dt}$ = 0. When a pseudo-steady state concentration profile is achieved on the inside of the biofilm, the consumption rate will be equal to the diffusion rate as seen in Equation 2.55 (Ntwampe *et al.*, 2008).

$$D_f\left(\frac{d^2C_{O_2}}{dx^2}\right)=\frac{kXC_{O_2}}{K_m+C_{O_2}} \qquad \textbf{2.55}$$

The inverse of each part in Equation 2.55 is taken, to yield a linear function between the inverse of the second derivative and the inverse of the oxygen concentration, represented by Equation 2.56 (Hibiya *et al.*, 2003; Ntwampe *et al.*, 2008).

$$\left(\frac{d^2C_{O_2}}{dx^2}\right)^{-1}=\frac{D_fK_m}{kX}\frac{1}{C_{O_2}}+\frac{D_f}{kX} \qquad \textbf{2.56}$$

The Monod saturation constant, K_m was calculated by dividing the slope $\left(\frac{D_fK_m}{kX}\right)$ by the intercept $\left(\frac{D_f}{kX}\right)$. Using the exponential Equation 2.57, the second derivative that fits the experimental profile of oxygen distribution in the biofilms was calculated. Equation 2.57 was the exponential equation that best fitted the experimental data (Hibiya *et al.*, 2003).

$$C_s=a_1+a_2\exp\left(-\frac{x}{a_3}\right) \qquad \textbf{2.57}$$

According to Frank-Kamenetskii (1969), the mass balance equation at steady state can be transformed to an equation (Equation 2.58) that represents the first derivative of oxygen concentration distribution across the biofilm (Hibiya *et al.*, 2003).

$$\left(\frac{dC_{O_2}}{dt}\right)_b=\sqrt{2\frac{kX}{D_f}\left(C_{O_2}-K_m\ln\frac{K_m-C_{O_2}}{K_m}\right)} \qquad \textbf{2.58}$$

This was further developed by Ntwampe (2005) for a multi-capillary MBR system, as shown in Equation 2.59.

$$\left(\frac{dC_{O_2}}{dt}\right)_b = -\sqrt{2\frac{kX}{D_f}\left(C_{O_2} - K_m \ln\frac{K_m + C_{O_2}}{K_m}\right)} \qquad 2.59$$

By utilising the parameters calculated from the experimental profiles, namely $\left(\frac{D_f}{kX}\right)$ and K_m the first derivative of oxygen concentration distribution across the biofilm was simulated using Equation 2.59. The oxygen distribution can be simulated by the finite difference method, using the kinetic parameters and effective diffusion coefficient. The substrate molecules must travel across the boundary layer before reaching the biofilm surface via diffusion. Without convective mass transfer the oxygen concentration profile would be linear, therefore the oxygen concentration profile in the boundary layer can be described by the empirical exponential function (Hibiya *et al.*, 2003).

2.4.4.3 Oxygen flux values within an MGR

During operation of an MGR system of *P. chrysosporium*, immobilised on the external surface of an ultrafiltration capillary membrane, oxygen flux values of 0.27 to 0.7 g/m^2.h were obtained. The oxygen consumption rate in the range 894.53 to 2739.70 g/m^3.h and Monod's saturation constants in the range of 0.041 to 0.999 g/m^3 was used in the modelling of the oxygen distribution (Ntwampe *et al.*, 2008).

Maximum oxygen flux values, measured with the aid of oxygen microsensors, of approximately 10 g/m^2.d, was measured by Nishidome *et al.* (1994), a value similar to that measured by Tijhuis *et al.* (1994) and corresponds to a calculated oxygen penetration depth of 100 µm. Actual oxygen flux values depend on the specific oxygen uptake rate of the micro organism, the density of the biofilm and the effective diffusivity of oxygen in the biofilm. Generally, overall biofilm thickness exceeds the oxygen penetration depth into the biofilm, thus preventing a large part of the biofilm from participating in aerobic substrate degradation processes (Casey *et al.*, 1999). The oxygen saturation concentration of air in water at atmospheric pressure is approximately 8 mg/L and of oxygen in water at atmospheric pressure is 40 mg/L (Casey *et al.*, 1999).

2.5 Scale-up of a SFMGR to multifibre membrane gradostat bioreactor (MFMGR)

Successful scale-up and operational control of aerobic microbial processes requires knowledge regarding the oxygen kinetic and metabolic parameters (Ozergin-Ulgen and Mavituna, 1998). The scale-up step from the laboratory to industrial scale is complicated. The main scale-up parameters are aeration, shear stress, biofilm growth and the ratio

between membrane surface area and volumetric flux (Govender *et al.*, 2003). A problem observed with scale-up is that the actual productivity is less than the predicted theoretical maximum, due to the utilised operational parameters being based on empirical assumptions made after single fibre membrane gradostat reactor (SFMGR) analysis, thus not adequately reproducing the axial flow of oxygen along the membranes as observed in the SFMGR's (Govender *et al.*, 2003). Kinetic growth models are required by engineers in the design process as these models are an excellent scientific method for predicting a system's behaviour for the design of scaled-up systems (Sheldon *et al.*, 2008).

CHAPTER 3

MATERIALS AND METHODS

CHAPTER THREE
MATERIALS AND METHODS

All experimental work was done at Synexa Life Sciences (www.synexagroup.com), a biotechnology company located in Bellville (Cape Town). Unfortunately, due to non-disclosure agreements and intelectual property not all procedures can be elaborated on within the materials and methods chapter.

3.1 Construction of the 1 x 3 reactor rig and the 1 x 12 reactor rig

The following steps were followed in the construction and set-up of a 1 x 3 single fibre membrane gradostat reactor (SFMGR) rig and a 1 x 12 SFMGR rig.

3.1.1 CAD drawing of the reactor set-up

Before the rig was constructed and the reactors were set-up, the rig was drawn to scale using a three dimensional drawing program, Solid Edge version 18. This was to ensure that when the rig was physically constructed, the different sections all fitted together perfectly.

3.1.2 Actual construction of the reactor set-up

The drawing templates, with all the dimensions for the 1 x 3 SFMGR Quorus rig, designed by Synexa Life Sciences, were sent to Techno Surfaces located in Bellville (Cape Town), a company specialising in plastics. The rig (as shown in Figures 3.1 and 3.2) was built to scale according to the drawing templates. The 1 x 12 SFMGR rig was constructed on site at Synexa Life Sciences, using aluminium tubing (2 x 2 cm) and perspex sheeting.

Figure 3.1: Photograph of the 1 x 3 SFMGR Quorus rig constructed of white Corian plastic

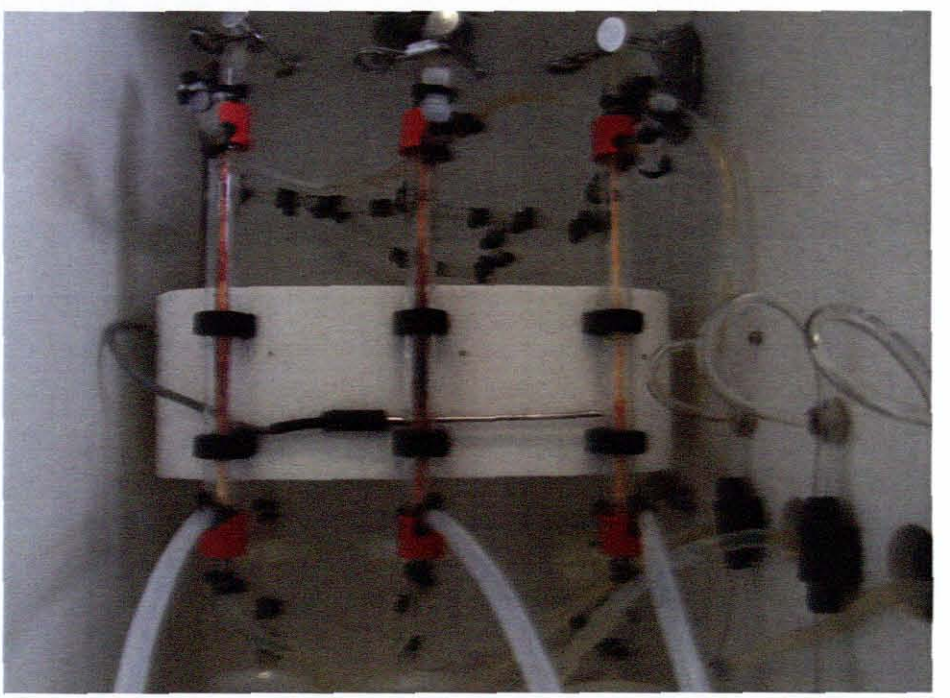

Figure 3.2: Photograph of 1 x 3 SFMGR's in the Quorus rig

3.1.3 Circuit diagram of the wiring in the 1 x 3 SFMGR Quorus rig

Proior to wiring the rig, to ensure correct wiring and to make sure that all the electronic equipment and wiring fitted within the space provided in the Quorus rig, a circuit diagram was drawn in Microsoft Office Power Point 2003. All the electronic equipment that was utilised had a basic wiring diagram attached from where the circuit diagram was constructed. The wiring diagram was drawn to ensure that anyone could wire the rig.

3.1.4 Wiring the Quorus rig

Only after the wiring diagram was completed, could the electronic equipment in the rig be wired and made operational. This was to ensure that incorrect wiring did not occur, which would have resulted in time wastage trying to find the problem, as well as possible damage to the electronic equipment.

3.1.5 Valve tuning of the proportional valves

All the Burkett Proportional valves (Type 2821), supplied by Burkett located in Germany, that were utilised in the reactor set-up required tuning. The valves were tuned to ensure that at 0% the valve was completely closed and at 100% the valve was fully open, thus ensuring the valves were calibrated to function optimally. Each valve was tuned separately as per the in-house procedure at Synexa Life Sciences.

3.1.6 Tuning of the proportional-integral-derivative (PID) controller in the JCS Shinko controllers

The PID controller of the JCS Shinko pressure controller had to be tuned to ensure that the percentage difference between the set value (SV) and the process valve (PV) (i.e. actual value) of the JCS Shinko pressure controller was as small as possible. The SV and the PV should be the same. However, if the PID controller was not tuned there would be a large difference between these two values. The PID controller was tuned either manually or automatically, as per in-house procedure.

3.2 Ceramic membranes

The assymetric capillary ceramic membranes utilised were made of high purity aluminium oxide (α-Al_2O_3) and had an inside coating of aluminium oxide (α-Al_2O_3) with an average pore size of 40 nm (see Figure 3.3a - d). The ceramic membranes used in the SFMGR systems were supplied by Hyflux CEPAration BV in the Netherlands, a company specialising in hollow fibre ceramic membranes and modules. Ceramic membranes fall into the category of integrally skinned asymmetric membranes. Aluminium oxide is known for its strength, chemical resistance and extreme hardness resulting in membranes having a very high abrasion resistance.

3.2.1 Characteristics and dimensions of the ceramic membranes

In the experimental procedures conducted, two types of ceramic hollow fibre membranes were utilised. The inner and outer diameters of the two membranes were the only difference between them. All other characteristics and dimensions of the two membranes were identical, as seen in Table 3.1.

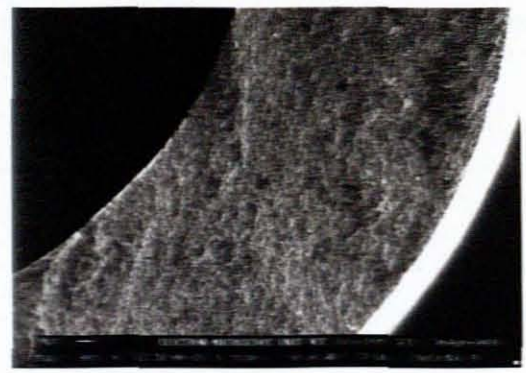

(a) Cross section of a 3 mm x 2 mm ceramic membrane (Magnification of 400x)

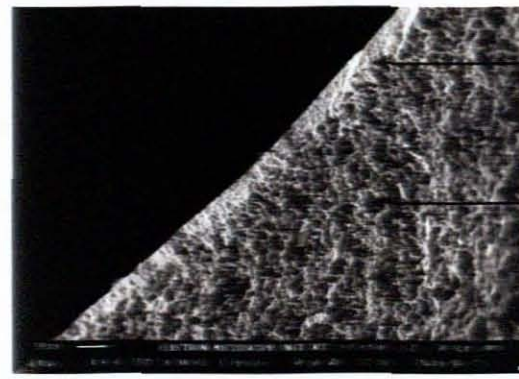

(b) Inside coating layer and outer layer composed of α-Al_2O_3 (Magnification of 2240x)

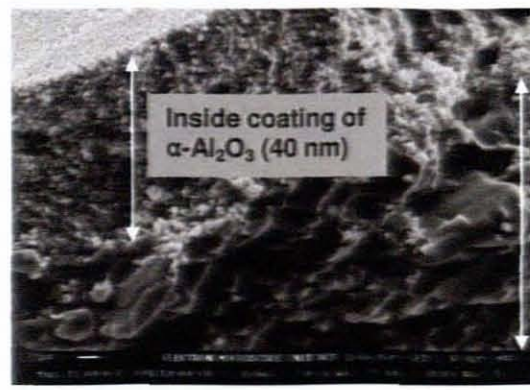

(c) Inside coating layer of α-Al_2O_3 with a pore size of 40 nm (Magnification of 15000x)

(d) The inside surface of the 40 nm inside coating of α-Al_2O_3 (Magnification of 2000x)

Figure 3.3: Scanning-Electron Microscopy (SEM) images of 3 mm x 2 mm asymmetric capillary ceramic membrane

Table 3.1: Characteristics and dimensions of the ceramic membranes (Hyflux Ceparation, 2008)

Parameters	Small membrane	Large membrane
Material	α-Al_2O_3	α-Al_2O_3
Outer diameter (mm)	2.8	3.8
Inner diameter (mm)	1.8	2.8
Wall thickness (mm)	0.5	0.5
Length (mm)	225	225
Pore size (nm)	40	40
Inside coating	Yes	Yes
Coating material	α-Al_2O_3	α-Al_2O_3
pH resistance	1 – 14	1 - 14
Maximum temperature (°C)	1000 +	1000 +
Burst pressure (kPa)	5000 +	5000 +
CWF (L/h.m^2.kPa)	5	5
Porosity	~30%	~30%

3.2.2 Integrity testing

Before using the ceramic membranes, all the membranes were autoclaved for 20 min at a temperature of 121°C and a pressure of 1 atm. Autoclaving was used to identify any membranes with weaknesses such as cracks or holes, as these ceramic membranes would break and could be eliminated before use. Following autoclaving, the membranes were submerged in distilled water for 30 min so that the membranes were saturated and then integrity tested.

Integrity testing measured a membrane's ability to withstand and remain intact at a high pressure. The integrity of the ceramic membranes was tested at a pressure of 150 kPa, a pressure higher than at which the membranes would be operated. If the membranes could

withstand a pressure of 150 kPa during integrity testing then the membranes would withstand the operating pressure. Any membranes that were damaged (i.e. a hole or crack) or had weak areas would leak, in the form of air bubbles, during integrity testing, and could thus be eliminated from use.

3.2.3 Porosity/flux testing of the membranes

Although all the ceramic membranes were subjected to the same manufacturing conditions, the porosity of the membranes differed slightly. It was therefore necessary to test the flux of each membrane, to allow the grouping of membranes with similar porosities so that they could be used together. Therefore, the effect of different porosities could be eliminated as a factor that influenced the outcome of the experimental procedures.

After the flux testing with distilled water was completed, a graph of the measured pressure (kPa) against the volume of distilled water collected (ml) over a set period of time was plotted for each membrane. A trendline was added to each graph and the slope obtained for each trendline compared. The percentage difference between the trendline slopes was calculated and the membranes with a percentage difference of less than 5 % were grouped together.

3.2.4 Drying and weighing the ceramic membranes

After the ceramic membranes were autoclaved and the integrity and clear water flux tests completed the ceramic membranes were dried in an oven at a temperature of 70°C for 24 hr. The membranes were dried in an oven to ensure that all the water that was trapped inside the pores was removed and that the membranes were completely dry when weighed. After drying, the dry weights of the membranes were determined and used in the biomass and growth kinetics calculations.

3.2.5 Cleaning of the ceramic membranes after use for re-use

After the bioreactors were disconnected, the membranes were removed and the wet and dry biomass determined. The ceramic membranes were then submerged in a 10% hydrogen peroxide (H_2O_2) solution for 5 days. A H_2O_2 solution was utilised to clean the membranes after use, because it is a powerful oxidising agent that removes all organic compounds from the membranes. After 5 days the membranes were removed, rinsed with distilled water for 30 sec and dried in an oven for 24 hr at a temperature of 70°C. Once clean and dry the membranes were ready for re-use. The flux and integrity tests were not repeated.

3.3 Set-up of reactors and ancillary equipment

3.3.1 Construction of the reactors

Table 3.2 lists the components necessary for assembling one SFMGR as patented by Edwards *et al.* (2007). All the components on the list should be available prior to initiating the assembly process. The construction of a SFMGR is illustrated schematically in Figure 3.4.

Table 3.2: Components required to assemble a Single fibre membrane gradostat reactor (SFMGR) (Edwards *et al.*, 2007)

Component	Dimensions (size)	Number per SFMGR
Glass housing manifold (A)	16 mm OD; 200 mm length	1
Ceramic membrane (B)	3 mm OD; 2 mm ID or 4 mm OD; 3 mm ID 230 mm length for both membrane sizes	1
Silicone disk gaskets (C_1 & C_2)	16 mm OD x 2.8 mm ID; 5 mm thickness	2
Stainless steel end plates (D_1 & D_2)		2
Schott GL18 end caps (E_1 & E_2)	17.5 mm	2

After inserting a silicone disc gasket (C1) onto one end of the ceramic membrane (B), the membrane was inserted into the glass housing manifold (A). A second silicone disc gasket (C2) was placed onto the opposite end of the ceramic membrane. At both ends of the glass housing manifold a stainless steel end plate (D1 & D2) was aligned on top of the silicone disc gaskets and held in place by Schott GL18 end caps (E1 & E2) by rotating the end caps in a clockwise direction. The membrane gradostat bioreactor (MGR) was patented by Leukes *et al.*, (1999).

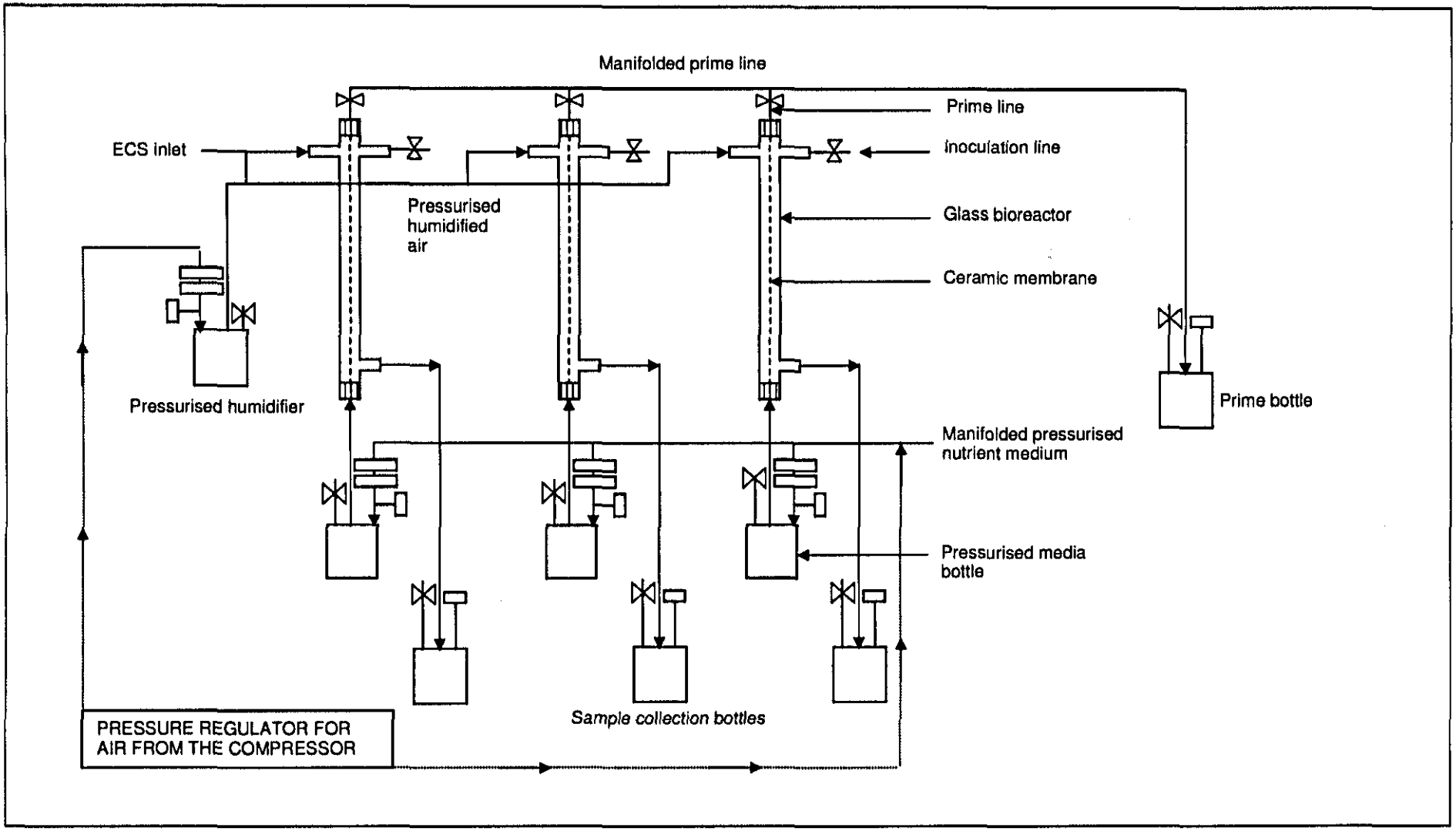

Figure 3.5: Schematic diagram of the 1 x 3 manifolded single fibre membrane gradostat reactor module set-up with ancillaries

3.3.4 Construction of the 1 x 3 SFMGR rig to measure oxygen profiles

These SFMGR's were set up as for a 1 x 3 module SFMGR, ready for inoculation once assembled with ancillaries. The only difference between these SFMGR's and those described in section 3.3.3 and Figure 3.5 being that the glass housing of each bioreactor had a port located at either the bottom, middle or top of the glass housing (refer to Figure 3.6). The design templates were taken to Glasschem Bk., a company located in Stellenbosch (SA), specialising in the design and construction of glass products. See Figure 3.5 for a schematic diagram of the 1 x 3 module SFMGR rig set-up and Appendix D for the design of these bioreactors.

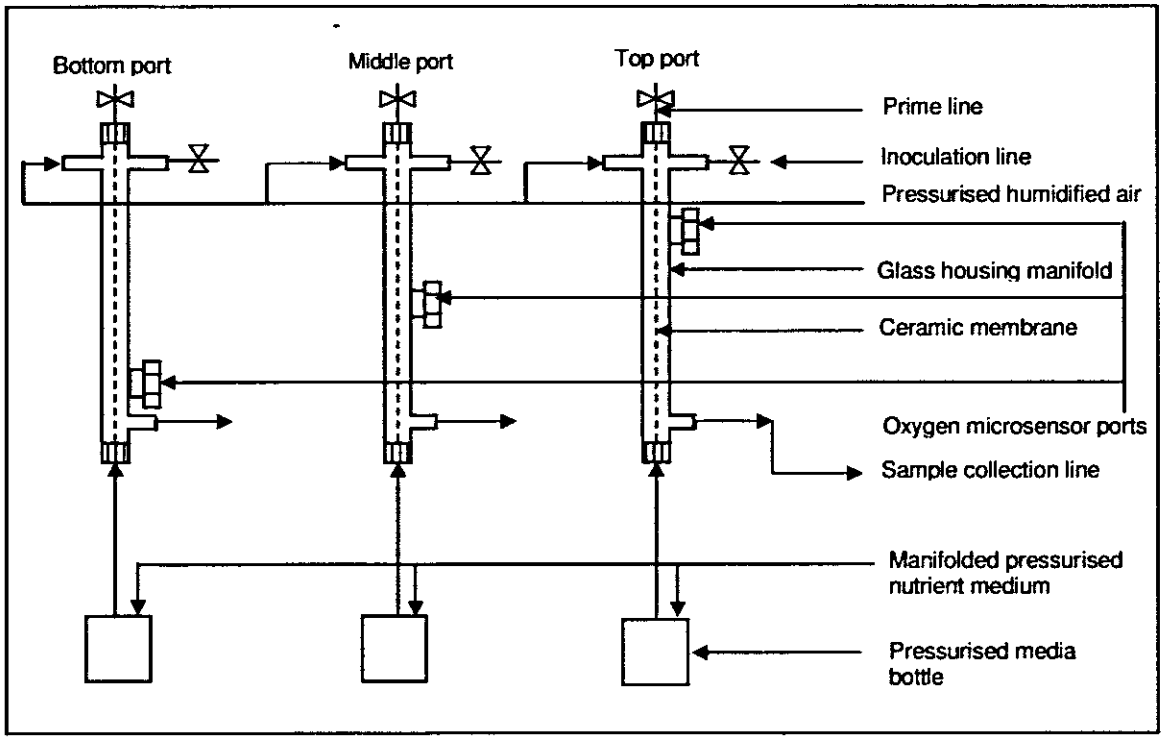

Figure 3.6: Set of 3 manifolded single fibre membrane gradostat reactors (SFMGR) with bottom, middle and top ports for oxygen measurements

3.3.5 Test runs

3.3.5.1 Pure water flux testing

Prior to operating the 3 or 12 module SFMGR rigs, pure water flux testing was conducted. Pure water flux testing was carried out to ensure transmembrane flux was occurring across the ceramic membranes from the membrane lumen to the ECS and to ensure that all the SFMGR's maintained pressure and were not leaking air.

Pure water flux testing was performed by filling all the media bottles with equal volumes of distilled water. The JCS Shinko pressure controllers were set at increasing pressure

differentials of between 1 and 4 kPa and the rig was operated for 30 min at each new differential. The volume of water collected was measured and the flux for each reactor determined, as the time elapsed between start and finish was recorded. Due to different liquids having different densities the pressure differential had to be adjusted accordingly to achieve the desired flux.

3.3.5.2 Control run with media to be utilised during the experiment

A control run was conducted with the growth medium that was to be utilised during the experimental procedure in order to establish the pressure differential at which the system was to be operated so that the flow rate would be approximately 1ml/hr.

All the media bottles were filled with an equal volume of growth medium and the JCS Shinko pressure controllers were set to a starting pressure differential of 0.5 kPa. After running the system for an hour, the volume of permeate was measured, and the pressure differential altered by increasing or decreasing the set pressure of the growth medium controller. Whether to increase or decrease the set pressure of the controller was determined by the volume of growth medium measured after an hour. The process was repeated until a pressure differential was established that resulted in a flow rate of approximately 1ml/hr.

3.3.6 Post set-up sterilisation

After construction, the glass bioreactors with ceramic membranes, media bottles, humidifier, sample collection bottles and prime bottle were removed from the rig and sterilised before inoculation by autoclaving at a temperature of 121°C and a pressure of 1 atm for 20 min. All the Schott GL18 end caps attached to the ends of the reactors were loosened before autoclaving to prevent the ceramic membranes from breaking. Before the reactors and ancilliaries were removed from the autoclave the Schott GL18 end caps were re-tightened and the lids of all the glass schott bottles checked to ensure they were securely fastened. Should one of the lids have come loose after the reactors and ancillaries had been removed from the autoclave, everything would have to be re-autoclaved to prevent the possibility of contamination. Following sterilisation, the reactors and ancillaries were set up in the rig ready for inoculation.

3.4 Growth medium preparation

The medium required for an experimental procedure was prepared and sterilised by autoclaving for 20 min at 121°C, after the rig had been set-up, and prior to inoculation.

Two different types of media were utilised: (1) an International *Streptomyces* Project, medium 2 (ISP2) as described by Shirling and Gottlieb (1966) and (2) a defined growth

medium (Hobbs *et al.*, 1989). The ISP2 growth medium is a complex medium that provided the micro organism being cultured with the basic components required to survive; namely a carbon source, in the form of glucose; a nitrogen and phosphate source both present in the yeast and malt extract found in the medium (as listed in Table 3.3). In the defined medium each component present in the media was known as shown in Table 3.4. In the defined medium glucose was the carbon source; NaCl the chloride source; $NaNO_3$ the nitrate source; K_2PO_4 the phosphate source; Na_2SO_4, $MgSO_4.7H_2O$ and $ZnSO_4$ the sulphate sources; the TRIS (hydroxymethyl) aminomethane base was the GR buffer substance and the trace element solution provided the micro organism with the metals and minerals required in trace (i.e. minute) amounts.

Table 3.3: Complex International *Streptomyces* Project, medium 2 (ISP2) growth medium preparation (Shirling & Gottlieb, 1966)

Glucose	4.0 g
Yeast extract	4.0 g
Malt extract	10.0 g
Distilled water	1 litre

Adjust to pH 7.5 with 1M NaOH. Autoclave at 1 atm and 121 °C for 20 min.

Table 3.4: Defined Hobbs *et al.* (1989) growth medium preparation

NaCl	5.0 g
Na_2SO_4	4.5 g
$NaNO_3$	2.0 g
K_2HPO_4	2.0 g
Glucose	2.0 g
TRIS Base	1.2 g
$MgSO_4.7H_2O$	1.0 g
$ZnSO_4$	0.01 g
Distilled water	1 litre

Adjust to pH 7.2 with 1M NaOH. Autoclave at 1 atm and 121°C for 20 min. The phosphate and glucose solutions were prepared and sterilised separately and added to the rest of the medium solution after autoclaving.

The salt solution in Table 3.4 was supplemented with 1 ml of filter sterilised trace element solution described in Table 3.5.

Table 3.5: Trace element solution (Hobbs *et al.*, 1989)

$FeCl_3$	8.775 g
$ZnCl_2$	2.040 g
$MnCl_2.4H_2O$	1.015 g
$CuCl_2.2H_2O$	0.425 g
NaI	0.415 g
H_3BO_3	0.310 g
$CaCl_2.6H_2O$	0.238 g
$Na_2MoO_4.2H_2O$	0.242 g
Distilled water	1 litre

3.4.1 Growth medium transfer

After the sterilisation process, the growth medium was sterilely transferred to all the media bottles present in the rig. In order to sterilely transfer the medium, a stainless steel connector held with diagonal pliers, was heated in a Bunsen burner flame until red hot and inserted into the silicone tubing attached to the medium top-up bottle. Two cable ties were used to keep the sterile connection in place. The open end of the sterile connection was then heated in the Bunsen burner flame until red hot and then inserted into the medium top-up line connected to the reactor's medium bottle. After the connection was secured in place by two cable ties, the cable ties sealing the silicone lines from both the medium top-up bottle and the medium bottle were released.

The vent line attached to the medium top-up bottle was closed with a cable ti.e. The silicone lines to which the respective double air filters of both the medium top-up bottle and the medium bottle were attached were opened. The volume of medium required was then

transferred from the medium top-up bottle to the medium bottle of the reactor by attaching an air line to the double air filters attached to the medium top-up bottle.

Note: As the air is pumped into the medium top-up bottle the pressure in the bottle increases and forces the medium into the medium bottle. If the vent line of the medium top-up bottle remains open no medium transfer will occur as all the air being pumped into the medium top-up bottle will escape through the vent and there will be no pressure increase in the medium top-up bottle. If the double air filters on the medium bottle is not opened the medium bottle will eventually explode, due to a pressure build up.

Once the required volume of medium had been transferred, the air line was disconnected; the silicone tubing on both sides of the sterile connection was closed off by bending the silicone tubing over itself and then cable tying. The cable ties securing the stainless steel sterile connection to the silicone tubing of the medium bottle was released and the sterile connection removed. The stainless steel sterile connection remained attached to the medium top-up bottle ready for the next medium transfer.

3.5 Inoculum preparation

Inoculum preparation was of vital importance as the inoculum had to remain uncontaminated. A Gram stain was conducted on the inoculum prior to inoculation to test for contamination. The inoculum with which the reactors were inoculated contained colonies the size of a pin head that could easily adhere to the surface of the ceramic membranes. If the inoculum became contaminated, fresh inoculum was prepared and the experiment placed on hold until uncontaminated inoculum was available. All inoculum was cultured from a spore stock solution prepared as described in section 3.5.1.

3.5.1 Preparation of the spore stock solution

A spore stock solution was cultured from where all future inoculum were prepared. Before the spore stock solution could be cultured three empty 100 ml flasks sealed with cotton wool bungs and covered with aluminium foil, as well as 500 ml ISP2 growth medium was prepared (see Table 3.3 for ISP2 growth medium preparation procedure) and autoclaved at 121 °C for 20 min.

Once the flasks and ISP2 growth medium were sterilised, 40 ml ISP2 growth medium was transferred to each of the sterile 100 ml flasks, under the laminar flow hood with the aid of an electronic pipette using sterile techniques. Prior to using the laminar flow hood, the hood was cleaned with 70% ethanol.

Colonies of *S. coelicolor* A3(2) were then transferred from a stock agar plate to each flask with a sterile inoculation loop. An extra flask was prepared in case contamination occurred. After inoculation, the flasks were placed in a shaking-incubator for 4 days at 200 revolutions per minute (rpm) and a temperature of 27°C. While the flasks were being incubated, 20 ISP2 agar plates were prepared (see Table 3.6).

Table 3.6: International *Streptomyces* Project, medium 2 (ISP2) agar preparation (Shirling & Gottlieb, 1966)

Glucose	4.0 g
Yeast extract	4.0 g
Malt extract	10.0 g
Agar	12.0 g
Distilled water	1 litre

Adjust to pH 7.5 with 1M NaOH. Autoclave at 121°C for 20 min. Sterilely pour approximately 20 to 25 ml of hot agar into 20 sterile Petri dishes under the laminar flow hood. Allow to cool and solidify.

After the 4 day incubation period had elapsed and the flask cultures were pink in colour with visible suspended pellets, 100 µl of the inoculum was sterilely transferred to each of the 20 ISP2 agar plates with the aid of a Gilson pipette. Using a sterile glass rod bent to resemble a hockey stick, the 100 µl inoculum was evenly spread over the surface of the agar to ensure that a "lawn" of growth would be achieved. This procedure was performed under the laminar flow hood using sterile techniques. The 20 inoculated ISP2 agar plates were placed in an incubator for 7 to 10 days at a temperature of 28°C. Once sufficient sporulation from the colonies on the agar plates were observed, the plates were removed from the incubator. The ISP2 agar plates could not be left in the incubator for too long as this would cause the agar to dry out and the plates would then have to be discarded.

A stock solution of spores was obtained by filling each IPS2 agar plate with 5 ml of a wetting agent (also known as a buffer solution), namely 0.1% Tween 80 and gently scraping the surface of the plate with a bent glass rod. Either 0.1% Tween 80 or 0.0001% Triton x 100 could have been utilised as the wetting agent. A wetting agent was necessary to separate the individual spores from each other as the spores were hydrophobic, therefore the wetting agent prevented the spores from aggregating. The loosened spores were then transferred to

a sterile 50 ml centrifuge tube with the aid of a Gilson pipette. The 50 ml centrifuge tube containing a mixture of the harvested spores and 0.1% Tween 80 wetting agent was centrifuged at 4000 rpm for 10 min. After centrifugation the supernatant was poured off and the pellet left at the bottom of the centrifuge tube was resuspended in 0.1% Tween 80. The volume with which the pellet was resuspended was equivalent to half the volume present in the 50 ml centrifuge tube before centrifugation (eg. if before centrifugation the volume was 10 ml, then the pellet would have been resuspended in 5 ml 0.1% Tween 80).

Once the pellet had been resuspended a serial dilution was prepared in eppendorf tubes as described in Table 3.7.

Table 3.7: Serial dilution

Concentration of dilution	Volume of resuspended spore solution (µl)	Volume of 0.1% Tween 80 (µl)	Vortex
1x dilution	1 ml of the undiluted resuspended spore solution	0	Yes
2x dilution	500 µl of the 1x diluted solution	500 µl	Yes
5x dilution	200 µl of the 1x diluted solution	800 µl	Yes
10x dilution	500 µl of the 5x diluted solution	500 µl	Yes
100x dilution	100 µl of the 10x diluted solution	900 µl	Yes
1000x dilution	100 µl of the 100x diluted solution	900 µl	Yes

300 µl of each dilution concentration was transferred in duplicate to the wells of a microtitre plate. Table 3.8 represents the layout of the microtitre plate; the blank is represented by the Bl symbol. 0.1% Tween 80 was utilised as the blank. Each dilution was read in duplicate.

Table 3.8: Microtitre plate layout

Bl	1 x	2 x	5 x	10 x	100 x	1000 x
Bl	1x	2 x	5 x	10 x	100 x	1000 x

After the absorbance values had been determined for each dilution the average absorbance values were plotted against the serial dilutions, shown in Figure 3.7. The sequential serial

dilutions that resulted in the best R^2 value was then utilised in all calculations to prepare the stock spore solution.

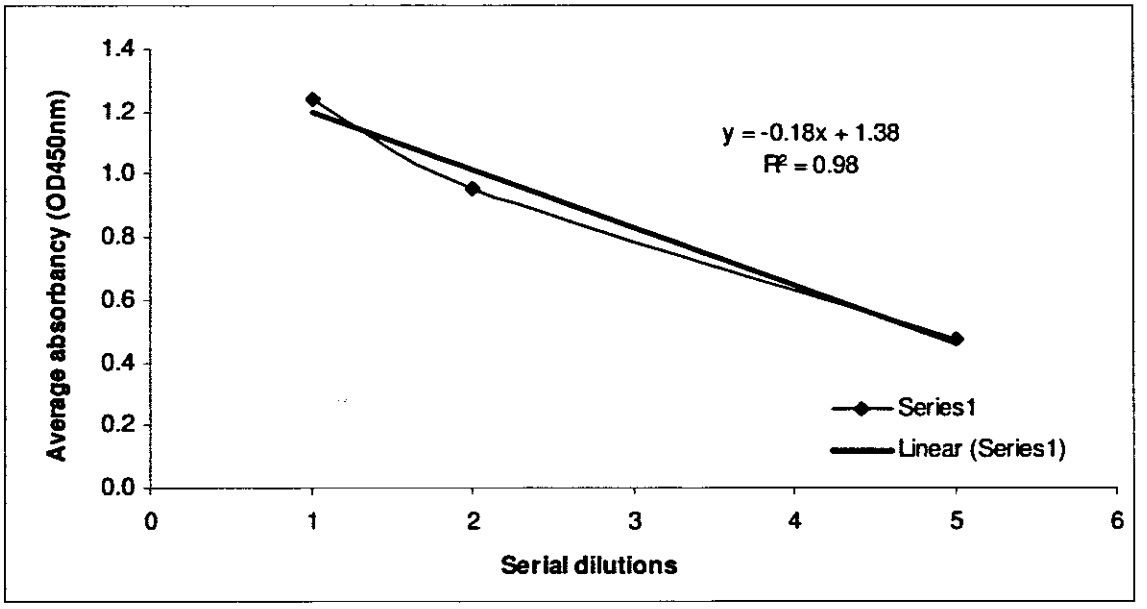

Figure 3.7: Sequential serial dilutions with the best R^2 fit

.....

Once the sequential dilutions with the best R^2 values had been identified the average absorbency for each serial dilution was determined. The spore concentration of *Streptomyces* species read at an optical density (OD_{450}) of 450 nm in a cuvette with a 1 cm^{-1} pathlength is 5 x 10^7 spores/ml (Kieser *et al.*, 2000). Since a microtire plate reader was utilised instead of a spectrophotometer the average absorbancy had to be multiplied by 0.8 pathlength. The undiluted spore concentrations of each serial dilution in the chosen sequential dilutions were determined using Equation 3.1.

$$\text{Undiluted spore concentration} = \left(\frac{5\times10^7}{\text{Average absorbance}}\right)\times \text{Serial dilution} \qquad \textbf{3.1}$$

For example, the 1x serial dilution had an average absorbency of 1.033, therefore:

$$\text{Undiluted spore concentration} = \left(\frac{5\times10^7}{1.033\times0.8}\right)\times1$$

$$\text{Undiluted spore concentration} = 3.87\times10^6 \text{ spores/ml}$$

The spore concentration (C_1) of the spore stock solution was determined by averaging the undiluted spore concentrations calculated using Equation 3.1, the undiluted spore stock

solution was calculated to be $C_1 = 3.69 \times 10^7$ spores/ml. From literature (Keiser *et al.*, 2000) the standard spore concentration utilised when inoculating with *Streptomyces* species is 1 x 10^7 spores/ml. Equation 3.2 was utilised to determine the dilution of the spore stock solution required.

$$\text{Dilution of spore stock solution} = \left(\frac{\text{Desired concentration } (C_2)}{\text{Spore concentration you have } (C_1)} \right) \qquad \textbf{3.2}$$

The dilution desired was the standard spore concentration, therefore $C_2 = 1 \times 10^7$ spores/ml.

$$\text{Dilution of spore stock solution} = \left(\frac{1 \times 10^7}{3.69 \times 10^7} \right)$$

$$\text{Dilution of spore stock solution} = 0.27 \text{ dimensionless}$$

Utilising Equation 3.5 the volume (V) of 20% glycerol to be added to the undiluted spore stock solution to obtain a concentration of 1 x 10^7 spores/ml was calculated. Equation 3.3 is known to be true. The volume of undiluted spore stock solution is represented by (V_1).

$$V_1 C_1 = V_2 C_2 \qquad \textbf{3.3}$$

Therefore:

$$V_1 = \frac{V_2 C_2}{C_1} \qquad \textbf{3.4}$$

$$V_1 = \left(\frac{(20) \times (1 \times 10^7)}{3.69 \times 10^7} \right)$$

$$V_1 = 5.42 \text{ ml}$$

$$V = V_2 - V_1 \qquad \textbf{3.5}$$

$$V = 20 - 5.42$$

$V = 14.58$ ml

The final volume(V_2) of the diluted spore stock solution was chosen to be 20 ml. V_1 was determined to be 5.42 ml. From Equation 3.5 it was determined that 14.58 ml of 20% glycerol was required to be added to 5.42 ml of the undiluted spore stock solution and 0.1% Tween 80 solution to obtain a final concentration of 1 x 10^7 spores/ml.

The microtitre plate was read on a microtitre plate reader (FLUOstar OPTIMA BMG LABTECH) at a wavelength of 450 nanometres (nm). For a spore concentration of 1 x 10^7 spores/ml at a wavelength of 450 nm in a 1 cm cuvette with a path length of 0.8 the absorbance should be 0.03 (Keiser *et al.*, 2000). Glycerol (20% w/v, final concentration) was added to the spore stock suspension which was stored at -80°C in 1 ml aliquots, (~10^7 spores/ml). The 20% glycerol solution allowed the spores to be stored at -80°C without being damaged.

3.5.2 Inoculum preparation for the inoculation of a SFMGR reactor

Working under a sterile laminar flow hood, 40 ml ISP2 medium was transferred to sterile autoclaved flasks sealed with a cotton wool bung and aluminium foil. After defrosting a frozen 1 ml cryo-tube containing the spore stock solution and ensuring the contents was well mixed, 100 µl of the spore stock solution was transferred to each flask with the aid of a Gilson pipette (i.e. 1 x 10^6 spores per flask). The culture flasks were then incubated in a shaker-incubator for 3 days at 27°C and 200 rpm. The 1 x 3 SFMGR rig required 2 inoculated flasks, while 3 flasks had to be inoculated for the 1 x 12 SFMGR rig.

$$\frac{1\times10^7 \text{ spores}}{1\,\text{ml}} = \frac{1\times10^7 \text{ spores}}{1000\,\mu\text{l}}\left(\frac{\div 100}{\div 100}\right) = \frac{1\times10^6 \text{ spores}}{100\,\mu\text{l}}$$

3.5.3 Testing to ensure the inoculum was free of contamination

All inoculum was checked for contamination before a reactor was inoculated. After the culture flasks were removed from the shaking-incubator, using sterile techniques under the laminar flow hood, 100 µl of the inoculum was placed in the centre of a glass slide with the aid of a Gilson pipette. The inoculum was heat fixed to the glass slide by passing the glass slide through the flame of a Bunsen burner until all the liquid had evaporated off the glass slide.

Note: Ensure the glass slide is not held in the flame for too long, as this would cause the glucose present in the growth medium to caramelise, resulting in artefacts when looked at the slide under the microscope.

Once the inoculum sample was heat fixed on the glass slide, the slide was stained with the Gram stain using the method described below:

1. Cover the glass slide with Crystal Violet for 30 sec.
2. Rinse off the Crystal Violet with distilled water.
3. Cover the glass slide with Iodine for 1 min.
4. Wash off the Iodine with 70% ethanol for 20 sec.
5. Rinse off the 70% ethanol with distilled water.
6. Cover the slide with Saffrine for 30 sec.
7. Rinse off the Saffrine with distilled water.
8. Dry the slide carefully with paper towel.

The stained slide was then observed under a microscope, first under the 10x/0.25x magnification and then under the 100x oil immersion magnification.

Note: If the inoculum was uncontaminated purple mycelia would be visible under the microscope. The presence of pink or purple rods (bacilli) or dots (cocci) would indicate contamination.

3.5.4 Inoculation procedure

Under the laminar flow hood a sterile syringe, to which a needle had been attached, was filled with the uncontaminated inoculum and the rig being utilised was prepared for inoculation. Utilising the pressure regulator the pressure of the air entering the rig from the compressor was increased to 100 kPa. The CN40 temperature controller was used to adjust the temperature to 28°C; while the respective JCS Shinko controllers for the extracapillary space (ECS) and growth medium were in the off position. All tubing exiting the reactors were clamped off as close as possible to the reactor, with Hoffman clamps being utilised to close off the ECS lines.

After spraying the tubing of the inoculation line with 70% ethanol, the needle attached to the sterile syringe containing the uncontaminated inoculum was flamed in a Bunsen burner until red hot. 2 ml of the inoculum was then injected into the inoculation line. Prior to injection, the content of the syringe was well mixed. Once the needle was removed from the inoculation line, the line was sealed off with two cable ties and sprayed with 70% ethanol.

Once all the reactors had been inoculated, the JCS Shinko controller of the medium was switched on; the vent attached to the humidifier opened; the Hoffman clamps closing the ECS lines opened; the clamps closing the medium lines opened and all the reactors primed. When a reactor was completely filled with medium, the ECS line, medium line and humidifier vent were all re-clamped and the JCS Shinko controller of the growth medium switched off. The contents of all the reactors, the 2 ml of inoculum together with the added medium, was mixed by tilting the reactor back and forth and allowing the air bubble present in the reactor to mix the contents. Once sufficiently mixed the JCS Shinko controller of the ECS was switched on and the pressure increased to 80 kPa; the Hoffman clamp on both the ECS and prime lines were removed allowing the reactor's contents to drain.

When all the reactors were drained of their contents the clamps closing off the permeate lines were removed; the ECS pressure decreased to the calculated set value using the JCS Shinko controller; the prime lines were re-clamped; the were clamps removed from the medium lines feeding the reactors and the JCS Shinko controller of the medium switched on and adjusted to the calculated set value. All the reactors were then primed until bubble free medium passed through the prime line to remove any air bubbles present in the lumen of the membranes and medium lines.

3.6 Experimental procedures

3.6.1 Nutrient flow rate and air flow rate

After sterilisation, the nutrient medium was supplied to the membrane lumen, in dead end flow, at a flow rate of 0.001 L/hr. Humidified air was supplied to the ECS of the bioreactor at a flow rate of 2.4 L/hr. Using pressure transducers, a pressure differential was created within the system by applying pressure to both the nutrient medium and the humidifier. The pressure applied to the nutrient medium was higher than the pressure applied to the humidifier to ensure transmembrane flux occurred. Two JCS Shinko controllers (PID) were used to display the set pressure and actual pressure of the nutrient medium and ECS, respectively.

3.6.2 Bioreactor operation

As shown in Figure 3.4, three vertically orientated manifolded SFMGR's, operated under pressure, were used to culture the bacteria, *S. coelicolor*, at 28 °C on the external surface of the capillary ceramic membrane. The airlines to the ECS of each reactor were manifolded from a single humidifier; therefore all three SFMGR's had the same air source. The pressure applied to the media bottle of each reactor was also manifolded from the same source.

A pneumatic bioreactor system can be operated in one of two ways; either via flux control or via pressure control (Defrance & Jaffrin, 1999). The pneumatic MGR system in this study was operated via pressure control. The pressures at which the ECS (i.e. air) and the medium were set were determined during the control run (see section 3.3.5.2). A schematic diagram of the pressurised SFMGR is shown in Figure 3.5, the ceramic membrane dimensions and SFMGR system parameters are shown in Table 3.9, respectively.

Table 3.9: SFMGR system parameters

Model parameter	Symbol	Unit	Basic measured value
Membrane initial hydraulic permeability	k_m	m/Pa.s	6.95×10^{-10}
Fraction retentate	f		0
Membrane inner radius	R_L	m	9.0×10^{-4}
Membrane outer radius	R_x	m	1.4×10^{-3}
Pitch	R_2	m	3.95×10^{-3}
Glass manifold inner radius	R_3	m	6.5×10^{-3}
Glass bioreactor length	L_b	m	2.09×10^{-1}
Effective membrane length	L_m	m	1.939×10^{-1}
Inlet hydrostatic pressure	p_0	Pa	$53.0 \pm 0.5 \times 10^3$
Outlet hydrostatic pressure	p_1	Pa	$52.0 \pm 0.5 \times 10^3$
Growth medium flow rate	Q	m^3/s	2.78×10^{-10}
Growth medium viscosity	μ_g	Pa.s	1.2×10^{-3}

3.6.3 Experimental overview

Tables 3.10 to 3.13 show an overview of all the experimental procedures conducted in the various rigs; including the time duration of the experiments, the growth medium, size and

amount of ceramic membranes utilised, as well as the pressure differential at which the system was operated.

Table 3.10: 1 x 3 SFMGR rig

Experiment	Duration	Growth medium	Membranes utilised	Pressure differential
1	28 days	ISP2 growth medium	3 mm x 2 mm (Small ceramic membrane)	Continually adjusted pressure differential to maintain a flux of 0.708 $L/m^2.hr$
2	28 days	ISP2 growth medium for 163 hr, Hobbs defined nutrient medium for 163 to 499 hr, ISP2 growth medium for 499 to 667 hr	4 mm x 3 mm (Large ceramic membrane)	1 kPa for the first 24 hr, 3.5 kPa for the remainder of the experiment
3	28 days	ISP2 growth medium	4 mm x 3 mm (Large ceramic membrane)	1 kPa for the first 24 hr, 3.5 kPa for the remainder of the experiment
4	14 days Fouling experiment	ISP2 growth medium	3 mm x 2 mm (Small ceramic membrane)	1 kPa for the first 24 hr, 3.5 kPa for the remainder of the experiment

Table 3.11: 1 x 12 SFMGR rig

Experiment	Duration	Growth medium	Membranes utilised	Pressure differential
1	18 days	ISP2 growth medium	3 mm x 2 mm (Small ceramic membrane)	Adjusted pressure differential to maintain a flux of 0.708 L/m^2.hr
2	18 days	ISP2 growth medium	3 mm x 2 mm (Small ceramic membrane)	1 kPa for the first 24 hr, 3.0 kPa for the remainder of the experiment
3	28 days	ISP2 growth medium	3 mm x 2 mm (Small ceramic membrane)	1 kPa for the first 24 hr, 3.0 kPa for the remainder of the experiment
4	28 days	ISP2 growth medium	3 mm x 2 mm (Small ceramic membrane)	1 kPa for the first 24 hr, 3.0 kPa for the remainder of the experiment
5	6 days	ISP2 growth medium	3 mm x 2 mm (Small ceramic membrane)	1 kPa for the first 24 hr, 3.0 kPa for the remainder of the experiment
6	17 days	ISP2 growth medium	3 mm x 2 mm (Small ceramic membrane)	1 kPa for the first 24 hr, 3.0 kPa for the remainder of the experiment

Table 3.11: 1 x 12 SFMGR rig

Experiment	Duration	Growth medium	Membranes utilised	Pressure differential
1	18 days	ISP2 growth medium	3 mm x 2 mm (Small ceramic membrane)	Adjusted pressure differential to maintain a flux of 0.708 L/m^2.hr
2	18 days	ISP2 growth medium	3 mm x 2 mm (Small ceramic membrane)	1 kPa for the first 24 hr, 3.0 kPa for the remainder of the experiment
3	28 days	ISP2 growth medium	3 mm x 2 mm (Small ceramic membrane)	1 kPa for the first 24 hr, 3.0 kPa for the remainder of the experiment
4	28 days	ISP2 growth medium	3 mm x 2 mm (Small ceramic membrane)	1 kPa for the first 24 hr, 3.0 kPa for the remainder of the experiment
5	6 days	ISP2 growth medium	3 mm x 2 mm (Small ceramic membrane)	1 kPa for the first 24 hr, 3.0 kPa for the remainder of the experiment
6	17 days	ISP2 growth medium	3 mm x 2 mm (Small ceramic membrane)	1 kPa for the first 24 hr, 3.0 kPa for the remainder of the experiment

Table 3.12: 28x Ceramic membrane MFR rigs

Experiment	Duration	Growth medium	Membranes utilised	Pressure differential
1	36 days	29 days ISP2 nutrient medium, 8 days ISP2 growth medium with 25% glucose and malt extract, 8 days ISP2 growth medium with 25% glucose	28x (3 mm x 2 mm) Small ceramic membranes	Pressure differential was adjusted by an automated computer program to maintain a flux of 0.506 L/m^2.hr
1	36 days	29 days ISP2 growth medium, 8 days ISP2 growth medium with 25% glucose and malt extract, 8 days ISP2 growth medium with 25% glucose	28x (4 mm x 3 mm) Large ceramic membrane	Pressure differential was adjusted by an automated computer program to maintain a flux of 0.337 L/m^2.hr

Table 3.13: Oxygen experiments conducted in the 1 x 3 SFMGR Quorus rig

Experiment	Duration	Microsensor location	Growth medium	Membranes utilised	Pressure differential
1	5 days	Bottom oxygen port	ISP2 growth medium	3 mm x 2 mm (Small ceramic membrane)	1 kPa for the first 24 hr, 3.0 kPa for the remainder of the experiment
2	7 days (Test run)	Bottom oxygen port	ISP2 growth medium	3 mm x 2 mm (Small ceramic membrane)	1 kPa for the first 24 hr, 3.0 kPa for the remainder of the experiment
3	7 days (Control run) 21 days (Experiment)	Middle oxygen port	ISP2 growth medium	3 mm x 2 mm (Small ceramic membrane)	1 kPa for the first 24 hr, 1.5 kPa for the remainder of the experiment
4	45 days 47 days 48 days	Middle oxygen port	ISP2 growth medium	3 mm x 2 mm (Small ceramic membrane)	1 kPa for the first 24 hr, 2.5 kPa for the remainder of the experiment
5 (repeat of experiment 4)	24 days	Middle oxygen port	ISP2 growth medium	3 mm x 2 mm (Small ceramic membrane)	1 kPa for the first 24 hr, 2.5 kPa for the remainder of the experiment

3.6.4 Sampling

Permeate from each SFMGR was collected and analysed daily. The amount of permeate collected daily was dependent on the pressure differential and the resistance to transmembrane flux by the biofilm. When collecting permeate from the respective bottles the silicone tubing connecting the reactor to the permeate collection bottle was clamped off with a Hoffman clamp. The sample line attached to the permeate collection bottle was opened and permeate flushed out by the residual pressure remaining in the permeate collection bottle. Once the bottle was empty the sample line was re-clamped and the Hoffman clamp on the line connecting the reactor to the permeate collection bottle slowly released until the pressure in the reactor and the permeate bottle had equalised. The attachment of the Hoffman clamp to the silicone tubing prevented a sudden decrease in pressure within the system and decreased the risk of the biofilm being sloughed off the membrane.

3.6.5 Disconnecting of reactors

Prior to starting an experiment it was decided in which order to disconnect the reactors. Once a reactor had run for its predetermined time duration, the reactor was disconnected. All silicone tubing exiting the reactor was sealed with cable ties. Using diagonal pliers the silicone tubing on the side closest to the reactor was cut and the reactor and its ancillaries removed from the rig. 70% Ethanol was sprayed on the ends of the cut silicone tubing.

After removing the membrane and biofilm from the reactor, the empty reactor and its ancillaries were decontaminated by autoclaving, at 121 °C for 20 min. The silicone tubing and cable ties were removed from the decontaminated reactor and ancillaries, with diagonal pliers, and discarded. The reactor and its ancillaries were then washed, dried and stored, ready for re-use.

3.6.6 Decontamination of the 1 x 3 and 1 x 12 SFMGR rigs

After all the reactors in a rig were disconnected, the JCS Shinko controllers for both the growth medium and ECS were switched off, the pressure regulator decreased to zero, the temperature controller switched off and the entire rig decontaminated with biocide.

3.7 Biofilm analysis

After a reactor was disconnected the membrane with wet biofilm attached within the reactor were carefully removed from the reactor's glass housing manifold. A calibrated Vernier calliper and a specially constructed stand was then utilised to measure the biofilm thickness at the top and bottom of the wet biofilm at a distance of 3 cm from both ends of the membrane. Since the diameter of the ceramic membranes utilised was known, the biofilm thickness could be calculated by subtracting the diameter of the membrane from the measured wet biofilm thickness and dividing the result by 2.

Once the top and bottom diameters of a wet biofilm had been measured and recorded, the membrane and wet biofilm was placed in an empty test tube on known weight. The weight of the test tube, membrane and wet biofilm was then determined and recorded. After drying overnight (i.e. 12 hr) in an oven at 70 °C, the weight of the test tube, membrane and dry biofilm was determined and recorded.

Before starting with an experimental procedure the membranes that were to be utilised were weighed and their weights recorded. Since the weight of both the membrane and empty test tube was known, the weight of the wet and dry biofilm could be determined.

3.8 Sample analysis

After the volume, pH and redox potential of a permeate sample had been measured and recorded, a small amount, approximately 3 ml, of the sample was transferred to an eppendorf tube and stored in the refrigerator at 4°C until the actinorhodin, glucose and phosphate assay could be performed.

3.8.1 Volume

The volume (ml) of permeate collected daily into a centrifuge tube from each reactor was measured and recorded. The permeate volume was calculated by subtracting the mass of the empty centrifuge tube, weighed prior to the start of the experimental procedure; from the mass of the centrifuge tube filled with collected permeate. The volume of permeate collected had to be calculated as this was used to determine the rate at which nutrients was supplied to the biofilm. After use the centrifuge tube was sprayed with 70% ethanol and rinsed with distilled water for re-use the following day.

3.8.2 pH and redox potential

The pH and redox potential (mV) of all permeate samples collected daily was measured with a Cyberscan 2500 pH meter and recorded, as the pH and mV profiles of the cell free permeate can be used to track the metabolic activity of the *S. coelicolor* biofilm. Prior to use at the start of each day the pH meter was calibrated with buffer solutions (supplied by Kimix, Cape Town, South Africa), one with a pH of 4.0 the other with a pH of 7.0, to ensure the pH meter was giving accurate pH and mV readings.

3.9 Assays

The assays in section 3.9.1, 3.9.2 and 3.9.3 were conducted on all permeate samples in order to determine which growth medium component had the largest effect on actinorhodin production. Substrate utilisation profiles could be calculated from the level of residual substrate present in the permeate samples. Thus allowing the component that negatively effects actinorhodin production to be decreased or eliminated, and the component that positively effects actinorhodin production to be increased. This allows for process optimisation and thus increased secondary metabolite production, in this case, actinorhodin.

3.9.1 Actinorhodin assay

Actinorhodin concentrations (total blue pigment), in milligrams per litre (mg/L) were determined as described by Doull and Vining (1990) and utilised by De Orduña and Theobald (2000). After centrifuging the permeate samples at 4000 rpm for 10 min, to remove suspended cells and other solids, equal volumes (600 µl) of supernatant and 2 M NaOH were added together in a one to one ratio. The absorbance of the supernatant was measured

at 640 nm in triplicate on a microtitre plate reader (Fluostar Optima supplied by BMG Labtech, Milnerton, Cape Town). The final actinorhodin concentration was calculated using an extinction coefficient ($E_{1\%,1cm}$ = 355 $g^{-1}.L.cm^{-1}$) as given by Doull and Vining (1990). Crude actinorhodin levels present in the permeate was monitored spectrophotometrically as described in Appendix A.

3.9.2 Glucose assay

The reducing sugar content (i.e. glucose concentration) of the permeate samples was determined using the dinitrosalicylic acid method (Miller, 1959; Choi *et al.*, 2001) on a microtitre plate reader (Fluostar Optima supplied by BMG Labtech, Milnerton, Cape Town). The absorbance of the supernatant was measured in triplicate, at a wavelength of 590 nm, for each permeate sample collected from each reactor. An average was then calculated for each day from the data obtained. The concentration of glucose was calculated from the absorbance values obtained from the assay, and a linear correlation determined from the respective standard curves. The glucose assay was conducted on all samples to test for glucose consumption or utilisation by the bacteria and the resulting effect on biofilm development and secondary metabolite production. Refer to Appendix B for the glucose assay procedure.

3.9.3 Phosphate assay

The phosphate concentration within the permeate samples was measured using the ascorbic assay method (Chen *et al.*, 1956; Plisova *et al.*, 2005). The absorbance, measured in triplicate for all permeate samples on a microtitre plate reader (Fluostar Optima supplied by BMG Labtech, Milnerton, Cape Town), was determined at a wavelength of 650 nm (see Appendix C for the phosphate assay procedure). The concentration of phosphate was calculated from the absorbance values obtained from the assay conducted, and a linear correlation determined from the respective standard curves. The phosphate assay was conducted on each sample collected from each reactor to test for phosphate consumption or utilisation from the growth medium. The phosphate assay indicated how the presence or absence of phosphate in the growth medium affected secondary metabolite production. An average was then calculated for each day from the data obtained.

CHAPTER 4

RESULTS

GROWTH MEDIUM COMPARISON USING CULTURE FLASKS

CHAPTER FOUR

GROWTH MEDIUM COMPARISON USING CULTURE FLASKS

4.1 Introduction

Growth media can be divided into two categories: complex and defined. In a defined growth medium each component present in the medium is known, as well as the quantity of the component to be used in the medium preparation. In a complex growth medium not all the components are known since extracts, such as malt extract, are utilised and not all the components present in the extract are defined. A complex medium provides the micro organism being cultured with the basic components required to survive, such as carbon in the form of glucose.

4.1.1 Background

According to Ozergin-Ulgen and Mavituna (1994) researchers utilise defined growth medium in batch and fed-batch cultures although, complex growth medium is preferred when working with *S. coelicolor*. Complex growth medium results in higher biomass yields and product concentrations, as well as the presence of suspended solids which interferes with the dry weight measurements of the biomass (Ozergin-Ulgen & Mavituna, 1994).

4.1.2 Objectives

The primary aim of this part of the study was to determine in which growth medium the filamentous bacterium *S. coelicolor* displayed optimum growth and secondary metabolite production (i.e. actinorhodin).

The objectives for this part of the study were to:

- Compare *S. coelicolor* growth using two growth media (complex and defined).
- Quantify and compare the production of actinorhodin in the two growth media.

4.2 Materials and methods

Three culture flasks containing complex growth medium and three culture flasks containing defined growth medium were inoculated with the *Streptomyces* strain *S.coelicolor* A3(2) (prepared as explained in section 3.5.1) and incubated to observe the micro organism's response to the different growth media. The micro organism was maintained as a frozen spore suspension in 20% glycerol at a temperature of -80 °C.

4.2.1 Culture flask preparation and incubation

Six sterile culture flasks were utilised in this experimental procedure: (1) three culture flasks contained 40 ml of the sterile complex growth medium International *Streptomyces* Project, medium 2 (ISP2) as described by Shirling & Gottlieb (1966) (refer to Table 3.3 in section 3.4 for the preparation procedure); and (2) three culture flasks contained 40 ml sterile defined media as described by Hobbs *et al.* (1989) (refer to Tables 3.4 and 3.5 in section 3.4 for the preparation procedure). Each of the six flasks was inoculated with 100 µl of the defrosted spore suspension with a concentration of 1×10^7 spores/ml (i.e. 1×10^6 spores/flask). The six inoculated culture flasks were incubated in a shaker-incubator for 192 hr at 27°C and 200 rpm.

4.3 Analytical methods

The actinorhodin concentration described by Doull and Vining (1990), of each culture flask was determined daily, in order to quantify the secondary metabolite production. Refer to Appendix A for a detailed actinorhodin assay procedure description.

4.4 Results and discussion

A culture sample was taken from each of the six culture flasks daily. With the aid of Sigma Plot (Version 8) the actinorhodin assay results for the three culture flasks with the same growth medium were averaged and the standard error for each point determined. The standard error bars represent the spread of data for a particular point around the average value calculated for that point, as shown in Figure 4.1.

4.4.1 Actinorhodin production in ISP2 complex growth medium versus Hobbs defined growth medium

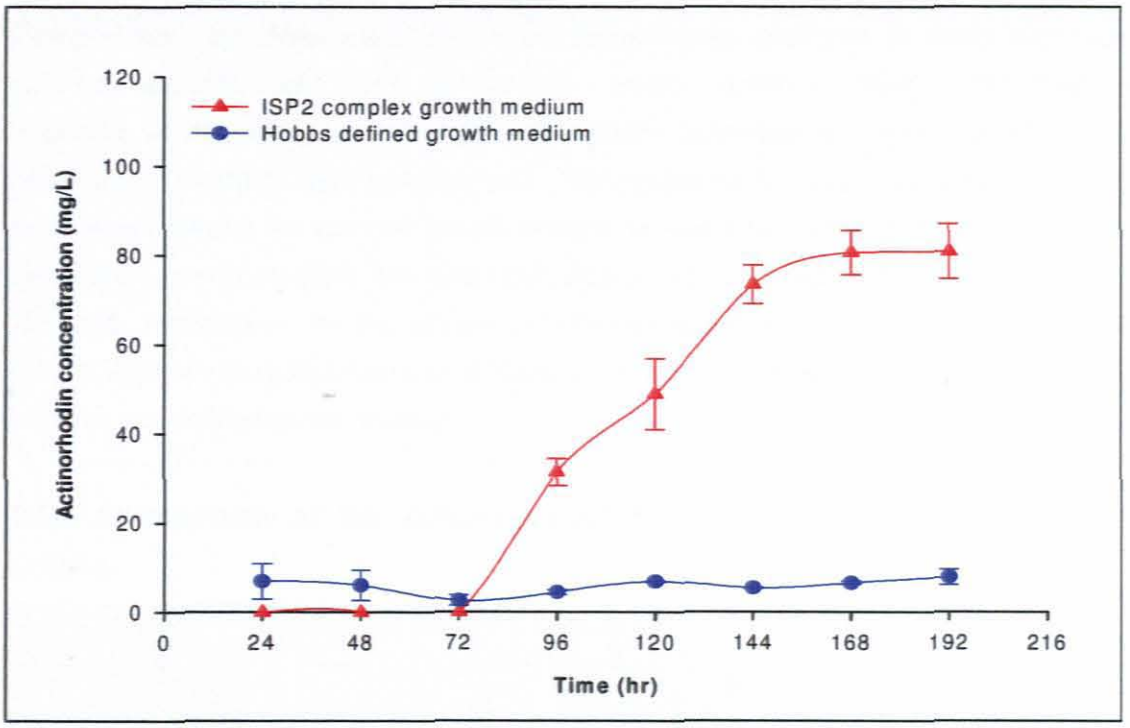

Figure 4.1: Actinorhodin production in ISP2 complex growth medium versus Hobbs defined growth medium (The error bars represent the standard error using Sigma Plot 8.0)

Figure 4.1 indicates that the complex growth medium, ISP2, produced higher concentrations of the secondary metabolite (i.e. actinorhodin). Using the ISP2 complex growth medium, actinorhodin production increased from 0 to 86.9 mg/L over 192 hr, while actinorhodin production remained consistent at approximately 6.2 mg/L for the Hobbs defined growth medium. In Figure 4.1, using ISP2 growth medium the actinorhodin production started around 72 hr after inoculation and accumulated over time. The maximum actinorhodin concentration obtained was 86.9 mg/L and 7.7 mg/L, with ISP2 and the defined growth medium, respectively. The maximum actinorhodin concentration obtained with the complex growth medium was approximately eleven times higher than the maximum concentration obtained with the defined growth medium. Although the biomass was not measured, it was observed that a higher concentration of culture pellets formed in the flasks inoculated with ISP2 complex growth medium compared to the flasks containing the Hobbs defined growth medium. The higher actinorhodin production using ISP2 complex growth medium was therefore attributed to the higher biomass observed in the culture flasks.

According to Ates *et al.* (1997), for batch fermentations the maximum actinorhodin concentration attained, also using the defined growth medium described by

Hobbs *et al.* (1989), after ±115 hr was 28.5 mg/L. At ±115 hr the actinorhodin concentration obtained using the defined growth medium during this study was approximately 6.8 mg/L.

Ozergin-Ulgen and Mavituna (1994) grew *Streptomyces coelicolor* in freely suspended cultures operated with both a complex growth medium, YEME, described by Hopwood *et al.* (1985) and the defined medium described by Hobbs *et al.* (1989). According to Ozergin-Ulgen and Mavituna (1994) actinorhodin production was 50 times as much when utilising the complex growth medium as when compared to the production with the defined growth medium. The maximum actinorhodin concentration was 2.12 mg/L and 125 mg/L, respectively, for the defined and complex growth media in the freely suspended culture. Actinorhodin was excreted extracellularly in the freely suspended culture for both the complex and defined growth media.

4.4.2 Comparison of the culture media after actinorhodin production has started

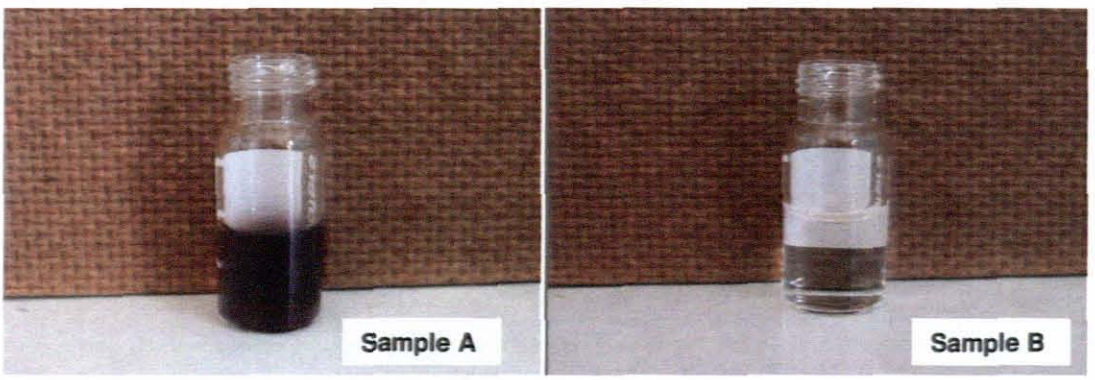

Figure 4.2: Actinorhodin production culture sample comparison. (A) ISP2 complex growth medium and (B) Hobbs defined growth medium

In Figure 4.2, sample A represents the actinorhodin production when ISP2 complex growth medium was used. This growth medium was initially yellow in colour and as actinorhodin production increased the colour of the growth medium in the culture flasks changed to pink and eventually dark purple. After inoculation the culture pellets changed from white in colour to yellow for the duration of the experimental procedure. Sample B in Figure 4.2, represents the actinorhodin production when the Hobbs defined growth medium was utilised. This medium started out clear in colour and remained clear in colour up to ±120 hr, after which the growth medium in the culture flasks developed a slight dark blue tinge and the culture pellets became pink in colour. According to Ozergin-Ulgen and Mavituna (1994) actinorhodin should be navy blue in the defined growth medium and dark purple in the complex growth medium.

was not tested therefore it is unknown if these were being produced as the secondary metabolite instead of actinorhodin.

From literature it can be assumed that when utilising a defined growth medium in a freely suspended culture, most of the product formation is intracellular. However, when utilising a complex growth medium with a pH close to neutral and the product is dark blue-purple in colour, it can be assumed that product formation is both intracellular and extracellular. *The lactone derivative γ-actinorhodin accounts for the dark blue/purple colour of the product* and indicates that γ-actinorhodin is extracellular while actinorhodin is produced intracellularly.

From their studies Doull and Vining (1990) concluded that a decrease in the growth rate triggered actinorhodin production. While Hobbs *et al.* (1990) concluded that actinorhodin is mainly produced during the stationary phase and that production is sensitive to both ammonium ions and phosphate to a lesser extent. From the Luedeking-Piret model Ozergin-Ulger and Mavituna (1993) found that actinorhodin production was growth-associated with growth rate being the dominant parameter. According to Bystrykh *et al.* (1996) the depletion of glucose stops pigment synthesis, while the depletion of other nutrients, such as ammonium or nitrate, phosphate and trace elements resulted in pigment synthesis (Melzoch *et al.*, 1997). Actinorhodin is produced by actively growing cells, in nitrogen- or carbon-limited cultures; with the highest specific production rate occurring at the intermediate growth rate in carbon-limited cultures (Melzoch *et al.*, 1997).

4.5 Summary

From the experiments conducted during this section of the study, the complex growth medium, ISP2 yielded higher biomass as well as secondary metabolite concentrations when compared to the defined growth medium described by Hobbs *et al.* (1989).

It can be concluded that when the main objective is to stimulate the production of high concentrations of the secondary metabolite, actinorhodin by *Streptomyces coelicolor* then ISP2 complex medium is the growth medium of choice. However, when the calculation of kinetic parameters is priority and not secondary metabolite production the Hobbs *et al.* (1989) defined medium is the recommended growth medium.

In Chapter 5 both ISP2 complex growth medium and Hobbs et al. (1989) defined growth medium were used, in order to compare biofilm growth in a continuously operated MGR. In Chapters 6 to 8 the ISP2 complex growth medim was utilised. However, in Chapter 7 variations of ISP2 growth medium were used as well.

CHAPTER 5

RESULTS

SUBSTRATE CONSUMPTION KINETICS AND ACTINORHODIN PRODUCTION USING CONTINUOUS PRESSURISED SINGLE FIBRE MEMBRANE GRADOSTAT REACTORS (SFMGR)

PUBLICATION:

De Jager, D., Sheldon, M.S. & Edwards, W. 2009. Modelling growth kinetics of *Streptomyces coelicolor* A3(2) in a pressurised membrane gradostat reactor (MGR). *Enzyme and Microbial Technology*, 45:449-456.

CHAPTER FIVE

SUBSTRATE CONSUMPTION KINETICS AND ACTINORHODIN PRODUCTION USING CONTINUOUS PRESSURISED SINGLE FIBRE MEMBRANE GRADOSTAT REACTORS (SFMGR)

5.1 Introduction

Secondary metabolism is suppressed when a micro organism is growing at its full potential under optimum conditions. In order to optimise secondary metabolite production certain nutrients, such as glucose, a carbon source for *Streptomyces coelicolor* A3(2), is limited resulting in increased actinorhodin production.

5.1.1 Background

Quantitative characterisation of the activity of an enzyme or microbe on a particular substrate is an essential requirement for the detailed understanding of the dynamics of any process (Goudar & Devlin, 2001). The quantification process involves estimating several parameters in the kinetic models using experimental data. A simple unstructured kinetic model is used to describe the interaction between the substrate and the enzyme or microbe (Gouder & Devlin, 2001). Substrate utilisation by a micro organism normally results in the removal of a chemical contaminant, increase in microbial biomass and the subsequent biodegradation of the contaminant. Several microbial growth and biodegradation kinetic models exist (Okpokwasili & Nweke, 2006). The growth limiting substrate concept was introduced by the Monod model. In continuous cultures the limiting nutrient is the substrate controlling or limiting the growth of the micro organism, while in batch systems the limiting nutrient refers to the substrate that limits the extent of growth of the culture (Bazin, 1982).

Substrate depletion by enzymes and non-growing bacterial suspensions are generally described by the Michaelis-Menten equation, while the Monod equation generally describes growth associated substrate consumption (Goudar & Devlin, 2001). The Monod empirical equation (refer to Equation 2.7a in section 2.3.4.1) defines the relationship between the growth rate and the concentration of the limiting nutrient. An important feature of this model is that the growth rate is zero when there is no substrate and when the substrate is in excess the growth rate tends to the upper limit (Lobry *et al.*, 1992).

$$\mu = \frac{\mu_{max} C_s}{K_m + C_s} \qquad \textbf{2.7a}$$

Where μ represents the specific growth rate (hr^{-1}); μ_{max} represents the maximum specific growth rate (hr^{-1}); C_s represents the substrate concentration (g/m^3) and K_m the Monod saturation constant (g/m^3), which is equivalent to the substrate concentration at half μ_{max} (Okpokwasili & Nweke, 2006).

A method commonly utilised to express the kinetic constants is the Monod equation, derived from the Michaelis-Menton hypothesis, previously described by Equation 2.8 in section 2.3.4.1 (Shuler & Kargi, 2002).

$$r_B = \frac{r_m C_s}{K_m + C_s} \qquad 2.8$$

Where C_s is the substrate concentration (g/m^3); r_B is the biological consumption rate ($g/m^3.hr$); r_m is the maximum substrate consumption rate ($g/m^3.hr$); and K_m the Monod saturation constant (Shuler & Kargi, 2002).

The Lineweaver-Burke (double-reciprocal plot) and Eadie-Hofstee methods are two linearisation techniques in which the hyperbolic relationship between the rate of the reaction and the substrate concentration is arranged linearly (Shuler & Kargi, 2002). According to Ntwampe (2005) for the MGR system the Lineweaver-Burke linearisation method gave the best fit with correlation coefficients (R^2) of 0.9 and higher.

The yield coefficient (refer to Equation 2.21 in section 2.3.4.6) describes the relationship between the biomass generated and the amount of substrate consumed to produce the biomass. The maintenance coefficient (refer to Equation 2.22 in section 2.3.4.6) describes the specific rate of substrate uptake for biomass maintenance when biomass production is negligible (Shuler & Kargi, 2002; Ntwampe & Sheldon, 2006).

5.1.2 Objectives

The primary aim of this part of the study was to determine whether the Monod single-substrate limited model could be fitted to this system.

The objectives of this study were to:

- Compare the effect of different growth media on microbial growth and secondary metabolite production within continuous systems.
- Quantify the substrate kinetics using ISP2 complex growth medium and Hobbs defined growth medium.
- Quantify actinorhodin production.

5.2 Materials and methods

Except for the type of growth medium and the size of ceramic membrane utilised, all the experiments were run under identical operating conditions (i.e. pressure, temperature and duration).

5.2.1 Micro organism

The micro organism used in this study was *Streptomyces coelicolor* A3(2) (Yul-Min & Jae-hoen, 2004), the model representative of a group of soil dwelling micro organisms. The micro organism was maintained as a frozen spore suspension in 20% glycerol at a temperature of -80°C, prepared as explained in section 3.5.1.

5.2.2 Inoculum preparation and inoculation

The inoculum was prepared and tested for contamination as explained in sections 3.5.2 and 3.5.3, respectively. Each single fibre membrane gradostat reactor (SFMGR) was inoculated as explained in section 3.5.4.

5.2.3 Growth medium

Two different growth media, a complex growth medium and a defined growth medium were used during the operation of the SFMGR's. The complex growth medium that was used was the International *Streptomyces* Project, medium 2 (ISP2) (Shirling & Gottlieb, 1966); refer to Table 3.3 in section 3.4 for the preparation procedure. The defined growth medium that was used was described by Hobbs *et al.* (1989); refer to Tables 3.4 and 3.5 in section 3.4 for the preparation procedure.

5.3 Experimental set-up

The new 1 x 3 single fibre membrane gradostat reactor (SFMGR) Quorus rig (see sections 3.1.2, 3.3 and 3.3.3 for the experimental set-up) was used to test the linearity between the three manifolded SFMGR's. Linearity was both qualified and quantified by immobilising the filamentous bacteria *S. coelicolor* A3(2) on the surface of the ceramic membranes.

The construction of a Single Fibre Membrane Gradostat Reactor (SFMGR) as patented by Edwards *et al.* (2007) was illustrated schematically in Figure 3.4 and explained in section 3.3.1. After the SFMGR was constructed the reactor with ceramic membrane was pressure tested to check their ability to withstand high pressures and that no leaks were present as explained in section 3.3.2. Three SFMGR's were then manifolded together with 5 mm (ID) by 8 mm (OD) silicone tubing, as shown in Figure 3.5 and explained in section 3.3.3.

A total of three experiments were performed. Two experiments were conducted utilising ISP2 complex growth medium; one with 3 mm x 2 mm ceramic membranes and the other with 4 mm x 3 mm ceramic membranes. The remaining experiment was conducted with Hobbs (1989) defined growth medium and 4 mm x 3 mm ceramic membranes. The two sizes of capillary ceramic membranes utilised are explained in Table 3.1 in section 3.2.1.

After inoculation, the nutrient medium was supplied to the membrane lumen, in dead end flow, as explained in section 3.6.1.

5.3.1 Bioreactor operation

Three vertically orientated SFMGR's operated under pressure utilising the MGR concept as patented by Leukes *et al.* (1999), were used to culture the bacteria, *S. coelicolor* A3(2), at 28°C on the external surface of the capillary ceramic membrane. The airlines to the ECS of each reactor were manifolded from a single humidifier, therefore all three SFMGR's had the same air source. The pressure applied to the medium bottle of each reactor was also manifolded from the same source.

A pneumatic bioreactor system can be operated in one of two ways; either via flux control or via pressure control (Defrance & Jaffrin, 1999). The pneumatic MGR system in this study was operated via pressure control, as seen in Figure 5.1. For the first 24 hr it was attempted to maintain the transmembrane pressure (TMP) at 1 kPa to allow the micro organism to adhere to the membrane surface. For the remainder of the study the medium and ECS were operated at pressures of 53.5 and 50 kPa, respectively, to attempt to maintain a transmembrane pressure (TMP) of 3.5 kPa. As the pressure differential was kept constant, the flux decreased over time as the biofilm increased in thickness and thus resistance to transmembrane flux increased. The flux started at a rate of ±0.708 and 0.472 $L/m^2.hr$ for the 3 mm (ID) X 2 mm (OD) and 4 mm (ID) x 3 mm (OD) ceramic membranes, respectively. The bioreactor system was operated for 28 days (±672 hr).

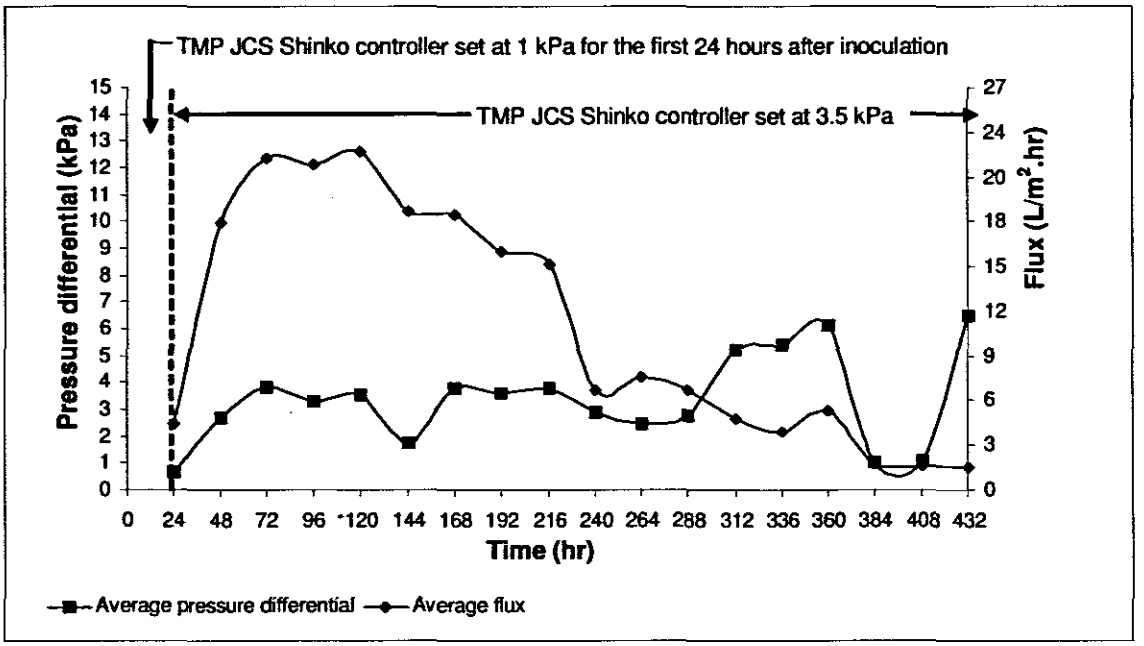

Figure 5.1: Plots of the permeate flux and the transmembrane pressure as functions of operation time for a pressure controlled SFMGR

Two experiments were operated using the International *Streptomyces* Project, medium 2 (ISP2) growth medium (Shirling & Gottlieb, 1966) for the duration of the experiment. One of these two experiments was run using 3 mm (OD) x 2 mm (ID) ceramic membranes, while the other was run using 4 mm (OD) x 3 mm (ID) ceramic membranes. A third experiment was first operated with ISP2 growth medium for ±163 hr, then with Hobbs (1989) defined growth medium until 499 hr, then again ISP2 growth medium until 667 hr, using the 4 mm (OD) x 3 mm (ID) ceramic membranes. ISP2 growth medium was utilised initially for ±163 hr to ensure a well established biofilm was present on the ceramic membrane of each reactor before changing to the defined growth medium.

5.4 Analytical methods

Permeate from each SFMGR was collected and analysed daily. The amount of permeate collected daily was dependent on the pressure differential and the resistance to transmembrane flux by the biofilm. The volume and pH of the permeate samples were measured and recorded daily, including the time elapsed between sampling; thus allowing the flux to be calculated for each SFMGR.

On completion of the experiments the wet biomass of each reactor was recorded, as well as the dry biomass, after the biofilm had been dried for 12 hr at 70°C in an oven. The biofilm thickness was measured, with a Vernier calliper, along the length of the membrane at 2 cm intervals after the bioreactor set-up was disconnected. It was not possible to determine the

thickness of the biofilm with a Fluorescence microscope as the biofilm was too thick (refer to section 3.7).

Actinorhodin concentrations were determined as described in section 3.9.1. Refer to Appendix A for a detailed description of the actinorhodin assay procedure. The glucose concentration of the permeate samples were measured as described in section 3.9.2. Refer to Appendix B for the detailed glucose assay procedure. The phosphate concentration within the permeate samples was measured as described in section 3.9.3. Refer to Appendix C for the detailed procedure of the phosphate assay. The concentration of both glucose and phosphate was calculated from the absorbance values obtained from the assays conducted, and a linear correlation determined from the respective standard curves.

5.5 Results and discussion

Three SFMGR's were used in each experiment. One permeate sample was taken from each bioreactor daily. The daily flux, pH, actinorhodin, glucose and phosphate results obtained from the three bioreactors were averaged (with the aid of Sigma Plot (Version 8)), for each of the three experiments and the standard error for each point determined. The standard error bars on the figures represent the spread of data for a particular point around the average value calculated for that point.

5.5.1 Average flux

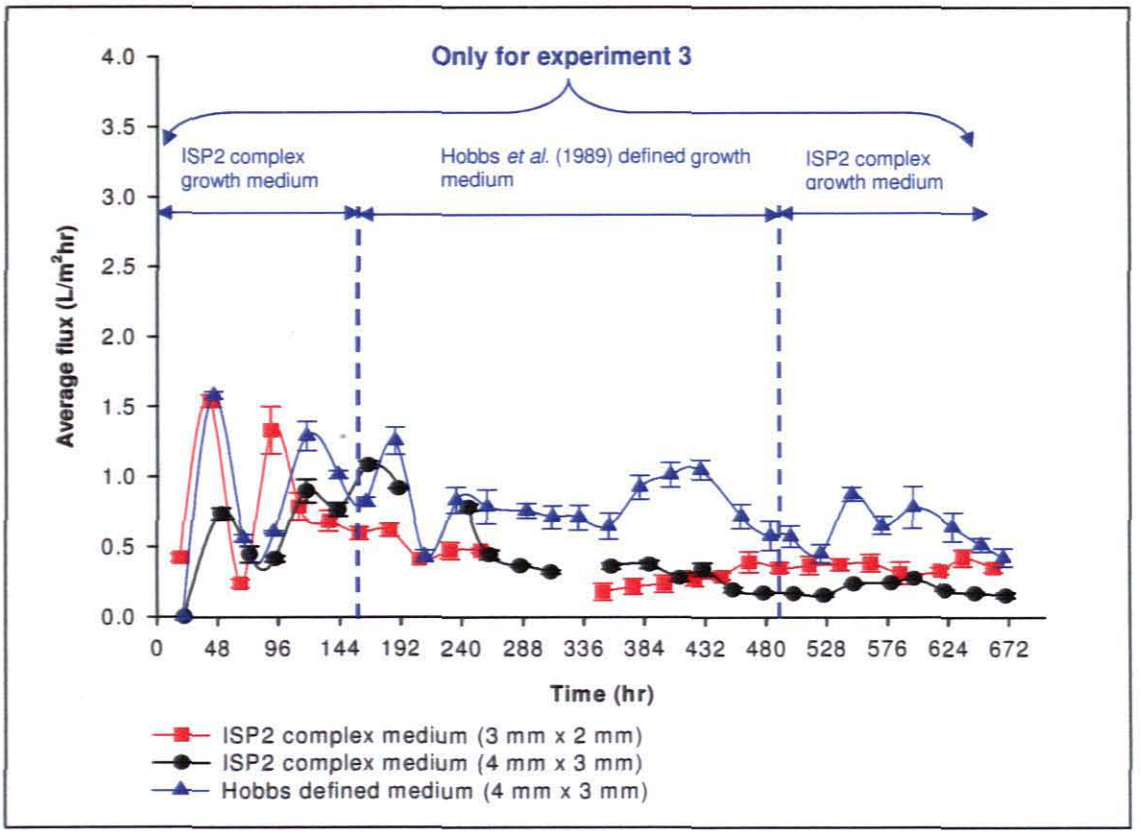

Figure 5.2: Average flux in the 1 x 3 SFMGR rig (The error bars represent the standard error using Sigma Plot 8.0)

Figure 5.2 is a plot of the average flux ($L/m^2.hr$) against time (hr), and indicates how the flux decreased over time when the TMP was kept constant, and a well established biofilm was present to provide increased resistance to flux as the biofilm thickness increased.

The curves in Figure 5.2 representing the ISP2 complex medium (3 mm x 2 mm and 4 mm x 3 mm) were both operated with the complex growth medium for the duration of the experimental procedure. The only difference being the size of the ceramic membranes utilised. The curve representing Hobbs defined medium (4 mm x 3 mm) was operated with ISP2 growth medium for the first 163 hr, then Hobbs defined growth medium for 163 to 499 hr, and ISP2 growth medium for 499 to 677 hr. The similarity between the three experimental procedures was that all three procedures were operated with ISP2 growth medium for the first 163 hr and the same pressure differential of 3 kPa. The difference between the ISP2 complex medium (4 mm x 3 mm) experiment and the Hobbs defined medium (4 mm x 3 mm) experiment was that different growth medium was utilised after 163 hr, but the same size ceramic membranes were utilised.

The low flux observed at 336 hr on the ISP2 comlpex medium (3 mm x 2 mm) curve occurred as a result of two interelated reasons: (1) the pressure differential was decreased to a value of 2 kPa; and (2) the well developed biofilm. The pressure differential was decreased to starve the biofilm, in order to stimulate secondary metabolite production.

The absent data point at 336 hr, for the ISP2 comlex medium (4 mm x 3 mm) curve was removed due to a power failure, which caused the medium to overflux. When the power failure occurred, the ECS pressure decreased to zero, while the medium pressure remained at its set pressure. As it was a closed system, a large pressure differential was thus established across the membrane, resulting in an extremely high transmembrane flux.

Figure 5.2 indicates that after 240 hr the flux became stable, due to the presence of a well established biofilm at this time. Slight variation occurred in the flux after 240 hr, due to the fact that the actual pressures of the medium and ECS varied slightly from the respective set pressures. This variation in pressures resulted in the pressure differential varying from the set 3.5 kPa, which influenced the transmembrane flux.

Similar flux was observed for both ISP2 complex medium curves, even though different sized ceramic membranes were utilised. A higher flux was observed for the Hobbs defined medium curve. During the study it was observed that after 163 hr when the growth medium had been changed from the complex medium to the defined medium, the biofilms decreased in thickness. The cause of the higher flux observed for the Hobbs defined medium, was due to the decreased biofilm thickness, which provided decreased resistance to transmembrane flux. 24 hr after changing the defined medium back to the complex medium, an increase in the thickness of the biofilms was observed; especially in the biofilm located at the bottom end of the ceramic membrane in the vertically orientated SFMGR. According to Ozergin-Ulgen and Mavituna (1994) complex growth medium is favoured by researchers when working with *S. coelicolor* as it yields higher biomass and product concentrations than defined growth medium.

5.5.2 Average pH

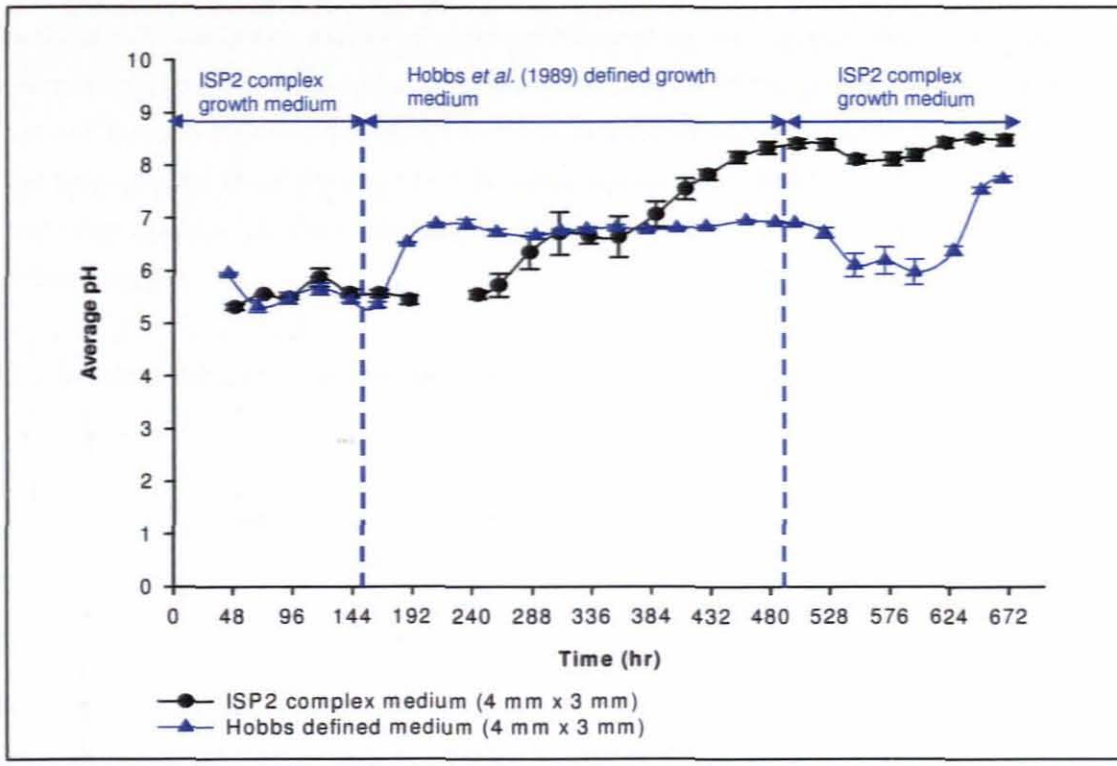

Figure 5.3: Average pH of the 3 Single Fibre Membrane Gradostat Reactors (The error bars represent the standard error using Sigma Plot 8.0)

The initial pH of the complex growth medium ISP2 was 7.5, while the initial pH of the defined growth medium, described by Hobbs *et al.* (1989), was 7.2. For the first 163 hr both experiments were operated with ISP2 growth medium. After 163 hr the pH of the ISP2 complex medium (4 mm x 3 mm) curve continued increasing, while the Hobbs defined medium (4 mm x 3 mm) graph remained stable at pH of approximately 7.0. At 624 hr, about 120 hr after the growth medium was changed to ISP2 complex medium the pH started increasing again. The trend observed in Figure 5.3 was that after inoculation the pH of ISP2 complex medium decreased initially and stabilised at pH of approximately 5.5 for 120 hr before increasing. According to Bystrykh *et al.* (1996) at growth medium pH values of 4.5 to 5.5 significant amounts of actinorhodin occurs. However, it is located almost exclusively intracellularly. At growth medium pH values of 6.0 to 7.5 a different blue pigment was produced both intracellularly and extracellularly. *S. coelicolor* A3(2) is therefore capable of producing large amounts of two actinorhodin-related pigments (Bystrykh *et al.* 1996).

The stable pH noticed between 163 and 499 hr in the curve for Hobbs defined medium (4 mm x 3 mm) corresponds to the time period when the growth medium was changed from the complex medium to the defined medium. In Figure 5.4 there was a stable, yet minute

production of secondary metabolites when the system was operated with the defined medium. After changing the growth medium back to IPS2 complex medium at 499 hr, the actinorhodin production and pH decreased followed by an increase after 24 hr and 72 hr, respectively (seen in Figures 5.3 and 5.4). The final pH of the growth medium, rather than specific nutrient limitation has been identified as the determining factor in which blue pigment will be produced. Bystrykh *et al.* (1996) reported that when grown at a neutral pH the major exported product of the actinorhodin biosynthetic pathway by *S. coelicolor* A3(2) is γ-actinorhodin.

5.5.3 Average actinorhodin production

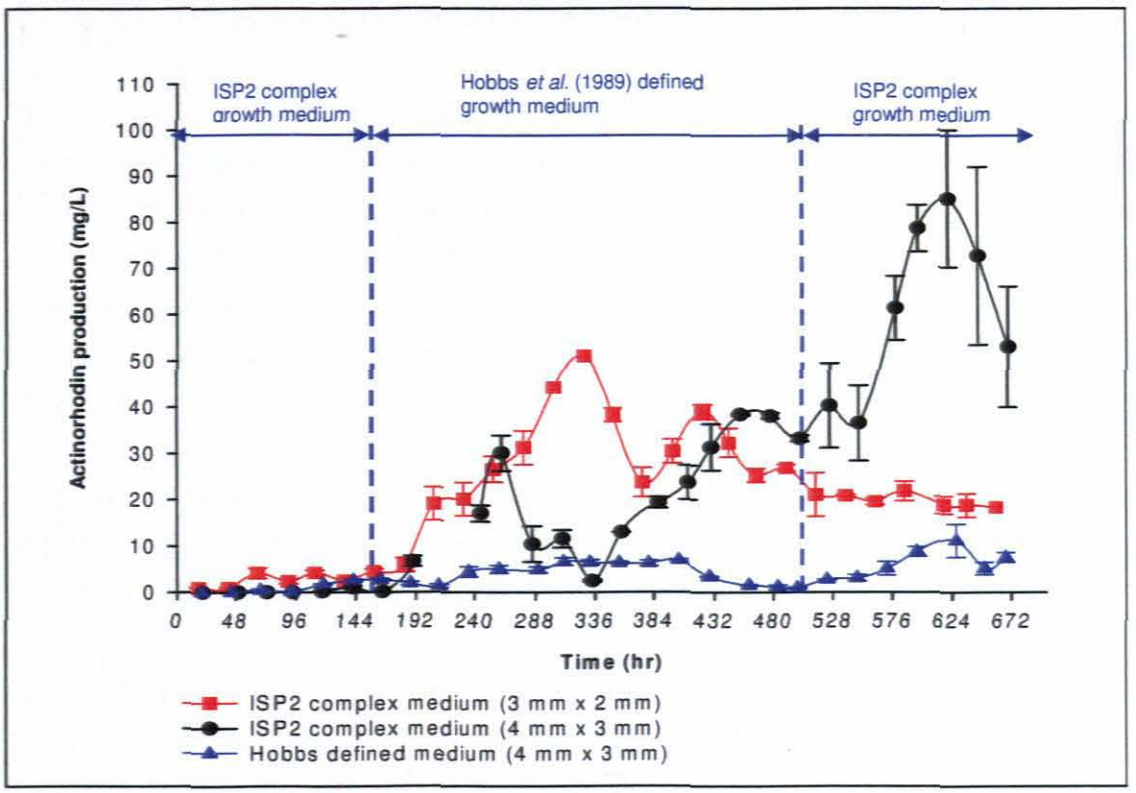

Figure 5.4: Average actinorhodin production in the 1 x 3 SFMGR rig (The error bars represent the standard error using Sigma Plot 8.0)

Figure 5.4 indicates that higher actinorhodin production was achieved with the complex growth medium than with the defined growth medium. About 72 hr after changing the Hobbs defined growth medium back to ISP2 complex medium, actinorhodin production started increasing. In Figure 5.3 the average pH when the bioreactors were operated with the defined growth medium was 6.8. Therefore, the low amounts of actinorhodin produced, when the bioreactors were operated with Hobbs defined medium, could be because the actinorhodin was mainly produced intracellularly.

During this study the maximum actinorhodin concentration produced by *S. coelicolor* A3(2), utilising the complex medium ISP2, immobilised on the surface of ceramic membranes, was 51.0 mg/L and 85.12 mg/L for the 3 mm x 2 mm and 4 mm x 3 mm ceramic membranes, respectively. In the flask cultures utilising the complex growth medium ISP2, the maximum actinorhodin concentration produced was 86.9 mg/L. The maximum actinorhodin concentration produced by *S. coelicolor* A3(2) immobilised on a ceramic membrane and in flask cultures during the experimental procedures performed, utilising Hobbs defined medium, was 6.89 and 6.2 mg/L, respectively. According to Ozergin-Ulgen and Mavituna (1994) the maximum actinorhodin production in an immobilised culture, utilising the defined growth medium was 0.538 mg/L. The actinorhodin concentrations obtained during this study was therefore higher than that obtained by Ozergin-Ulgen and Mavituna (1994).

Ozergin-Ulgen and Mavituna (1994) grew Streptomyces coelicolor in immobilised cultures operated with both a complex growth medium, YEME, described by Hopwood *et al.* (1985) and the defined medium described by Hobbs *et al.* (1989). Actinorhodin was excreted extracellularly in the immobilised culture when the complex growth medium was utilised and intracellularly when the defined growth medium was used. In immobilised cultures operated with the complex growth medium YEME (Hopwood *et al.,* 1985) actinorhodin production occurred after glucose depletion, indicating that the product formation was non-growth-associated. The actinorhodin concentrations obtained during this study were about half when compared to literature (Ozergin-Ulgen & Mavituna, 1994). This could be because two different complex media were utilised, YEME growth medium was utilised in the literature and ISP2 growth medium for this study.

With ISP2 growth medium actinorhodin was produced mainly extracellularly, this was confirmed by the permeate being dark purple (opaque) in colour and an average pH of 8.1. According to Ozergin-Ulgen and Mavituna (1994) immobilised cultures of *S. coelicolor* operated with a complex growth medium produces the secondary metabolite actinorhodin extracellularly, resulting in higher actinorhodin concentrations than obtained with the defined growth medium, where it was assumed actinorhodin production is intracellular hence the low actinorhodin concentrations.

With Hobbs defined medium the permeate was clear, indicating actinorhodin production was intracellular. If the actinorhodin production was extracellular the permeate would have been dark blue (clear), as was seen with the flask cultures in section 4.5.2. Similar amounts of actinorhodin was produced in the flask cultures as with the 1 x 3 SFMGR Quorus rig. The actinorhodin assay used (see section 3.9.1) was only capable of determining extracellular actinorhodin.

The highest secondary metabolite (actinorhodin) production was measured when operating the SFMGR's with ISP2 growth medium and the 4 mm x 3 mm ceramic membranes. The pressure differential and therefore the flow rate for both experimental procedures were identical. However, the 4 mm x 3 mm capillary ceramic membranes had a larger surface area than the 3 mm x 2 mm, resulting in a lower flux per square meter surface area for the 4 mm x 3 mm ceramic membranes. Thus, it is postulated that the micro organism was under nutrient limitation, which stimulated a higher production of secondary metabolites.

Figure 4.1 in section 4.4.1 represents actinorhodin production in flask cultures, while Figure 5.4 represents actinorhodin production in continuous immobilised cultures. A comparison of the graphs show that batch cultures (Figure 4.1) have a short phase (±72 hr) during which no actinorhodin was produced followed by a rapid increase in actinorhodin production. The continuous cultures (Figure 5.4) showed a longer inactive phase (±192 hr) followed by a slow increase in actinorhodin production, until maximum production was reached. Although the continuous cultures took a long time to reach maximum actinorhodin production, the total amount of actinorhodin produced was much higher than the batch cultures were capable of producing. Over time the amount of actinorhodin produced by the batch cultures decreased, due to the nutrients in the growth medium being depleted, while the amount of actinorhodin produced by continuous cultures remained at a maximum as long as the operating parameters of the system were being optimised. Ozergin-Ulgen and Mavituna (1994) reported that immobilised cells of *S. coelicolor* A 3(2) were more efficient producers of actinorhodin than freely suspended cultured cells.

Immobilised cultures of *S. coelicolor* operated with a complex growth medium produce the secondary metabolite actinorhodin extracellularly, resulting in higher actinorhodin concentrations than obtained with the defined growth medium where it was assumed actinorhodin production was intracellular hence the low actinorhodin concentrations (Ozergin-Ulgen and Mavituna, 1994).

5.5.4 Average phosphate concentration

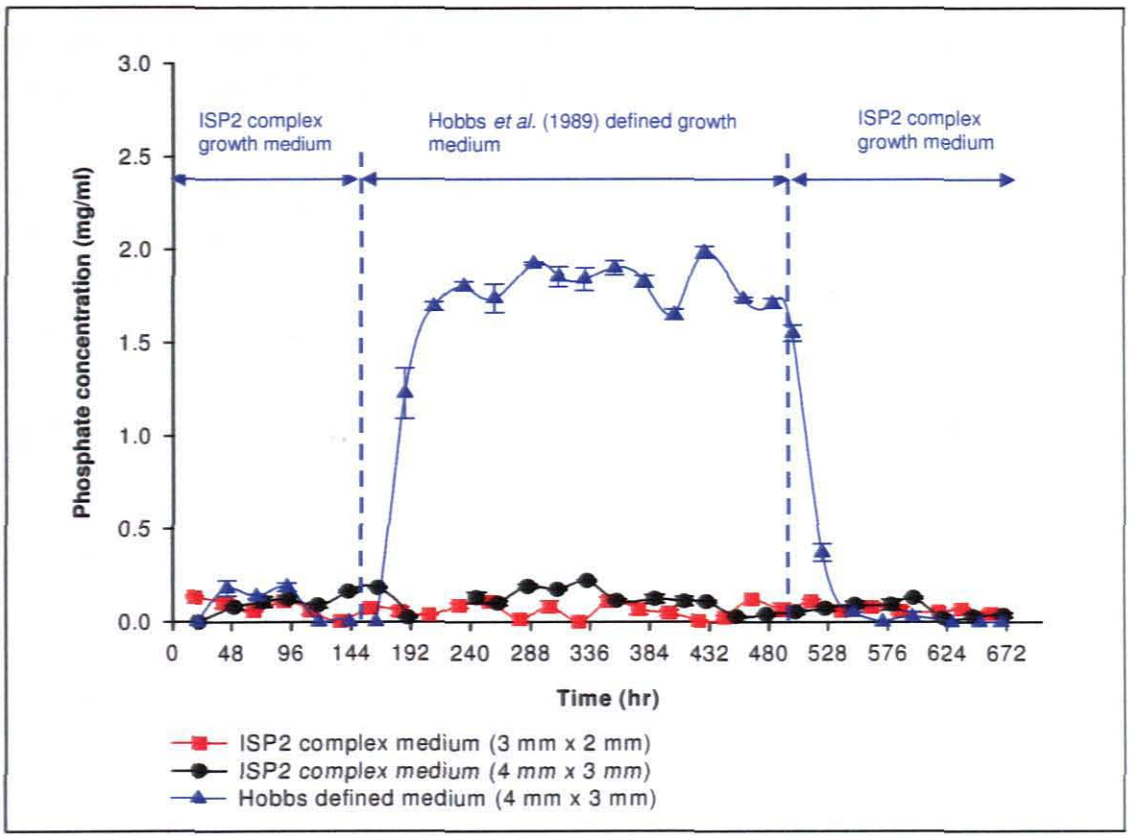

Figure 5.5: Average phosphate concentration for the 1 x 3 SFMGR rig (The error bars represent the standard error using Sigma Plot 8.0)

The original phosphate concentration in the two growth media was 0.083 and 1.37 mg/ml for ISP2 complex medium and Hobbs (1989) defined medium, respectively. Hence, the increase in phosphate concentration observed between ±192 and 576 hr in Figure 5.5 when the ISP2 complex growth medium was switched to Hobbs defined growth medium.

From the graphs in Figure 5.5 it appears the phosphate concentration remains relatively stable at 0.079 mg/ml for the complex growth medium. However, from the values obtained the micro organism was not utilising phosphate, since a phosphate concentration of 0.079 mg/ml and 1.76 mg/ml was present in the permeate samples of the complex and defined growth media, respectively. This value obtained for the permeate of the defined growth medium was higher than the phosphate concentration present in the growth medium initially.

According to Bibb (2005) an excessive level of inorganic phosphate, such as K_2HPO_4 present in Hobbs *et al.* (1989) defined medium, prevents the production of structurally diverse secondary metabolites, like actinorhodin. How the elevated levels of intracellular phosphate

exert an inhibitory effect on secondary metabolism is speculative (Bibb, 2005). Therefore, the actinorhodin concentration increases with decreasing phosphate concentration (Hobbs *et al.* 1989). Figures 5.4 and 5.5 verify this statement, as the defined growth medium which had a high concentration of inorganic phosphate had a corresponding low actinorhodin concentration. Phosphate concentrations in the range of 0.3 to 300 mM supports cell growth. However, phosphate concentrations of 10 mM and higher repress the biosynthesis of many antibiotics (Ates *et al.,* 1997). Hobbs *et al.* (1989) reported that actinorhodin production was completely inhibited when the phosphate concentration in the growth medium was higher than 24 mM. Regarding actinorhodin production by *S. coelicolor* Hobbs *et al.* (1990) reported that an interrelationship exists between the nitrogen and phosphate levels present in the growth medium, with phosphate having an epistatic control over nitrogen.

5.5.5 Average glucose concentration

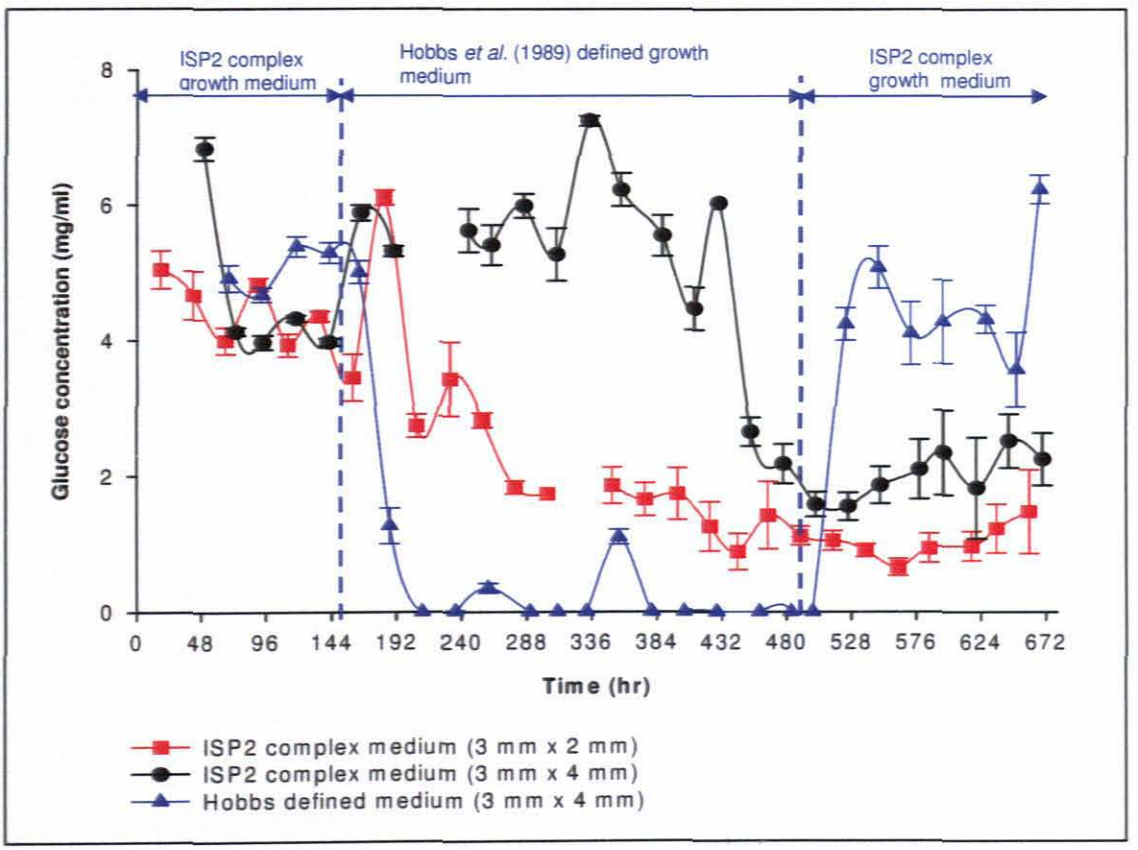

Figure 5.6: Average glucose concentration for 1 x 3 SFMGR rig (The error bars represent the standard error using Sigma Plot 8.0)

The initial glucose concentration present in ISP2 complex medium was 4.96 and 1.74 mg/ml for Hobbs (1989) defined medium. Hence, the decrease in glucose concentration observed between ±163 and 499 hr in Figure 5.6 when ISP2 complex growth medium was switched to Hobbs defined growth medium.

From the graphs in Figure 5.6 the micro organism was consuming glucose, since the glucose concentration present in the permeate samples was lower than the amount originally present in the two growth media. The original glucose concentration present in the defined growth medium described by Hobbs (1989) was about a third of that present in the ISP2 growth medium; the amount of glucose present in the permeate samples collected between ±163 and 499 hr when the SFMGR's were operated with Hobbs (1989) defined medium was zero.

A correlation of Figure 5.6 with Figures 5.2, 5.3 and 5.4 revealed that when the flux increased, the glucose concentration increased. However, when the pH and actinorhodin concentration increased, the glucose concentration decreased and vice versa.

Comparing the graphs in Figure 5.6 shows the quantity of actinorhodin produced was significantly higher for ISP2 growth medium than for Hobbs (1989) defined medium. This was due to the difference in glucose concentrations present in the two growth media. It has been reported that actinorhodin is extremely sensitive to the glucose concentration present in the growth medium (Ates *et al.*, 1997; Elibol & Mavituna, 1998; Elibol, 2004). This is observed in Figures 5.4 and 5.6, where the ISP2 complex medium (3 mm x 2 mm) and ISP2 complex medium (4 mm x 3 mm) graphs show a high glucose concentration as well as a corresponding high actinorhodin production. In contrast the Hobbs growth medium (4 mm x 3 mm) graph in Figures 5.4 and 5.6 indicate a low glucose concentration and a corresponding low actinorhodin production. Elibol (2002) stated that glucose is consumed by *S. coelicolor* for biomass formation. Glucose is an independent variable while actinorhodin, biomass concentrations, volumetric oxygen and glucose uptake rate are all dependent variables (Elibol, 2002). An increase in biomass concentration is accompanied by a decrease in the residual glucose concentration (Elibol, 2001).

In the ISP2 growth medium sufficient glucose was present for actinorhodin production without complete depletion of the substrate, since there was still glucose present in the permeate samples. Hence, glucose was not the limiting nutrient in the system when ISP2 growth medium was utilised. When the system was operated with Hobbs (1989) defined medium, glucose was the limiting nutrient as the substrate was depleted during the production of the secondary metabolite actinorhodin, as seen in Figure 5.6.

5.5.6 Single substrate limited growth kinetics

The general response of *S. coelicolor* A3(2) to a depletion of glucose is the cessation of blue pigment synthesis; and to growth limitation by nitrogen (either ammonium or nitrate), phosphate, or trace elements is the synthesis of blue pigment (Bystrykh *et al.*, 1996). When the pressurised MGR system was operated with Hobbs (1989) defined medium from

±163 and 499 hr, the permeate became clear and lost its blue pigment; the disappearance of this blue pigment indicated a depletion of glucose. This was confirmed by the glucose results which indicated complete consumption of glucose over time, as seen in Figure 5.6 for the Hobbs growth medium (4 mm x 3 mm) graph. Therefore, glucose was the limiting nutrient in the Hobbs defined growth medium as the substrate was completely depleted during the study.

Various single-substrate growth kinetic models exist, such as the Monod, Tessier, Moser and Contois growth kinetic models, refer to Table 2.4 in section 2.3.3.1 for the equations representing these models. The two methods for determining (K_s) are (1) to measure the nutrient concentrations at known growth rates; or (2) to measure the growth rate at known concentrations of the rate limiting nutrient (Beyenal *et al.*, (2003). In this study different substrate (i.e. glucose) concentrations were not tested and the biomass was only determined at 28 days (refer to section 3.5.6) and not for different time durations. The substrate saturation constant (K_s) could therefore not be calculated or extrapolated and an empirical model with experimental data was required. The Monod single-substrate growth kinetic model was therefore utilised to quantify the glucose consumption kinetics, as the initial glucose concentration present in the growth medium remained unchanged for the duration of the study.

5.5.6.1 Substrate consumption rate

The accumulative glucose concentration consumed was determined by adding the daily glucose consumed over ±672 hr. The glucose consumed was calculated by determining the difference between the glucose initially present in the growth medium and the glucose present in the permeate samples. The accumulative glucose consumption (shown in Figure 5.7) curve was quantified over ±672 hr. A third-order polynomial function best described the graph of accumulative glucose consumed plotted against time with a correlation coefficient (R^2) value of 0.99. The derivative of the third-order polynomial function was equivalent to the glucose consumption rate (r_B).

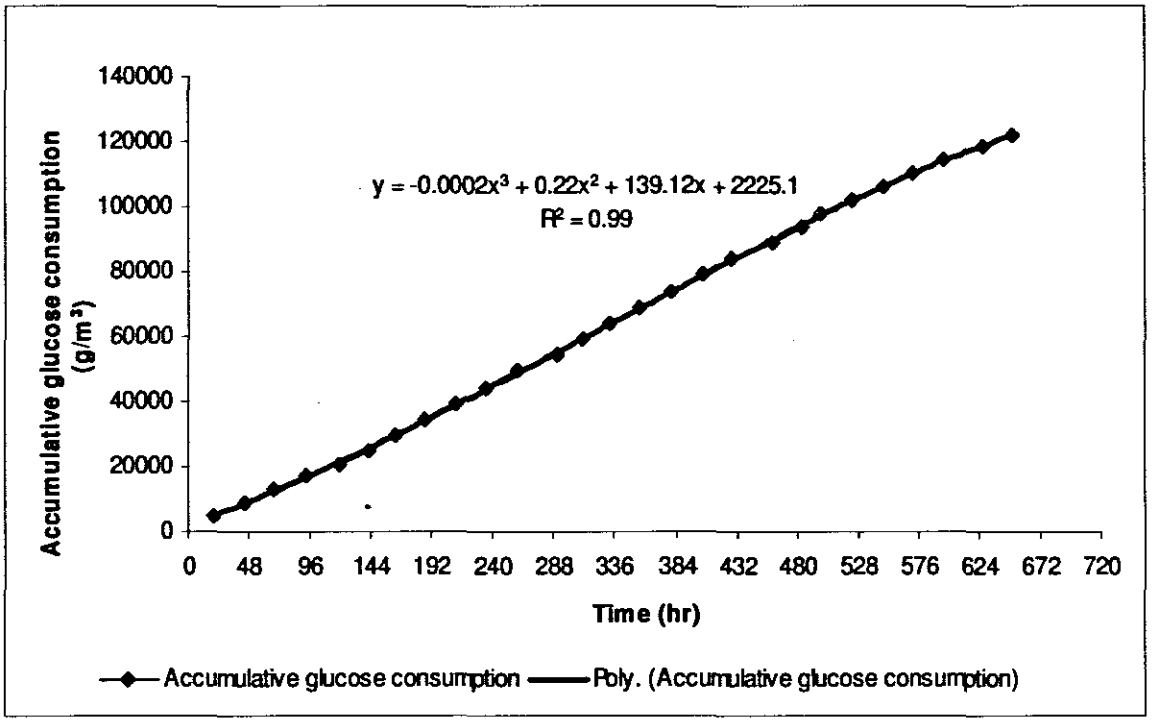

Figure 5.7: Accumulative glucose consumption profile over ±672 hr

The average glucose consumption rate(r_B), calculated by dividing the total accumulative glucose consumed by the total time the pressurised MGR system was operated (±672 hr) was approximately 92.27 g/m^3.hr. Ntwampe and Sheldon (2006) utilised this method for determining the substrate consumption kinetics for the white rot fungus *Phanerochaete chrysosporium*, immobilised in a non-pressurised MGR system. The average glucose consumption rate(r_B) for their system was defined as 94.0 g/m^3.hr. Sheldon *et al.* (2008) quantified the nutrient consumption of *P. chrysosporium* (BKMF-1767) immobilised in single-capillary flow-cell MGR's operated under different spore concentrations and air flow rates. The average glucose consumption was 17.09 and 48.9 g/m^3.hr for the 0.5 and 1 million spores, respectively.

5.5.6.2 Monod saturation constant (K_m) and the maximum substrate consumption rate (r_m)

The method and equation used for determining the Monod kinetic constants were explained in sections 2.3.4.1 and 2.3.4.3. The inverse of the derivative of the third-order polynomial function described the relationship between the inverse of the first-order derivative and the inverse of the Monod equation (shown in Figure 5.8).

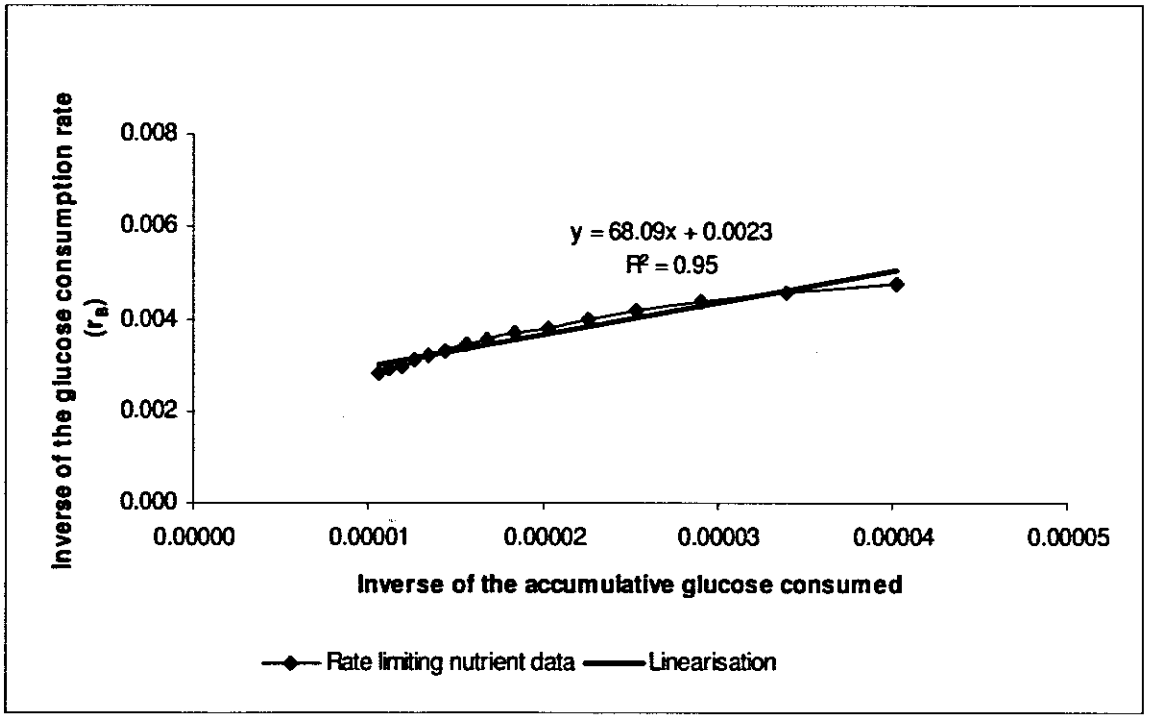

Figure 5.8: Lineweaver-Burke linearisation method

The Lineweaver-Burke method, as described by Shuler and Kargi (2002), was utilised to linearise the rate limiting nutrient's data, by rearranging the hyperbolic relationship between the rate reaction and the glucose concentration. The Monod saturation constant (K_m) was calculated by dividing the slope of the linear trendline by the intercept obtained from the graph in Figure 5.8. The Lineweaver-Burke linearisation method gave the best fit with correlation coefficients (R^2) of 0.9 and higher for the MGR system utilised by Ntwampe (2005). Sheldon *et al.* (2008) utilising an MGR for the immobilisation of used the Lineweaver-Burke method to linearise the rate limiting nutrient's data.

In this study, the Monod saturation constant (K_m) and the maximum substrate consumption rate (r_m) were calculated to be 29605.65 g/m^3 and 434.78 g/m^3.hr, respectively from ±163 to 499 hr, when the pressurised MGR system was operated with Hobbs *et al.* (1989) defined growth medium. It was therefore postulated that the pressure within the system facilitated the mass transfer of the nutrients, such as glucose, across the biofilm, resulting in a higher Monod saturation constant. Since the biofilm was more saturated with nutrients than observed in non-pressurised systems, the rate of glucose consumption by the biofilm would be higher due to higher concentrations of nutrients being more readily available to the biofilm.

5.5.6.3 Yield coefficient

A yield coefficient, determined by plotting the mass of the dry biofilm (determined as explained in section 3.7) against the mass of glucose consumed (shown in Figure 5.9), could only be determined for the ISP2 complex medium from ±20 to 142 hr. The biomass was initially established using ISP2 complex growth medium and then changed to Hobbs *et al.* (1989) defined medium after ±163 hr once a well-established biofilm was present. A yield coefficient determined utilising the substrate data from ±163 to 499 hr for the defined growth medium would therefore not be a true reflection due to the growth medium being changed during the experimental procedure. The yield coefficient, determined from Figure 5.9, was defined as 0.603 g biofilm/g glucose for ISP2 complex growth medium over a time period of ±142 hr. However, the accuracy of this value is questionable since there are not enough data points in Figure 5.9 due to conflicting biomass and glucose consumption results..

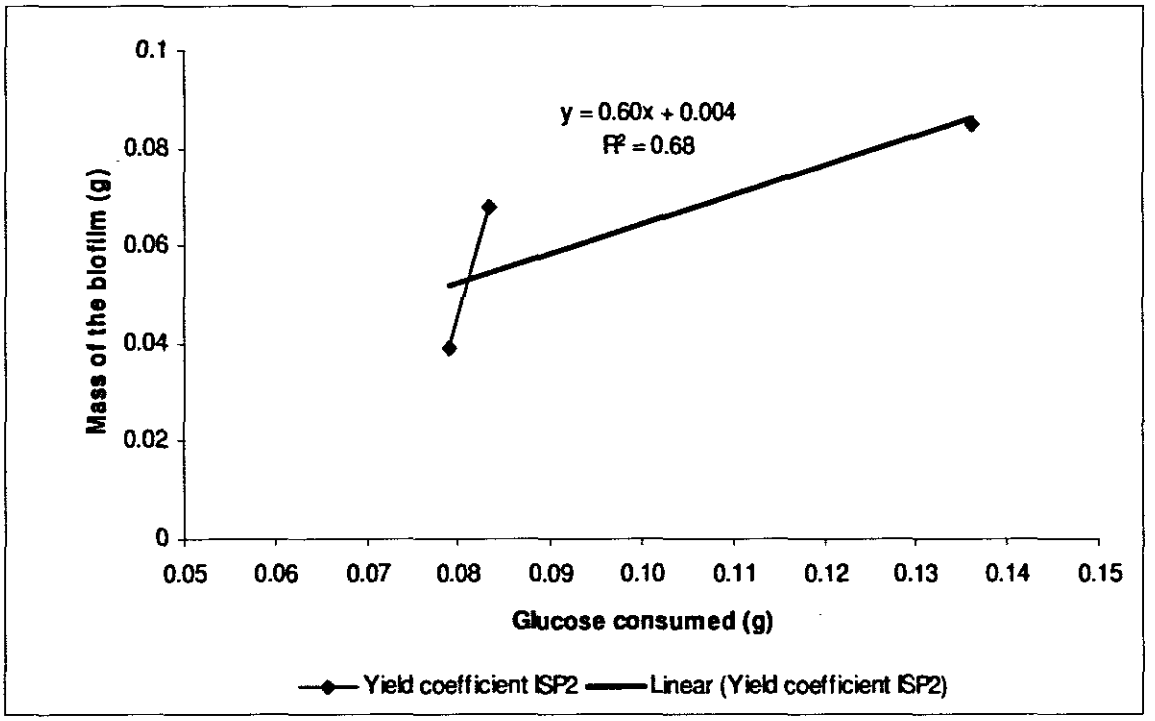

Figure 5.9: Glucose consumed against the biofilm generated over time

Using a non-pressurised vertically orientated SFMGR operated at 37°C for 264 hr Ntwampe and Sheldon (2006) quantified the growth parameters of *P. chrysosporium* (BKMF-1767) based on the utilisation rate of glucose and biofilm. The average glucose-based yield coefficient was determined to be 0.202 g biofilm/g glucose over a period of 264 hr. The glucose-based growth yield parameter estimated by Barclay *et al.* (1993) for the Monod model was 0.441 g biofilm/g glucose in a batch culture.

Beyenal *et al.* (2003) obtained a yield coefficient of 0.628 g micro organism/g glucose for *Pseudomonas aeruginosa* grown in a 2 L chemostat culture with an artificial growth medium. This value was an order of magnitude higher than those reported in literature, which Beyenal *et al.* (2003) attributed to the glucose concentration utilised in the artificial medium being higher than in the other systems previously tested.

5.5.6.4 Significance of the substrate limited results

When comparing the results obtained in this study with non-pressurised systems (shown in Table 5.2), the pressure within the system appears to influence the substrate consumption rate. With a higher consumption rate and therefore higher maximum consumption rate being observed in the pressurised system utilised during this study. However, the Monod saturation constant is unaffected by the presence or absence of pressure within the system. The saturation constant for glucose was lower in the pressurised system than in the non-pressurised system, and still lower in the non-pressurised chemostat culture. The Monod saturation constant appears to be influenced by the residual concentration of the rate limiting substrate. Glucose was not limited during the study conducted by Sheldon *et al.* (2008), which might explain why the Monod saturation constant was higher in this system than during the current study. The higher the residual concentration of the limiting substrate the higher the yield coefficient, especially if the limiting substrate is the carbon source of the micro organism, such as glucose, which stimulates biomass formation.

Table 5.2: Comparison of substrate limitation results from literature with the current studies results

	Current study	Sheldon *et al* (2008)		Beyenal and Lewandowski (2003)
Substrate consumption rate ($g/m^3.hr$)	92.27	1.25 (0.5 million spores) 1.18 (1 million spores)	17.09 (0.5 million spores) 18.9 (1 milliom spores)	-
Monod saturation constant (g/m^3)	434.78	1.41 (0.5 million spores) 1.34 (1 million spores)	1200.61 (0.5 million spores) 3190.34 (1 million spores)	26.9 (glucose) 1.18 (oxygen)
Maximum substrate consumption rate ($g/m^3.hr$) *	29605.65	9.32 (0.5 million spores) 17.67 (1 million spores)	48.31 (0.5 million spores) 121.62 (1 million spores)	-
Yield coefficient (g biomass/g substrate)	0.603	-	-	0.628 (glucose) 0.635 oxygen)
Limited substrate(s)	Glucose	Ammonia (depleted)	Glucose (not depleted)	Glucose and oxygen
Dual or single substrate limitation	Single	Single	-	Dual
System	Pressurised MGR	Non-pressurised single fibre capillary flow cell MGR		Chemostat
Micro organism	*Streptomyces coelicolor* A3(2)	*Phanerochaete chrysosporium* (BKMF-1767)		*Pseudomonas aeruginosa*

5.6 Summary

At a constant transmembrane pressure (TMP) as the biofilm increased in thickness, flux decreased due to increased resistance. *S. coelicolor* utilised glucose for biomass growth during this study confirmed by the thick biofilm growth resulting when the complex growth medium was utilised and the poor biofilm growth observed when Hobbs defined medium was used and glucose was the limiting nutrient in the system. The dark blue colour of the permeate indicated extracelullar actinorhodin production, while the clear colour of the permeate indicated intracellular actinorhodin production when utilising the complex and defined medium respectively. High phosphate concentrations present in the growth medium have an inhibitory effect on biofilm growth and secondary metabolite production, confirmed when Hobbs defined growth medium with a high phosphate concentration was used.

For the complex growth medium a constant TMP with increasing biofilm thickness caused decreased flux, which resulted in nutrient limitation stimulating extracellular actinorhodin production. The Hobbs defined medium with the combined effect of low glucose and high phosphate concentrations resulted in poor biofilm growth and intracellular production of actinorhodin. It can be concluded that ISP2 complex growth medium is both a growth and secondary metabolite producing medium, while Hobbs defined growth medium is a production medium, as this medium did not stimulate biofilm growth, but did stimulate the intracellular production of the secondary metabolite, actinorhodin.

If glucose is the limiting nutrient within an MGR system, whether the system is pressurised or non-pressurised, the average glucose consumption rate is in the range of 90 - 95 $g/m^3.hr$. However, if glucose is not completely depleted within the system the average glucose consumption rate will be much lower.

In pressurised MGR systems in which glucose is the limiting nutrient, higher Monod saturation constants and maximum glucose consumption rates are observed than in non-pressurised MGR systems. MGR systems inoculated with the higher spore concentration operated over the same time period will have both a higher Monod saturation constant and maximum glucose consumption rates due to increased spore concentrations resulting in thicker and denser biofilm growth.

Although the filamentous bacterium *Streptomyces coelicolor* utilises glucose for biofilm growth, from the yield coefficient values obtained during the study conducted and from literature, this micro organism requires a similar amount of glucose to the white rot fungi *Phanerochaete chrysosporium* for biofilm generation. However, it is recommended that the experiment be repeated to confirm the yield coefficient value obtained during the study.

CHAPTER 6

RESULTS

QUANTIFYING GROWTH KINETICS IN CONTINUOUSLY OPERATED PRESSURISED SINGLE FIBRE MEMBRANE GRADOSTAT REACTORS (SFMGR)

PUBLICATIONS:

Godongwana, B., **De Jager, D.**, Sheldon, M.S. & Edwards, W. 2009. The effect of *Streptomyces coelicolor* on the hydrodynamics of a vertically orientated capillary membrane gradostat reactor. *Journal of Membrane Science*, 333:79-87.

De Jager, D., Sheldon, M.S. & Edwards, W. 2009. Modelling growth kinetics of *Streptomyces coelicolor* A3(2) in a pressurised membrane gradostat reactor (MGR). *Enzyme and Microbial Technology*, 45:449-456.

CHAPTER SIX

QUANTIFYING GROWTH KINETICS IN CONTINUOUSLY OPERATED PRESSURISED SINGLE FIBRE MEMBRANE GRADOSTAT REACTORS (SFMGR)

6.1 Introduction

A fast emerging area of membrane bioreactor (MBR) applications is the immobilisation and culturing of micro organisms, such as fungi and bacteria for the production of high-value low-volume secondary metabolites such as antibiotics, anti-inflammatories, anticancer drugs and vitamins (Luekes, 1999; Burton, 2001; Charcosset, 2006). A number of MBR applications have been reported in literature with various micro organisms (Belfort, 1989; Beeton *et al.*, 1993; Zhang *et al.*, 2006); fungi (Venkatadri & Irvine, 1993; Leukes, 1999; Solomon & Petersen, 2002; Hai *et al.*, 2006; Ntwampe *et al.*, 2007) and enzymes (Govender *et al.*, 2003; Charcosset, 2006; Diaz *et al.*, 2006) that were successfully cultured and/or immobilised on the external surface of membranes.

6.1.1 Background

Various empirical kinetic profiles have been described in solid state fermentation (SSF) systems including linear, exponential, logistic and fast acceleration/slow deceleration. The modelling of microbial growth kinetics plays an important role in the design and optimisation of MBR systems. Mathematical models are used to describe the overall performance of the MBR's. The models must describe not only the microbial growth kinetics but also the transport phenomena within the substrate bed and the mass and energy exchanges between the bed and subsystems of the MBR, such as the membrane wall and the extracellular space gases (Mitchell *et al.*, 2003).

In flowing systems, such as a membrane gradostat reactor (MGR), where the nutrient solution passes through the membrane lumen to the extracellular space (ECS) and air is supplied on the shell side of the bioreactor, three-dimensional biofilms develop. Therefore, studying and quantifying the growth kinetics within a continuous MGR is important as this can be utilised in the development of an efficient nutrient gradostat within the biofilm as well as to model the mass transfer of the bioprocess (Sheldon *et al.*, 2008). A large amount of information regarding growth kinetics of micro organisms in batch, fed-batch and non-pressurised systems are available in literature (Mitchell, 1991; Ates, 1997; Ikasari & Mitchell, 2000; Ooijkaas *et al.*, 2000; Sheldon & Small, 2005; Van de Lagemaat & Pyle, 2005; Ntwampe & Sheldon, 2006; Sheldon *et al.*, 2008). However, to date limited information has

been published with regards to the microbial growth kinetics of bacteria immobilised in continuously operated pressurised MGR's.

Table 6.1: Equations representing various growth models (Ikasari & Mitchell, 2000; Mitchell *et al.*, 2004)

Growth model	Equation	Equation number
Exponential	$\frac{dX}{dt} = \mu X$	2.2a
Logistic	$\frac{dX}{dt} = \mu X\left(1-\frac{X}{X_m}\right)^n, n=1$	2.3a
TWO-PHASE: Fast acceleration (Exponential)	$\frac{dX}{dt} = \mu X$	2.4a
Slow deceleration	$\frac{dX}{dt} = \left[\mu L e^{-k(t-t_a)}\right] X, t \geq t_a$	2.5a
Power law	$\frac{dX}{dt} = \mu X\left(1-\frac{X}{X_m}\right)^n, n<\text{or}>1$	2.6a

The models shown by Equations 2.2a to 2.6a in Table 6.1, respectively, were tested to determine which model(s) best describes the growth of *S.coelicolor* A3(2) in the pressurised SFMGR's used in this study.

6.1.2 Objectives

The purpose of this study was to quantify the growth kinetics of the filamentous bacterium *Streptomyces coelicolor* A3(2) immobilised on the external surface of single fibre ceramic membrane MGR's, operated under continuously pressurised air and nutrient supply.

The objectives for this part of the study were to:

- Quantify *S. coelicolor* growth on ceramic membranes.
- Model the growth kinetics of *Streptomyces coelicolor* A3(2) in a continuously operated pressurised membrane gradostat reactor (MGR).
- Investigate the correlation between the measured parameters (eg. average flux, pH, actinorhodin production, glucose and phosphate concentrations) and the growth curve.

6.2 Materials and methods

6.2.1 Micro organism

A 1 x 12 SFMGR rig was run with the complex growth medium, ISP2, and the filamentous bacterium *Streptomyces coelicolor* A3(2), prepared as explained in section 3.5.1.

6.2.2 Inoculum preparation and inoculation

The inoculum was prepared and tested for contamination as explained in sections 3.5.2 and 3.5.3, respectively. Each single fibre membrane gradostat reactor (SFMGR) was inoculated as explained in section 3.5.4.

6.2.3 Growth medium

The nutrient medium used for the both inoculum preparation and bioreactor operation was ISP2 (*Shirling &Gottlieb, 1966), a complex growth medium (refer to Table 3.3 in section* 3.4 for the preparation procedure).

6.3 Experimental set-up

The experimental set-up used in this section was the 1 x 12 SFMGR rig as explained in *sections* 3.3 *and* 3.3.3 *and Figure* 3.5. *The ceramic membranes used were the* 3 *mm x* 2 *mm* ceramic membranes supplied by Hyflux CEPAration BV. The characteristics of the capillary ceramic membranes that were used in the SFMGR system, are listed in Table 3.1 in section 3.2.1.

A schematic diagram of the SFMGR, as patented by Edwards *et al.* (2007), was illustrated schematically in Figure 3.4 and explained in section 3.3.1. After the SFMGR was constructed, the reactor with ceramic membranes was pressure tested using water to check its ability to withstand high pressures and that no leaks were present as explained in section 3.3.2. Three SFMGR's were then manifolded together with 5 mm (ID) by 8 mm (OD) silicone tubing, as shown in Figure 3.5 and explained in section 3.3.3.

6.3.1 Bioreactor operation

After sterilisation and inoculation, the nutrient medium was supplied to the membrane lumen at a flow rate of 0.001 L/hr. The air was supplied to the ECS of the bioreactor at a flow rate of 2.4 L/hr. A pressure differential, measured with pressure transducers, was created across the membranes by applying pressure to both the nutrient medium and the humidifier. The pressure applied to the nutrient medium was higher than the pressure applied to the humidifier to ensure transmembrane flux occurred. The SFMGR system was operated in the dead-end mode with a constant shell side pressure supplied by a JCS Shinko proportional-integral-derivative (PID) controller.

Four sets of three vertically orientated manifolded SFMGR's (shown in Figure 3.5) were used to culture the bacteria, *S. coelicolor*, at 28°C on the capillary ceramic membranes. The system and reactor parameters are shown in Table 6.2.

Table 6.2: System and reactor parameters

Model parameter	Unit	Basic value
Membrane outer diameter	m	0.0028
Membrane inner diameter	m	0.0018
Membrane wall thickness	m	0.0005
Effective membrane length	*m*	*0.225*
Glass manifold inner radius	m	6.5×10^{-3}
Glass bioreactor length	m	2.09×10^{-1}
Nutrient flow rate	L/hr	1.0×10^{-3}
Nutrient medium viscosity	Pa.s	1.2×10^{-3}

Four experiments were performed during this study. Two experiments were operated for 18 days, with two reactors sacrificed every third day. The remaining experiments were run for 8 days, with two reactors sacrificed daily after day 3.

6.4 Analytical methods

Permeate from each SFMGR was collected daily. The amount of permeate collected daily was dependent on the pressure differential and the resistance to transmembrane flux by the biofilm. The volume and pH of the permeate samples were measured, including the time elapsed between sampling; thus allowing the flux to be calculated. After disconnecting a reactor the wet biomass was measured, as well as the dry biomass after the biofilm was dried for 12 hr at 70°C (refer to section 3.7).

Actinorhodin concentrations were determined as described in section 3.9.1. Refer to Appendix A for a detailed description of the actinorhodin assay procedure. The glucose and phosphate concentrations of the permeate samples were determined as described in sections 3.9.2 and 3.9.3, respectively. Refer to Appendices B and C for detailed descriptions of the glucose and phosphate assays.

6.5 Results and discussion

All the data collected from the experiments operated for the same time period under identical conditions with the same growth medium were averaged together, this included flux, pH, actinorhodin, glucose and phosphate results. Figures 6.7 to 6.11 represent the average results and include standard error bars, generated using Sigma Plot (Version 8.0). The growth curve obtained for this study was constructed from the average dry biomass obtained from the two reactors disconnected after 66, 90, 114, 140, 162, 212, 282 and 354 hr of operation.

6.5.1 Dry biomass growth curve

Figure 6.2 depicts the average dry biomass results obtained for *S. coelicolor* A3(2) cultivated on the external surface of the ceramic membrane in the continuous pressurised SFMGR's. A limited understanding of the kinetic model for actinorhodin production exists due to the unstable, complex heterogeneous nature of *Streptomyces coelicolor* (Elibol & Mavituna, 1999a). The data point at 354 hr is devoid of standard error bars due to repeated sloughing of the biofilm from the membranes at this time (as shown in Figure 6.5), resulting in very little data being accumulated for this point. A similar growth curve, to that in Figure 6.2, shown in Figure 6.3, was obtained from a plot of the wet biofilm thickness as a function of time (Godongwana *et al.*, 2009), thus validating the shape of the growth curve.

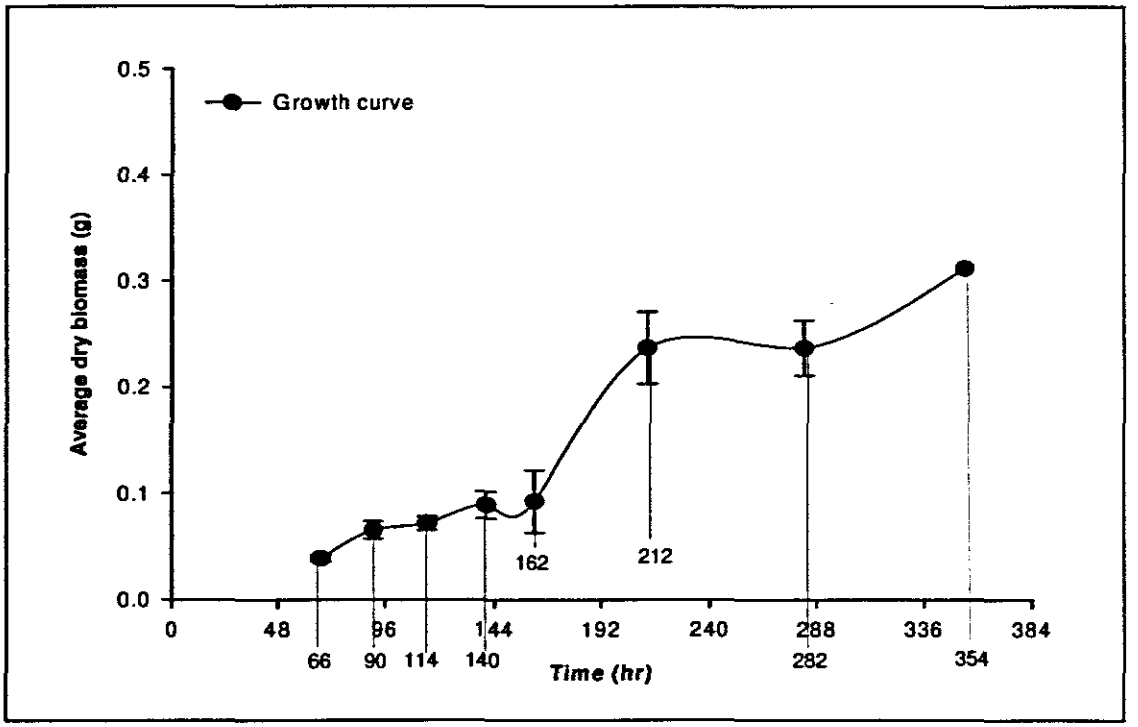

Figure 6.1: Growth curve obtained from the experimental data using the average dry weight of the biomass (The error bars represent the standard error using Sigma Plot 8.0)

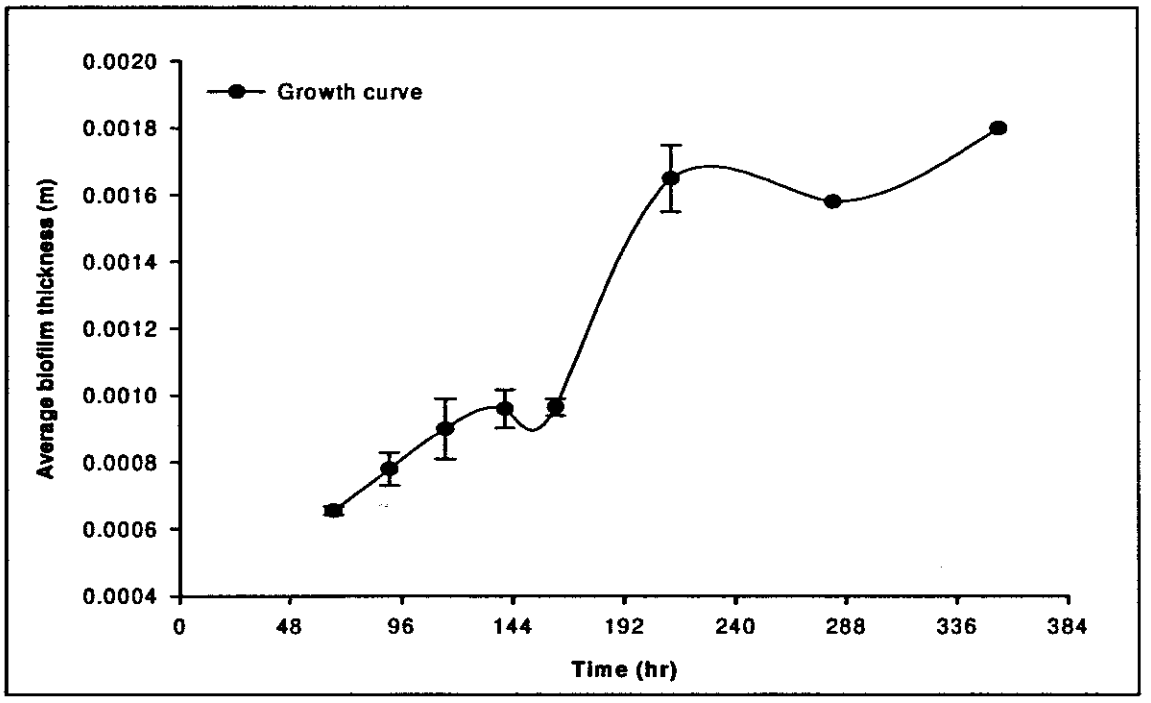

Figure 6.2: Growth curve obtained from the experimental data using the average biofilm thickness (The error bars represent the standard error using Sigma Plot 8.0)

An independent t-test was done to determine whether two growth cycles were present. The t-test measures the significant difference between data for 2 points, either dependent or independently, by comparing the means of the two points. The t-value, (which can be negative as absolute values are not used when calculating the t-value) and p-value take both the sample size and standard deviation into account. A p-value smaller than and equal to 0.05 ($p \leq 0.05$) was interpreted as significant as it indicated a probability of 5 % or less.

Table 6.3: Results from the One-way ANOVA run with SPSS

t-test between:	t-value	p-value
66 to 90 hr	-3.77	0.0024
90 to 114 hr	-0.58	0.5776
114 to 140 hr	-1.03	0.3341
140 to 162 hr	-0.13	0.8995
162 to 212 hr	-3.22	0.0323
212 to 282 hr	5.78×10^{-16}	1

The p-values, in Table 6.3, indicate that the increase in dry biomass between ±66 to 90 hr and ±162 to 212 hr was significant, as the p-values between these data groups were below 0.05. The significant difference between ±66 and 90 hr occurred as the biofilm was still in the exponential growth phase. The significant difference between ±162 and 212 hr can only be explained by a second exponential growth phase. Therefore, the first growth cycle ends and the second growth cycle starts around 162 hr. A t-test could not be run between the data groups at ±212 to 354 hr as there was too little data available, therefore no statistics were computed.

Therefore, Figure 6.2 shows the presence of two growth cycles, confirmed by the t-test, indicating biphasic growth. The growth curve showed two typical s-shaped growth cycles with what appeared to be the start of a third growth cycle. Therefore, the first growth cycle was identified between ±66 and 162 hr, with the second growth cycle occurring between ±162 and 354 hr with no evident intermediate lag phase. The shape of the growth curve after 282 hr indicates the possibility of a third growth cycle. However, this could not be confirmed due to biofilm sloughing after 354 hr (as shown in Figure 6.5). Biphasic growth occurs when a micro organism exhibits two growth phases due to the use of two different substrates for growth. Upon depletion of the first substrate the micro organism starts utilising a second substrate (Meunier & Choder, 1999). However, during this study a complex growth medium was utilised and except for glucose, which was not depleted in the system, the usage of the remaining substrates were not quantified, as the substrates were unknown.
From the experimental data obtained by integrating Equation 2.20 (Shuler & Kargi, 2002), average specific growth rates of 0.053 hr^{-1} and 0.012 hr^{-1} average specific growth rate was calculated, for the first growth cycle (±66 to 162 hr) and second growth cycle (±162 to 354 hr), respectively. However, utilising Ordinary Differential Equations Solver (ODE) in the software program Polymath 5.1 together with Solver in Microsoft Excel 2003 to minimise the sum of squares of the differences (SSD) between the experimental and calculated data, a specific growth rate value of 0.049 hr^{-1} for the first growth cycle was found to provide a better fit to the growth curve. Specific growth rate values of 0.013 hr^{-1} (±162 to 212 hr) and 0.019 hr^{-1} (±212 to 354 hr) was found to provide a better fit to the growth curve, when the two-phase growth model was fitted.

$$\mu = \frac{1}{X}\frac{dX}{dt} \qquad \textbf{2.20}$$

Where X is the microbial biomass (g); t represents time (hr) and μ the specific growth rate constant (hr^{-1}) (Shuler & Kargi, 2002).

According to Naeimpoor and Mavituna (2000), Shahab *et al.* (1996) determined a specific growth rate of 0.048 hr^{-1} for *S. coelicolor* grown in a continuous culture. This value corresponds to the specific growth rate value of 0.049 hr^{-1} caculated for the first growth cycle during this study.

6.5.1.1 Modelling the growth curve

The ODE in the software program Polymath 5.1, as well as non-linear regression in Microsoft Excel 2003 was utilised to fit the logistic, power law, exponential and two-phase growth models to the two growth cycles of the growth curve in Figure 6.2 by minimising the sum of square differences (SSD), as shown in Figure 6.4. By determining the correlation coefficient (R^2) values the best fit of the calculated data to the experimental data was validated. The best model was selected based on the minimum SSD and best R^2 values between the experimental and calculated data.

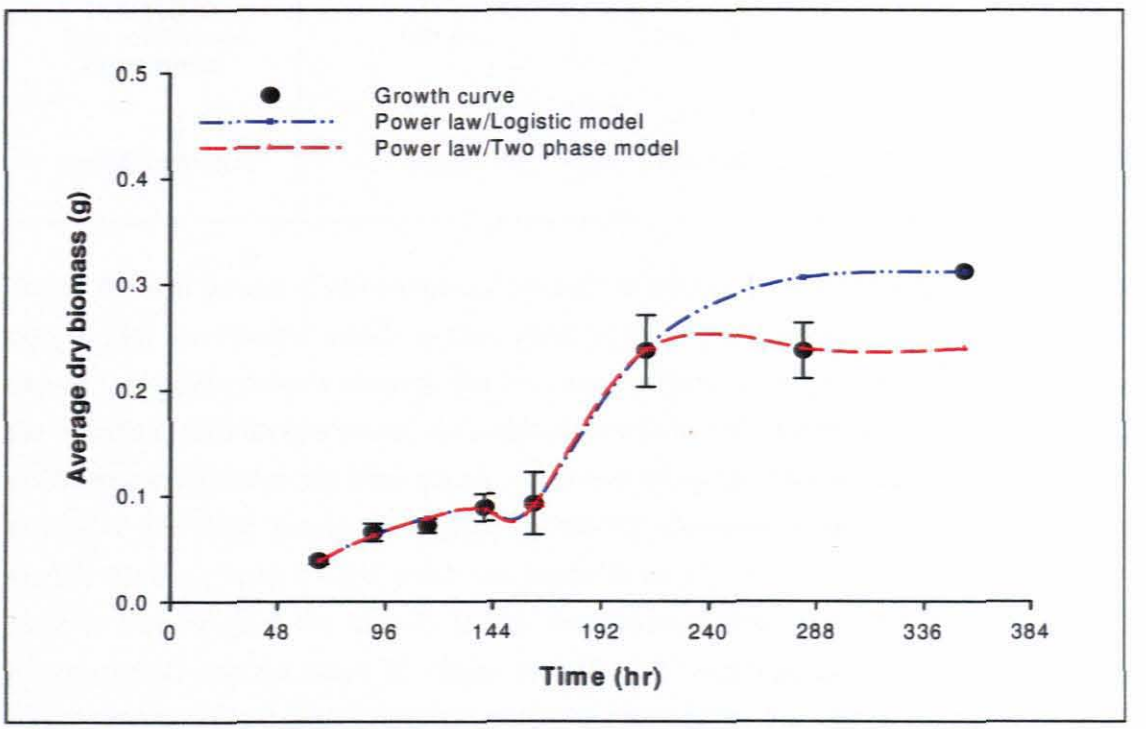

Figure 6.3: Growth models fitted to the growth curve obtained from the experimental data (The error bars represent the standard error using Sigma Plot 8.0)

Table 6.4: Growth model fitting to the first growth cycle (66 to 162 hr)

Growth model	Specific growth rate (μ)	SSD	R^2	*n*
Logistic	0.049 hr^{-1}	1.01×10^{-4}	0.95	N/A
Power law	0.049 hr^{-1}	6.85×10^{-5}	0.96	1.1
Exponential	0.049 hr^{-1}	19.1	0.56	N/A

Table 6.5: Growth model fitting to the second cycle (162 to 354 hr)

Growth model	Specific growth rate (μ)	SSD	R^2	Notes
Logistic	0.040 hr^{-1}	4.76×10^{-3}	0.89	N/A
Exponential	0.0063 hr^{-1}	1.37×10^{-2}	0.73	N/A
TWO-PHASE: Fast acceleration (Exponential)	0.019 hr^{-1}	5.49×10^{-6}	1	
Slow deceleration	0.013 hr^{-1}	5.34×10^{-3}	0.25	L = 1.47 k = 1

Tables 6.4 and 6.5 are a comparison of the sum of square differences (SSD) and R^2 values obtained for the different growth models fitted to the growth curve in Figure 6.2. Figure 6.4 depicts the growth models showing the two best fits fitted to the growth curve obtained from the experimental data (the power law model from ±66 to 162 hr and logistic model from ±162 to 354 hr; power law model from ±66 to 162 hr and two-phase model (fast acceleration: ±162 to 212 hr and slow deceleration: ±212 to 354 hr). However, when comparing the growth models fitted in Figure 6.4 the power law model from ±66 to 162 hr and logistic model from ±162 to 354 hr gave the best fit to the experimental data. This was confirmed by the minimum SSD and maximum R^2 values of 6.85×10^{-6} and 0.96 obtained for the power law model (±66 to 162 hr) and 4.76×10^{-3} and 0.89 obtained for the logistic model (±212 to 354 hr), respectively. The SSD value for the power law (fitted from 66 to 162 hr) was an order of magnitude smaller than the logistic model. Although the fast acceleration phase of the two-phase model showed a smaller SSD and higher R^2 value than the logistic model (fitted from ±212 to 354 hr), when the SSD and R^2 values of the slow deceleration phase was taken into account this growth model was eliminated.

Due to biofilm sloughing from the ceramic membrane (shown in Figure 6.5), the shape of the growth curve could not be confirmed after 354 hr, even with repeated experiments. Changing

the nutrient and airflow rates to minimise the probability of the biofilm sloughing was not an option, as the resulting graph would have been obtained under different operating conditions from earlier experiments and could therefore not be compared.

Figure 6.4: A ceramic membrane showing biofilm sloughing during operation of the SFMGR system

In Figure 6.6 and Table 6.6 the data point at 354 hr was excluded due to biofilm sloughing. Therefore, for the second growth cycle the growth models were only fitted from ±162 to 282 hr.

According to the minimum SSD and best R^2 values, the power law model still gave the best fit for the first growth cycle, from ±66 to 162 hr. Table 6.6 is a comparison of SSD and R^2 values obtained for the different growth models fitted to the second growth cycle of the growth curve from ±162 to 282 hr only. The two-phase model (fast acceleration phase from around ±162 to 212 hr and slow deceleration phase from around ±212 to 282 hr) gave the best fit for the second growth cycle. From the minimum SSD values of 5.46×10^{-6} for the fast acceleration phase and 3.90×10^{-6} for the slow deceleration phase, an order of magnitude smaller than for the logistic model, and a maximum R^2 value of 1 the two-phase model

provided the better fit to the growth curve. A comparison of Figures 6.4 and 6.6 indicate the best growth model fit is obtained when the point at around 354 hr on the growth curve is excluded.

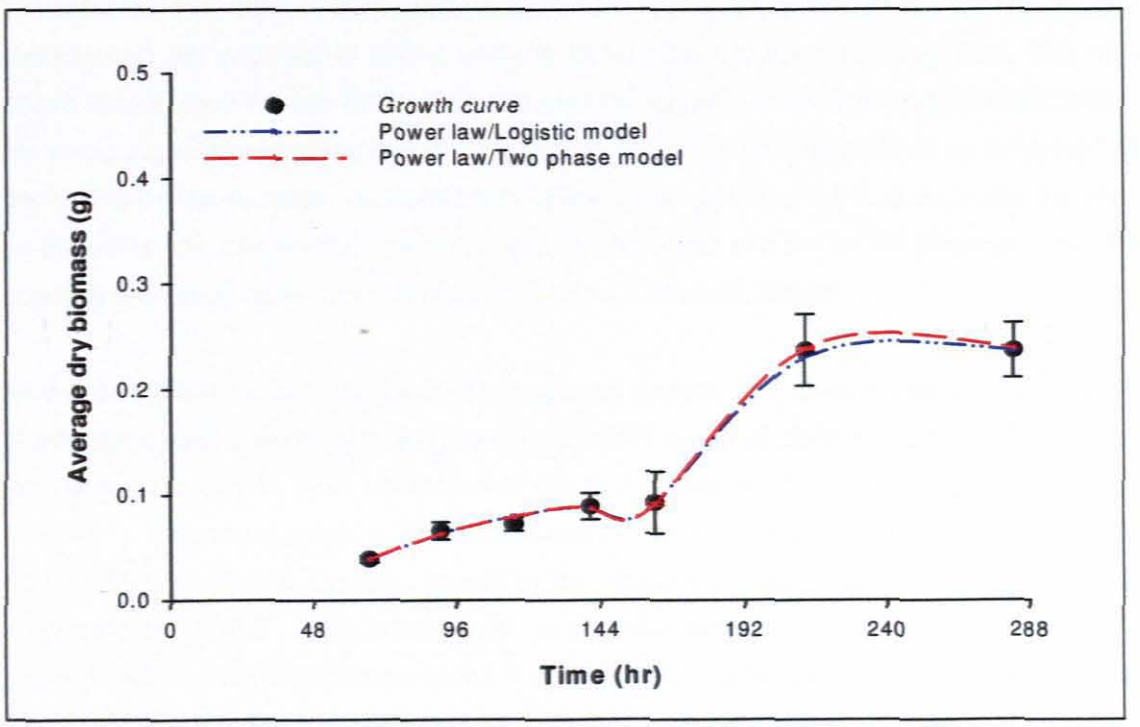

Figure 6.5: Two-phase growth models fitted to the growth curve obtained from the experimental data; excluding 354 hr (The error bars represent the standard error using Sigma Plot 8.0)

Table 6.6: Growth model fitting to the second growth cycle (162 to 282 hr)

Growth model	Specific growth rate (μ)	SSD	R^2	Notes
Logistic	0.075 hr^{-1}	6.96×10^{-5}	0.75	N/A
Exponential	0.019 hr^{-1}	4.48×10^{-1}	0.75	N/A
TWO-PHASE: Fast acceleration (Exponential)	0.019 hr^{-1}	5.49×10^{-6}	1	
Slow deceleration	0.013 hr^{-1}	3.90×10^{-6}	N/A	L = 1.47 k = 1

The two-phase model was developed to describe the growth of fungal micro organisms and although *S. coelicolor* is a filamentous bacterium it behaves like fungi to some extent, because Streptomycetes are mycelial bacteria resembling filamentous fungi in their apical growth (Flärdh, 2003), which explains why the two-phase growth model provided the best fit. To describe the growth of a filamentous micro organism a two-phase growth model, representing the exponential phase and the deceleration phase was developed. The two-phase model complements rather than replaces the logistic model (Ikasari & Mitchell, 2000). For micro organisms showing filamentous growth, the growth rate should not be described as depending on the substrate concentration, because the growth of a micro organism depends on the substrate concentration within its local environment and not on the average substrate concentration and usage within the biofilm (Ikasari & Mitchell, 2000).

As biphasic growth was demonstrated two specific growth rates were obtained, one for each growth cycle, with a lower specific growth rate (in the range of ±0.013 to 0.019 hr^{-1}) obtained for the second growth cycle compared to the first growth cycle (in the range of ±0.033 to 0.073 hr^{-1}). This corresponds to literature where similar MGR systems were utilised. Sheldon *et al.* (2008) confirmed biphasic growth in the filamentous white rot fungi *Phanerochaete chrysosporium* (BKMF-1767) immobilised on a polysulphone membrane in a flow-cell MGR operated with a peristaltic pump system. Two exponential growth phases were identified with specific growth rates in the range of 0.07 to 0.1 hr^{-1} for the first growth cycle and in the range of 0.015 to 0.05 hr^{-1} for the second growth cycle. This occurred due to the biofilm being exposed to ammonium starvation. Ntwampe and Sheldon (2006) also reported a primary and secondary growth phase for the white rot fungi *P. chrysosporium* (BKMF-1767) immobilised on a vertically orientated polysulphone capillary membrane in an MGR.

A comparison of the results (refer to Table 6.7) obtained in this study with a non-pressurised MGR system (Sheldon *et al.*, 2008) showed a similar trend, with a lower specific growth rate obtained for the second growth cycle compared to the first growth cycle. However, the ranges of the specific growth rate values were not similar, this could be attributed to a filamentous bacterium being utiilsed in this study and a white-rot fungi being utilised in the non-pressurised MGR system.

Karandikara *et al.* (1997) studied the life cycle of *Streptomyces coelicolor* on solid medium from a physiological perspective. In this study a biphasic growth pattern was identified, with a continuous transition from an initial exponential growth cycle into a slower growth cycle of biomass accretion. The change from the initial exponential growth cycle to the slower growth cycle coincided with the depletion of nitrate in the growth medium. The depletion of nitrate caused an increased production of α-ketoglutarate by the micro organism which resulted in a

decrease in the pH of the growth medium (Karandikara *et al.* 1997). A biphasic growth pattern was identified when *S. coelicolor* was cultured on a solid medium. Therefore, it would appear that a solid substratum (i.e. solid medium, membrane surface in an MGR) onto which the micro organism can immobilise is required to initiate the phenomenon of biphasic growth, as this was not observed in batch and fed-batch cultures.

Table 6.7: Comparison of literature with data from this study

	Current study	**Sheldon et al. (2008)**	**Karandikara *et al.* (1997)**
Micro organism	*S. coelicolor* A3(2)	*Phanerochaete chrysosporium* (BKMF-1767)	*S. coelicolor*
System	Pressurised continuous MGR	Non-pressurised flow-cell MGR	Solid medium
Specific growth rate (first growth curve)	±0.013 to 0.019 hr^{-1}	0.07 to 0.1 hr^{-1}	-
Specific growth rate (second growth curve)	±0.033 to 0.073 hr^{-1}	0.015 to 0.05 hr^{-1}	-
Reason identified for biphasic growth	Not identified	Ammonium starvation	Nitrate depletion

During this study the nitrogen concentration present in the permeate samples was not determined, therefore it was unknown whether the system experienced nitrate depletion; resulting in the biphasic growth identified. However, the pH of the system was determined daily and no decrease was noticed at ±162 hr when the first growth cycle ended and the second growth cycle started. This was possibly due to the fact that the system used in this study was a continuous system and not a batch system. The carbon concentration present in the permeate samples, in the form of glucose, was determined during this study. However, although the filamentous bacterium *S. coelicolor* A3(2) consumed glucose as indicated by the amount of glucose present in the permeate samples decreasing continuously over time, glucose was not the limiting substrate in this system as glucose was never completely depleted within the system.

Utilising linear programming Naeimpoor and Mavituna (2000) analysed the specific growth rate of *Streptomyces coelicolor* grown in chemostat cultures under various nutrient limitations. The maximum theoretical growth rate was 0.093 hr^{-1} for nitrogen limitation,

decrease in the pH of the growth medium (Karandikara *et al.* 1997). A biphasic growth pattern was identified when *S. coelicolor* was cultured on a solid medium. Therefore, it would appear that a solid substratum (i.e. solid medium, membrane surface in an MGR) onto which the micro organism can immobilise is required to initiate the phenomenon of biphasic growth, as this was not observed in batch and fed-batch cultures.

Table 6.7: Comparison of literature with data from this study

	Current study	**Sheldon et al. (2008)**	**Karandikara *et al.* (1997)**
Micro organism	*S. coelicolor* A3(2)	*Phanerochaete chrysosporium* (BKMF-1767)	*S. coelicolor*
System	Pressurised continuous MGR	Non-pressurised flow-cell MGR	Solid medium
Specific growth rate (first growth curve)	±0.013 to 0.019 hr^{-1}	0.07 to 0.1 hr^{-1}	-
Specific growth rate (second growth curve)	±0.033 to 0.073 hr^{-1}	0.015 to 0.05 hr^{-1}	-
Reason identified for biphasic growth	Not identified	Ammonium starvation	Nitrate depletion

During this study the nitrogen concentration present in the permeate samples was not determined, therefore it was unknown whether the system experienced nitrate depletion; resulting in the biphasic growth identified. However, the pH of the system was determined daily and no decrease was noticed at ±162 hr when the first growth cycle ended and the second growth cycle started. This was possibly due to the fact that the system used in this study was a continuous system and not a batch system. The carbon concentration present in the permeate samples, in the form of glucose, was determined during this study. However, although the filamentous bacterium *S. coelicolor* A3(2) consumed glucose as indicated by the amount of glucose present in the permeate samples decreasing continuously over time, glucose was not the limiting substrate in this system as glucose was never completely depleted within the system.

Utilising linear programming Naeimpoor and Mavituna (2000) analysed the specific growth rate of *Streptomyces coelicolor* grown in chemostat cultures under various nutrient limitations. The maximum theoretical growth rate was 0.093 hr^{-1} for nitrogen limitation,

0.071 hr^{-1} for phosphate limitation and 0.065 hr^{-1} for both sulphur and potassium limitations. In this study, the specific growth rate was determined to be 0.049 hr^{-1} for the first growth cycle; 0.013 hr^{-1} for the fast acceleration phase and 0.019 hr^{-1} for the slow deceleration phase of the two-phase growth model. When compared to the specific growth rates determined by Naeimpoor and Mavituna (2000) it would appear that the system utilised in this study was not experiencing limitation from any of the nutrients analysed by Naeimpoor and Mavituna (2000).

According to Bystrykh *et al.* (1996) the general response of *S. coelicolor* A3(2) to a depletion of glucose is the abolishment of blue pigment synthesis; and to growth limitation by nitrogen (either ammonium or nitrate), phosphate, or trace elements is the synthesis of blue pigment (i.e. actinorhodin). The phosphate concentration of the permeate samples was determined daily and remained stable for the duration of the study. Blue pigment synthesis did not cease for the duration of the study. Therefore, the possibility exists that the system experienced trace element limitation since this was not measured and the amount of trace elements present in the nutrient medium was unknown, as a complex medium was utilised for the study.

For batch cultures of *S. coelicolor* A3(2) with an air-flow rate of 2 to 6 L/min a maximum specific growth rate of 0.03 hr^{-1} was achieved (Ozergin-Ulgen & Mavituna, 1993). For a batch culture with a lower air flow rate of 2 L/min a maximum specific growth rate of 0.017 hr^{-1} was determined (Ates *et al.*, 1997), while for a fed-batch culture with an air flow rate of 2 L/min a maximum specific growth rate of 0.022 hr^{-1} was determined (Ozergin-Ulgen & Mavituna, 1993). In batch cultures of *S. coelicolor* A3(2) with a continuous glucose feed, higher maximum specific growth rates were obtained at higher airflow rate.

The results for the first growth cycle in this study is in agreement with the specific growth rate obtained for the same filamentous bacterium cultured in a non-pressurised batch system (Ozergin-Ulgen & Mavituna, 1993). However, in non-pressurised batch and fed-batch systems of *S. coelicolor* A3(2) operated at lower airflow rates than utilised in this study, the specific growth rates were similar to the specific growth rate range obtained for the second growth cycle in this study. For *S. coelicolor* A3(2) a combination of pressure and airflow rate influences the specific growth rate, with higher specific growth rates obtained when the airflow rate is higher and the system pressurised.

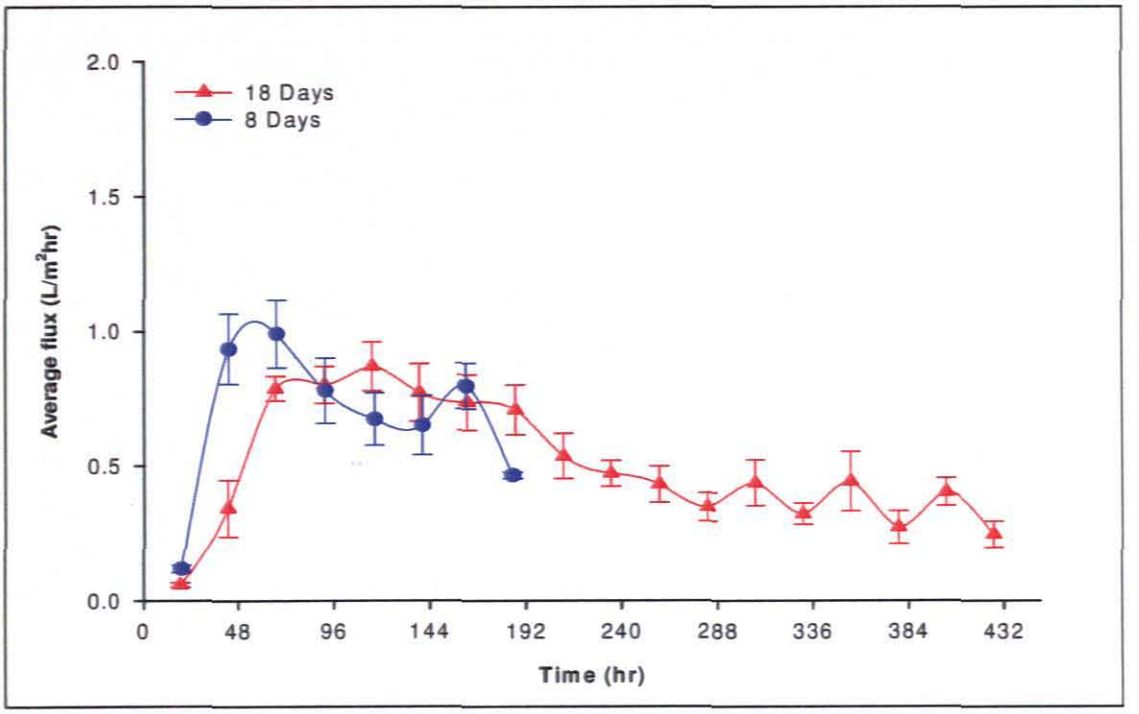

Figure 6.6: Average flux for the 1 x 12 SFMGR rig (The error bars represent the standard error using Sigma Plot 8.0)

Two experiments were operated for a time duration of 18 days, while two experiments were operated for 8 days. In Figure 6.7 it was observed that the flux gradually decreased over time due to an increase in the biofilm thickness and therefore an increase in resistance to flux. *Refer to section 5.5.1 in Chapter 5 for an expanded discussion and comparison to various* literature sources regarding flux and *S. coelicolor* A3(2).

6.5.3 Average pH

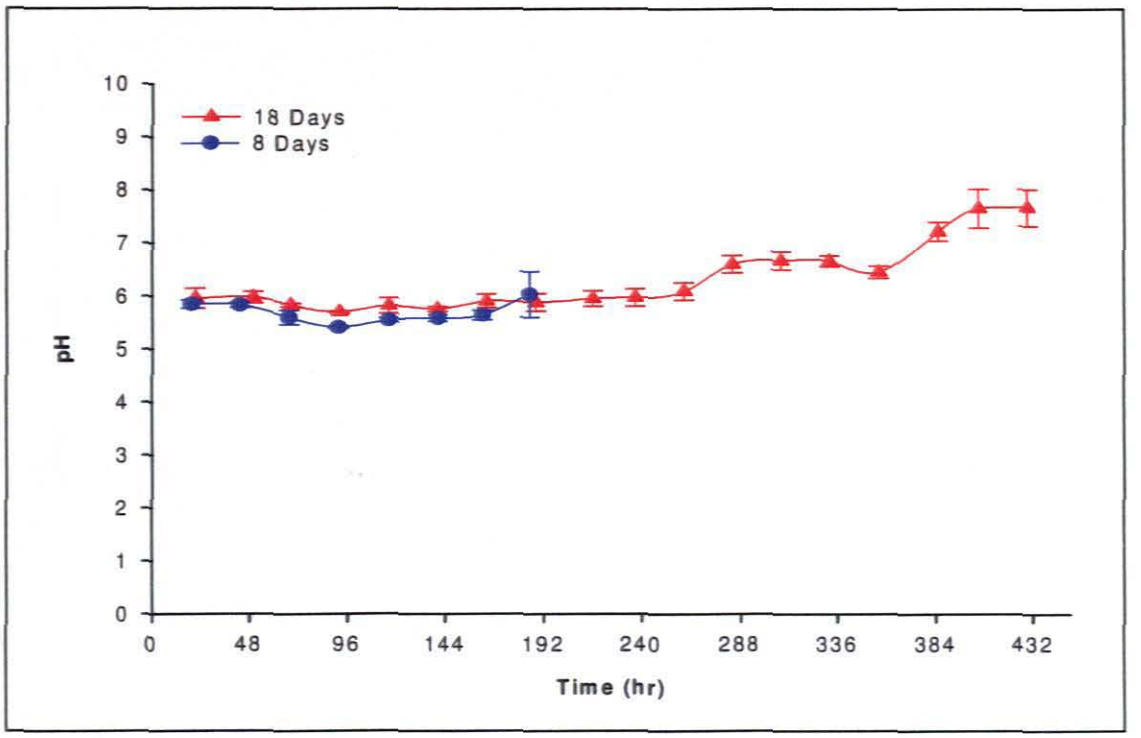

Figure 6.7: Average pH obtained for the 1 x 12 SFMGR rig (The error bars represent the standard error using Sigma Plot 8.0)

The initial pH of the ISP2 complex growth medium was 7.5 and as is characteristic with this growth medium the pH of the permeate samples first decreased to about 5.5 while the biofilm was establishing itself before increasing. In the curve representing 8 days, in Figure 6.8, the pH had only just started increasing when the reactors in these experiments were disconnected. The graph representing 18 days in Figure 6.8 followed the same trend observed in the results obtained for the 1 x 3 SFMGR rig in section 5.5.2. The maximum pH obtained over the 18 day time period was 7.8. Refer to section 5.5.2 in Chapter 5 for an *expanded discussion and comparison to various literature sources regarding pH and S. coelicolor* A3(2).

6.5.4 Average actinorhodin production

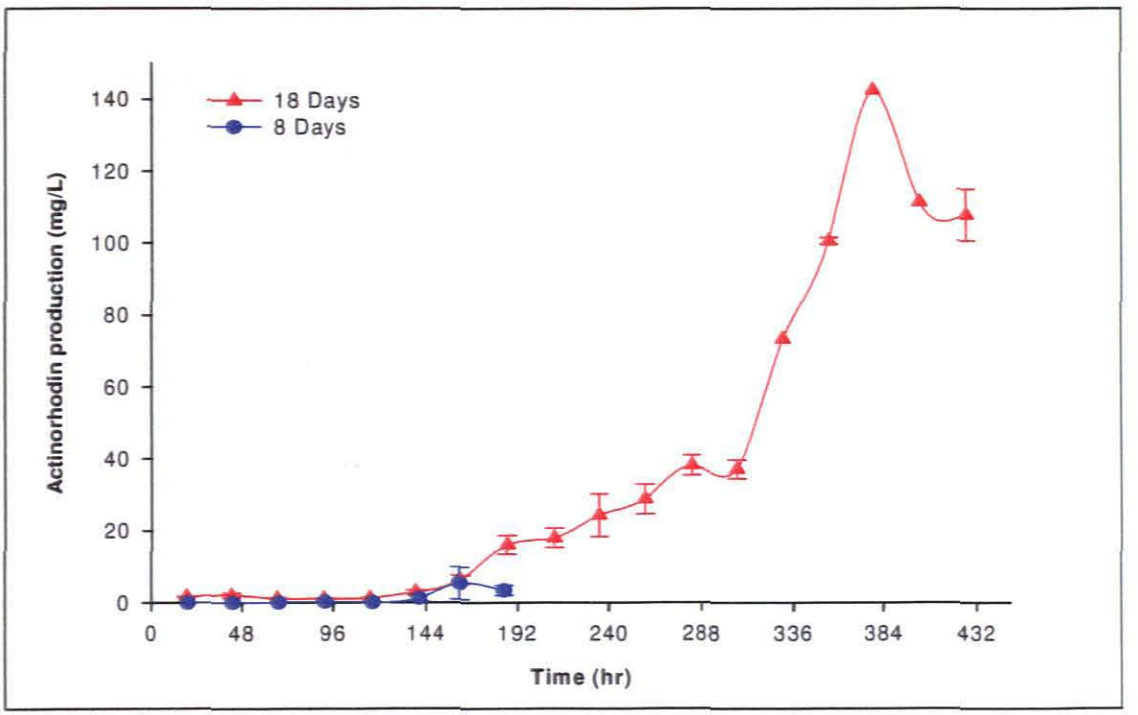

Figure 6.8: Average secondary metabolite production obtained for the 1 x 12 SFMGR rig (The error bars represent the standard error using Sigma Plot 8.0)

A comparison of Figure 6.8 and Figure 6.9 revealed that secondary metabolite production is directly proportional to an increase in pH. In other words as the pH increases so to does the production of the secondary metabolite, actinorhodin. When the pH decreased actinorhodin production also decreased as seen at 360 hr in Figures 6.8 and 6.9 on the curve representing 18 days in each of the Figures. Refer to section 5.5.3 in Chapter 5 for an expanded discussion and comparison to various literature sources regarding secondary metabolite (actinorhodin) production and *S. coelicolor* A3(2).

6.5.5 Average phosphate concentration

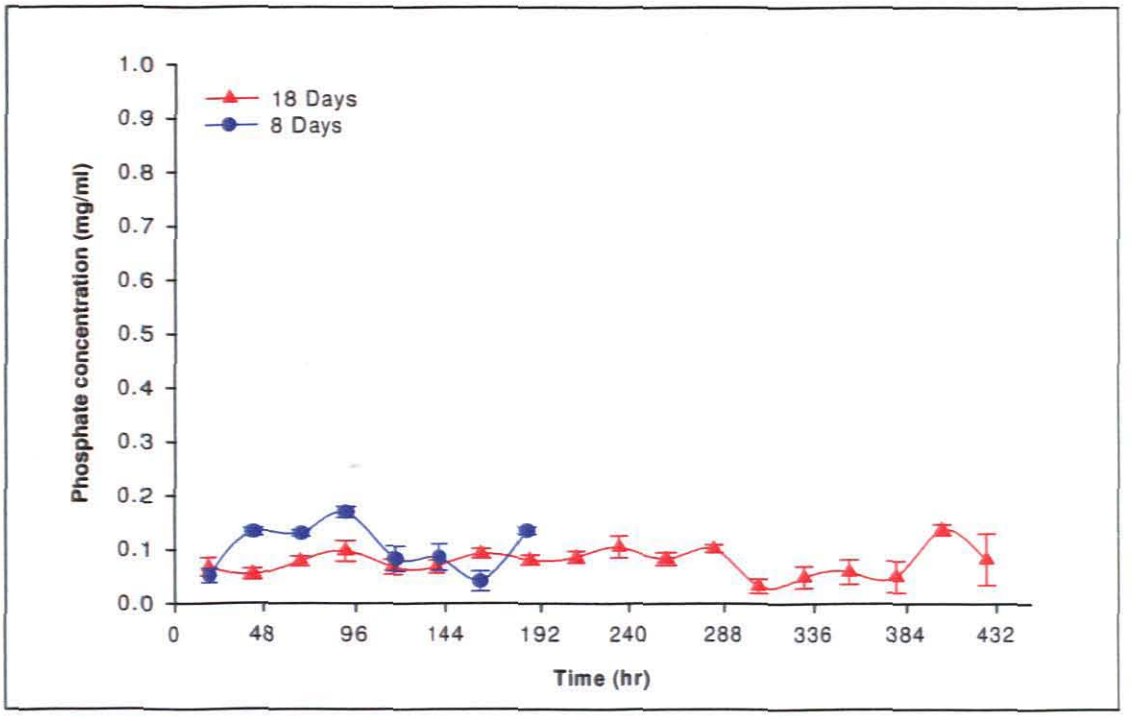

Figure 6.9: Average phosphate for the 1 x 12 SFMGR rig (The error bars represent the standard error using Sigma Plot 8.0)

The original concentration of phosphate in the ISP2 complex growth medium was 0.083 mg/ml. From the curves in Figure 6.10 and the corresponding phosphate concentration values the micro organism was not consuming or producing phosphate as the phosphate concentration present in the permeate samples remain stable around 0.083 mg/ml for the duration of the experiments. Refer to section 5.5.4 in Chapter 5 for an expanded discussion and comparison to various literature sources regarding the average phosphate concentration present in the permeate samples and *S. coelicolor* A3(2).

6.5.6 Average glucose concentration

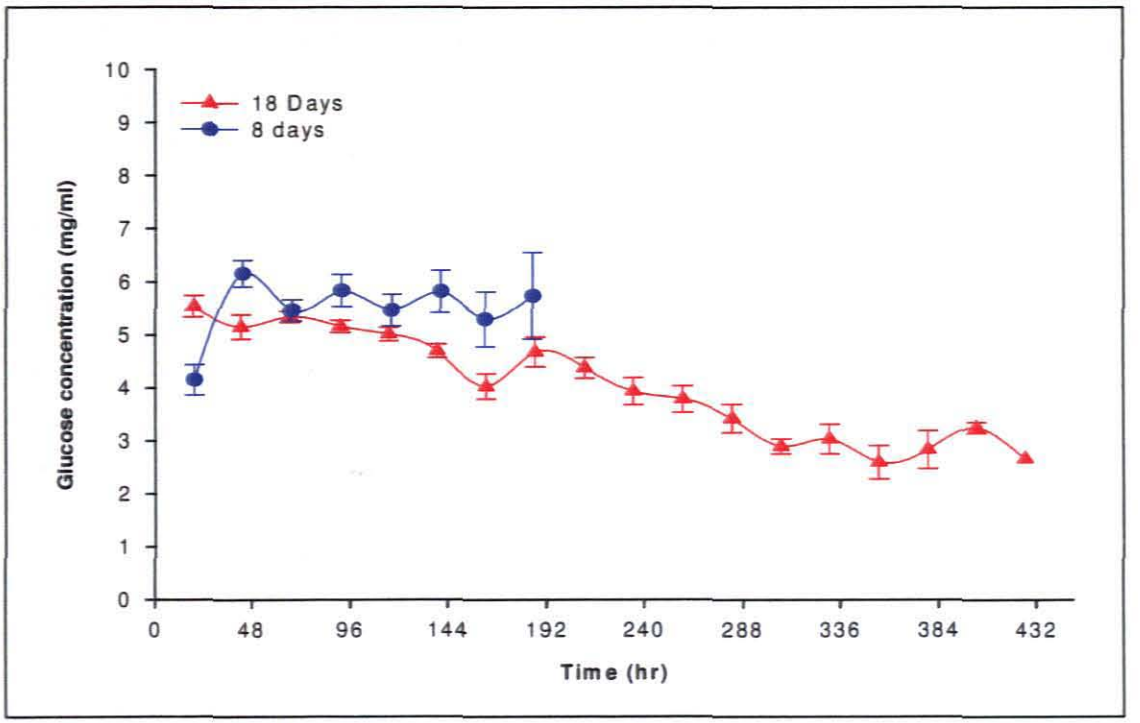

Figure 6.10: Average glucose concentration for the 1 x 12 SFMGR rig (The error bars represent *the standard error using Sigma Plot 8.0*)

The original glucose concentration present in ISP2 complex growth medium was 4.97 mg/ml. Figure 6.11 indicates that the filamentous bacterium *S. coelicolor* A3(2) consumed glucose as the amount of glucose present in the permeate samples decreased continuously over time. However glucose was not the limiting substrate in this system as glucose was never completely depleted by the system. Refer to section 5.5.5 in Chapter 5 for an expanded discussion and comparison to various literature sources regarding the average glucose concentration present in the permeate samples and *S. coelicolor* A3(2).

6.5.7 Correlation of measured parameters and the growth curve

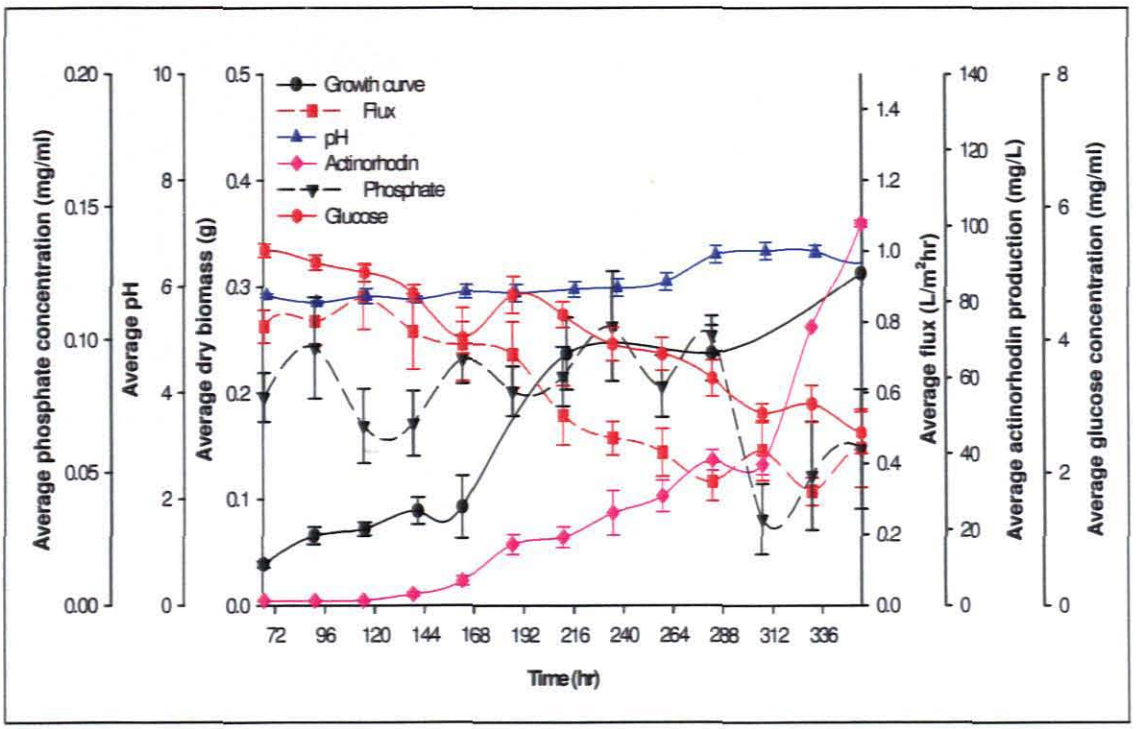

Figure 6.11: Growth curve, average flux, pH, actinorhodin production, phosphate and glucose consumption profiles (The error bars represent the standard error using Sigma Plot 8.0)

Figure 6.12 allows all the measured parameters (i.e. average flux, average pH, average actinorhodin production, average phosphate concentration and average glucose consumption) to be compared to the growth curve obtained from the average dry biomass. *The average phosphate and average pH curves in Figure 6.12 do not follow the same trend* as the other curves of either significantly increasing or decreasing. These two curves appear to remain relatively stable over the time course of the growth curve, with no significant increase or decrease observed.

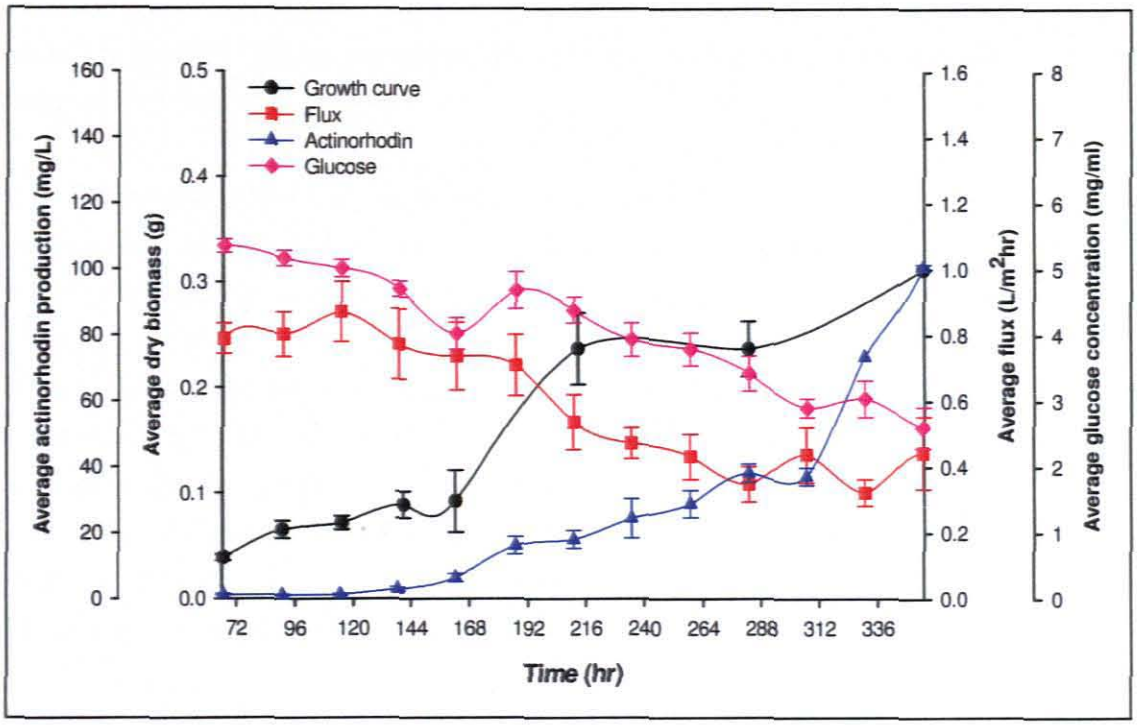

Figure 6.12: Growth curve, average flux, actinorhodin production and glucose consumption profiles (The error bars represent the standard error using Sigma Plot 8.0)

Figure 6.13 is similar to Figure 6.12; however the average pH and average phosphate curves were removed to facilitate clearer interpretation of trends by the curves with respect to each other and the growth curve.

According to Elibol (2002) most of the glucose consumed by *S. coelicolor* A3(2) is utilised for biomass formation, which accounts for the glucose concentration decreasing as the biomass increased in Figure 6.13. However, as the biomass increased, the flux decreased, this was expected as the pressure differential was kept constant for the duration of the experimental procedures. Therefore, as the biofilm increased in thickness due to glucose consumption, the flux decreased due to increased resistance from the growing biofilm. An increase in biofilm thickness resulted in decreased flux, which in turn caused the biofilm to experience nutrient limitation and therefore increased secondary metabolite, actinorhodin, production. Actinorhodin production is initiated by nutrient limitation, the more significant the nutrient limitation the higher the actinorhodin production.

6.6 Summary

The growth kinetics of the filamentous bacterium *Streptomyces coelicolor* A3(2) immobilised in a pressurised MGR exhibits biphasic growth. From the growth models fitted to the growth curve obtained from the experimental data, the power law model described the first growth cycle and the two-phase model the second growth cycle In this study, the specific growth

rate was determined to be in the range of ±0.033 to 0.073 hr^{-1} for the first growth cycle and ±0.013 to 0.019 hr^{-1} for the second growth cycle and the two-phase growth model provided a better fit than the logistic model.

It is recommended that the experiments be repeated with the same growth medium but at lower nutrient and airflow rates, to try prevent biofilm sloughing and thus confirm the shape of the growth curve and possibility of a third growth cycle after 354 hr. An assay to determine the nitrate concentration present in the permeate samples should be performed to identify if nitrate depletion occurs in continuously operated pressurised SFMGR systems. Identical pressurised and non-pressurised systems of *S. coelicolor* A3(2) should be compared with regards to specific growth rates, biofilm thickness and biomass to determine the effect of pressure on the system. Experiments with other bacteria should be conducted in pneumatic systems to confirm whether the two-phase growth model phenomenon applies only to filamentous micro organisms or include bacteria.

CHAPTER 7

RESULTS

MULTI-FIBRE MEMBRANE GRADOSTAT REACTOR (MFMGR) SCALE-UP

CHAPTER SEVEN

MULTI-FIBRE MEMBRANE GRADOSTAT REACTOR (MFMGR) SCALE-UP

7.1 Introduction

The scale-up step from laboratory to industrial scale is complicated (Govender *et al.*, 2003). Currently, scale-up is an empirical, imprecise art (Shuler & Kargi, 2002).

7.1.1 Background

A problem observed with scale-up, is that the actual productivity is less than the predicted theoretical maximum, due to the utilised operational parameters being based on empirical assumptions made after single fibre membrane gradostat reactor (SFMGR) analysis (Govender *et al.*, 2003). Kinetic growth models are required by engineers in the design process, as these models are an excellent scientific method for predicting a system's behaviour for the design of scaled-up systems (Sheldon *et al.*, 2008). Possible methods for improving scale-up are therefore, kinetic growth models and scale-down procedures since microenvironmental conditions are scale dependent (Shuler & Kargi, 2002).

7.1.2 Objectives

This study was conducted to gain information regarding how scale-up from a SFMGR to a MFMGR would effect secondary metabolite production. Therefore, the primary aim for this part of the study was process scale-up from a single fibre membrane gradostat reactor (SFMGR) to a multi-fibre membrane gradostat reactor (MFMGR).

The objectives of the experimental procedure were to:

- Culture *S. coelicolor* in a MFMGR utilising ceramic membranes with a larger inner and outer diameter.
- Quantify the substrate (i.e. glucose and phosphate) consumption.
- Quantify the product (i.e. actinorhodin) formation.

7.2 Materials and methods

7.2.1 Micro organism

Two MFMGR's were run with the complex growth medium, ISP2, and the filamentous bacterium *Streptomyces coelicolor* A3(2) (Yul-Min and Jae-hoen, 2004), maintained as a frozen spore suspension in 20% glycerol at a temperature of -80°C. The frozen spore suspension had a spore concentration of 1 x 10^7 spores/ml, and was prepared as explained in section 3.5.1.

7.2.2 Inoculum preparation and inoculation procedure

The inoculum was prepared as explained in section 3.5.2. The same reverse filtration inoculation procedure (Govender *et al.*, 2004) that was used for the SFMGR, explained in section 3.5.4, was utilised to inoculate each MFMGR. However, the MFMGR's were inoculated with 1 L of sterilised ISP2 growth medium, to which the 40 ml sterile ISP2 growth medium inoculated with 100 µl of the defrosted spore suspension in the shaker-flask had been sterily added.

7.2.3 Growth medium

The growth medium used for the inoculum preparation and operation of the MFMGR's was ISP2, a complex growth medium, refer to Table 3.3 in section 3.4 for the preparation procedure.

7.3 Experimental set-up

The experimental set-up used in this section was two stainless multi-fibre membrane gradostat reactors (MFMGR's), shown in Figure 7.1, housing 28 ceramic capillary membranes, operated using the gradostat concept.

Two types of ceramic hollow fibre membranes were utilised. The inner and outer diameter of the two membranes was the only difference between the two, as explained in Table 3.1 in section 3.2.1.

Following construction; the glass MFMGR's and ceramic membranes, medium bottles, humidifier, sample collection bottles and prime bottle were sterilised by autoclaving at a temperature of 121 °C and a pressure of 1 atm for 20 min.

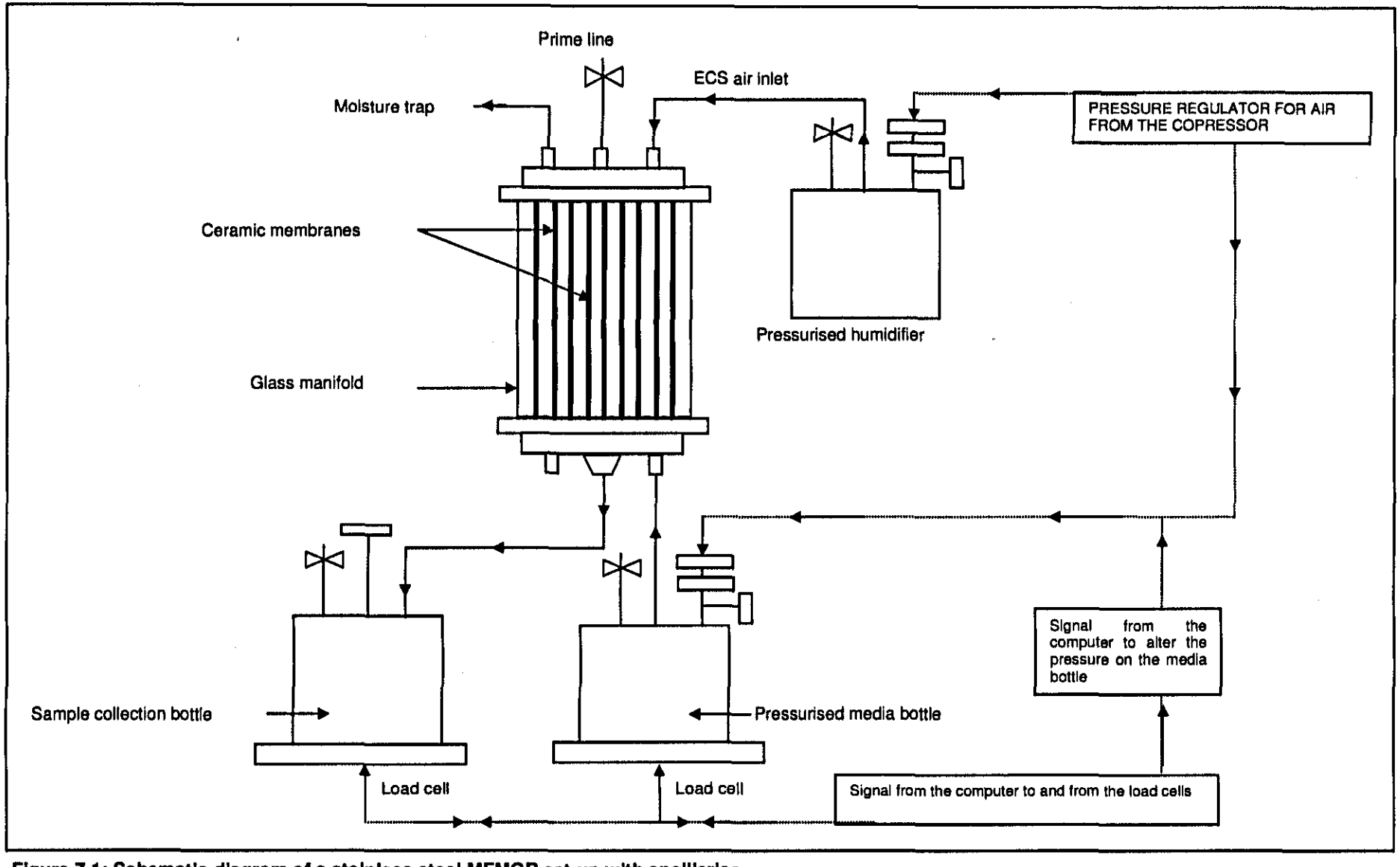

Figure 7.1: Schematic diagram of a stainless steel MFMGR set-up with ancillaries

7.3.1 Nutrient flow rate and airflow rate

The growth medium was supplied to the lumen of the ceramic membranes at a flow rate of 0.02 L/hr (per module) and the air was supplied to the extracellular space (ECS) of the bioreactor at a flow rate of 2.4 L/hr per module. Using pressure transducers controlled by an automated computer program, a transmembrane pressure differential was created within the system by applying pressure to both the growth medium and the humidifier.

7.3.2 Bioreactor operation

Two vertically orientated MFMGR's operated under pressure utilising the MGR concept as patented by Leukes *et al.* (1999), were used to culture the bacteria *S. coelicolor* at 28°C. The MFMGR system was operated in a dead-end mode with a constant shell side pressure supplied by a JCS Shinko pressure controller. One MFMGR was run with 28 ceramic membranes with an inner diameter (ID) of 3 mm and an outer diameter (OD) of 4 mm, while the second MFMGR was operated with 28 ceramic membranes with an ID of 2 mm and an OD of 3 mm. Both MFMGR's were operated with ISP2 growth medium, as described by Shirling and Gottlieb (1966), for ±711 hr before the glucose and malt content of the ISP2 growth medium was reduced to 25% of the original amount. The medium thus contained per litre distilled water: 1 g glucose, 4 g yeast extract and 2.5 g malt extract. The MFMGR's were operated with this altered growth medium from ±711 to 902 hr. Between ±902 and 1233 hr the growth medium was altered to contain per litre distilled water: 1 g glucose, 4 g yeast extract and 10 g malt extract. The MFMGR's were operated with this altered growth medium until the bioreactors were disconnected. The composition of the growth medium was altered during this study to observe how altering the amount of glucose (i.e. carbon source) would influence secondary metabolite production by *S. coelicolor*. The effects of nutrient limitation are easier to observe on a larger scale, such as a MFMGR than on small scale, as a larger volume of permeate can be collected daily.

A bioreactor system can be operated in one of two ways, either via constant flux control or via constant pressure control in a pneumatic system. The system in this study was operated via pressure control and the creation of a pressure differential to ensure trans-membrane flux occurred. The growth medium and ECS were operated at set pressures of 53.0 kPa and 50 kPa respectively, to maintain a constant flux of 0.506 L/m^2.hr (per module) for the MFMGR housing the 3 mm (OD) x 2 mm (ID) ceramic membranes and 0.337 L/m^2.hr (per module) for the MFMGR housing the 4 mm (OD) x 3 mm (ID) ceramic membrane. The two MFMGR's had different flux rates because of the size difference between the ceramic membranes housed in the MFMGR's. The growth medium and permeate bottle of each MFMGR was placed on a load cell that was connected to a computer. The pressure for the medium bottles was adjusted, according to the data received from the load cells by the

automated computer program, to maintain a constant flow rate of 20 ml/hr (i.e. 480 ml/day) to each MFMGR. Both MFMGR's were operated for 52 days (±1233 hr) before disconnecting.

7.4 Analytical methods

Permeate from each MFMGR was collected and analysed daily. The amount of permeate collected daily was dependent on the pressure differential and the resistance to transmembrane flux by the biofilm. The volume and pH of the permeate samples were measured and recorded daily, including the time elapsed between sampling; thus allowing the flux to be calculated for each MFMGR.

On completion of the experimental procedure the wet biomass of each MFMGR was recorded, as well as the dry biomass, after the biofilm had been dried for 12 hr at 70°C in an oven (refer to section 3.7).

Actinorhodin concentrations were determined as described in section 3.9.1. Refer to Appendix A for a detailed description of the actinorhodin assay procedure. The glucose and phosphate concentrations were determined as described in sections 3.9.2 and 3.9.3, respectively. Refer to Appendices B and C for detailed descriptions of the glucose and phosphate assays, respectively.

7.5 Results and discussion

One permeate sample was taken from each MFMGR daily. The flux, pH, actinorhodin, glucose and phosphate results obtained daily were plotted with the aid of the statistical program, Sigma Plot (Version 8).

automated computer program, to maintain a constant flow rate of 20 ml/hr (i.e. 480 ml/day) to each MFMGR. Both MFMGR's were operated for 52 days (±1233 hr) before disconnecting.

7.4 Analytical methods

Permeate from each MFMGR was collected and analysed daily. The amount of permeate collected daily was dependent on the pressure differential and the resistance to transmembrane flux by the biofilm. The volume and pH of the permeate samples were measured and recorded daily, including the time elapsed between sampling; thus allowing the flux to be calculated for each MFMGR.

On completion of the experimental procedure the wet biomass of each MFMGR was recorded, as well as the dry biomass, after the biofilm had been dried for 12 hr at 70°C in an oven (refer to section 3.7).

Actinorhodin concentrations were determined as described in section 3.9.1. Refer to Appendix A for a detailed description of the actinorhodin assay procedure. The glucose and phosphate concentrations were determined as described in sections 3.9.2 and 3.9.3, respectively. Refer to Appendices B and C for detailed descriptions of the glucose and phosphate assays, respectively.

7.5 Results and discussion

One permeate sample was taken from each MFMGR daily. The flux, pH, actinorhodin, glucose and phosphate results obtained daily were plotted with the aid of the statistical program, Sigma Plot (Version 8).

7.5.1 Average flux

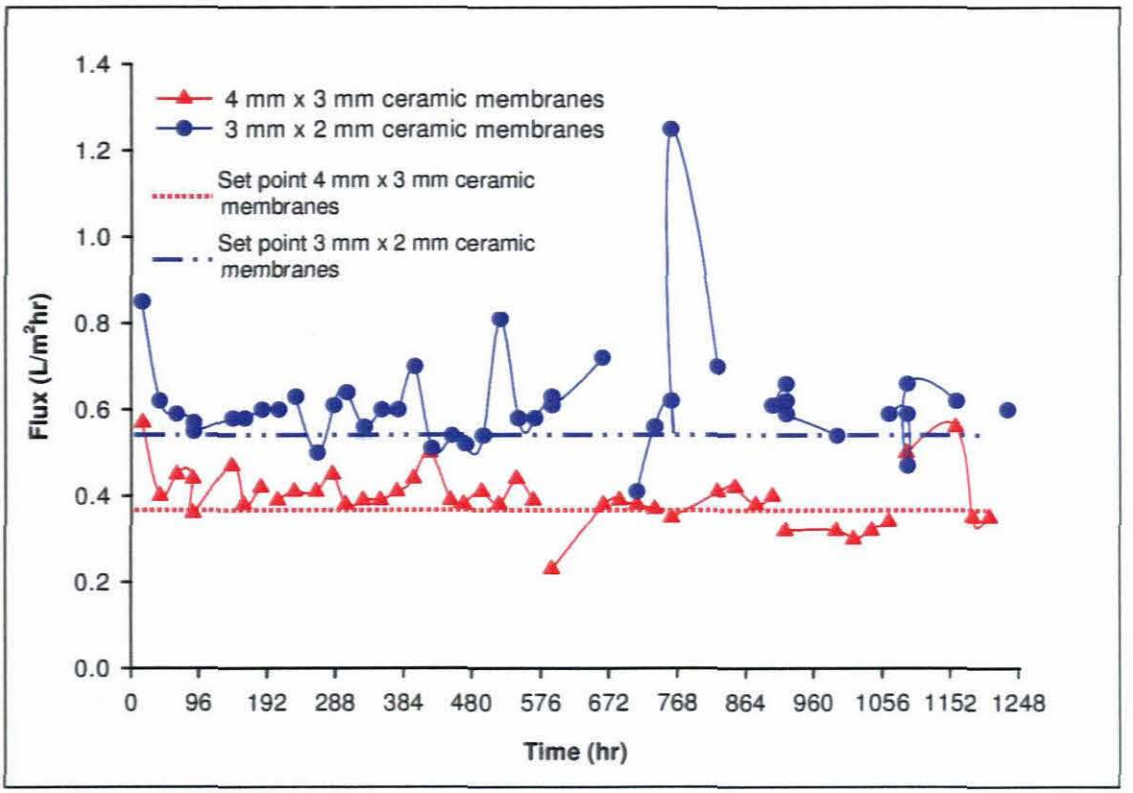

Figure 7.2: Average flux for the multi-fibre membrane gradostat reactors (MFMGR's)

The two MFMGR's were operated with a new automated computer program. The flux across both the 4 mm x 3 mm and 3 mm x 2 mm ceramic membranes was relatively stable over the 52 days (±1233 hr) of operation, with the actual flux of both MFMGR's operating slightly above their respective set fluxes.

However, after ±576 the flux in both MFMGR's was significantly higher and lower than the flux set point for the smaller and larger membranes, respectively, due to a problem experienced with the automated program. A technician was contacted and the problem solved with the flux returning to close to the set point.

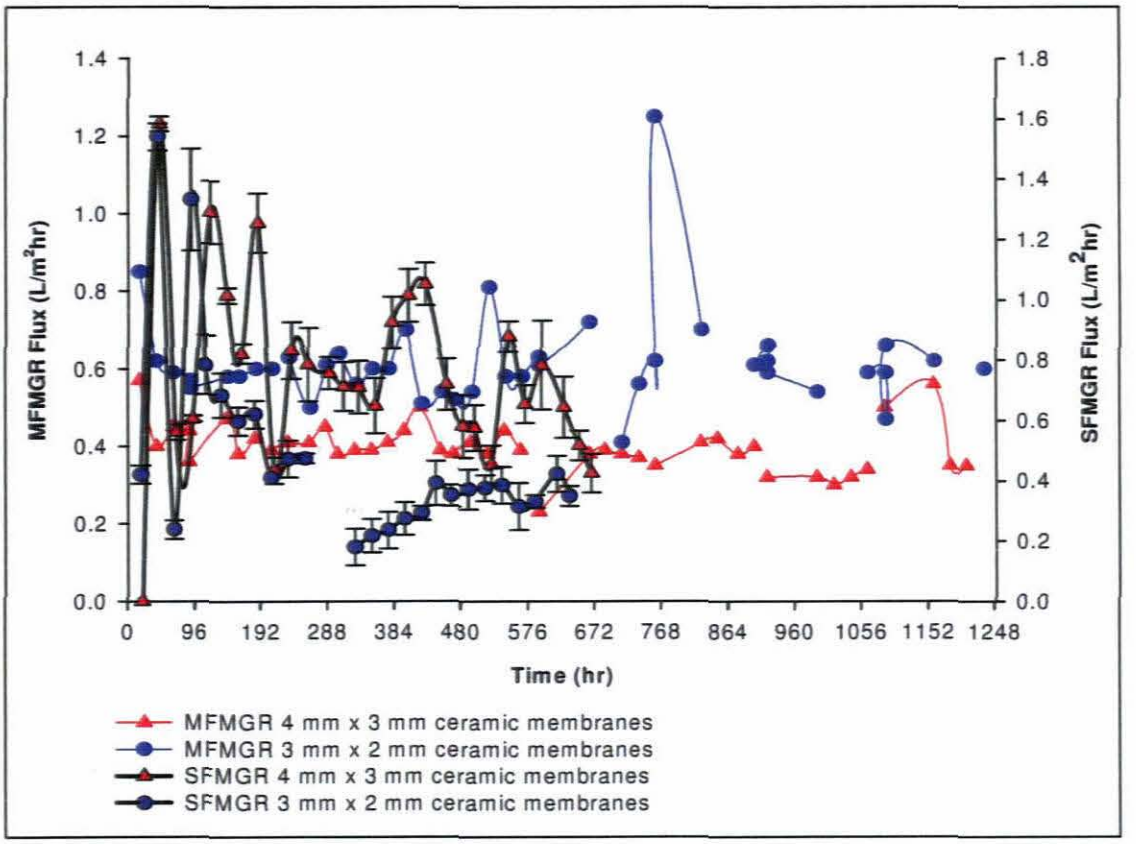

Figure 7.3: Comparison of the average flux for the multi-fibre membrane gradostat reactors (MFMGR's) and the single fibre membrane gradostat reactors (SFMGR's) (The error bars represent the standard error using Sigma Plot 8.0)

The SFMGR's were only operated for 672 hr before being disconnected, while the MFMGR's were operated for 1233 hr. In Figure 7.3 the fluxes were relatively stable for the larger and smaller membranes in the MFMGR's, while only the smaller membranes in the SFMGR's showed relatively stable flux.

The same pressure differential was utilised for both the 4 mm x 3 mm and 3 mm x 2 mm ceramic membranes in the SFMGR's. Therefore, the flux across the larger membranes was unstable when compared to the smaller membranes; this could be due to the pressure differential being too low to result in a stable transmembrane flux. In order to have maintained a stable flux similar to the smaller membranes the pressure differential should have been increased accordingly with an increase in membrane diameter.

7.5.2 Average pH

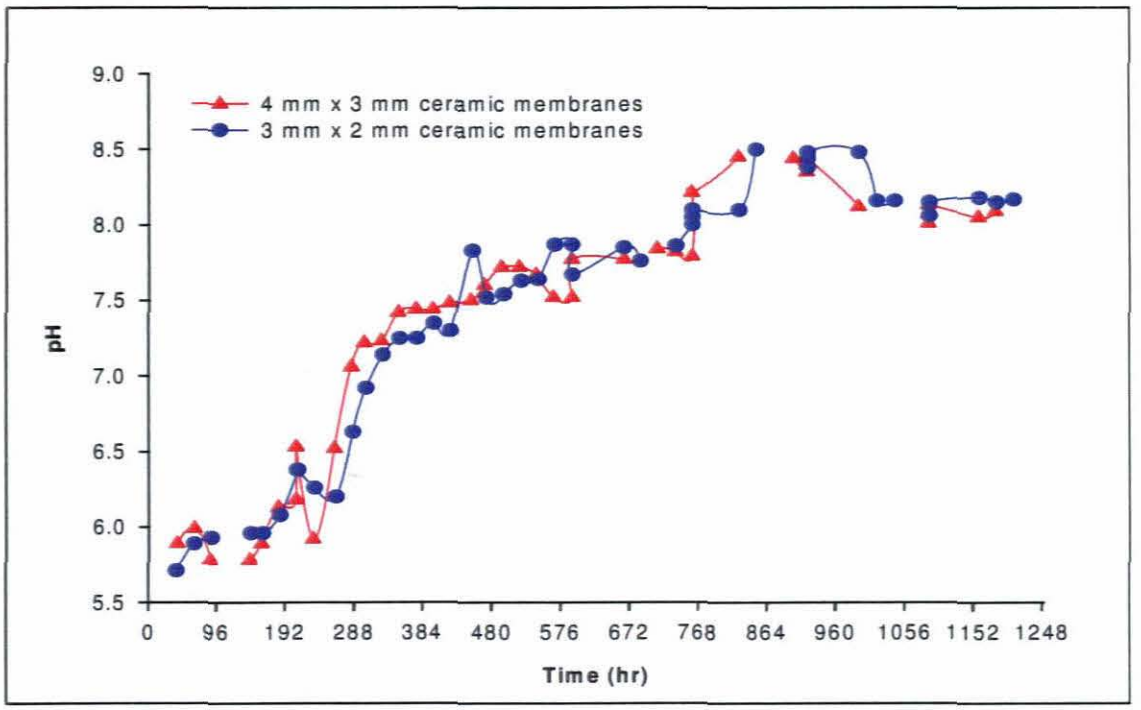

Figure 7.4: Average pH for the multi-fibre membrane gradostat reactor (MFMGR's)

The initial pH of the ISP2 growth medium was 7.5 first decreased for the first 24 hr, while the biofilm was establishing itself before increasing after 96 hr. As the MFMGR's were operated for ±1233 hr the pH could reach a maximum pH of about 8.5 in both MFMGR's. At growth medium pH values of 6.0 to 7.5 a different blue pigment is produced both intracellularly and extracellularly. *S. coelicolor* A3(2) is therefore capable of producing larger amounts of two actinorhodin-related pigments (Bystrykh *et al.*, 1996).

In Figure 7.4 at 720 hr a sudden increase in pH is seen in both curves. This corresponds to when the growth medium was changed from normal ISP2 growth medium to ISP2 growth medium containing 25% of the normal amount of glucose, 25% of the normal amount of malt extract and 100% of the normal amount of yeast extract. The decrease seen in both curves at ±912 hr corresponds to when the growth medium was changed to ISP2 growth medium containing 25% of the normal amount of glucose and 100% of both malt extract and yeast extract.

Comparing the pH in Figure 7.4 and the actinorhodin production in Figure 7.6, when the pH increases the actinorhodin production increases, and vice versa. This applies to both the 4 mm x 3 mm and 3 mm x 2 mm ceramic membranes. According to Bystrykh *et al.* (1996) at growth medium pH values of 4.5 to 5.5 significant amounts of the main intracellular pigment, actinorhodin occurs. At growth medium pH values of 6.0 to 7.5 a different blue pigment,

actinorhodin's lactone derivative γ-actinorhodin, responsible for the blue colour of the permeate, is produced both intracellularly and extracellularly. The pH of the permeate, seen in Figure 7.4, was in the range of 7.5 to 8.5 for most of the study. It was observed the permeate was blue in colour, therefore it was postulated γ-actinorhodin was being produced by the micro organism.

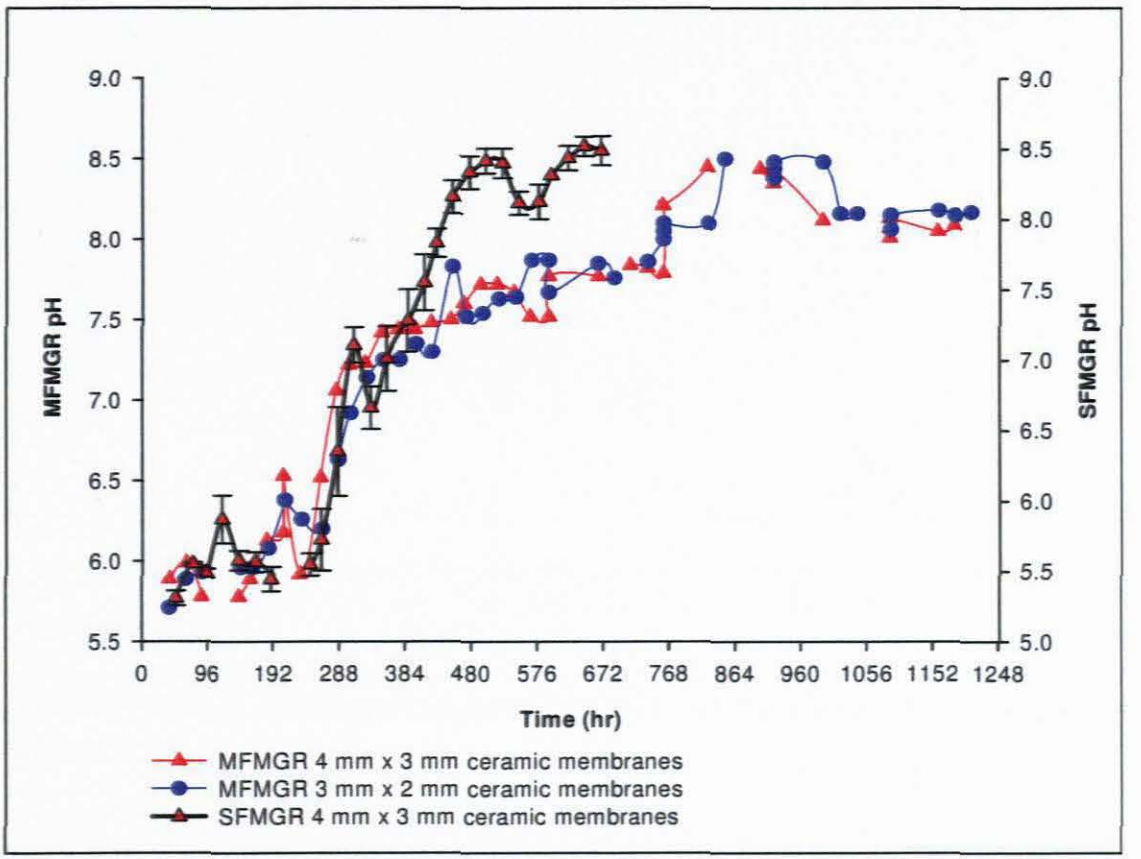

Figure 7.5: Comparison of average pH for the multi-fibre membrane gradostat reactor (MFMGR's) with single fibre membrane gradostat reactors (SFMGR's) (The error bars represent the standard error using Sigma Plot 8.0)

The pH curves followed the same trend in both the MFMGR and SFMGR rigs when operated with the complex growth medium, ISP2. In Figure 7.5 there is no curve for the 3 mm x 2 mm ceramic membranes in the SFMGR as pH was not measured when this experimental procedure was conducted. A maximum pH of approximately 8.5 was obtained with both membranes in the MFMGR's and the larger membranes in the SFMGR's.

The maximum pH was reached more rapidly in the SFMGR'S than in the MFMGR's. This is attributed to the fact that the SFMGR's operated with the larger membranes were operated at the same pressure differential as for the smaller membranes. Therefore, the flux across the

large membranes was lower, resulting in reduced growth medium to the biofilm and thus nutrient limitation. Nutrient limitation results in the onset of secondary metabolism which is indicated by the rapidly increasing pH.

7.5.3 Average actinorhodin production

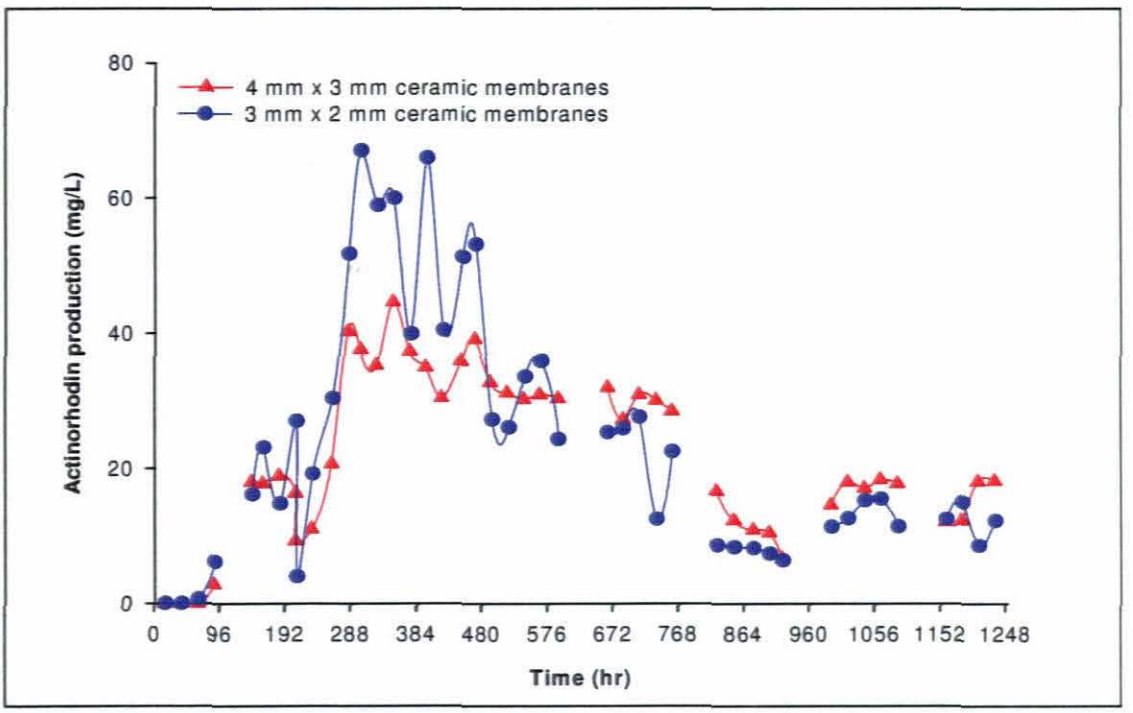

Figure 7.6: Average actinorhodin production for the multi-fibre membrane gradostat reactor (MFMGR's)

While the two MFMGR's were operated with normal ISP2 growth medium the MFMGR with the 3 mm (OD) x 2 mm (ID) ceramic membranes had a higher actinorhodin production than the MFMGR with the 4 mm (OD) x 3 mm (ID) ceramic membranes. However, in Figure 7.6 when the growth medium was changed at ±711 hr the MFMGR with the larger ceramic membranes showed a higher actinorhodin production. This phenomenon remained even after increasing the malt extract in the ISP2 growth medium back to 10 g/L.

The results in Figures 7.2, 7.4 and 7.6 indicated that flux, pH and actinorhodin production are all related. While the flux and actinorhodin production were inversely related, the pH and actinorhodin production were proportional to each other. If either the flux or the pH was not at an optimum, the actinorhodin production was adversely affected. A dynamic balance thus exists between these three parameters.

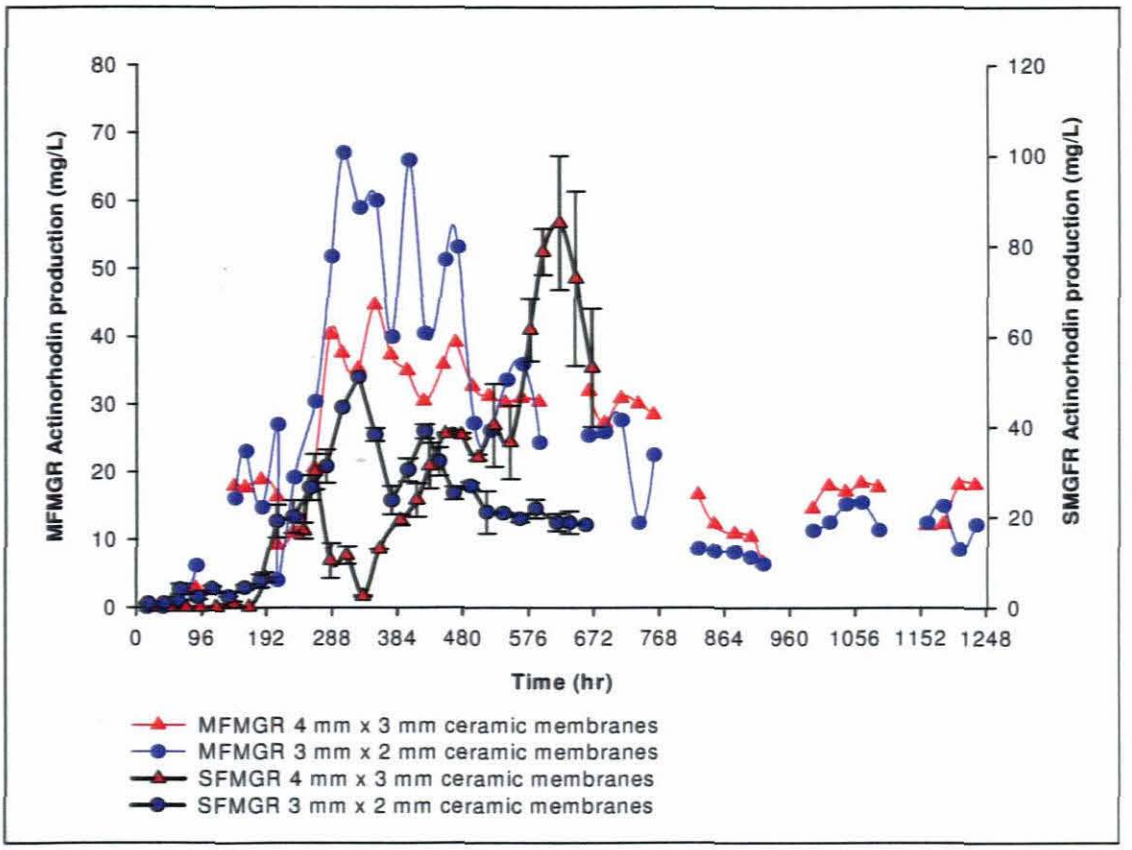

Figure 7.7: Comparison of the actinorhodin production in the multi-fibre membrane gradostat reactor (MFMGR's) with the single fibre membrane gradostat reactors (SFMGR's) (The error bars represent the standard error using Sigma Plot 8.0)

The results in Figure 7.7 indicate the highest actinorhodin concentration (85.12 mg/L) was produced by the SFMGR housing the larger membranes. The same pressure differential was utilised for both the larger and smaller ceramic membranes in the SFMGR's. Therefore, the flux across the larger membranes (refer to Figure 7.3) was unstable when compared to the smaller membranes; this could be due to the pressure differential being too low to result in a stable transmembrane flux. In order to have maintained a stable flux similar to the smaller membranes the pressure differential should have been increased accordingly with an increase in membrane diameter. Thus, it is postulated that the micro organism was under nutrient limitation, which stimulated a higher production of secondary metabolites.

The smaller membranes in the MFMGR's produced higher actinorhodin concentrations than the smaller membranes in the SFMGR's. The growth medium flux across the smaller ceramic membranes in the MFMGR of 0.506 L/m^2.hr was 28.5% lower than the flux of 0.708 L/m^2.hr across the smaller membranes in the SFMGR's. The biofilms immobilised in the MFMGR's

were receiving a lower volume of growth medium and therefore subjected to nutrient limitation resulting in higher concentrations of actinorhodin being produced.

7.5.4 Average phosphate concentration

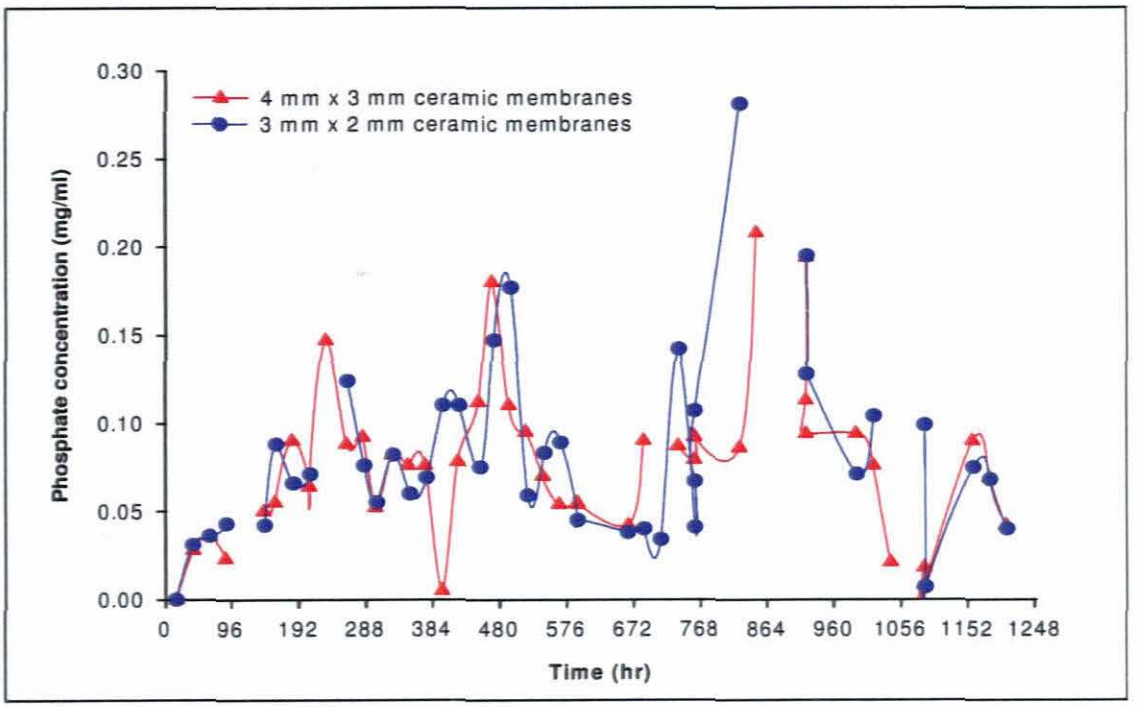

Figure 7.8: Average phosphate concentration for the multi-fibre membrane gradostat reactors (MFMGR'S)

The original phosphate concentration in the ISP2 growth medium was 0.083 mg/ml and when the medium was changed at ±711 hr the growth medium contained 0.073 mg/ml phosphate. The phosphate concentration in the growth medium, changed at 902 hr, to contain 25% of the normal amount of glucose and 100% malt extract, was 0.110 mg/ml.

The results in Figure 7.8 indicate that the phosphate concentration present in the permeate samples decreased when the malt extract was decreased (±711 hr) and increased when the malt extract was increased (±902 hr) to its original amount. Therefore, the phosphate concentration was influenced by the absence and presence of the malt extract in the growth medium.

The increased phosphate present in the permeate samples from ±711 to 902 hr influenced actinorhodin production (Figure 7.6), during this time period. According to Bibb (2005) an excessive level of inorganic phosphate in the growth medium prevents the production of many structurally diverse secondary metabolites, such as actinorhodin. Phosphate concentrations in the range of 0.3 to 300 mM support cell growth. However, phosphate

concentrations of 10 mM and above repress the biosynthesis of many antibiotics (Ates *et al.*, 1997).

Once the amount of phosphate present in the growth medium was returned to normal (±902 hr) the actinorhodin production increased even though the glucose concentration was still decreased by 75%. The filamentous bacterium *S. coelicolor* therefore consumed almost all of the glucose (as seen in Figure 7.10 from ±902 to 1000 hr) for biomass formation, which resulted in an increased secondary metabolite production as the biofilm was subjected to nutrient limitations.

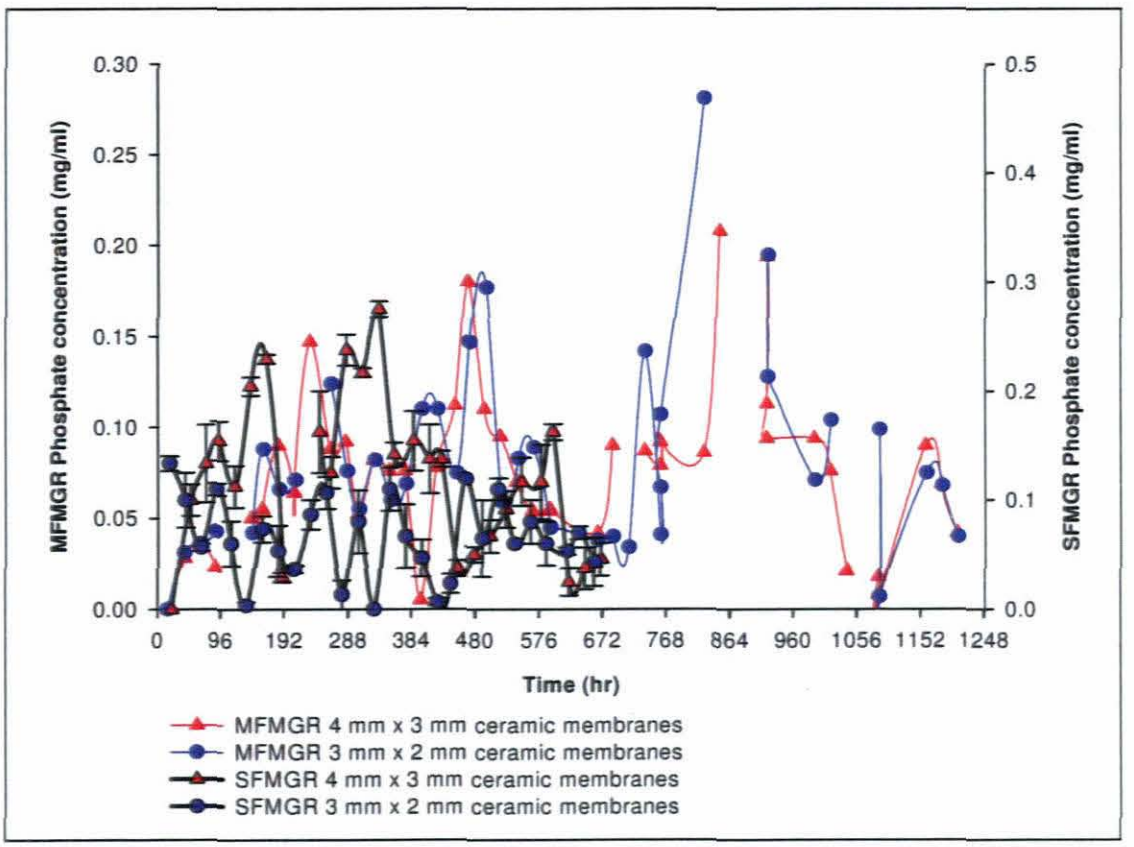

Figure 7.9: Comparison of the actinorhodin production in the multi-fibre membrane gradostat reactor (MFMGR's) with the single fibre membrane gradostat reactors (SFMGR's) (The error bars represent the standard error using Sigma Plot 8.0)

The phosphate concentration present in the permeate samples of both the SFMGR's and MFMGR'S were similar, with trace amounts of phosphate present, except at ±711 to 902 hr on the curves representing the MFMGR's. This is attributed to the malt extract and glucose amounts being decreased in the ISP2 growth medium at this time.

7.5.5 Average glucose concentration

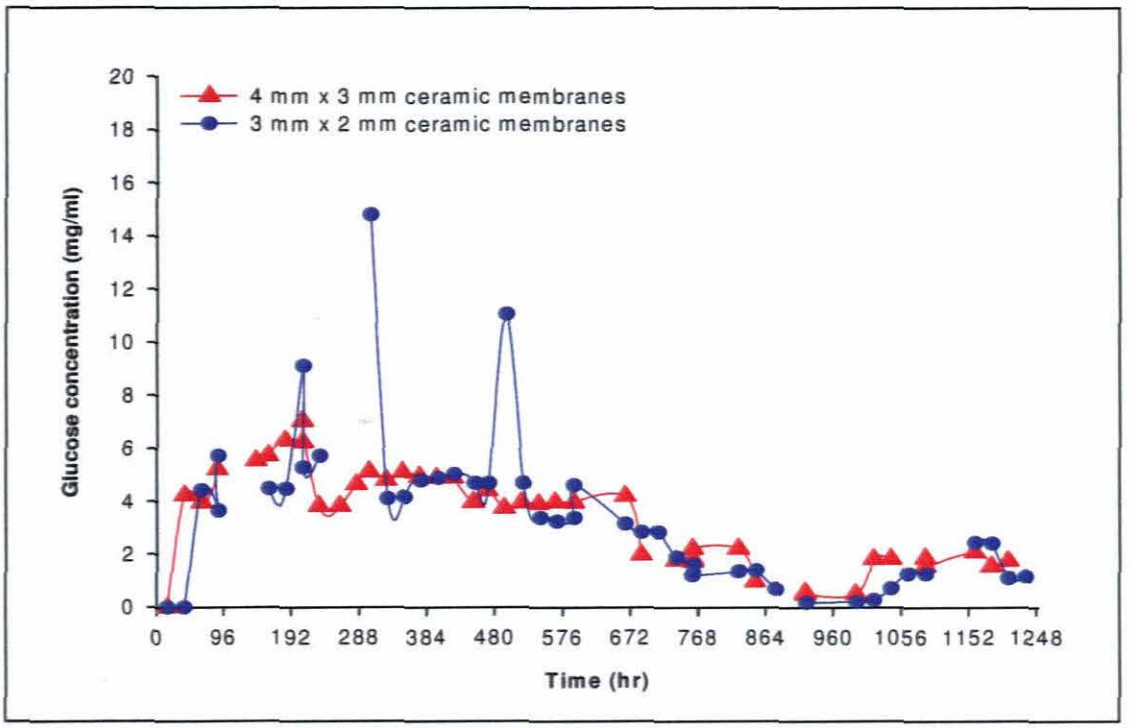

Figure 7.10: Average glucose concentration for the multi-fibre membrane gradostat reactors (MFMGR's)

The original glucose concentration of the complex growth medium ISP2 was ≈5 mg/ml. At ±711 hr the growth medium containing 25% of glucose and malt extract contained 1.825 mg/ml glucose. When the medium was changed at ±902 hr the glucose concentration was 2.415 mg/ml.

In Figure 7.10, ≈5 mg/ml of glucose was utilised by the micro organism, while the biofilm was being established in the first 48 hr, which is supported by literature in which Elibol (2002) states that glucose is consumed by *Streptomyces coelicolor* for biomass formation. Once the biofilm was established there was a decrease in the amount of glucose utilised by the micro organism. The glucose concentration present in the permeate samples steadily decreased as the biofilm increased in thickness with time. This was due to the filamentous bacterium *S. coelicolor* consuming glucose to form new biomass and also replace dead or dying biomass.

The rapid decrease in glucose concentration at ±711 hr was due to the amount of glucose present in the growth medium being decreased to 25%. At ±902 hr when the malt extract was increased to normal amount, the amount of phosphate present in the permeate samples decreased and a continuous decrease in glucose concentration was observed, until ±1008 hr. Between ±864 and 1008 hr the glucose and actinorhodin (Figure 7.6)

concentrations in the permeate samples were low, while the pH (Figure 7.4) was at a maximum of 8.5. When the glucose concentration increased after ±1008 hr the actinorhodin production also showed an increase, while the pH decreased to ±8.0. It was therefore postulated *S. coelicolor* was consuming glucose to form new biomass, since the micro organism was not utilising the glucose to produce secondary metabolites as seen in Figure 7.6.

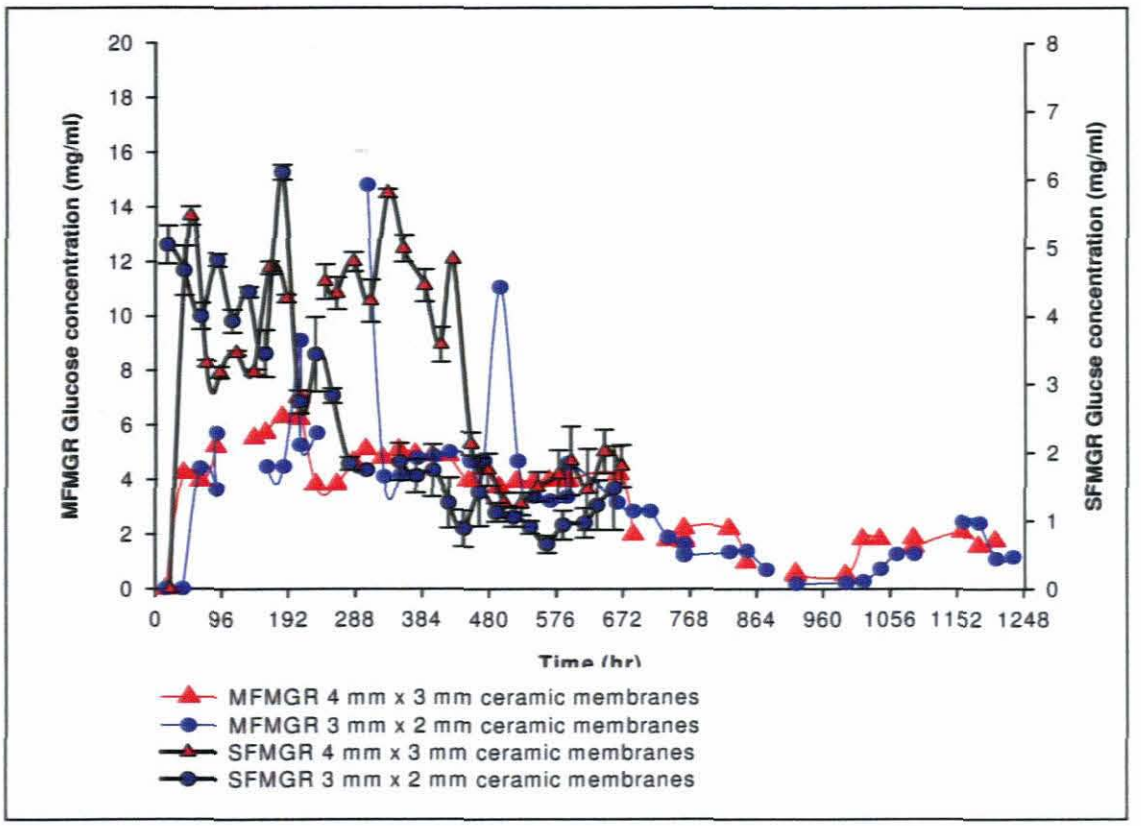

Figure 7.11: Comparison of the glucose production in the multi-fibre membrane gradostat reactors (MFMGR's) with the single fibre membrane gradostat reactors (SFMGR's) (The error bars represent the standard error using Sigma Plot 8.0)

The trend observed in both the SFMGR's and MFMGR's was that the glucose concentration present in the permeate samples steadily decreased with time. This is attributed to the filamentous bacterium consuming glucose for biomass formation (Elibol, 2002).

7.6 Summary

MFMGR's were operated as a scale-up experiment of the SFMGR's utilised earlier in this study. The amount of actinorhodin produced was influenced by the amount of phosphate present in the growth medium. Reduced actinorhodin concentrations were achieved, due to the increased phosphate concentration and large volume of growth medium diluting the actinorhodin concentration. A pH of above 8 was achieved and maintained in both MFMGR's

that allows for the production of both intracellular and extracellular actinorhodin. The highest actinorhodin concentration was however produced by the larger ceramic membranes in the SFMGR's. From the results it was concluded that *S. coelicolor* not only utilises glucose for biomass formation, but also actinorhodin production, as the actinorhodin production decreased when the glucose concentration in the growth medium was decreased.

Scale-up from SFMGR's to MFMGR's with *S. coelicolor* in MFMGR's is possible. However, for scale-up to be a success, the correct process parameters (i.e. growth medium composition, nutrient and air flow rates, membrane size) need to be utilised in order for the system to function optimally.

CHAPTER 8

RESULTS

MODELLING OXYGEN MASS TRANSFER WITHIN BIOFILMS OF *S. coelicolor* IMMOBILISED IN A CONTINUOUS PRESSURISED SINGLE FIBRE MEMBRANE GRADOSTAT REACTORS (SFMGR)

CHAPTER EIGHT

MODELLING OXYGEN MASS TRANSFER WITHIN BIOFILMS OF *S. coelicolor* IMMOBILISED IN CONTINUOUS PRESSURISED SINGLE FIBRE MEMBRANE GRADOSTAT REACTORS (SFMGR)

8.1 Introduction

The main problem of oxygen supply in aerobic biological systems, such as MBR's and MGR's utilised for the industrial production of antibiotics (Ozergin-Ulgen *et al.* 1998), is oxygen's nominal solubility in water (Hibiya *et al.*, 2003). Inadequate oxygen transfer results in reduced microbial activity (Thibault *et al.*, 2000). Reduced microbial activity can result in decreased production of low volume high value secondary metabolites.

The production of secondary metabolites, such as actinorhodin by *Streptomyces coelicolor,* is strongly affected by the dissolved oxygen (DO) concentration (Ozergin-Ulgen *et al.* 1998). To determine the effect of oxygen limitation on the production of secondary metabolites, oxygen profiles within the biofilm can be measured utilising microsensors (Frederick *et al.*, 1991). Microsensors were introduced through the work of Revsbech (1989), who constructed reliable oxygen microsensors, to be utilised in the profiling of oxygen distribution in sediments and biofilms. The mathematical modeling of the oxygen concentration profiles recorded with the oxygen microsensors, allowed the determination of oxygen kinetic parameters (Frederick *et al.*, 1991). The oxygen profiles obtained within biofilms not only added to increased understanding with regards to biological processes on a microscale, but also increased the information available regarding physical processes, such as diffusion and convection (Kuenen *et al.*, 1986).

The oxygen profiles obtained in this study will provide increased understanding of both the biological (microscale) and physical (diffusion and convection) processes within a pressurised MGR system. Therefore, more data will be available with regards to oxygen distribution within gradostat systems, thereby increasing the limited amount of information that is currently available.

8.2 Objectives

The main purpose of performing this part of the study was to determine the oxygen mass transfer kinetics, including the diffusive and convective parameters using *Streptomyces coelicolor* biofilms, immobilised on the external surface of a ceramic membrane in a continuously operated pressurised single fibre membrane gradostat reactor (SFMGR).

Figure 8.1: 1 x 3 SFMGR Quorus rig

8.4.1 Bioreactor design and construction

A schematic diagram of the SFMGR, as patented by Edwards *et al.* (2007), was illustrated schematically in Figure 3.4 and explained in section 3.3.1. The glass housing manifolds were specially designed (see Appendix D) for the oxygen measurements with a port located at the bottom; middle and top of the glass housing. After the SFMGR was constructed, the reactor with ceramic membranes was pressure tested using water to check its ability to withstand high pressures and that no leaks were present as explained in section 3.3.2. Three SFMGR's were manifolded together with 5 mm (ID) by 8 mm (OD) silicone tubing, as shown in Figure 3.6.

8.4.2 Clark-type ampoteric oxygen microsensor

All the oxygen microsensors utilised during this study were provided by Unisense (Denmark). Unisense produces high performance oxygen sensors for a variety of tasks. The oxygen microsensor used during this study was a Clark-type ampoteric oxygen sensor (shown in Figure 8.2) with a tip diameter of 10 µm, with a built-in guard cathode and reference anode. Ampoteric indicates that the sensor measures the concentration of an analyte by the current generated by the electrochemical reaction involving the analyte. Clark-type sensors are

based on the diffusion of oxygen through a silicone membrane to an oxygen reducing cathode that is polarised against an internal Ag/AgCl anode. The flow of electrons from the anode to the oxygen reducing cathode linearly indicates the oxygen partial pressure around the sensor tip and the signal is generated in the pA range. The current is measured by a PA2000 picoammeter (shown in Figure 8.3) that provides a stable polarisation potential of -0.8 V to both the sensing cathode and the guard cathode (Unisense, n.d.).

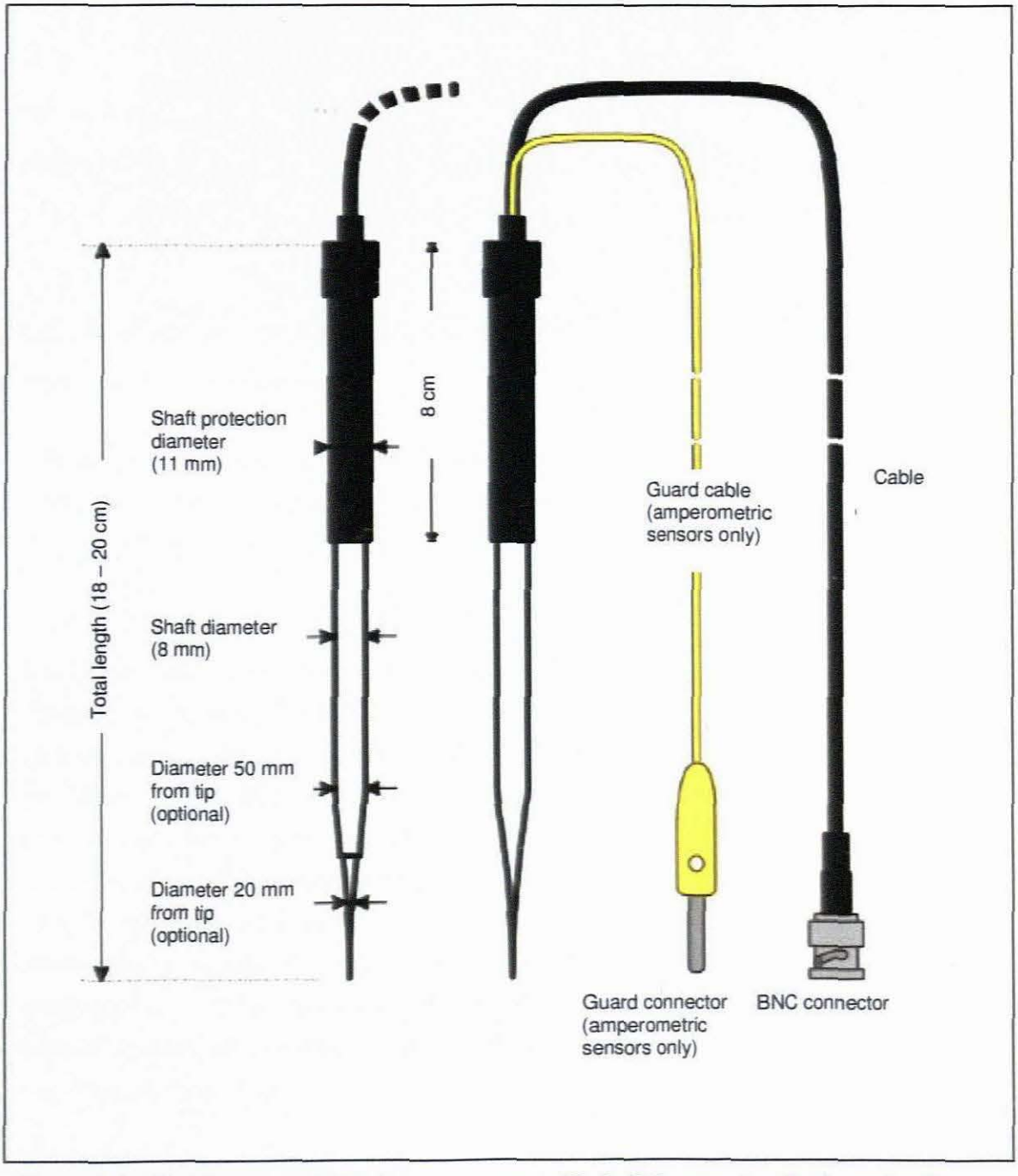

Figure 8.2: Clark-type ampoteric oxygen sensor with built-in guard cathode and reference anode (Unisense, n.d.)

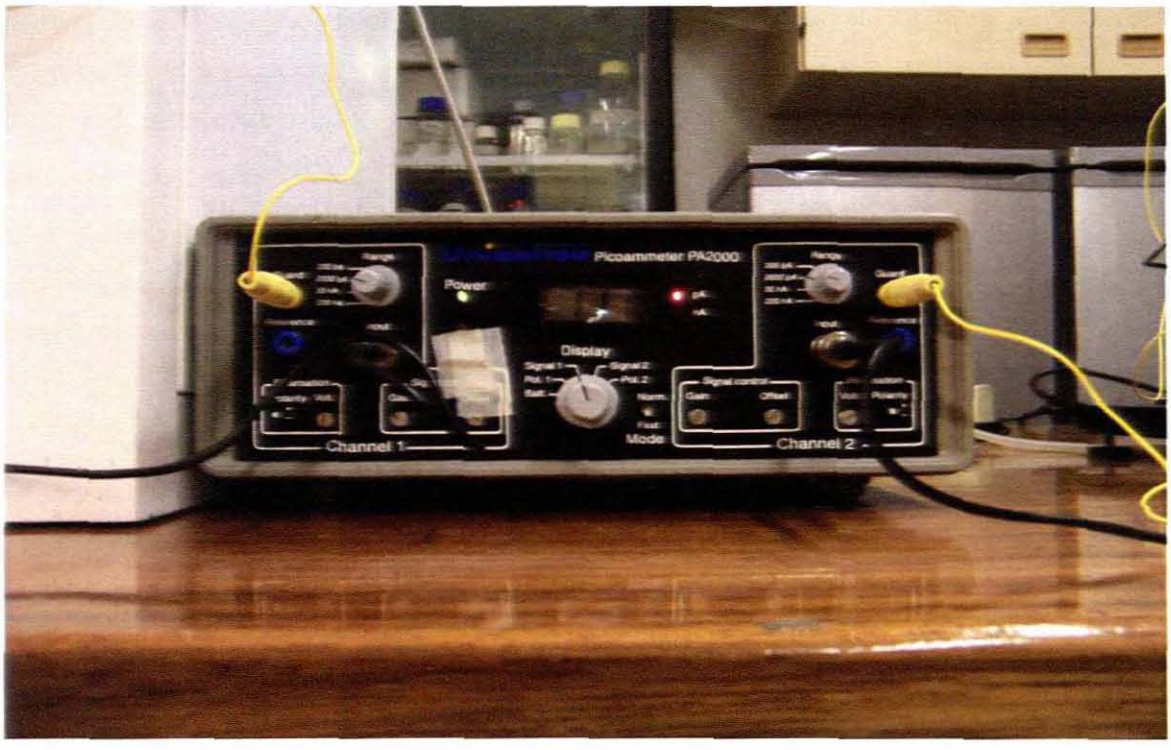

Figure 8.3: PA2000 picoammeter

A tip diameter of 10 µm and increments of 20 µm were used during the study to maintain the structure of the biofilm, by using the least invasive procedure to keep damage to the biofilm at a minimum when taking DO measurements.

8.4.2.1 Microsensor polarisation

The 10 µm oxygen microsensor to be utilised during the study was placed securely inside the designed manipulator. The BNC connector, containing both the reference and sensing cathode, was connected to the input terminal of channel A of the PA2000 picoammeter. Then the yellow guard cathode connector was connected to the guard terminal of the picoammeter. The oxygen microsensor was then polarised by immersing the tip of the microsensor in continuously aerated distilled water in the calibration chamber for at least an hour. Polarisation was required to remove any oxygen present in the electrolyte. During polarisation the oxygen present is consumed by both the sensing and guard cathode before stable operation of the microsensor is possible, as stated in the oxygen sensor's Users' manual provided by Unisense (Denmark). Polarisation was continued until a stable signal was obtained for at least 10 min.

8.4.2.2 Microsensor calibration

Following polarisation the oxygen microsensor was calibrated by immersing the tip of the sensor in an anoxic solution to obtain a zero reading and then in continuously well aerated

distilled water for an atmospheric reading. The anoxic solution was prepared by mixing in a 1:1 ratio 0.1 M sodium ascorbate and 0.1 M NaOH. After immersing the tip of the sensor in the anoxic solution the signal was allowed to stabilise before obtaining the zero oxygen partial pressure reading (S_0). The atmospheric partial pressure (S_a) reading was obtained, after allowing the signal to stabilise, by immersing the tip of the microsensor in distilled water that was continuously aerated in the calibration chamber, as stated in the oxygen sensor's User's manual provided by Unisense (Denmark).

According to the oxygen sensor's User's manual provided by Unisense (Denmark), to convert a signal (S) from the partial pressure to the equivalent oxygen concentration (C_{O_2}), a linear conversion is performed and the results multiplied by the atmospheric level solubility (a_{tm}) of oxygen in the relevant liquid at the relevant temperature, as shown in Equation 8.1.

$$C_{O_2} = a_{tm} \times \left(\frac{S - S_0}{S_a - S_0} \right) \qquad 8.1$$

8.4.3 Design of the microsensor manipulator

It was required to measure *in-situ* dissolved oxygen (DO) measurements within the biofilm, as the system utilised in this study was operated under pressure, a manipulator had to be designed that would allow the microsensor to remain attached to the glass housing of the bioreactor for the duration of each experiment. Once attached to the system, the manipulator was required not only to house the microsensor, while maintaining the pressure within the system, but allow the operator to manipulate the microsensor into and out of the biofilm immobilised on the surface of the ceramic membrane.

Prior to manufacturing the manipulator set-up, the manipulator was drawn to scale using a three dimensional drawing program, Solid Edge (Version 18). This was to ensure that when the manipulator set-up was constructed, all parts fitted together perfectly and moved as designed. See Appendix E for all the Solid Edge microsensor manipulator designs; as well as Figures 8.4a and 8.4b for images of the actual design attached to the middle oxygen port of a bioreactor.

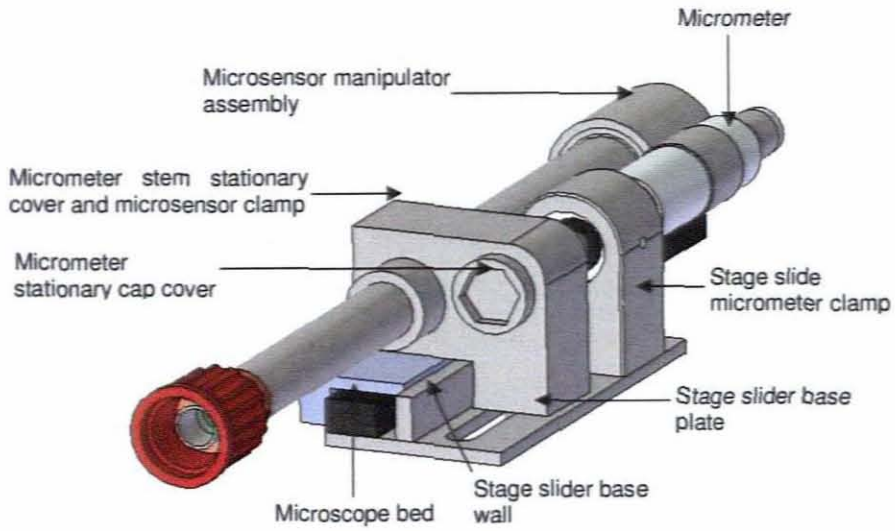

(a) Side view of the three-dimensional design in Solid Edge

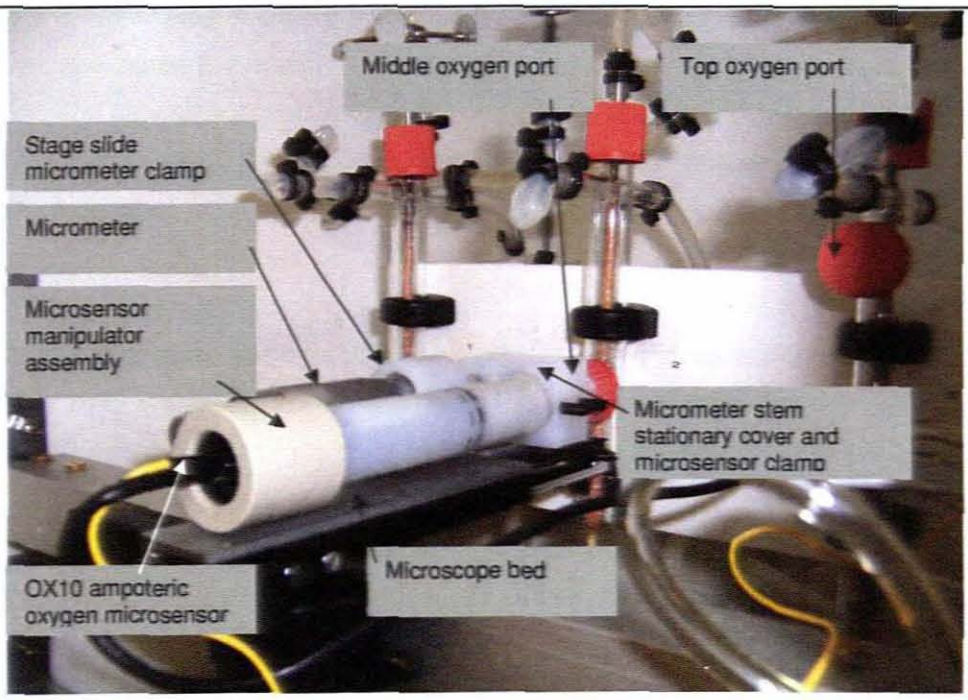

(b) Side view of the actual design attached to the middle oxygen port

Figure 8.4: The microsensor manipulator designed to house the microsensor

8.4.4 Connecting the oxygen microsensor and manipulator to the SFMGR system

After inoculation, before pressurising the system, the microsensor housed in the designed manipulator was attached to the middle oxygen port of the reactor for *in-situ* measurements (refer to Appendix D for the design templates of the bioreactor glass housing with oxygen measuring ports). The microsensor and the inside of the designed manipulator was sterilised with 70% ethanol before being attached. To maintain the sterility of the system the entrance of the oxygen port was sealed with a flat sheet membrane during construction of the SFMGR. Upon attaching the manipulator, the flat sheet membrane was broken, thereby not compromising the sterility of the system. Once securely in place the micrometer that formed part of the manipulator design was utilised to carefully move the tip of the microsensor to slightly above the surface of the ceramic membrane. The micrometer was then locked in place to ensure the tip of the sensor did not move during operation of the system. After the ECS had been pressurised any air leaks observed resulting in the system not maintaining the set ECS pressure were sealed.

8.4.5 SFMGR operation

Three vertically orientated manifolded SFMGR's (1 x 3) operated under pressure, as shown in Figure 8.5, were used to culture the bacteria, *S. coelicolor*, at 28°C. After sterilisation and inoculation, the nutrient medium was supplied to the membrane lumen at a flow rate of 0.001 L/hr. The air was supplied to the ECS of the bioreactor at a flow rate of 2.4 L/hr. of the nutrient medium and ECS, respectively. The SFMGR system was operated in the dead-end mode with a constant shell side pressure supplied by a proportional-integral-derivative (PID) controller.

The system in this study was operated using pressure control, as explained in section 3.6.2. For the first 24 hr it was attempted to maintain the transmembrane pressure (TMP) at 1 kPa to allow the micro organism to adhere to the membrane surface. For the remainder of the study, the medium and ECS were operated at pressures of 53 and 50 kPa, respectively (refer to Table 3.9 in section 3.6.3), to attempt to maintain a TMP of 3 kPa. The humidified air supplied to the ECS displaced the permeate produced, as a result of flux from the shell side, by the micro organism.

Figure 8.5: 1 x 3 Vertically orientated SFMGR set-up

Two experiments were performed during this study. One experiment was operated for 48 days (±1079 hr), with one reactor disconnected on days 45 (±1007 hr), 47(±1057 hr) and 48. The remaining experiment was run for 24 days (±569 hr), with all three reactors disconnected on day 24.

8.5 Analytical methods

8.5.1 *In-situ* dissolved oxygen (DO) biofilm measurements

The manipulator housing the microsensor for the *in-situ* DO measurements was attached to the middle oxygen port for all the experiments conducted during this study. Each day three sets of 11 *in-situ* dissolved oxygen (DO) measurements were taken with the Unisense Profix 3.0 software utilised for data acquisition and automated profiling for the microsensors.

8.5.2 Atmospheric dissolved oxygen (DO) biofilm measurements

After each reactor was disconnected, the diameter of the biofilm was measured with an electronic Vernier calliper at distances of 50 mm, 118 mm (position of the middle oxygen port) and 170 mm from the bottom of the ceramic membrane, shown in Figure 8.6. Utilising

the measured diameter the biofilm thickness at each of these locations could be calculated, since the outer diameter (2.8 mm) of the ceramic membrane was known.

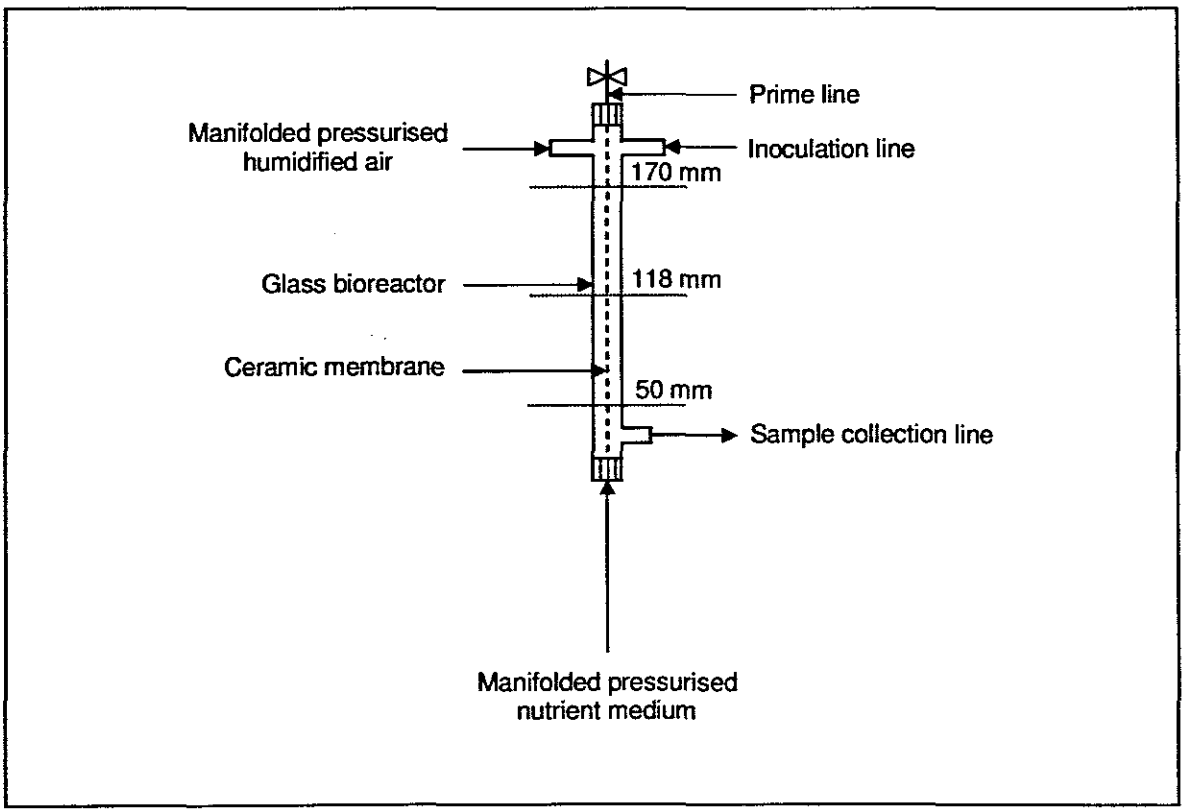

Figure 8.6: Positions at which the atmospheric dissolved oxygen measurements were taken with respect to the bioreactor

The tip of the OX10 microsensor (shown in Figure 8.7) was moved to above the biofilm surface. DO readings where taken as soon as possible after disconnecting the reactors using Profix 3.0 by manually moving the tip of the sensor in 20 µm increments until a DO reading of zero was reached. If a reading of zero was not reached the tip was moved to a depth of 350 µm away from the outside surface of the ceramic membrane to prevent the tip from breaking. Three sets of DO readings were taken at each location, to obtain an average oxygen profile.

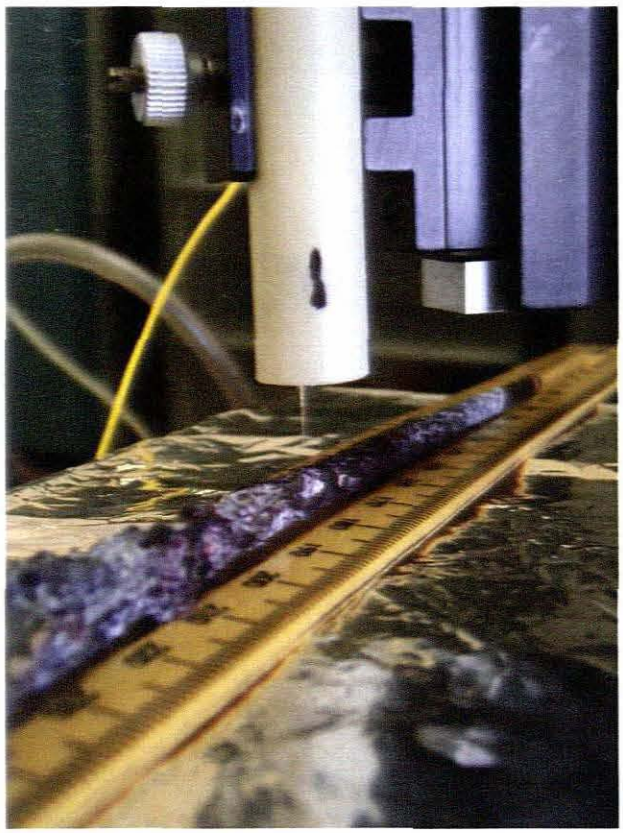

Figure 8.7: An image of dissolved oxygen measurements with an OX10 Clark-type ampoteric oxygen sensor

8.5.3 Biomass activity and biofilm measurements

The volume, pH and redox potential (mV) of the permeate samples were measured and recorded daily; including the time elapsed between sampling, thus allowing the flux to be calculated for each SFMGR. On completion of the experiments, the wet biomass of each reactor was recorded, as well as the dry biomass after the biofilm had been dried for 12 hr at 70℃ in an oven (refer to section 3.7).

8.5.4 Actinorhodin assay

Actinorhodin concentrations were determined as described in section 3.9.1. Refer to Appendix A for a detailed description of the actinorhodin assay procedure. actinorhodin assay procedure description).

8.6 Development of a mathematical model for oxygen mass transfer within a biofilm grown in a pressurised SFMGR

For this part of the study the system was divided into three sections (as shown in Figure 8.8), namely the extra capillary space (ECS), the boundary layer and the biofilm.

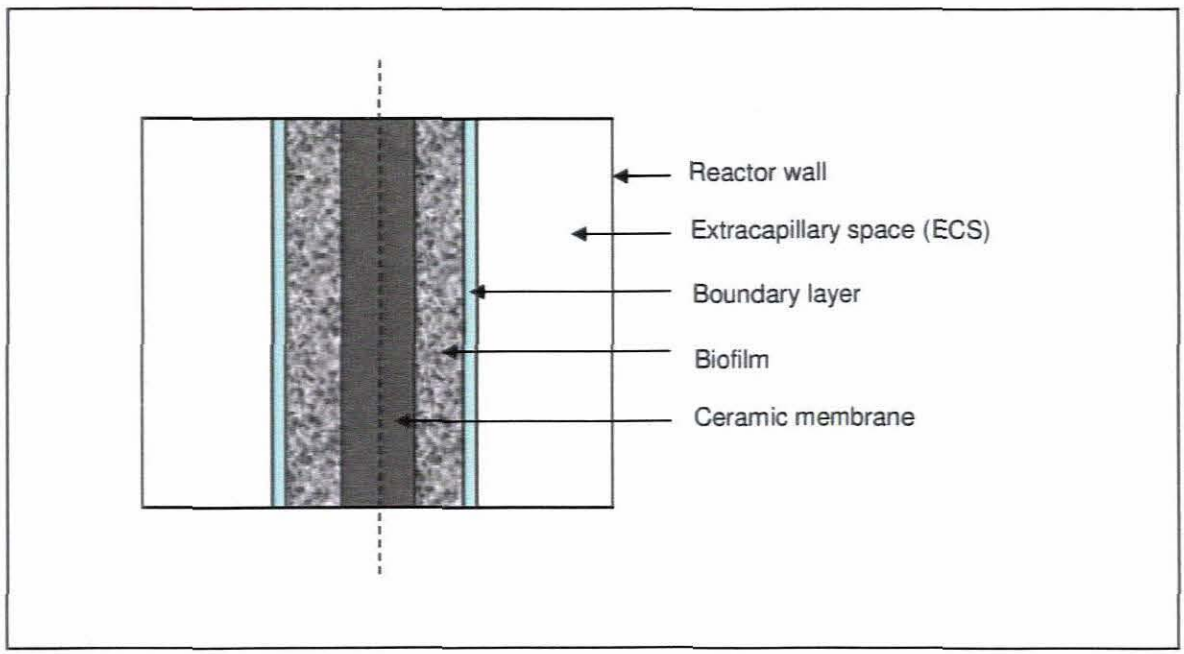

Figure 8.8: Three sections of the pressurised MGR system for modelling purposes

The diffusive, convective and reaction terms were therefore separated as shown in Equations 2.47 and 2.48 (Bird *et al.* 2002; Eberl *et al.* 2006),

$$\frac{\partial C_{sub}}{\partial t} + \bar{u}\nabla C_{sub} = D_{AB}\nabla^2 C_{sub} + r_A \qquad \textbf{2.47}$$

Where C_{sub} represents the local substrate concentration (g/m^3); t represents the time (hr); $\bar{u}$ represents the axial velocity vector; ∇ represents the gradient operator; D_{AB} represents the substrate diffusivity (m^2/s) which was assumed to be constant and r_A represents the rate of substrate production or consumption $(-r_A)$ (g/m^3.hr). The substrate production or consumption, r_A, is a function of the local growth rate, biofilm density, and time. The left hand side of Equation 2.47 represents bulk transport (convective); and the right hand side excluding r_A represents diffusive transport within the biofilm. Equation 2.47 can be rearranged so that both methods of substrate mass transport is on the right hand side of the equation, as shown in Equations 2.48.

$$\frac{\partial C_{sub}}{\partial t} = D_{AB}\nabla^2 C_{sub} - \bar{u}\nabla C_{sub} + r_A \qquad \textbf{2.48}$$

For the development of the DO mass balance Equation 2.48 becomes:

$$\frac{\partial C_{O_2}}{\partial t} = diffusion - convection - biological\ consumption \qquad 8.1$$

8.6.1 Model assumptions

1. In the extracapillary space no reaction occurred.
2. The ECS was at pseudo-steady state.
3. In the boundary layer no reaction occurred.
4. The boundary layer was at pseudo-steady state.
5. Oxygen transfer within the boundary layer only occurred radially and not axially, therefore the oxygen concentration changed in a radial direction and not an axial direction. DO mass transfer was therefore assumed to be one-dimensional; from the gaseous ECS across the biofilm towards the substratum, in this case the surface of the ceramic membrane.
6. The biofilm immobilised on the ceramic membrane was at psuedo-steady state with respect to the transport of DO into the inner mycelia. Psuedo steady state occurs when the oxygen concentration does not change for a period of time at the biofilm surface and aerial mycelia, when oxygen is transported from the gaseous phase into the mycelia (Ntwampe *et al.*, 2008).
7. In the biofilm oxygen was only transported in a radial direction, therefore the oxygen concentration only changed radially and not axially.
8. The rates of DO mass transfer in the biofilm are proportional to the concentration difference across the biofilm thickness.
9. *The proportionality factors are directly related to DO mass transfer constants.*
10. *S. coelicolor* is an aerobic micro organism, therefore oxygen uptake rate through biological reaction was assumed to be described by Monod's equation.
11. The biofilm is uniform, therefore a single effective diffusivity value was used for the entire biofilm. For biofilms with a heterogeneous non-uniform structure, the effective diffusivity varies from one location to another (Beyenal & Lewandowski, 2002; Lewandowski & Beyenal, 2003b).
12. The density of the biomass and the rate of oxygen consumption are uniform within the biofilm, therefore the oxygen profile will only vary with the radial position (Thibault *et al.*, 2000).

8.6.1.1 Mathematical model describing the extracapillary space and boundary layer

In the bulk ECS, it was assumed that no biological consumption occurred $(r_A = 0)$ and the ECS was at pseudo-steady state $(\partial C_{O_2}/\partial t = 0)$ as oxygen was not utilised, therefore in the bulk ECS diffusion was equal to convection.

In the boundary layer it was assumed that no biological consumption occurred $(r_A = 0)$; the DO in the boundary layer was at pseudo-steady state $(\partial C_{O_2}/\partial t = 0)$; oxygen was only transported radially in the boundary layer and not axially $(u(\partial C_{O_2}/\partial z) = 0)$ and the oxygen concentration changed in a radial direction and not an axial direction $(r(\partial^2 C_{O_2}/\partial z^2) = 0)$ (Eberl *et al.*, 2006). It was therefore assumed that the oxygen concentration did not change vertically along the length of the biofilm, but only in depth into the biofilm. In the boundary layer the oxygen concentration was therefore a function of r, as represented by Equation 8.2.

$$v\frac{\partial C_{O_2}}{\partial r} = \frac{D_{AB}}{r}\left[\frac{\partial C_{O_2}}{\partial r} + r\frac{\partial^2 C_{O_2}}{\partial r^2}\right] \qquad \textbf{8.2}$$

The partial derivatives in Equation 8.2 were therefore replaced by total derivatives as shown in Equation 8.3.

$$v\frac{dC_{O_2}}{dr} = \frac{D_{AB}}{r}\left[\frac{dC_{O_2}}{dr} + r\frac{d^2 C_{O_2}}{dr^2}\right] \qquad \textbf{8.3}$$

In Equation 8.4 the first and second derivatives were separated onto the left and right hand side of the equivalent sign and then combined to make single terms, respectively.

$$\frac{D_{AB}}{r}\frac{d^2 C_{O_2}}{dr^2} = \left(v - \frac{D_{AB}}{r}\right)\frac{dC_{O_2}}{dr} \qquad \textbf{8.4}$$

Equation 8.5 was obtained by multiplying Equation 8.4 by $\frac{r}{D_{AB}}$. Equation 8.5 describes the DO mass transport in the boundary layer of the SFMGR system.

8.6.1.1 Mathematical model describing the extracapillary space and boundary layer

In the bulk ECS, it was assumed that no biological consumption occurred $(r_A = 0)$ and the ECS was at pseudo-steady state $(\partial C_{O_2}/\partial t = 0)$ as oxygen was not utilised, therefore in the bulk ECS diffusion was equal to convection.

In the boundary layer it was assumed that no biological consumption occurred $(r_A = 0)$; the DO in the boundary layer was at pseudo-steady state $(\partial C_{O_2}/\partial t = 0)$; oxygen was only transported radially in the boundary layer and not axially $(u(\partial C_{O_2}/\partial z) = 0)$ and the oxygen concentration changed in a radial direction and not an axial direction $(r(\partial^2 C_{O_2}/\partial z^2) = 0)$ (Eberl *et al.*, 2006). It was therefore assumed that the oxygen concentration did not change vertically along the length of the biofilm, but only in depth into the biofilm. In the boundary layer the oxygen concentration was therefore a function of r, as represented by Equation 8.2.

$$v\frac{\partial C_{O_2}}{\partial r} = \frac{D_{AB}}{r}\left[\frac{\partial C_{O_2}}{\partial r} + r\frac{\partial^2 C_{O_2}}{\partial r^2}\right] \qquad \textbf{8.2}$$

The partial derivatives in Equation 8.2 were therefore replaced by total derivatives as shown in Equation 8.3.

$$v\frac{dC_{O_2}}{dr} = \frac{D_{AB}}{r}\left[\frac{dC_{O_2}}{dr} + r\frac{d^2 C_{O_2}}{dr^2}\right] \qquad \textbf{8.3}$$

In Equation 8.4 the first and second derivatives were separated onto the left and right hand side of the equivalent sign and then combined to make single terms, respectively.

$$\frac{D_{AB}}{r}\frac{d^2 C_{O_2}}{dr^2} = \left(v - \frac{D_{AB}}{r}\right)\frac{dC_{O_2}}{dr} \qquad \textbf{8.4}$$

Equation 8.5 was obtained by multiplying Equation 8.4 by $\frac{r}{D_{AB}}$. Equation 8.5 describes the DO mass transport in the boundary layer of the SFMGR system.

$$\frac{d^2C_{O_2}}{dr^2}=\left(\frac{vr}{D_{AB}}-1\right)\frac{dC_{O_2}}{dr} \qquad 8.5$$

8.6.1.2 Mathematical model within the biofilm

The biofilm was at pseudo-steady state since the MGR was operated at a constant TMP, therefore $(\partial C_{O_2}/\partial t=0)$; oxygen was only transported radially in the biofilm and not axially $(u(\partial C_{O_2}/\partial z)=0)$; oxygen concentration changed in a radial direction and not an axial direction $(r(\partial^2 C_{O_2}/\partial z^2)=0)$. This was validated by the DO profiles obtained during the study; each data point was an average of three sets of readings measured axially with regards to each other. The standard error for each data point was extremely small. It was therefore assumed that the oxygen concentration did not change vertically (i.e. z co-ordinate) along the length of the biofilm, but only in depth towards or away from surface of the ceramic membrane. DO concentration occured within the biofilm. Since the biofilm was a function of both diffusion and consumption, r_A was negative. A substrate consumption model (shown in Equation 8.6) was therefore utilised to represent r_A.

$$-r_A=\frac{\mu_{max}C_{O_2}X_\rho}{Y_{X/S}(K_s+C_{O_2})} \qquad 8.6$$

Where r_A represents the rate of substrate production or consumption (g/m^3.hr); C_{O_2} represents oxygen concentration (g/m^3); t represents time (hr); μ_{max} represents the maximum specific growth rate (hr^{-1}); X_ρ represents the biofilm density (g/m^3); $Y_{X/S}$ represents the growth yield coefficient (g biomass/g substrate) and K_s represents the substrate saturation constant (g/m^3) (Monod, 1949; Blanch, 1981).

From the above mentioned assumptions, Equation 2.53 combined with the rate expression given in Equation 8.6 becomes:

$$v\frac{\partial C_{O_2}}{\partial r}=\frac{D_{AB}}{r}\left[\frac{\partial C_{O_2}}{\partial r}+r\frac{\partial^2 C_{O_2}}{\partial r^2}\right]-\frac{\mu_{max}C_{O_2}X_f}{Y_{X/Z}(K_S+C_{O_2})} \qquad 8.7$$

The partial derivatives in Equation 8.7 were therefore replaced by total derivatives as shown in Equation 8.8.

$$v\frac{dC_{O_2}}{dr}=\frac{D_{AB}}{r}\frac{dC_{O_2}}{dr}+\frac{D_{AB}}{r}r\frac{d^2C_{O_2}}{dr^2}-\frac{\mu_{max}C_{O_2}X_f}{Y_{X/Z}\left(K_S+C_{O_2}\right)} \quad \textbf{8.8}$$

By removing the common denominator on the left side of Equation 8.8, Equation 8.9 which represented oxygen mass transfer within the biofilm was obtained.

$$\left(v-\frac{D_{AB}}{r}\right)\frac{dC_{O_2}}{dr}=D_{AB}\frac{d^2C_{O_2}}{dr^2}-\frac{\mu_{max}C_{O_2}X_f}{Y_{X/Z}\left(K_S+C_{O_2}\right)} \quad \textbf{8.9}$$

Dividing Equation 8.9 by $-D_{AB}$ resulted in Equation 8.10.

$$\left(-\frac{v}{D_{AB}}+\frac{1}{r}\right)\frac{dC_{O_2}}{dr}=-1\frac{d^2C_{O_2}}{dr^2}-\frac{\mu_{max}C_{O_2}X_f}{Y_{X/Z}\left(K_S+C_{O_2}\right)D_{AB}} \quad \textbf{8.10}$$

Equation 8.11 was obtained by rearranging Equation 8.10, so that all the terms were located on the left hand side of the equation.

$$\frac{d^2C_{O_2}}{dr^2}+\left(-\frac{v}{D_{AB}}+\frac{1}{r}\right)\frac{C_{O_2}}{dr}+\frac{\mu_{max}C_{O_2}X_f}{Y_{X/Z}\left(K_S+C_{O_2}\right)D_{AB}}=0 \quad \textbf{8.11}$$

For simplicity let $\frac{\mu_{max}X_f}{Y_{X/Z}D_{AB}}=A$ **8.12**

Note: $r_m=\frac{A}{D_{AB}}$, since $\frac{\mu_{max}X_f}{Y_{X/Z}}=r_m$. **8.13**

In Equation 8.13, r_m represents the maximum substrate consumption rate (g/m^3.hr). Therefore, substituting Equation 8.12 into Equation 8.11 resulted in Equation 8.14.

$$\frac{d^2C_{O_2}}{dr^2}-\left(\frac{v}{D_{AB}}-\frac{1}{r}\right)\frac{dC_{O_2}}{dr}+A\frac{C_{O_2}}{\left(K_S+C_{O_2}\right)}=0 \quad \textbf{8.14}$$

One of three scenarios exists in the system utilised in this study, to solve Eqaution 8.14. For simplicity allow:

$$A\frac{C_{O_2}}{\left(K_S+C_{O_2}\right)}=d \qquad \textbf{8.15}$$

Scenario 1: $K_S >> C_{O_2}$

Assuming $K_S >> C_{O_2}$, then $d=A\frac{C_{O_2}}{K_S}$. Substituting $d=A\frac{C_{O_2}}{K_S}$ into Equation 8.14 results in Equation 8.16.

$$\frac{d^2C_{O_2}}{dr^2}-\left(\frac{v}{D_{AB}}-\frac{1}{r}\right)\frac{dC_{O_2}}{dr}+A\frac{C_{O_2}}{K_s}=0 \qquad \textbf{8.16}$$

However, since A and K_S are constants let $G=\frac{A}{K_S}$. Equation 8.16 can be rewritten as Equation 8.17.

$$\frac{d^2C_{O_2}}{dr^2}-\left(\frac{v}{D_{AB}}-\frac{1}{r}\right)\frac{dC_{O_2}}{dr}+GC_{O_2}=0 \qquad \textbf{8.17}$$

Equation 8.17 can be solved with the Pertubation Theory.

Scenario 2: $C_{O_2} >> K_S$

Assuming $C_{O_2} >> K_S$, then $d=A\frac{C_{O_2}}{C_{O_2}}=A$ Substituting $d=A\frac{C_{O_2}}{C_{O_2}}=A$ into Equation 8.14 results in Equation 8.18, which can be rewritten as Equation 8.19

$$\frac{d^2C_{O_2}}{dr^2}-\left(\frac{v}{D_{AB}}-\frac{1}{r}\right)\frac{dC_{O_2}}{dr}+A=0 \qquad \textbf{8.18}$$

$$\frac{d^2C_{O_2}}{dr^2}-\left(\frac{v}{D_{AB}}-\frac{1}{r}\right)\frac{dC_{O_2}}{dr}=-A \qquad \textbf{8.19}$$

Equation 8.19 is an inhomogenous differential equation, indicating that Equation 8.14 can be solved with Laplace Transforms. An inhomogeneous differential equation is an ordinary differential equation in which all the terms are linear and the entire equation is equal to a non zero function of the variable, with respect to which derivatives are taken (Google, n.d.).

Scenario 3: $C_{O_2} \approx K_S$

Assuming $C_{O_2} \approx K_S$, a numerical technique like the finite difference technique will be required to solve Equation 8.14.

According to Howell and Atkinson (1976) scenario 2 ($C_{O_2} >> K_S$) only occurs away from the reaction zone within the biofilm. Therefore, K_S is only significant within the reaction (i.e. consumption or generation) regions in the biofilm and K_S is not important within the bulk transport regions, such as the ECS.

8.7 Results and discussion

The manipulator housing the microsensor was attached to the middle port for all the experiments during this study. The top oxygen port was not utilised for DO profiling as it was observed that the biofilm growth located opposite this port was sparse and the risk of breaking the microsensor tip was therefore high. The biofilm growth on the surface of the ceramic membrane located opposite the bottom oxygen port was sufficient for DO readings, however, this port was not utilised due to repeated sloughing of the bottom section of the biofilm.

The 1 x 3 SFMGR system was stopped at approximately 569, 1007, 1057 and 1079 hr respectively and oxygen profiles were taken for each reactor as explained in section 8.5.2. The average dissolved oxygen profiles, oxygen penetration ratio, pH, redox potential (mV) and actinorhodin production with standard error bars were plotted with the aid of the statistical program Sigma Plot (Version 8).

8.7.1 In-situ dissolved oxygen measurements

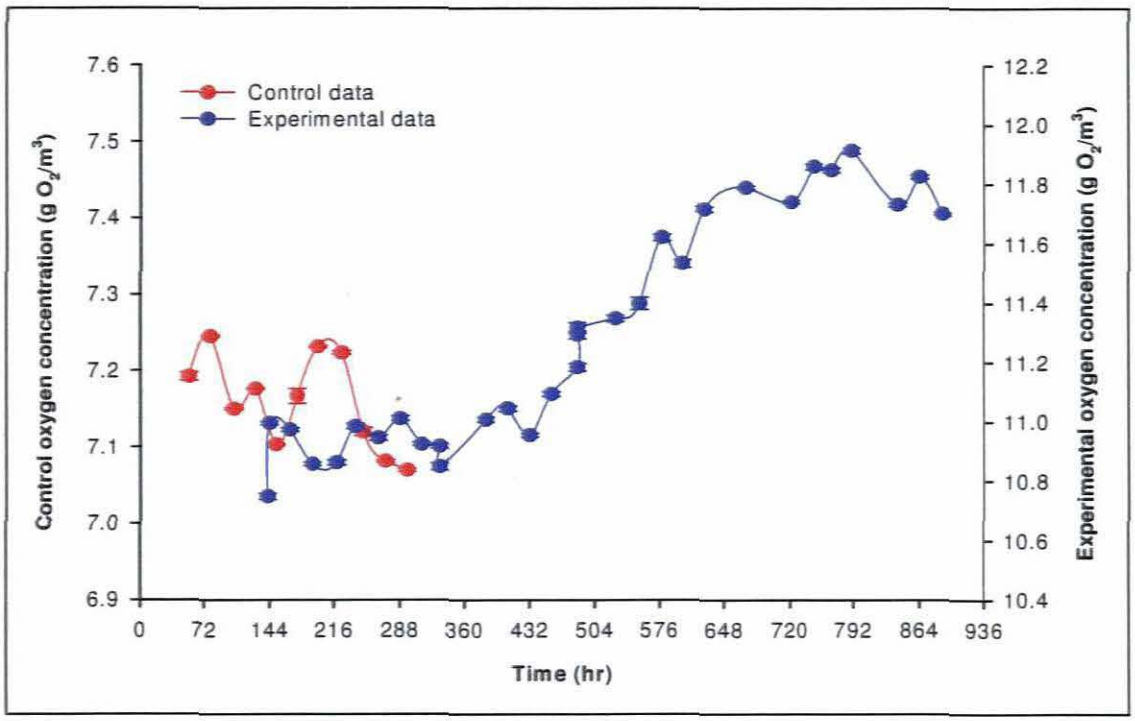

Figure 8.9: Control and *in-situ* dissolved oxygen (DO) profiles at the middle position within a pressurised SFMGR

During the control (a sterile uninoculated SFMGR) run, shown in Figure 8.9, the oxygen concentration was in the range of 7.05 to 7.25 g O_2/m^3. At atmospheric pressure (101.3 kPa) oxygen composes 21% of air by volume 21% which translates to a concentration of ±6.5 g O_2/m^3. The system utilised in this study was operated at a pressure of ±50 kPa (gauge), thereby increasing the partial pressure of the air present in the ECS of the system. Accounting for the high oxygen concentration in the range of 7.05 to 7.25 g O_2/m^3, this translates to ±33% increased oxygen in the air, during the control run.

Observed in the curve representing the experimental data (an inoculated SFMGR system) in Figure 8.9, the DO concentration continuously increased over the duration of the experiment. Due to the microsensor being attached to the middle oxygen port for the duration of the run, the sensor was only calibrated at the start of the study at atmospheric conditions. It was only discovered after completion of the study and after communication with Unisense sales representatives, that to obtain the best results the microsensor requires daily calibration under exactly the same conditions at which the system is to be operated. The microsensor could not be calibrated daily as the system utilised in the study would have been at risk of contamination, and a special chamber would have had to have been constructed to calibrate the microsensor under the pressurised operating conditions.

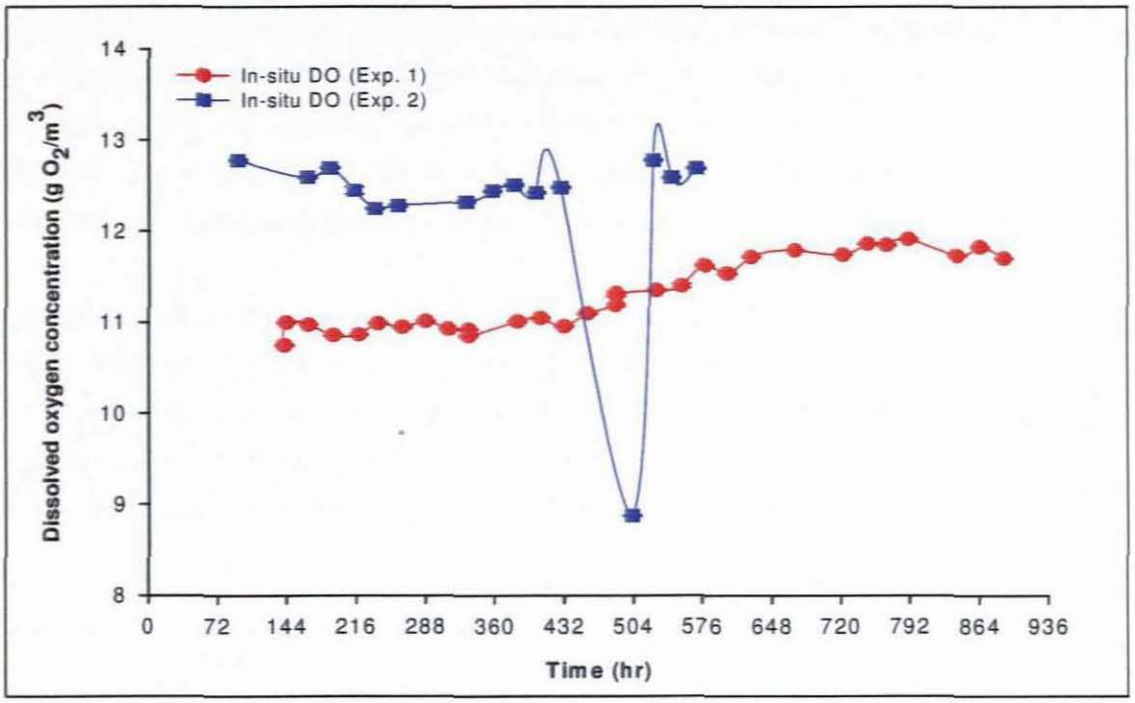

Figure 8.10: *In-situ* averaged dissolved oxygen (DO) profiles within the biofilm located at the middle position of the SFMGR (The error bars represent the standard error using Sigma Plot 8.0)

The experimental data curves in Figures 8.9 and 8.10 show a continually increasing signal over time. According to the oxygen sensors User's manual a high and drifting signal as observed during the studies could occur for two reasons. Either the sensor tip was broken and needed to be replaced or gas bubbles were present inside the sensor tip. The microsensor tip was not broken during the *in-situ* DO profiles recorded in Figure 8.10, therefore gas bubbles must have been present inside the sensor tip due to prolonged usage of the microsensor under high pressure. According to the microsensor User's manual supplied by Unisense (Denmark), to solve this problem the microsensor tip would have had to be immersed in degassed water for 20 minutes. Water is degassed by boiling and subsequent cooling or by 10 minutes of vacuum treatment (Anon., 1998). However, the microsensor would have had to be removed from the SFMGR system, risking possible breakage of the microsensor and contamination of the system. The high pressure within the system resulted in increased DO diffusivity in the membrane at the tip of the microsensor, which possibly could account for the continually increasing signal observed in Figures 8.9 and 8.10. Although the sensor was kept polarised between measurements, by keeping the picoammeter on for the duration of the study, according to Unisense sales representatives the membrane permeability changes with time and therefore requires calibration every 24 hr if the time between measurements exceeds several days. Kuenen *et al.*, (1986) observed

drift of less than 1% per hour during the study of oxygen micro profiles of photosynthetic and non-photosynthetic biofilms. Clark-type oxygen microsensors were used to study the biofilms of trickling filters from a sewage treatment plant. However, over a long period of time, such as ±1080 hr, the drift observed would have been much larger. It can be concluded that due to the high and drifting signal observed for the duration of both *in-situ* studies the profiles obtained are not accurate representations of the DO concentration within the biofilm.

The large decrease in DO concentration observed at ±504 hr during experiment 2 in Figure 8.10 was due to the experimental data being recorded when the pressure in the ECS was decreased after removing the permeate from the permeate collection bottles for daily analysis. This decrease in DO concentration observed at a decreased ECS pressure confirms that the pressurised air within the ECS affected the microsensor signal.

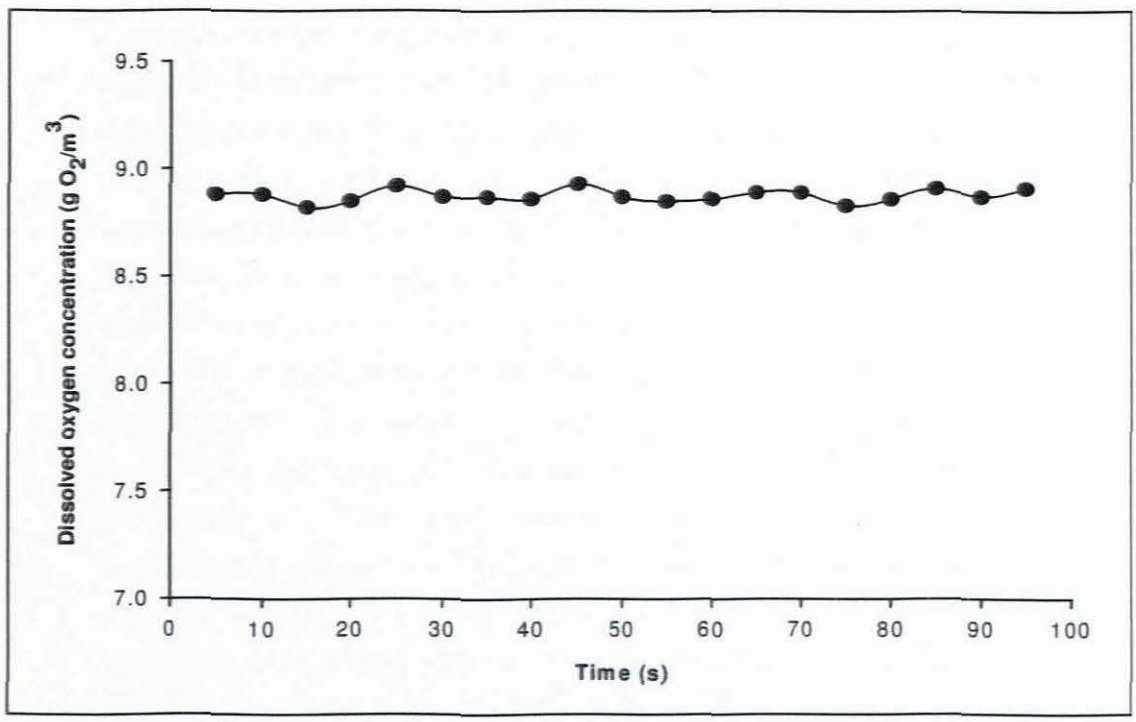

Figure 8.11: *In-situ* average dissolved oxygen (DO) profiles located at the middle position as the microsensor was removed from the biofilm at the end of the experiment after 569 hr (The error bars represent the standard error using Sigma Plot 8.0)

The graph in Figure 8.11 that was obtained *in-situ* as the microsensor was removed from the biofilm at the end of the experiment was not an accurate *in-situ* oxygen profile for the biofilm due to the high and drifting signal experienced during the study. The concentration at the different depths did not change as the microsensor was removed from the biofilm and remained unchanged even after the sensor was outside the biofilm in the ECS of the reactor.

drift of less than 1% per hour during the study of oxygen micro profiles of photosynthetic and non-photosynthetic biofilms. Clark-type oxygen microsensors were used to study the biofilms of trickling filters from a sewage treatment plant. However, over a long period of time, such as ±1080 hr, the drift observed would have been much larger. It can be concluded that due to the high and drifting signal observed for the duration of both *in-situ* studies the profiles obtained are not accurate representations of the DO concentration within the biofilm.

The large decrease in DO concentration observed at ±504 hr during experiment 2 in Figure 8.10 was due to the experimental data being recorded when the pressure in the ECS was decreased after removing the permeate from the permeate collection bottles for daily analysis. This decrease in DO concentration observed at a decreased ECS pressure confirms that the pressurised air within the ECS affected the microsensor signal.

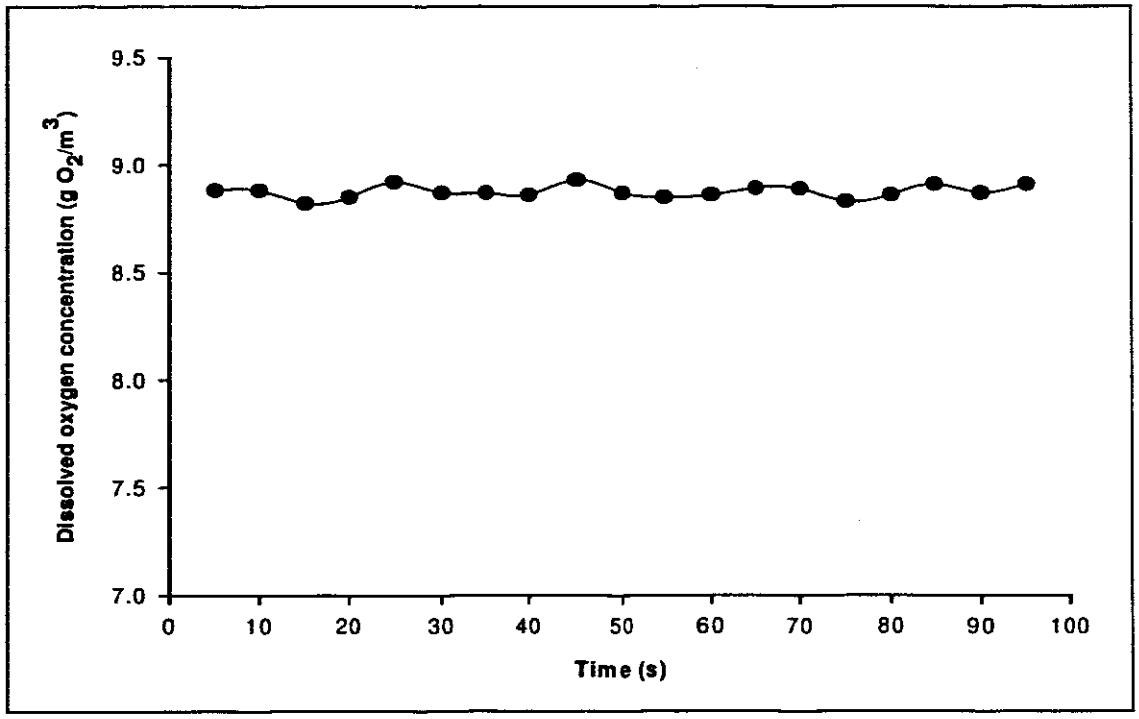

Figure 8.11: *In-situ* average dissolved oxygen (DO) profiles located at the middle position as the microsensor was removed from the biofilm at the end of the experiment after 569 hr (The error bars represent the standard error using Sigma Plot 8.0)

The graph in Figure 8.11 that was obtained *in-situ* as the microsensor was removed from the biofilm at the end of the experiment was not an accurate *in-situ* oxygen profile for the biofilm due to the high and drifting signal experienced during the study. The concentration at the different depths did not change as the microsensor was removed from the biofilm and remained unchanged even after the sensor was outside the biofilm in the ECS of the reactor.

This profile can therefore be disregarded. Therefore all subsequent analysis was performed on bioilfms directly after they had been removed from the pressurised reactors.

8.7.1.1 Problems experienced during the *in-situ* DO measurements

The following problems were experienced during the *in-situ* DO measurement section of this study.

1. The biofilm came loose from the membrane and became attached to the tip of the microsensor. As the microsensor and manipulator was attached to glass housing of the SFMGR it was not possible to remove the microsensor and clean the tip without compromising the sterility and therefore the integrity of the study.
2. The bottom port to which the microsensor could be attached to measure *in-situ* DO readings was not 100% straight (ie 90° to the glass housing of the reactor) therefore this port could not be utilised without risking breaking the microsensor tip.
3. The microsensor utilised in the study was handmade, as a result the tip as it extended from the microsensor body was not perfectly straight. Therefore, after placing the microsensor inside the designed manipulator tube, the tip was not centred inside the tube. The off-centre microsensor tip inside the manipulator tube, together with the angle of the bottom port, resulted in an increased risk of breakage of the microsensor tip when manipulating the microsensor into the bioreactor.
4. The ports were designed to lie opposite the membranes, unfortunately as the microsensor tips were not centred within the manipulator tube, which was attached to a port, the microsensor tips were not located over the middle of the membrane. Therefore, the tip sometimes moved past the biofilm and ceramic membrane depending on the degree with which the microsensor tip was off-centre.
5. The bottom half of the biofilm showed repeated sloughing. The same operating conditions was utilised for the duration of this study. Therefore, it was not possible to decrease the nutrient and air flow rates to try prevent sloughing from occurring.
6. The distance of the microsensor tip from the surface of the ceramic membrane after entering the biofilm, during *in-situ* DO measurements, was unknown.

8.7.2 Atmospheric dissolved oxygen measurements for different times at 50, 118 and 170 mm from the bottom of the reactor

Three reactors were disconnected at different times (24, 47 and 48 days). The ceramic membranes with biofilm were removed and DO measurements were taken outside at atmospheric pressure at 50, 118 and 170 mm, respectively from the bottom of the reactor (refer to Figure 8.6 for the locations from the bottom of the reactor).

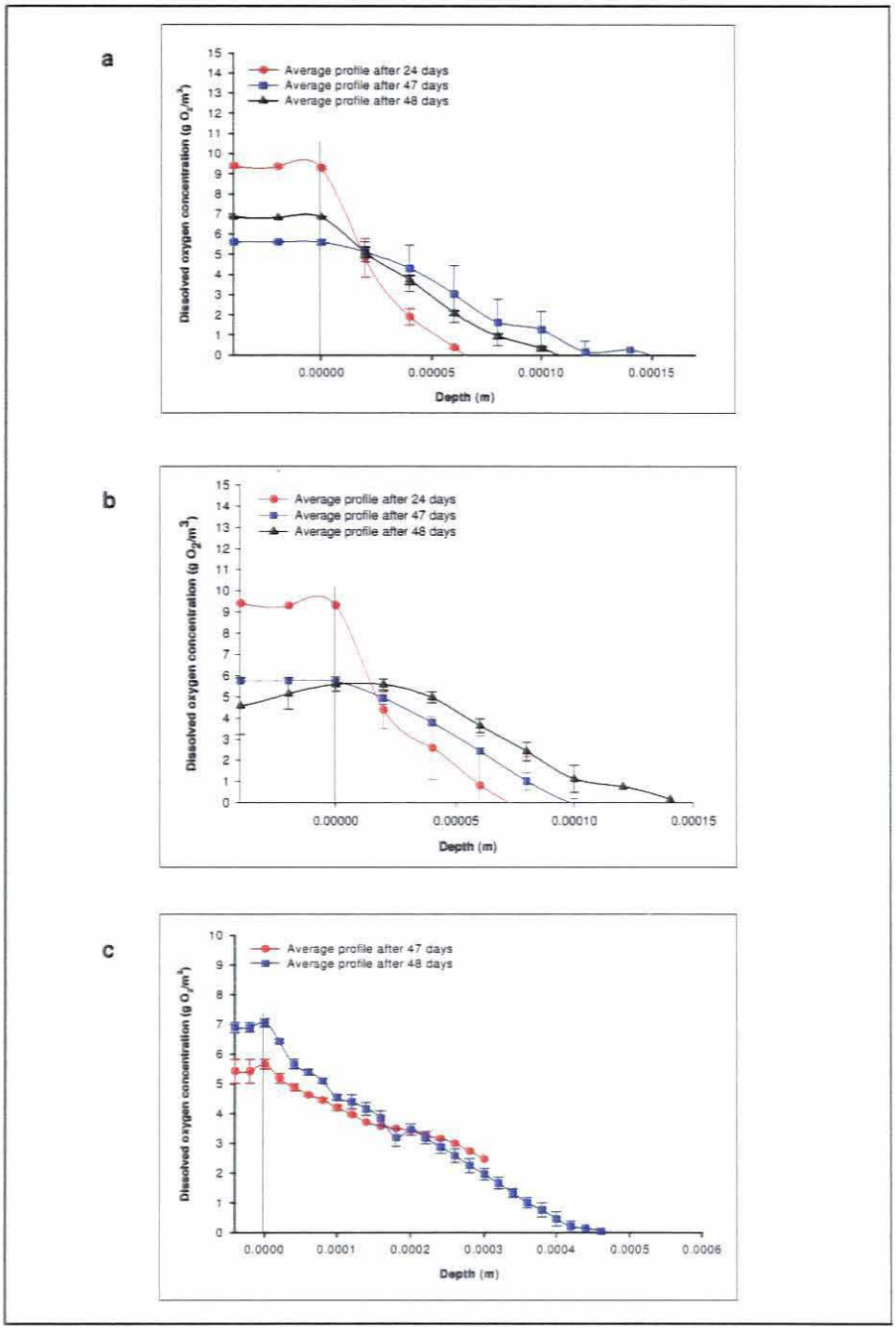

Figure 8.12: Average dissolved oxygen (DO) profiles at: (a) 50 mm; (b) 118 mm; and (c) 170 mm from the bottom of the bioreactor after 24, 47 and 48 days, respectively (The error bars represent the standard error using Sigma Plot 8.0)

Table 8.1: Average biofilm data at: (a) 50 mm; (b) 118 mm; and (c) 170 mm from the bottom of the bioreactor on days 24, 47 and 48, respectively

a	Time (Days)	24	47	48
	Biofilm thickness (mm)	1.22	2.17	1.36
	Average DO penetration depth (mm)	5.3×10^{-5}	1.2×10^{-4}	9.3×10^{-5}
	Penetration ratio	4.37×10^{-5}	5.3×10^{-5}	6.86×10^{-5}

b	Time (Days)	24	47	48
	Biofilm thickness (mm)	0.94	1.24	1.78
	Average DO penetration depth (mm)	8.0×10^{-5}	9.3×10^{-5}	9.3×10^{-5}
	Penetration ratio	2.4×10^{-5}	7.5×10^{-5}	5.2×10^{-5}

c	Time (Days)	24	47	48
	Biofilm thickness (mm)	-	0.87	0.96
	Average DO penetration depth (mm)	-	4.3×10^{-4}	4.1×10^{-4}
	Penetration ratio	-	4.9×10^{-4}	4.2×10^{-4}

According Howell and Atkinson (1976), oxygen concentration declines exponentially with depth; this was observed in Figures 8.12a – c and 8.14a - c. In Figure 8.12a, it was observed that the DO penetration depth was highest on day 47 and lowest on day 24. Day 48 showed less DO penetration than day 47, although the bioreactor was operated for a longer time period. Due to the bottom section of the biofilm sloughing, the biofilm on day 48 was thinner than the biofilm on day 47, as shown in the Table 8.1a. The thicker the biofilm, the higher the average DO penetration depth (refer to Table 8.1a). The penetration ratio at 50 mm for the different time durations were of the same order of magnitude, even on day 48 when biofilm sloughing was observed, therefore the profile for day 48 was still relevant to the study.

In Figure 8.12b, biofilm sloughing was only observed on day 48 at the bottom section (i.e. ±45 mm from the bottom of the bioreactor) of the membrane. The middle section of the biofilm unaffected by sloughing. Therefore, on day 48 the biofilm thickness at 118 mm was thicker than on day 47 (see Table 8.1b). The penetration depth was highest on day 48 and lowest on day 24. The penetration ratios at 118 mm for the different time durations were of the same order of magnitude.

Figure 8.12c represents the DO profiles of the biofilm located closest to the air supply of the extracapillary space (ECS) of the bioreactor. The biofilm at 170 mm from the bottom off the bioreactor was extremely thin, due to tapering of the biofilm observed from the bottom to the top of the bioreactor. It was postulated that the thickness of the biofilm located at the top of the membrane in the vertically orientated SFMGR was thinner than at the middle and bottom positions due to gravity and nutrient run down. According to Gondongwana *et al.* (2009) tapering of the biofilm towards the top of the bioreactor is often observed in vertically orientated SFMGR's. Therefore, no DO profile was measured at 170 mm on day 24, due to the biofilm being extremely thin and the high risk of breaking or damaging the oxygen microsensor if measurements were taken. Since no DO measurements were recorded no data could be provided for day 24 regarding DO penetration depth, biofilm thickness and penetration ratio in Table 8.1c. The shape of the profiles in Figure 8.12c, for days 47 and 48, indicate that $r_B \approx r_m$, therefore no biological reaction (i.e. consumption) was occurring at this location.

When comparing Figures 8.12a, b and c, the penetration depth was highest at 170 mm when taking the biofilm thickness into account. The increased penetration depth was due to the biofilm's location in terms of the air inlet. Since the pressurised air was entering the bioreactor at the top, biofilm located in the vicinity of the inlet experienced increased oxygen penetration. The combined effect of pressure and flow from the inlet promoted oxygen penetration.

8.7.2.1 Biofilm thickness and dissolved oxygen penetration depth

The biofilm thickness was measured with an electronic Vernier caliper every 0.02 m along the length of the ceramic membrane. As was expected the biofilm thickness increased with time. Utilising a similar non-pressurised MGR system an increase in biofilm thickness was observed over time with the fungi *Phanerochate chrysosporium* (Ntwampe *et al.*, 2008). According to Elibol and Mavituna (1999a; 1999b) in a fermentation system the biomass concentration of *S. coelicolor* increased with time. Table 8.1a, b and c shows that the DO penetration depth in the biofilm increased with time, therefore the DO penetration depth is linked to biofilm thickness. The penetration depth increased when the biofilm thickness

In Figure 8.12b, biofilm sloughing was only observed on day 48 at the bottom section (i.e. ±45 mm from the bottom of the bioreactor) of the membrane. The middle section of the biofilm unaffected by sloughing. Therefore, on day 48 the biofilm thickness at 118 mm was thicker than on day 47 (see Table 8.1b). The penetration depth was highest on day 48 and lowest on day 24. The penetration ratios at 118 mm for the different time durations were of the same order of magnitude.

Figure 8.12c represents the DO profiles of the biofilm located closest to the air supply of the extracapillary space (ECS) of the bioreactor. The biofilm at 170 mm from the bottom off the bioreactor was extremely thin, due to tapering of the biofilm observed from the bottom to the top of the bioreactor. It was postulated that the thickness of the biofilm located at the top of the membrane in the vertically orientated SFMGR was thinner than at the middle and bottom positions due to gravity and nutrient run down. According to Gondongwana *et al.* (2009) tapering of the biofilm towards the top of the bioreactor is often observed in vertically orientated SFMGR's. Therefore, no DO profile was measured at 170 mm on day 24, due to the biofilm being extremely thin and the high risk of breaking or damaging the oxygen microsensor if measurements were taken. Since no DO measurements were recorded no data could be provided for day 24 regarding DO penetration depth, biofilm thickness and penetration ratio in Table 8.1c. The shape of the profiles in Figure 8.12c, for days 47 and 48, indicate that $r_B \approx r_m$, therefore no biological reaction (i.e. consumption) was occurring at this location.

When comparing Figures 8.12a, b and c, the penetration depth was highest at 170 mm when taking the biofilm thickness into account. The increased penetration depth was due to the biofilm's location in terms of the air inlet. Since the pressurised air was entering the bioreactor at the top, biofilm located in the vicinity of the inlet experienced increased oxygen penetration. The combined effect of pressure and flow from the inlet promoted oxygen penetration.

8.7.2.1 Biofilm thickness and dissolved oxygen penetration depth

The biofilm thickness was measured with an electronic Vernier caliper every 0.02 m along the length of the ceramic membrane. As was expected the biofilm thickness increased with time. Utilising a similar non-pressurised MGR system an increase in biofilm thickness was observed over time with the fungi *Phanerochate chrysosporium* (Ntwampe *et al.*, 2008). According to Elibol and Mavituna (1999a; 1999b) in a fermentation system the biomass concentration of *S. coelicolor* increased with time. Table 8.1a, b and c shows that the DO penetration depth in the biofilm increased with time, therefore the DO penetration depth is linked to biofilm thickness. The penetration depth increased when the biofilm thickness

increased and decreased on day 48 when the biofilm thickness showed a decrease due to the biofilm sloughing. Howell and Atkinson (1976) defined the penetration depth as the depth of film for which the overall oxygen uptake would be 99% of that in a very thick biofilm. During this study penetration depth was defined as the depth of biofilm at which oxygen concentration first presented as 0%. Therefore, the depth the DO penetrated into the biofilm.

Table 8.2: Biofilm data

Time (Days)	Day 24	Day 45	Day 47	Day 48
Average biofilm thickness (mm)	0.453	2.025	1.355	0.885
Average wet biomass (g)	1.061	3.609	3.437	3.169
Average dry biomass (g)	0.121	0.309	0.317	0.209
Average density of the wet biofilm (g/m^3)	0.35	0.34	0.63	3.11

Table 8.2 shows all the biofilm data measured and calculated after disconnecting the bioreactors. The biofilm for day 48 experienced biofilm sloughing, therefore the data does not always follow the trends observed. The biofilms that experienced sloughing on day 24 were eliminated from the calculations. With increasing age the biofilms showed increasing dry biomass and wet density, the wet biomass and biofilm thickness did not show this trend. The biofilm on day 45 showed a heavier wet biomass and therefore biofilm thickness, this could be attributed to increased flux before disconnecting the bioreactor or a lower temperature within the rig resulting in less absorption of liquid from the biofilm surface. However, after being dried in an oven overnight the liquid was removed and the expected trend of increasing biomass with increasing time was observed, therefore excess liquid is the cause of the increased biofilm thickness and wet biomass observed on day 47.

Both the thickness and density of the biofilm have a significant affect on the distribution of oxygen within biofilms. The density of biofilms change in the depth direction. A thin biofilm has a dense homogeneous structure, and thus is expected to exhibit a lower substrate penetration depth due to the high density of the biofilm structure that results in a small diffusion coefficient. Thicker biofilms show a heterogeneous structure with large pores (Hibiya *et al.*, 2003), therefore the oxygen can penetrate further into the biofilm.

8.7.2.2 Oxygen penetration ratios within the biofilm

The oxygen penetration ratio was calculated by dividing the oxygen penetration depth by the biofilm thickness. In Table 8.1a, b and c the oxygen penetration depth increased with increasing biofilm thickness, while the oxygen penetration ratio decreased with increasing biofilm thickness. However, the increase in penetration depth was not proportional to the increase in biofilm thickness. Meaning that the penetration depth increased in smaller increments with time, when compared to the biofilm thickness. This resulted in a decreasing penetration ratio when the biofilm increased in thickness. According to Hibiya *et al.* (2003) a thick anaerobic zone exists at the bottom of thick biofilms, indicating the possibility of microbial denitrification. It has been concluded by Hibiya *et al.* (2003) that the oxygen penetration ratio decreases gradually with an increase in the thickness of the biofilm. In a similar non-pressurised MGR system Ntwampe *et al.* (2008) concluded the oxygen penetration ratio decreased with an increase in biofilm thickness. The penetration ratio decreased from an average of 0.42 at 72 hr to 0.12 after 264 hr, therefore the thickness of the anaerobic zones located close to the surface of the ceramic membranes increased with time (Ntwampe *et al.*, 2008).

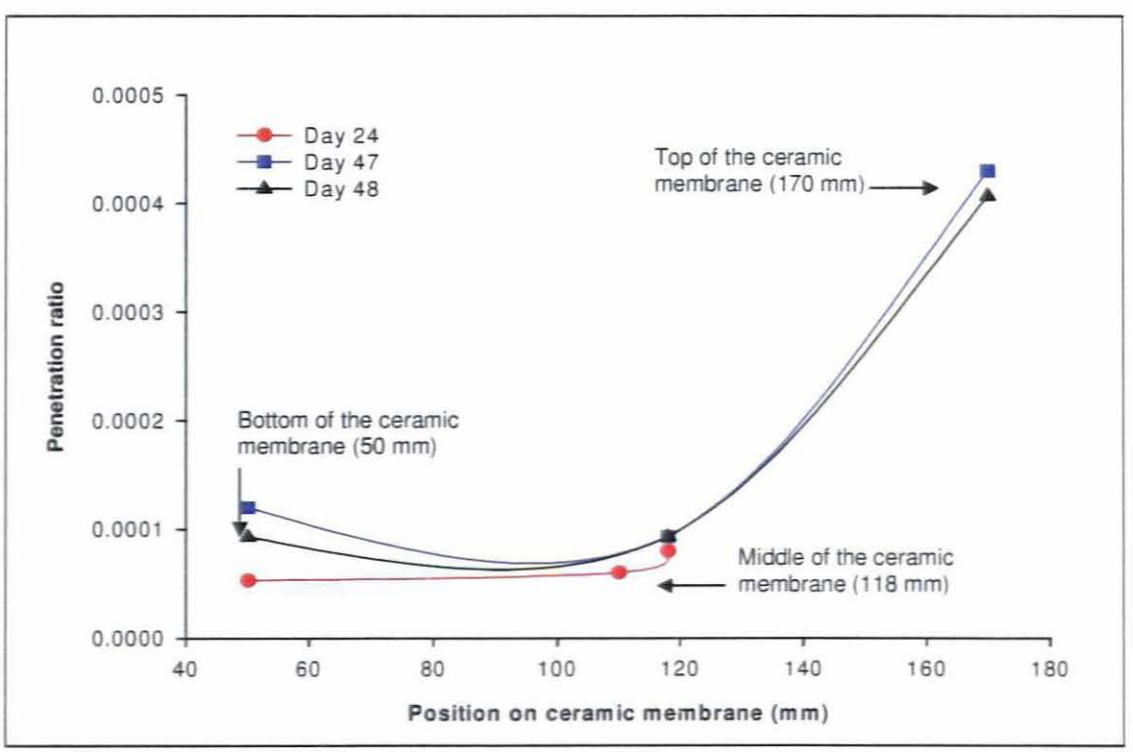

Figure 8.13: Penetration ratio at different locations on a single membrane measured on different days (The error bars represent the standard error using Sigma Plot 8.0)

In the pressurised SFMGR system utilised in the study the position at 50 mm was located furthest from the air supply, while the position at 170 mm was located closest to the air

supply of the system. Figure 8.13 indicates that the closer the biofilm was located to the air supply the higher the penetration ratio. It was observed that the biofilm located closest to the air supply in a pressurised SFMGR was the thinnest. Therefore, in a pressurised SFMGR the highest penetration ratio was determined to be in the thinnest part of the biofilm located closest to the air supply of the system.

8.7.3 Atmospheric dissolved oxygen measurements along the length of the biofilm

The type of DO mass transport into the biofilm, convection or diffusion, had to be identified as it determines the model to be utilised to determine the mass transport parameters within the immobilised biofilm. The ratio between the biofilm oxygen diffusivity coefficient ($D_{a,f}$) in the aerial mycelia and the oxygen diffusivity coefficient (D_w) in the nutrient medium, had to be determined. The oxygen diffusivity coefficient (D_w) in the nutrient medium was determined to be equivalent to 1.161 x 10^{-5} m^2/hr as the complex growth medium, ISP2, had 3% salinity as measured with a hydrometer. If the ratio$\left(D_w : D_{a,f}\right)$ was larger than and equal to 1 (≥1) then the transport was diffusive; if the ratio was much smaller than 1 (<<1) then the transport was convective (Ntwampe *et al.*, 2008). The ratio was calculated for each DO profile as shown in Table 8.3a - c.

The biofilm located at 50 mm from the bottom of the ceramic membrane was located furthest from the air inlet and the type of mass transport into the biofilm was identified as diffusion. The biofilm located at 118 mm from the bottom of the ceramic membrane was located in the middle of the bioreactor, half way between the bottom of the reactor and the air inlet. In Table 8.3b the type of mass transport into the biofilm was determined to be via a combination of diffusion and convection. The biofilm located at 170 mm from the bottom of the ceramic membrane was located closest to the air inlet and the type of transport into the biofilm was identified as convection. The shape and gradient of the DO profiles in Figure 8.14a - c indicate that depending on the location of the biofilm with regards to the air inlet, different types of mass transport into the biofilm were utilised.

Table 8.3: Type of mass transport into the biofilm at (a) 50 mm; (b) 118 mm; and (c) 170 mm from the bottom of the bioreactor on days 24, 47 and 48, respectively

a

Parameter	Day 24	Day 47	Day 48
D_w (m²/hr)	1.161 x 10^{-5}	1.161 x 10^{-5}	1.161 x 10^{-5}
$D_{a.f}$ (m²/hr)	3.85 x 10^{-6}	8.15 x 10^{-6}	3.08 x 10^{-6}
Ratio $\left(D_w : D_{a.f}\right)$	3.01	1.42	3.77
Type of transport	Diffusive	Diffusive	Diffusive

b

Parameter	Day 24	Day 47	Day 48
D_w (m²/hr)	1.161 x 10^{-5}	1.161 x 10^{-5}	1.161 x 10^{-5}
$D_{a.f}$ (m²/hr)	6.05 x 10^{-5}	1.75 x 10^{-5}	4.56 x 10^{-6}
Ratio $\left(D_w : D_{a.f}\right)$	0.19	0.66	2.55
Type of transport	Convective	Diffusive	Diffusive

c

Parameter	Day 24	Day 47	Day 48
D_w	1.161 x 10^{-5}	1.161 x 10^{-5}	1.161 x 10^{-5}
$D_{a.f}$ (m²/hr)	Not measured biofilm too thin	3.05 x 10^{-5}	4.52 x 10^{-5}
Ratio $\left(D_w : D_{a.f}\right)$	-	0.38	0.26
Type of transport	-	Convective	Convective

In Figure 8.14a no DO profile was obtained on day 24 for the 170 mm position as the biofilm was too thin to take measurements. Comparing the shape and gradient of the profiles in Figure 8.14a – c to the type of mass transport identified in Table 8.3a – c; indicated that the diffusive transport profiles obtained in the biofilm located at 50 mm and 118 mm, had a steep gradient. The convective mass transport identified in the biofilm at 170 mm from the bottom of the bioreactor had a gradual gradient, less steep than the profiles for 50 mm and 118 mm.

The biofilm at 170 mm was located closest to the air inlet and exhibited increased DO penetration depth when compared to 50 mm and 118 mm, although the biofilm located at 170 mm was the thinnest due to biofilm tapering. The increased DO penetration depth was due to a combination of the location of the biofilm with regards to the air inlet and the convective mass transport within the biofilm.

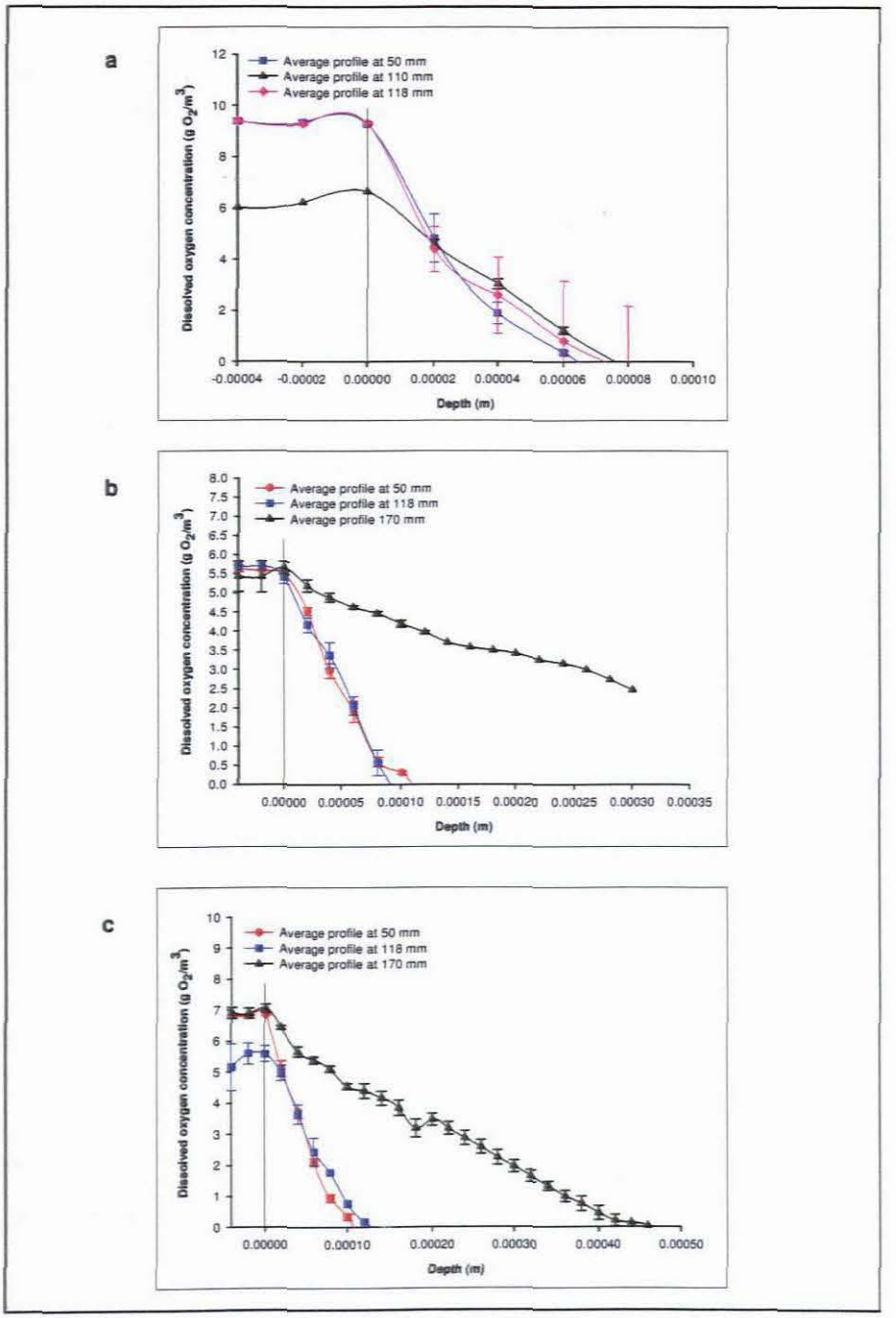

Figure 8.14: Average dissolved oxygen profiles on: (a) day 24; (b) day 47; and (c) day 48 at 50 mm, 118 mm and 170 mm from the bottom of the bioreactor, respectively (The error bars represent the standard error using Sigma Plot 8.0)

The biofilm at 170 mm was located closest to the air inlet and exhibited increased DO penetration depth when compared to 50 mm and 118 mm, although the biofilm located at 170 mm was the thinnest due to biofilm tapering. The increased DO penetration depth was due to a combination of the location of the biofilm with regards to the air inlet and the convective mass transport within the biofilm.

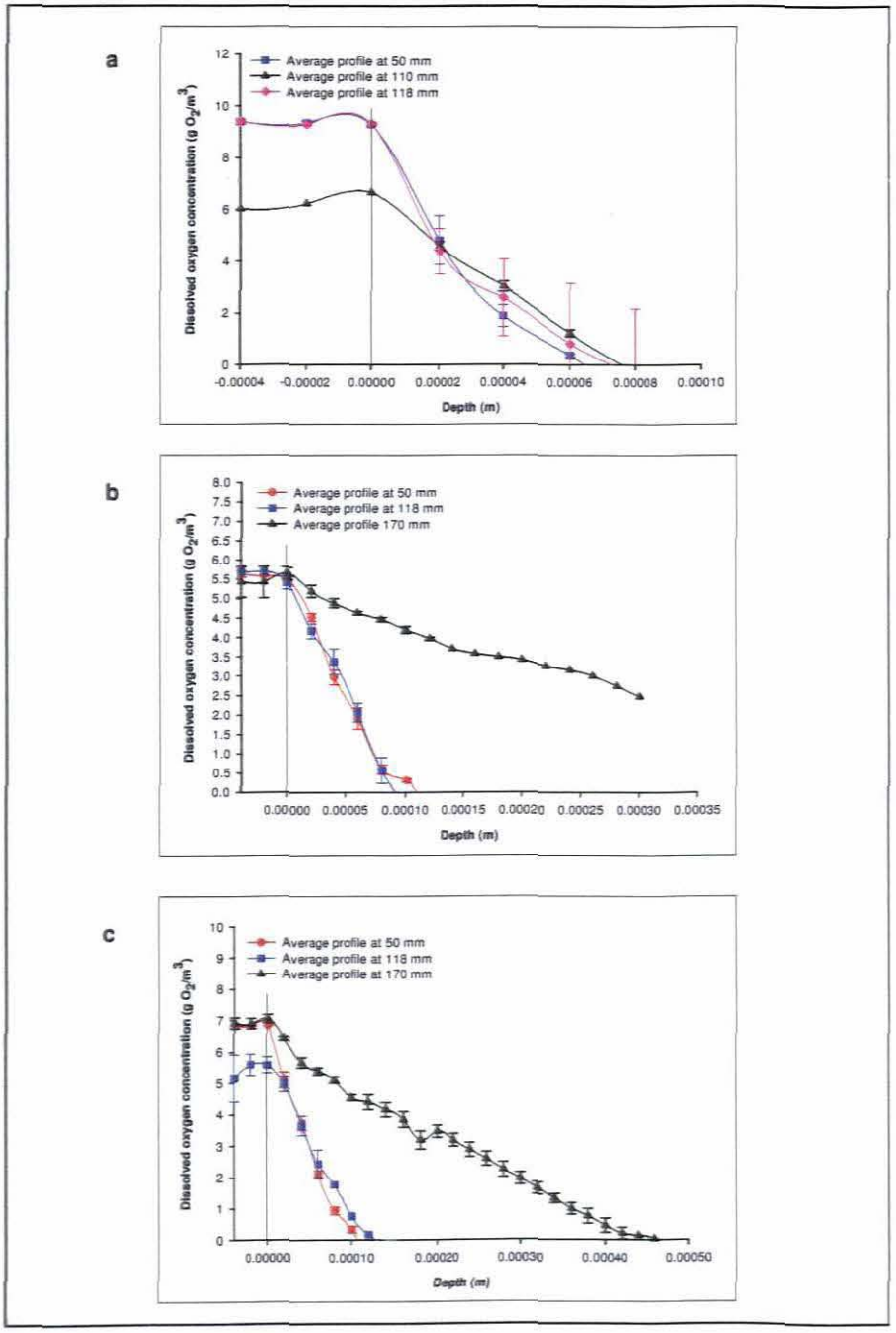

Figure 8.14: Average dissolved oxygen profiles on: (a) day 24; (b) day 47; and (c) day 48 at 50 mm, 118 mm and 170 mm from the bottom of the bioreactor, respectively (The error bars represent the standard error using Sigma Plot 8.0)

8.7.4 Atmospheric dissolved oxygen measurements influenced by the structure of the biofilm

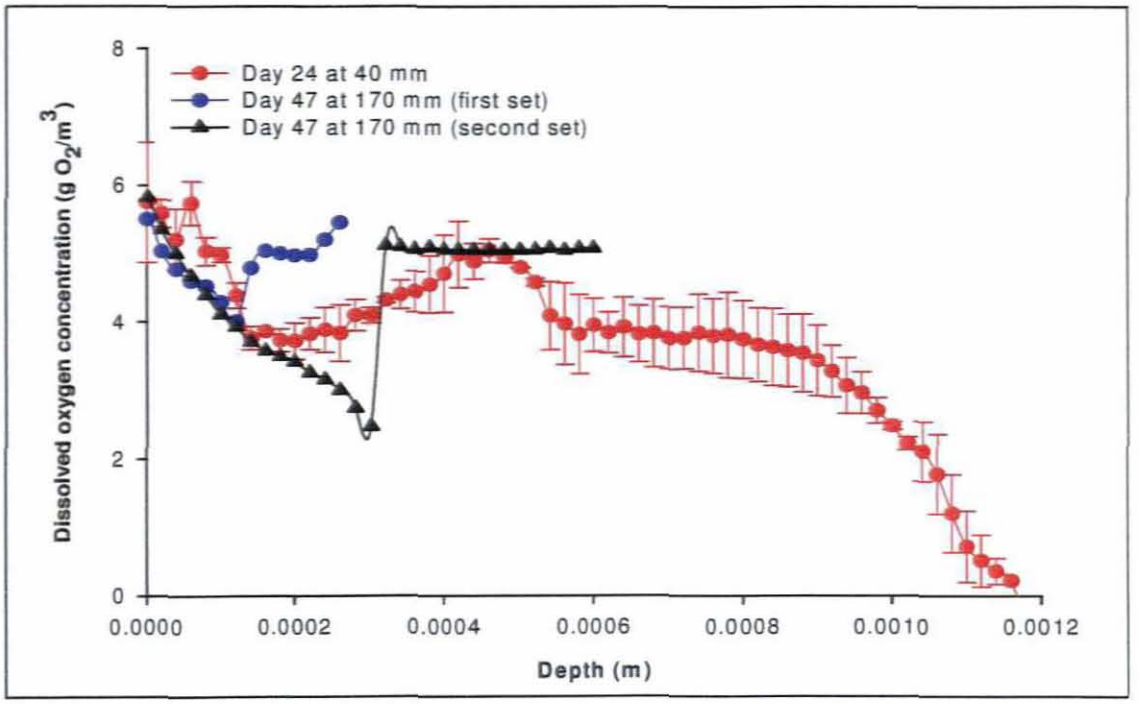

Figure 8.15: Average dissolved oxygen (DO) profile on day 24 at 40 mm from the bottom of the reactor and two profiles on day 47 at 170 mm (The error bars represent the standard error using Sigma Plot 8.0)

During the study the profiles in Figure 8.15 were obtained in addition to the profiles seen in Figure 8.12a - c. The shape of the profiles in Figure 8.15 differs from those in Figure 8.12a - c. The DO profiles in Figure 8.15 were not steadily decreasing as seen in Figure 8.12a - c. In the curves measured on day 47 in Figure 8.15 the DO concentration was steadily decreasing when the profile suddenly increased at 0.00013 and 0.0003 m for the first and second set of readings at 170 mm, respectively. This was due to the structure of the filamentous bacterium *Streptomyces coelicolor* utilised during the study, as shown in the SEM's in Figure 8.16. As the micro organism is filamentous in nature sometimes air pockets are created as seen in Figure 8.16 (b and c), which might be responsible for the phenomenon observed in the DO profiles in Figure 8.15.

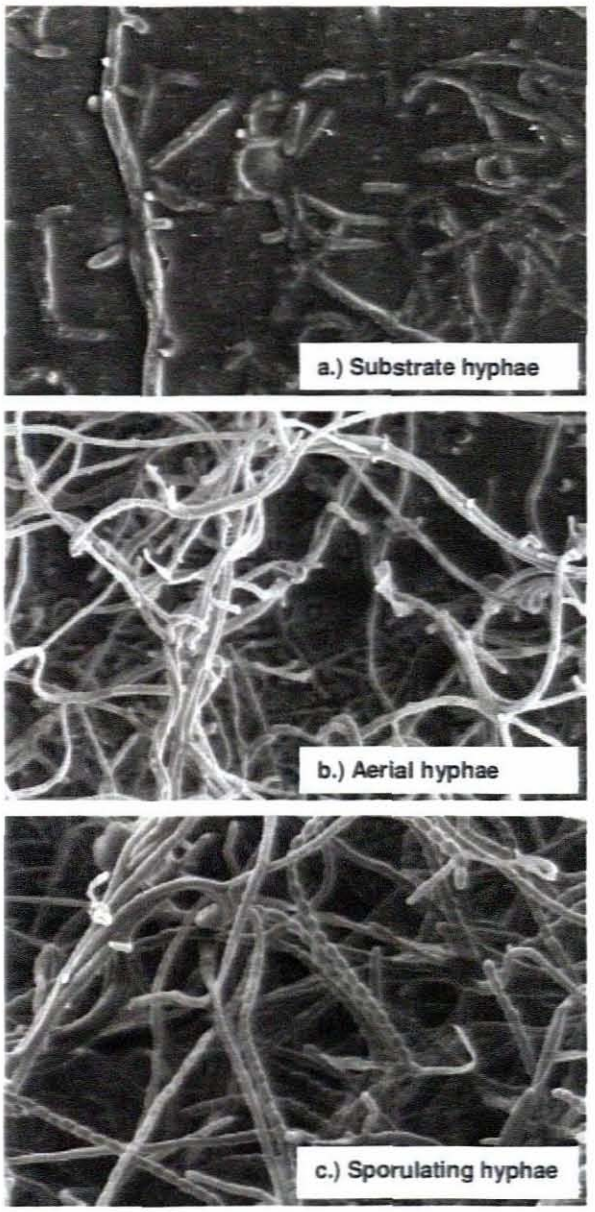

Figure 8.16: The life cycle of Streptomycetes grow mom solid media, such as the surface of a ceramic membrane (Claessen *et al.*, 2006)

8.7.5 Dissolved oxygen mass transport parameters

From the dissolved oxygen profiles obtained using the data acquisition software Profix 3.0, the dissolved oxygen mass transport parameters were calculated via two methods; (1) Profile 1.0 software, and (2) using Taylor's expansion series explained in section 2.4.3 in Chapter 2.

The oxygen profiles recorded using Profix 3.0 data acquisition software, were not only analysed with Profile 1.0 software, but also in Microsoft Excel 2003. Equation 8.1 was utilised to convert the signal recorded by Profix 3.0 (V) into dissolved oxygen concentrations

(g O_2/m^3). The inverse of each part in Equation 2.55 (refer to section 2.4.4.2 in Chapter 2) was taken, to yield a linear function between the inverse of the second derivative and the inverse of the DO concentration, represented by Equation 2.56 (Hibiya *et al.*, 2003). In Excel the inverse of the second derivative and the inverse of the DO concentration were plotted and a linear trendline inserted. The substrate saturation constant, K_s was calculated by dividing the slope of the trendline obtained by the intercept. The oxygen diffusion coefficient, $D_{a.f}$, was calculated using Equation 2.26 in section 2.4.1.2. The maximum rate of reaction, V_{max}, was then calculated by dividing the intercept of the linear trend line by the oxygen diffusion coefficient. To determine the oxygen diffusion coefficient, $D_{a.f}$, the flux through the biofilm, $J_{f_{O_2}}$, was required. The flux was determined with Profile 1.0 software. An input file (refer to Appendix F for an example of an input file) created in Notepad, was run in Profile 1.0 and an output file generated (refer to Appendix F for an example of an output file) for each DO profile measured. The output file contained data regarding the DO concentration at the surface and bottom of the biofilm close to the membrane, the oxygen flux through the biofilm, the type of biological activity (i.e. production or consumption), as well as the depth at which biological activity started in the biofilm.

The kinetic parameters K_s, V_{max}, $D_{a.f}$ and $J_{w.xs}$ and the experimental coefficients a, b and c were also calculated using Equations 2.32, 2.35, 2.38 to 2.39 of Taylor's expansion method explained in section 2.4.3 in Chapter 2 (these results were not included in this chapter).

8.7.5.1 Kinetic parameters calculated from the oxygen profiles and Profile 1.0

Table 8.4a indicated that as the biofilm decreased in thickness towards the top of the bioreactor due to biofilm tapering the substrate saturation constant, K_s, decreased. In this study the substrate was oxygen. In Table 8.4b the substrate saturation constant increased over time, therefore the older the biofilm the higher the substrate saturation constant. It was therefore postulated that in thin less dense biofilms the substrate saturation constant will be small, while in thicker older biofilms the substrate saturation constant will be larger.

The oxygen diffusion coefficient, $D_{a.f}$, in the aerial mycelia was highest at 170 mm from the bottom of the bioreactor, as seen in Table 8.4a. The biofilm at this location was situated closest to the air inlet, while the biofilm located further away from the air inlet at 50 mm and 118 mm was therefore not subjected to direct air flow as the biofilm at 170 mm.

Table 8.4: Average dissolved oxygen kinetic parameters at (a) 50, 118 and 170 mm from the bottom of the bioreactor; and (b) on days 24, 47 and 48, calculated from the dissolved oxygen profiles

a	Position on the ceramic membrane (mm)	50 mm	118 mm	170 mm
	K_s (g/m^3)	3.00	3.46	≈0
	$D_{a,f}$ (m^2/hr)	2.0 x 10^{-6}	2.0 x 10^{-6}	3.3 x 10^{-5}
	Biofilm thickness (mm)	1.33	1.43	0.92

b	Time (Days)	Day 24	Day 47	Day 48
	K_s (g/m^3)	2.45	3.78	4.25
	$D_{a,f}$ (m^2/hr)	2.0 x 10^{-6}	2.2 x 10^{-5}	2.0 x 10^{-6}
	Biofilm thickness (mm)	0.451	1.355	0.885 (Biofilm sloughed)

The maximum rate of reaction, V_{max}, was the same order of magnitude for the biofilm located at 50 mm and 118 mm (Table 8.4a), as well as on the different days (Table 8.4b) the bioreactors were disconnected. The values for the maximum rate of reaction were extremely large and therefore not reported in the study. A possible reason for the extreme values obtained could have been due to the pressure under which the system was operated, as well as the type of mass transport into the biofilm. The humidified air supplied to the ECS of the bioreactor and the growth medium supplied to the lumen of the membrane were pressurised. The pressure differential in the system therefore facilitated increased reaction rates within the biofilm regions dominated by maximum biological reaction and minimal transport.

In Table 8.5a it was observed that the closer the biofilm (170 mm) was located to the air inlet the lower the flux through the biofilm and the further the biofilm (50 mm) was located from the air inlet the higher the flux through the biofilm. Table 8.5b indicated that the flux through the biofilm decreased over time and increased biofilm thickness. Tables 8.5a and b indicate that the biological reaction occurring within the biofilms was consumption since the value calculated by Profile 1.0 was negative.

Table 8.5: Average dissolved oxygen parameters at (a) 50, 118 and 170 mm from the bottom of the bioreactor; and (b) on days 24, 47 and 48, calculated using Profile 1.0 software

a	Position on ceramic membrane (mm)	50 mm	118 mm	170 mm
	Calculated concentration at the top (g/m^3)	7.33	6.21	6.29
	Calculated concentration at the bottom (g/m^3)	1.39	1.65	0.69
	Calculated flux at the top ($g/m^2.hr$)	0.11	0.17	0.02
	Calculated flux at the bottom ($g/m^2.hr$)	0	0	0
	Production (Consumption)	Zone 1: -1103.60	Zone 1: -1457.95	Zone 1: -79.62 Zone 2: -86.90
	Depth (mm)	0.09	0.08	0.23 (Zone 1) 0.38 (Zone 2)

b	Time (Days)	Day 24	Day 47	Day 48
	Calculated concentration at the top (g/m^3)	7.58	5.66	7.01
	Calculated concentration at the bottom (g/m^3)	1.61	1.35	1.47
	Calculated flux at the top ($g/m^2.hr$)	0.29	0.09	0.13
	Calculated flux at the bottom ($g/m^2.hr$)	0	0	0
	Production (Consumption)	Zone 1: -6052.67	Zone 1: -880.65	Zone 1: -1680.90
	Depth (mm)	0.07	0.15	0.09

In the biofilm located at 50 mm and 118 mm from the bottom of the bioreactor the biological reaction occurs within 0.09 mm and 0.08 mm from the surface of the biofilm, respectively. At 170 mm the biological reaction (i.e. consumption) begins 0.23 mm from the surface of the biofilm. Therefore, the reaction zone within the biofilm at 50 mm, 118 mm and 170 mm was 1.24, 1.35 and 0.31 mm thick, respectively. The thickness of the reaction zones indicated

that at 170 mm, closer to the air inlet, there was minimal consumption and maximal transport, while at 50 and 118 mm consumption was high and transport low. This is confirmed by the type of transport identified at these locations, as well as the consumption values generated in the output file using Profle 1.0 software. Diffusive transport dominated at 50 and 118 mm, while convective transport dominated at 170 mm.

The shape and gradients of the profiles in Figure 8.12a – c were detemined by the type of transport. In the regions were the transport was via diffusion the biological reaction zones were large; therefore these regions were dominated by the biological reaction and not transport. In the regions were the transport was via convection the biological reaction zones were minimal, therefore these regions were dominated by maximal convective transport and minimal consumption. This was confirmed by the substrate saturation constant and maximum rate of reaction which were determined to be approximately zero at 170 mm, where the transport was convective. If the substrate saturation constant is much smaller than the initial concentration of the substrate (i.e. oxygen), C_{O_2}, then the biological reaction rate, r_B, will be equivalent to the maximum substrate consumption rate, r_m. However, if $K_s \approx 0$, then $r_B \approx r_m \approx 0$. This was observed in the biofilm at 170 mm from the bottom of the bioreactor, where consumption was minimal and convective transport at a maximum.

8.7.5.2 Comparison of parameters calculated utilising the oxygen profiles, Profile 1.0 and Taylor's expansion series

Ntwampe *et al.* (2008) determined DO mass transfer parameters using Taylor's expansion series for a similar non-pressurised MGR system utilised to immobilise *P. chrysosporium.* The Monod saturation constants were in the range of 0.041 to 0.999 g/m^3, the consumption of oxygen in the biofilm was in the range of 894.53 to 2739.70 g/m^3.hr, the oxygen diffusion coefficient in the range of 7.94 x 10^{-6} to 1.750 x 10^{-5} m^2/hr and dissolved oxygen flux through the biofilm 0.27 to 0.7 g/m^2.hr. The average oxygen penetration depth decreased with time and the penetration ratio decreased from 0.42 to 0.12 with anaerobic zones in the biofilms increasing from 602 µm after 72 hr to 1940 µm after 264 hr.

During this study, using Profile 1.0 software the substrate saturation constants were in the range of 2.45 to 4.25 g/m^3, the oxygen diffusion coefficient in the range of 8.15 x 10^{-6} to 1.75 x 10^{-5} m^2/hr and dissolved oxygen flux through the biofilm 0.13 to 0.29 g/m^2.hr. The average oxygen penetration depth decreased with time and the penetration ratio decreased from 1.6 to 0.26.

When the DO kinetic parameters determined for this study were compared to those obtained by Ntwampe *et al.* (2008) the range of substrate saturation constants and the rate of oxygen consumption range was higher. This was attributed to the system being operated under pressure while the MGR system utilsed by Ntwampe *et al.* (2008) was not. The oxygen diffusion coefficients obtained were of the same order of magnitude for both systems. Although different micro organisms were immobilised during the two studies both micro organisms, namely *Phanerochaete chrysosporium* and *Streptomyces coelicolor*, were filamentous in nature.For both the non-pressurised MGR system used by Ntwampe *et al.* (2008) and the pressurised MGR system used during this study the average penetration depth decreased over time with an increase in biofilm thickness, resulting in a decrease in penetration ratio over time. The penetration ratios determined for this study were higher than those determined by Ntwampe *et al.* (2008) due to the current study being operated for a longer duration; however both showed a decrease in penetration ratio over time. A higher flux of oxygen through the biofilm was observed in the non-pressurised system (Ntwampe *et al.*, 2008) than in the pressurised system utilised during the current study.

The DO kinetic parameters calculated using Taylor's expansion series were compared to the values obtained using Profile 1.0 software. However, except for the oxygen diffusion coefficient values which were of the same order of magnitude, the values determined for K_s, V_{max} and $J_{w,xs}$ were vastly different from those determined with Profile 1.0 software. Taylor's expansion method was utllised by Ntwampe *et al.* (2008) to determine the DO kinetic parameters in a similar non-pressurised system. The values determined by Ntwampe *et al.* (2008) are comparable to those determined for the current study using Profile 1.0 software. Therefore, Taylor's expansion method can be utilised to determine dissolved oxygen kinetic parameters for non-pressurised MGR systems, but was not suitable for the pressurised system utilised during this study.

8.7.6 Scenario to be utilised to solve the mathematical model developed

From this study it was determined that the initial oxygen concentration, C_{O_2}, supplied to the system in the range of 7.05 to 7.25 g O_2/m^3 and the substrate (i.e. oxygen) saturation constant, K_S, values (indicated in Tables 8.4b) were of the same order of magnitude, therefore $C_{O_2} \approx K_S$. A numerical technique is therefore required to solve Equation 8.14. However, the correct numerical technique first needs to be identified before the equation can be solved. This process of elimination and model solving would be extremely time consuming and was therefore not part of this study.

8.7.7 Dissolved oxygen measurements of the permeate samples

The DO present in the permeate samples was measured daily after removing the permeate from the permeate collection bottle of each reactor. When the permeate was collected from the pressurised collection bottles into centrifuge tubes, the permeate was exposed to air at atmospheric pressure allowing mixing to occur. The only way to collect the permeate from the pressurised collection bottles for analysis was by releasing the pressure in the collection bottles which facilitated the transfer of the permeate to the centrifuge tubes. The volume of permeate collected determined how well the air mixed with the permeate. The smaller the volume the higher the DO concentration within the permeate samples and the larger the volume the lower the DO concentration. Therefore, the DO concentration present in the permeate samples appeared to depend on the volume of permeate collected and possibly the temperature in the laboratory.

8.7.8 Dissolved oxygen measurements within the growth medium

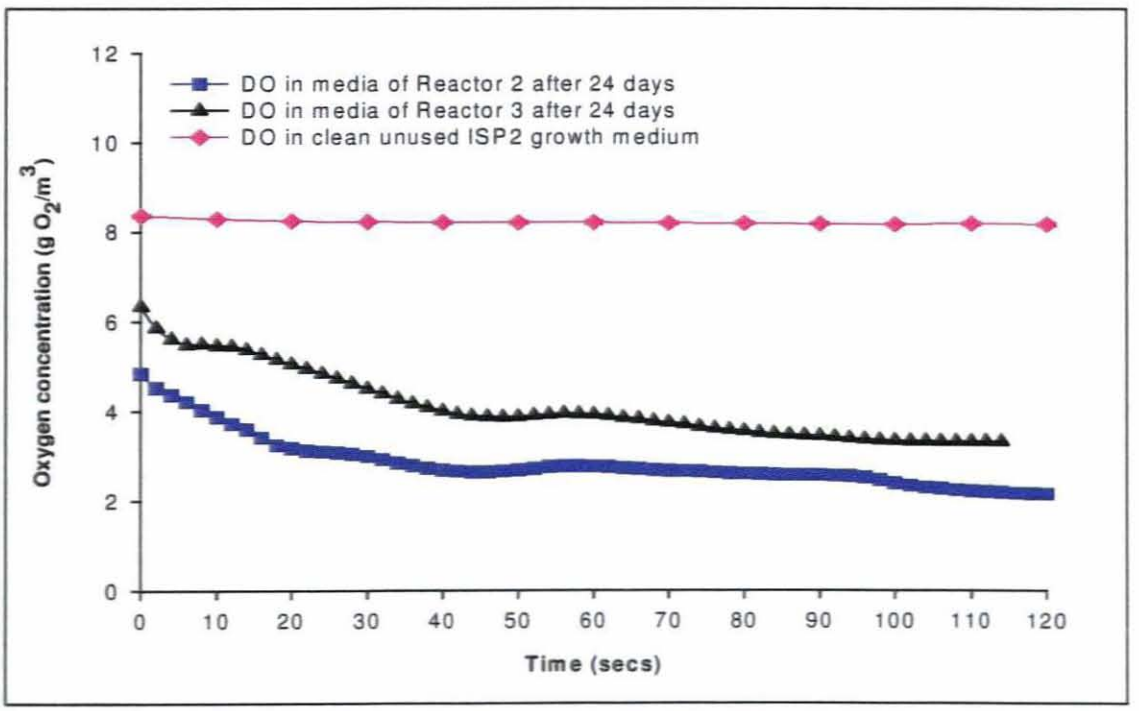

Figure 8.17: Average dissolved oxygen (DO) profiles in unused growth medium and used growth medium (24 days) (The error bars represent the standard error using Sigma Plot 8.0)

In Figure 8.17 the DO concentration within the media was measured with a Clark-type ampoteric microsensor. The two curves showing a gradual decrease in DO concentration over time was measured in the complex growth medium, ISP2, which had been utilised for 24 days by the system. When the DO readings were taken it was observed that there was back growth of the micro organism in the growth medium. In the pressurised SFMGR system

utilised in this study the longer the system is operated the higher the possibility of back growth of the micro organism within the growth medium. This accounts for the gradual decrease in DO concentration as the profile was measured, since the micro organism present in the growth medium was utilising the oxygen present in the medium. For these two curves readings were taken every 2 seconds with an OX10 microsensor.

The stable almost horizontal curve in Figure 8.17 represents the DO concentration measured in sterile unused fresh complex growth medium. As this growth medium was sterile and unused there was no back growth of the micro organism, therefore the oxygen present in the medium was not being utilised which explains why the curve is horizontal and does not fluctuate over time. For this curve readings were taken every 10 seconds with an OX10 microsensor, therefore there are less data points when compared to the two other curves in Figure 8.17.

The possibility of oxygen present in the growth medium influencing the DO concentration present in the biofilm, and resulting in increased concentration as observed in Figures 8.9 and 8.10 can therefore be eliminated. The micro organism present in the growth medium due to back growth utilised any oxygen present.

8.7.9 Average flux, pH, actinorhodin production and redox potential

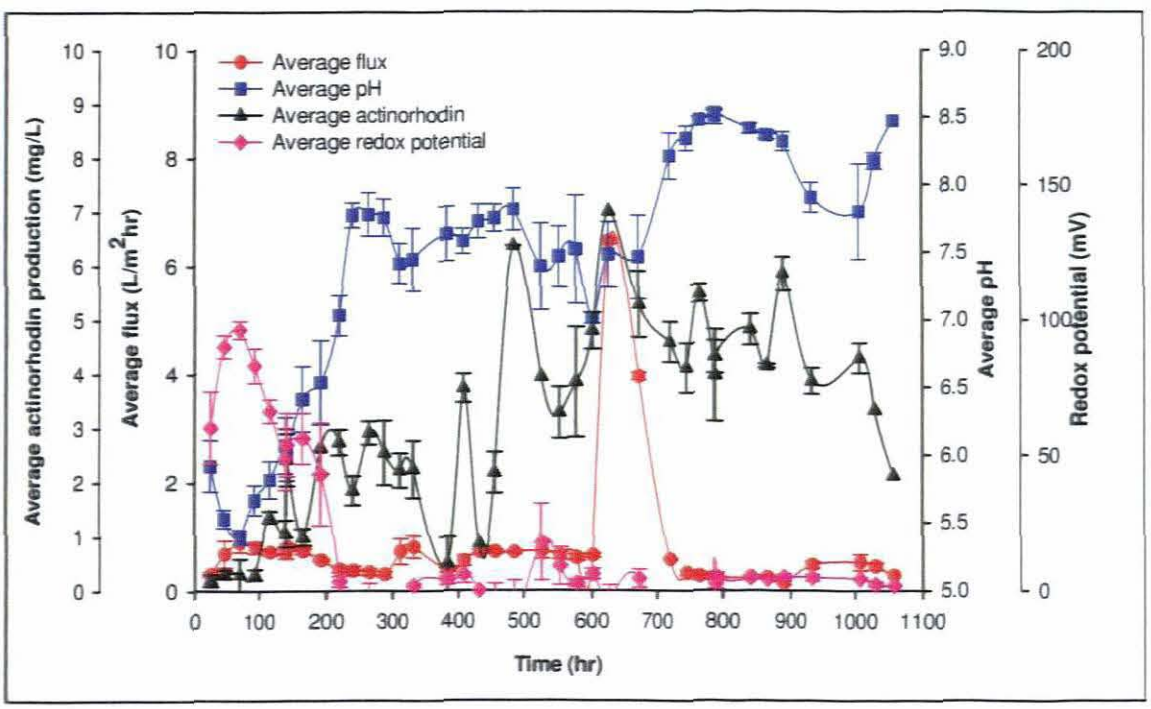

Figure 8.18: Time course of the average flux, pH, actinorhodin production and redox potential profiles (The error bars represent the standard error using Sigma Plot 8.0)

In Figure 8.18 the average flux, pH, actinorhodin production and redox potential was determined daily. Both the pH and redox potential was measured with a Metrohm 744 pH meter. Observed from the curves in Figure 8.18 the flux decreased gradually over time as the transmembrane pressure remained constant and the biofilm increased in thickness. Due to the flux decreasing over time and the micro organism consuming glucose for biomass formation the biofilm was subjected to nutrient limitation resulting in an increase in extracellular actinorhodin production. An increase in actinorhodin production resulted in an increase in pH. The redox potential was measured for the first time during this study. It was observed that as the pH increased the redox potential decreased, therefore the pH and redox potential showed an inverse relationship to each other.

8.8 Summary

To be able to measure *in-situ* dissolved oxygen (DO) measurements within a biofilm immobilised in a pressurised MGR a manipulator had to be designed. The manipulator had to allow the DO microsensor to remain attached to the glass housing of the bioreactor for the duration of each experiment. It was required that once attached to the system the manipulator not only housed the microsensor, while maintaining the pressure within the system, but allowed the operator to manipulate the microsensor into and out of the biofilm immobilised on the surface of the ceramic membrane. The manipulator was successfully designed and drawn to scale using a three dimensional drawing program, Solid Edge (Version 18).

On completion of this section of the study it was concluded that over time a biofilm immobilised on the surface of a ceramic membrane in a pressurised SFMGR increases in thickness, unless sloughing occurs. However, due to the vertical orientation of the bioreactor the thickest part of the biofilm was located at the bottom of the bioreactor and the thinnest at top. Convective mass transfer was identified in the thin biofilm located closest to the air inlet and diffusive mass transport in the thicker biofilm located in the middle and at the bottom of the bioreactor.

It is recommended that the study be repeated with an oxygen microsensor constructed by Unisense that is pressure tolerant. A pressure tolerant microsensor would allow the measurement of oxygen under high pressure, like observed in the ECS of the system utilised in this study. Thereby, hopefully eliminating the high and drifting signal observed during the *in-situ* DO measurements of this study.

It is important to understand how oxygen affects an immobilised biofilm in an MGR in order to optimise the SFMGR system for the commercial production of secondary metabolites, such

as actinorhodin. The measured oxygen profiles of the immobilised *Streptomyce coelicolor* biofilm can be used to quantify mass transfer parameters. Understanding dissolved oxygen mass transfer kinetic parameters in aerobic biofilms, such as *Streptomyces coelicolor* A3(2), is required to obtain optimal microbial activity.

It is recommended that should a similar study be conducted more than one method be utilised to determine the maximum rate of reaction, V_{max}, in order order to confirm the values obtained during this study. Since the values obtained were excessively high even for a pressurised system. By utilising different methods to determine the oxygen mass transfer parameters within a pressurised MGR system, the most appropriate method would be confirmed.

CHAPTER 9

OVERALL DISCUSSION OF RESULTS

CHAPTER NINE
OVERALL DISCUSSION OF RESULTS

9.1 Background

The main purpose for performing this research project was to determine the growth, substrate and oxygen mass transfer kinetics in a continuously operated pressurised Membrane Gradostat Bioreactor (MGR), using the soil dwelling Gram positive filamentous bacterium *Streptomyces coelicolor* A3(2).

9.2 Overall discussion of results

9.2.1 The quantification and comparison of *Streptomyces coelicolor* growth in defined and complex growth medium

Growth media is divided into two categories: complex and defined. In a defined growth medium each component present in the medium is known, as well as the quantity of the component to be used in the medium preparation. In a complex growth medium not all the components are known since extracts, such as malt extract, are utilised and not all the components present in the extract are defined on the label of the container. A complex medium provides the micro organism being cultured with the basic components required to survive, such as carbon in the form of glucose. A relationship normally exists between the composition of the growth medium and the biosynthesis of secondary metabolites such as actinorhodin.

From literature it was deducted that when utilising a defined growth medium, most of the product formation is intracellular. However, when utilising a complex growth medium with a pH close to neutral and the product is dark blue/purple in colour, it can be assumed that product formation is both intracellular and extracellular. The lactone derivative γ-actinorhodin accounts for the dark blue/purple colour of the product and indicates that γ-actinorhodin is extracellular, while actinorhodin is produced intracellularly.

The use of the complex growth medium, ISP2, utilised in this study resulted in thicker, more robust biofilms, as well as higher secondary metabolite (i.e. actinorhodin) production, than the defined growth medium. When utilising the complex medium, the biofilms increased in thickness due to glucose consumption. However, due to the biofilm continually increasing in thickness, the flux decreased since the TMP was kept constant for the duration of the study. Therefore, the biofilm experienced nutrient limitation, resulting in blue pigment synthesis that was visible in the permeate.

The biofilms generated when the defined medium was utilised were extremely thin due to nutrient limitation, identified as glucose. The glucose limitation, indicated by the cessation of blue pigment synthesis, resulted in poor biomass production. Therefore, when the defined growth medium was utilised the secondary metabolite production was intracellular and not visible in the permeate.

Both the complex and defined growth media stimulated secondary metabolite production, but for different reasons. The defined medium resulted in actinorhodin production due to glucose limitation, which also caused poor biomass growth. While the complex medium resulted in actinorhodin production, due to decreased flux across the biofilm.

9.2.2 Identifying glucose consumption kinetic parameters for *S. coelicolor* using both a complex (ISP2) and defined growth medium

Secondary metabolism is suppressed when a micro organism is growing at its full potential under optimum conditions. In order to optimise secondary metabolite production certain nutrients, such as glucose, a carbon source for *Streptomyces coelicolor* A3(2), is limited resulting in increased secondary metabolite production.

In this study the glucose concentration decreased as the biomass increased. When the complex growth medium was utilised glucose was not limited. However, glucose was identified as the limiting nutrient when the system was operated with the defined growth medium.

The Monod single-substrate growth kinetic model was utilised to quantify the glucose consumption kinetics, as the initial glucose concentration present in the growth medium remained unchanged for the duration of the study. The average glucose consumption rate, (r_g), was determined to be approximately 92.27 g/m^3.hr. Utilising the Lineweaver-Burke method to linearise the rate limiting nutrient's data, the Monod saturation constant, (K_m), and the maximum substrate consumption rate, (r_m), were calculated to be 29605.65 g/m^3 and 434.78 g/m^3.hr, respectively. While using Solver in Microsoft Excel 2003 for the non-linear regression method, the Monod saturation constant, (K_m), and the maximum substrate consumption rate, (r_m), were calculated to be 29605.67 g/m^3 and 4341.69 g/m^3.hr, respectively.

If glucose is the limiting nutrient within an MGR system, whether the system is pressurised or non-pressurised, the average consumption rate is in the range of 90 to 95 g/m^3.hr. However,

if glucose is not completely depleted within the system the average consumption rate is much lower. In pressurised MGR systems, higher Monod saturation constants and maximum glucose consumption rates are observed than in non-pressurised MGR systems.

9.2.3 Mathematical modelling of the growth kinetics of *S. coelicolor* biofilm growth in a pressurised MGR

The growth curve obtained for *S. coelicolor* A3(2) immobilised in a pressurised continuously operated MGR, showed the presence of two growth cycles (biphasic growth) from ±66 to 162 hr and ±162 to 354 hr, respectively, with no noticeable intermediate lag phase. Two specific growth rates were obtained, one for each growth cycle, with a lower specific growth rate (in the range of 0.013 to 0.019 hr^{-1}) obtained for the second growth cycle compared to the first growth cycle (in the range of 0.033 to 0.073 hr^{-1}), this trend corresponds to literature for non-pressurised MGR systems. The specific growth rate determined for the first growth cycle correspond to the specific growth rate obtained in literature for the same micro organism cultured in a non-pressurised batch system. However, the specific growth rate range obtained for the second growth cycle in this study corresponds to specific growth rates obtained in literature for non-pressurised batch and fed-batch systems operated at lower airflow rates than utilised in this study.

The various kinetic growth models (i.e. logistic, exponential, linear, power law and two-phase) were fitted to the growth curve obtained from the experiemental data. The power law model gave the best fit for the first growth cycle, from ±66 to 162 hr. The two-phase model (fast acceleration phase from ±162 to 212 hr and slow deceleration phase from ±212 to 282 hr) gave the best fit for the second growth cycle. The best growth model fit was obtained when the point at ±354 hr on the growth curve was excluded. Due to repeated biofilm sloughing from the ceramic membrane, the point at ±354 hr could not be confirmed after 354 hr, even with repeated experiments.

The cause of the biphasic growth during this study was not identified. However, from (1) the pH values recorded; (2) the glucose, actinorhodin and phosphate assays performed; (3) the specific growth rates obtained for the two growth cycles; as well as (4) the synthesis of the blue pigment (ie. actinorhodin), glucose and phosphate were eliminated as possible causes. Nitrogen, sulphur, potassium and trace elements were the components of the growth medium not eliminated. However, since a complex growth medium was utilised during the study the quantity of these components present in the growth medium was unknown.

9.2.4 The quantification and comparison of product formation in biofilms of *S. coelicolor* in both single fibre membrane gradostat reactor's (SFMGR's) and multifibre membrane gradostat bioreactor's (MFMGR's)

The highest actinorhodin concentration (85.12 mg/L) was produced by the SFMGR's housing the larger membranes. The same pressure differential was utilised for both the larger and smaller ceramic membranes in the SFMGR's. The flux across the larger membranes was unstable due to the pressure differential being too low to facilitate a stable transmembrane flux. The pressure differential should have been increased accordingly with an increase in membrane diameter. Therefore, it was postulated that the micro organism experienced nutrient limitation, resulting in increased actinorhodin production.

The highest actinorhodin concentration produced by the biofilm immobilised on the larger and smaller membranes in the MFMGR's, was 44.60 and 67.09 mg/L, respectively. The highest actinorhodin concentration produced by the biofilm immobilised on the smaller membranes in the SFMGR's was 51.0 mg/L. The growth medium flux across the smaller membranes in the MFMGR of 0.506 $L/m^2.hr$ was 28.5% lower than the flux of 0.708 $L/m^2.hr$ across the smaller membranes in the SFMGR's. The biofilms immobilised in the MFMGR's housing the smaller membranes were receiving a lower volume of growth medium and therefore subjected to nutrient limitation resulting in higher concentrations of actinorhodin being produced. The highest actinorhodin production occurred with the larger membranes in the SFMGR's and with the smaller membranes in the MFMGR's

A comparison of the results obtained for the SFMGR's in Chapter 5 with the results obtained for the MFMGR's in Chapter 8 indicated that for the MFMGR's when the pH increased the actinorhodin and glucose concentrations decreased. This occurred possibly due to the composition of the growth medium being altered and the maintenance of a constant flux across the membranes. The MFMGR's utilised an automated system with load cells that ensured the flux remained constant. In the SFMGR's an increase in pH resulted in an increase in actinorhodin production and a decrease in glucose concentration. However, due to a combination of increased biofilm thickness over time and a constant TMP, the flux in the SFMGR system decreased over time. Therefore the SFMGR's experienced nutrient limitation due to decreased flux, while the MFMGR's experienced nutrient limitation due to the growth medium being altered to contain decreased quantities of glucose and malt extract.

9.2.5 Atmospheric oxygen measurements and quantification of the oxygen kinetic parameters

On completion of this section of the study it was concluded that over time a biofilm immobilised on the surface of a ceramic membrane in a pressurised vertically orientated

SFMGR increases in thickness and exhibits tapering from the bottom to the top of the bioreactor. Both biofilm density and dry biomass increased with age.

The DO penetration depth depends on: (1) the location of the biofilm; (2) biofilm thickness; and (3) the type of transport into the biofilm. The closer the biofilm is located to the air inlet, the thinner the biofilm and if the mass transport is via convection the higher the penetration depth. Therefore, DO penetration depth increased from the bottom of the bioreactor towards the top, where the air inlet of the SFMGR was located. The penetration ratio increased with a decrease in biofilm thickness along the length of the ceramic membrane.

The type of transport depended on the thickness and location of the biofilm within the bioreactor with regards to the air inlet. Mass transport in biofilms less than 1 mm thick was via convection and via diffusion in biofilms thicker than 1 mm. At 50 and 118 mm from the bottom of the bioreactor, the type of transport was identified as diffusive. The substrate saturation constants were determined to be ≈3.00 and 3.46 g/m^3, respectively and the thickness of the reaction zone ≈1.24 and 1.35 mm, respectively, indicating minimal transport and maximum biological reaction, identified as consumption. At 170 mm from the bottom of the reactor, the type of transport was identified as convective. The substrate saturation constant was determined to be ≈0.00 g/m^3 and the thickness of the reaction zone ≈0.38 mm, indicating minimal consumption and maximal convective mass transport. However, the question arises if the air inlet was located at the bottom of the bioreactor; would the transport in the biofilm located at the top of the bioreactor still be via convection?

Anaerobic zones exist within the biofilm especially at 50 and 118 mm from the bottom of the reactor where the mass transport was via diffusion. At these locations transport was minimal and biological reaction maximal. The average penetration depth was determined to be ≈8.67×10^{-5} and 8.87×10^{-5} mm at 50 mm and 118 mm, respectively. Considering the average biofilm thickness at 50 mm from the bottom was ≈1.58 mm and 1.32 mm at 118 mm from the bottom of the reactor, the possibility that the biofilm experienced oxygen limitation exists.

Taylor's expansion method proved to be an unstuitable method to determine dissolved oxygen kinetic parameters for a continuously operated pressurised MGR system. Profile 1.0 proved to be a suitable method. During this study, using Profile 1.0 software the substrate saturation constants were in the range of 2.45 to 4.25 g/m^3; the oxygen diffusion coefficient in the range of 8.15×10^{-6} to 1.75×10^{-5} m^2/hr; and dissolved oxygen flux through the biofilm 0.13 to 0.29 $g/m^2.hr$. The average oxygen penetration depth decreased with time and the penetration ratio decreased from 1.6 to 0.26. The high flux through the biofilm at 50 and

118 mm was due to the minimal transport and maximum biological reaction at these locations, eventhough both these locations were far away from the air inlet.

An individual mathematical model can be developed for each location of the biofilm on the the membrane (i.e. 50, 118 and 170 mm). The scenario to be utilised to solve the model depends on the type of transport through the biofilm, the ratio of the substrate saturation constant to the initial substrate (i.e. oxygen) concentration, as well as the ratio of convective transport to diffusive transport at a particular location within the biofilm. In heterogeneous biofilms mass transport does not occur solely by diffusion or convection, but a combination of the two.

CHAPTER 10

CONCLUSIONS AND RECOMMENDATIONS

CHAPTER TEN
CONCLUSIONS AND RECOMMENDATIONS

10.1 Conclusions

It can be concluded that when the main objective is to stimulate the production of high concentrations of the secondary metabolite, actinorhodin by *Streptomyces coelicolor* then ISP2 complex medium is the growth medium of choice. However, when the calculation of kinetic parameters is priority and not secondary metabolite production the Hobbs *et al.* (1989) defined medium is the recommended growth medium

The presence of pressure within an MGR system influences the substrate consumption rate. A higher consumption rate and therefore higher maximum consumption rate is observed in pressurised systems than non-pressurised systems. However, the Monod saturation constant is unaffected by the presence or absence of pressure within the system, but rather affected by the residual concentration of the rate limiting substrate. The higher the residual concentration of the rate limiting substrate the higher the yield coefficient, especially if the limiting substrate is the nutrient which stimulates biomass formation.

From the results of this study and literature it was postulated, for *S. coelicolor* A3(2) a solid substratum (i.e. solid medium, membrane surface in an MGR) onto which the micro organism can immobilise is required to initiate the phenomenon of biphasic growth, as this was not observed in batch and fed-batch cultures. For this micro organism biphasic growth occurs in both pressurised and non-pressurised systems. For *S. coelicolor* the specific growth rates are similar, whether the micro organism is cultured in a batch, fed-batch, continuous MGR, pressurised or non-pressurised system

Scale-up from SFMGR's to MFMGR's with *S.coelicolor* was possible. However, for scale-up to be a success, the correct process parameters (i.e. growth medium composition, nutrient and air flow rate, membrane size) need to be utilised in order for the system to function optimally and efficiently produce high concentrations of secondary metabolites.

Oxygen mass transfer in a biofilm immobilised within a continuously operated pressurised MGR is influenced by the thickness of the biofilm and the location of the biofilm with regards to the air inlet. In vertically orientated SFMGR's tapering of the biofilm occurs, with the thinnest biofilm located at the top and the thickest biofilm at the bottom of the bioreactor. Penetration depth is influenced by the location of the biofilm with regards to the air inlet, biofilm thickness and type of mass transport. The type of mass transport depends on the

thickness and location of the biofilm in the bioreactor. Modelling oxygen mass transport is a complicated process as the type of mass transport in the biofilm needs to be identified. However, biofilms are not uniform therefore in heterogeneous biofilms mass transport does not occur via convection or diffusion only, but a combination of the two. Determining the extent of the convective or diffusive transport in the biofilm at a particular location will assist in the development of the mathematical model.

In conclusion there is now a better understanding of substrate kinetics, growth kinetics and oxygen mass transfer kinetics within a continuously operated pressurised MGR system. The information obtained contributed to a better understanding of reactor design, secondary metabolite production and process optimisation. The oxygen profiles obtained provided an increased understanding of both the biological (microscale) and physical (diffusion and convection) processes within a pressurised MGR system. More data is now available with regards to oxygen distribution within gradostat systems, increasing the limited amount of information currently available.

10.2 Recommendations

The following recommendations are made due to the problems experienced during the study, as well as from regular utilisation of the system.

1. The study should be repeated but at conditions that will eliminate the sloughing phenomenon observed.
2. The growth medium component responsible for the biphasic growth should be identified.
3. An assay to determine the nitrate concentration present in the permeate samples should be performed to identify if nitrate depletion occurs in continuously operated pressurised SFMGR systems.
4. Identical pressurised and non-pressurised systems of *S. coelicolor* A3(2) should be compared with regards to specific growth rates, biofilm thickness and biomass to determine the effect of pressure on the system.
5. Experiments with other bacteria should be conducted in pneumatic systems to confirm whether the two-phase growth model phenomenon applies only to filamentous micro organisms or includes bacteria.
6. Improved microsensors that are less invasive into the biofilm, therefore they do not disturb the structure of the biofilm when entering and leaving the biofilm.
7. Construction of microsensors that are more durable and do not break so easily, possibly using a different material for construction.

8. Construction of microsensors that are not pressure sensitive when operated under pressure for long periods of time. Thereby, eliminating the dissolving of air in the electrolyte causing increased readings and signal drift.
9. It is recommended that the experiments be repeated but instead of using microsensors to utilise smart holograms "programmed" to measure the dissolved oxygen, glucose concentration, actinorhodin concentration, nitrogen concentration, phosphate concentration and pH within the biofilm. The use of smart holograms will eliminate the increased readings and signal drift experienced with the normal microsensors due to their pressure sensitivity. The problem of off-centre tips will also be eliminated.
10. If microsensors are utilised for follow up studies, the ports onto which the microsensor tube is attached must be perfectly straight and attached at a 90° angle as the slightest deviation from this angle will result in the microsensor being skew which increases the possibility of breaking the microsensor tip.
11. The mathematical model developed to describe mass transfer within the pressurised MGR system utilised during this study must be completed and the curve fitting method utilised on experimental data to test the validity of the model developed.
12. Disolved oxygen kinetic parameters should be calculated using various methods such as Proifle 1.0 software and Taylor's expansion series. The method providing the most accurate values for the DO kinetic parameters determined via the curve fitting method with the best SSD and R^2 values determined with regards to the DO profiles measured.

REFERENCES

REFERENCES

Abbas, A.S. & Edwards, C. 1990. Effects of metals on *Streptomyces coelicolor* growth and actinorhodin production. *Applied and Environmental Microbiology,* 56:675-680.

Adour, L. & Couriol, C. & Amrane, A. 2005. Diauxic growth of *Penicillium camembertii* on glucose and arginine. *Enzyme and Microbial Technology,* 36:198–202.

Ahmadi Motlagh, A.R., Voller, V.R. & Semmens, M.J. 2006. Advective flow through membrane-aerated biofilms modelling results. *Journal of Membrane Science,* 273:143-151.

Amrane, A., Adour, L. & Couriol, C. 2005. An unstructured model for the diauxic growth of *Penicillium camembertii* on glucose and arginine. *Biochemical Enginerring Journal,* 24:124-133.

Anon. 1998. *Oxygen Sensor's. User's manual.* Denmark.

Ates, S., Elibol, M. & Mavituna, F. 1997. Production of actinorhodin by *Streptomyces coelicolor* in batch and fed-batch cultures. *Process Biochemistry,* 32:273-278.

Aunstrup, K., Andresen, O., Falch, E.A. & Nielsen, T.K. 1979. Production of microbial enzymes. In *Microbial Technology,* Vol. 1, 2nd ed. New York:Academic Press. pp.282-309.

Barclay, C.D., Legge, R.L. & Farquhar, G.F. 1993. Modelling the growth kinetics of *Phanerochaete chrysosporium* in submerged static culture. *Applied Enivironmental Microbiology,* 59(6):1887-1892.

Bazin, M.J. 1982. *Microbial Population dynamics.* Florida:CRC Press.

Beeton, S., Bellhouse, B.J., Knowles, C.J., Millward, H.R., Nicholson, A.M. & J.R. Wyatt. 1993. A novel membrane bioreactor for microbial growth. *Applied Microbiology and Biotechnology,* 40:812-817.

Belfort, G. 1989. Membranes and bioreactors: A technical challenge in biotechnology. *Biotechnology and Bioengineering,* 33:1047-1066.

Bentley, S.D., Chater, K.F., Cerdeño-Tárragam, A.-M., Challis, G.L., Thomson, N.R., James, K.D., Harris, D.E., Quail, M.A., Kieser, H., Harper, D., Bateman, A., Brown, S., Chandra, G., Chen, C.W., Collins, M., Cronin, a., Fraser, A., Goble, A., Hidalgo, J., Hornsby, T., Howarth, S., Huang, C.-H., Kieser, T., Larke, L., Murphy, L., Oliver, K., O'Neil, S., Rabbinowitsch, E., Rajandream, M.-A., Rutherford, K., Rutter, S., Seeger, K., Saunders, D., Sharp, S., Squares, R., Squares, S., Taylor, K., Warren, T., Wietzorrek, A., Woodward, J., Barrell, B.G., Parkhill, J. & Hopwood, D.A. 2002. Complete genome sequence of the model actinomycete *Streptomyces coelicolor* A3(2). *Nature,* 417:141-147.

Berg, P., Risgaard-Petersen, N. & Rysgaard, S. 1998. Interpretation of measured concentration profiles in sediment pore water. *Bioengineering and Biotechnology,* 43:1500-1510.

Beyenal, H. and Lewandowski, Z. 2002. Internal and external transfer in biofilms grown at various flow velocities. *Biotechnology Progess,* 18:55-61.

Beyenal, H., Chen, S.N. and Lewandowski, Z. 2003. The double substrate growth kinetics of *Pseudomonas aeruginosa. Enzyme and Microbial Technology,* 32:92-98.

Bibb, M. 1996. 1995 Colworth Prize Lecture. The regulation of antibiotic production in *Streptomyces coelicolor* A3(2). *Microbiology,* 142:1335-1344.

Bibb, M.J. 2005. Regulation of secondary metabolism in streptomycetes. *Current Opinion in Microbiology,* 8:208-215.

Blanch, H.W. 1981. Invited review microbial growth kinetics. *Chemical Engineering Communications,* 8:181-211.

Bird, R.B., Stewart, W.E. & Lightfoot, E.N. 2002. *Transport Phenomena.* 2ND ed. New York:John Wiley.

Bruheim, P., Sletta, H., Bibb, M.J., White, J. & Levine, D.W. 2002. High-yield actinorhodin production in fed-batch cultures by *Streptomyces lividans* strain overexpressing the pathway-specific activator gene *act*II-ORF4. *Journal of Industrial Microbiology and Biotechnology,* 28:103-111.

Burton, S.G. 2001. Development of bioreactors for application of biocatalysts in biotransformations and bioremediation. *Pure and Applied Chemistry,* 73:77-83.

Bystrykh, L.V., Fernández-Moreno, M.A., Herrema, J.K., Malpartida, F., Hopwood, D.A. & Dijkhuizen, L. 1996. Production of actinorhodin-related "blue pigments" by *Streptomyces coelicolor* A3(2). *Journal of Bacteriology,* 178:2238-2244.

Bystrykh, L.V., Herrera, J.K., Cruising, W. & Kellogg, R.M. 1997. 5-Hydroxyaloesapanarin II, a minor blue pigment in an actinorhodin-negative mutant of *Streptomyces* coelicolor A3(2). *Biotechnology and Applied Biochemistry,* 26:195-201.

Casey, E., Glennon, B. & Hamer, G. 1999. Oxygen mass transfer characteristics in a membrane-aerated biofilm reactor. *Biotechnology and Bioengineering,* 62:183-192.

Casey, E., Glennon, B. & Hamer, G. 2000. Biofilm development in a membrane-aerated biofilm reactor: Effect of intra-membrane oxygen pressure on performance. *Bioprocess Engineering,* 23:457-465.

Champness, W. 2000. Actinomycete development, antibiotic production and phylogeny: questions and challenges. In: Brun, Y.V. and Skimkets, L.J. (eds). *Prokaryotic development.* Washington DC: American Society for Microbiology. pp 11-13.

Champness, W.C. & Chater, K.F. 1994. Regulation and integration of antibiotic production and morphological differentiation in *Streptomyces* spp. In: Piggot, P.J., Moran Jr, C.P. and Youngman, P. (series eds). *Regulation of Bacterial Differentiation.* Washington D.C: American Society for Microbiology. pp. 61-65

Charcosset, C. 2006. Membrane processes in biotechnology: an overview. *Biotechnology Advances,* 24:482-492.

Chater, K.F. 2006. *Streptomyces* inside-out: a new perspective on the bacteria that provide us with antibiotics. *Philosophical transactions of the Royal Society B,* 361:761-768.

Chen, P.S., Toribara, T.Y. & Warner, H. 1956. Microdetermination of phosphorous. *Analytical. Chemistry*, 28:1756-1758.

Cho, M.H. & Wang, S.S. 1988. Enhancement of oxygen transfer in hybridoma cell culture by using a perfluorocarbon as an oxygen carrier. *Biotechnology Letters*, 10:855-860.

Choi, M.H., Ji, G.E., Koh, K.H, Ryu, Y.W., Jo, D.H. & Park., Y.H. 2002. Use of waste Chinese cabbage as a substrate for yeast biomass production. *Bioresources Technology*, 83:251-253.

Claessen, D., De Jong, W., Dijkhuizen, L. & Wösten, H.A.B. 2006. Review: Regulation of *Streptomyces* development: reach for the sky! *Trends in Microbiology*, 14:313

Coisne, S., Béchet, M. & Blondeau, R. 1999. Actinorhodin production by *Streptomyces coelicolor* A3(2) in iron-restricted media. *Letters in Applied Microbiology*, 28:199-202.

Cote, P., Bersillion, J., Huyard, A. & Faup, G. 1988. Bubble-free aeration using membranes: Process analysis. *Journal of Water Pollution Control Federation*, 60:1986-1992.

Curcio, E., De Bartolo, L., Barbieri, G., Rende, M., Giorno, L., Morelli, S. & Drioli, E. 2005. Diffusive and convective transport through hollow fibre membranes for liver cell culture. *Journal of Biotechnology*, 117:309-321.

Davey, M.E., Caiazza, N.C. & O'Toole, G.A. 2003. Rhamnolipid surfactant production affects biofilm architecture in *Pseudomonas aeriginosa* PAO1. *Journal of Bacteriology*, 185:1027-1036.

De Orduña, R.M. & Theobald, U. 2000. Intracellular glucose 6-phosphate content in *Streptomyces coelicolor* upon environmental changes in a defined medium. *Journal of Biotechnology*, 77:209-218.

Defrance, L. & Jaffrin, M.Y. 1999. Comparison between filtrations at fixed transmembrane pressure and fixed permeate flux: Application to a membrane bioreactor used for wastewater treatment. *Journal of Membrane Science*, 152:203-210.

Diaz, E.G., Catana, R., Ferreira, B.S., Luque, S., Fernandes, P. & Cabral, J.M.S. 2006. Towards the development of a membrane reactor for enzymatic inulin hydrolysis. *Journal of Membrane Science*, 273:152-158.

Doull, J.L. & Vining, L.C. 1990. Nutritional control of actinorhodin production by *Streptomyces coelicolor* A3(2): suppressive effects of nitrogen and phosphate. *Applied Microbiology and Biotechnology*, 32:449-454.

Eberl, H., Morgenroth, E., Noguera, D., Picioreanu, C., Rittmann, B., Van Loosdrecht, M. & Wanner, O. 2006. *Mathematical Modelling of Biofilms: Scientific and Tehcnical Report No.18*. London: IWA Publishing.

Edwards, W., Leukes, W.D. & Fraser, S.J. 2007. High throughput bioprocess apparatus, PCT application WO 2007/116266 A1.

Elibol, M. & Mavituna, F. 1998. Effect of sucrose on actinorhodin production by

Streptomyces coelicolor A3(2). *Process Biochemistry,* 33:307-311.

Elibol, M. & Mavituna, F. 1999a. A kinetic model for actinorhodin production by *Streptomyces coelicolor* A3(2). *Process Biochemistry,* 34:625-631.

Elibol, M. & Mavituna, F. 1999b. A remedy to oxygen limitation problem in antibiotic production: addition of perfluorocarbon. *Biochemical Engineering Journal,* 3:1-7.

Elibol, M. 2001. Improvement of antibiotic production by increased oxygen solubility through the addition of perfluorodecalin. *Journal of Chemical Technology and Biotechnology,* 76:418-422.

Elibol, M. 2002. Response surface methodological approach for inclusion of perfluorocarbon in actinorhodin fermentation medium. *Process Biochemistry,* 38: 667-673.

Elibol, M. 2004. Optimisation of medium composition for actinorhodin production by *Streptomyces* coelicolor A3(2) with response surface methodology. *Process Biochemistry,* 39:1057-1062.

Ernster, L. 1986. Oxygen as an environmental poison. *Chemica Scripta,* 26:525-534.

Fenn, P. & Kirk, T. K. 1981. Relationship of nitrogen to the onset and suppression of ligninolytic activity and secondary metabolism in *P. chrysosporium. Archives of Microbiology,* 130:59-65.

Fenn, P., Choi, S. & Kirk, T. K. 1981. Ligninolytic activity of *Phanerochaete chrysosporium*: Physiology of suppression by ammonia and l-glutamate. *Archives of Microbiology,* 130:66-71.

Flärdh, K. 2003. Growth polarity and cell division in *Streptomyces. Current opinion in Microbiology,* 6:564-571.

Fogler, H.S. 1999. *Elements of chemical reaction engineering.* 3RD ed. Prentice Hall: New Jersey.

Frank-Kamenetskii, D.A. 1969. *Diffusion and heat transfer in chemical kinetics.* New York: Plenum Press.

Frederick, C., Michael, J.R., Eric, A.G. & Adinarayana, R. 1991. Determination of the respiration kinetics for mycelial pellets of *Phanerochaete chrysosporium. Applied and Environmental Microbiology,* 58(5):1740-1745.

Gavalas, V.G., Wang, J. & Bachas, L.G. 2003. Membranes for the development of biosensors. In: Bhattacharyya, D. and Butterfield, D.A. (eds). *New insights into membrane science and technology: polymeric and biofunctional membranes.* Elsevier: Amsterdam. pp. 379-392.

Godongwana, B., De Jager, D., Sheldon, M.S. & Edwards, W. 2009. The effect of *Streptomyces coelicolor* development on the hydrodynamics of a vertically orientated capillary membrane gradostat reactor. *Journal of Membrane Science,* 333:79-87.

Godongwana, B., Sheldon, M.S. & Solomons, D.M. 2007. Momentum transfer inside a vertically orientated capillary membrane bioreactor. *Journal of Membrane Science,* 303:86-

99.

González Diaz, E., Catana, R., Ferreira, B.S., Luque, S., Fernandes, P. & Cabral, J.M.S. 2006. Towards the development of a membrane reactor for enzymatic inulin hydrolysis. *Journal of Membrane Science*, 273:152-158.

Gotoh, T., Mochizuki, G. & Kikuchi, K. 2001. Perfluorocarbon-mediated aeration applied to recombinant protein production by virus-infected cells. *Biochemical Engineering Journal*, 7:69-78.

Goudar, C.T. & Devlin, J.F. 2001. Nonlinear estimation of microbial and enzyme kinetic parameters from progress curve data. *Water Environment Research*, 73(3):260-265.

Govender, S., Jacobs, E.P., Leukes, W.D., Odhav, B. & Pillay, V.L. 2004. Towards an optimum spore immobilisation strategy using *Phanerochaete chrysosporium*, reverse filtration and ultrafiltration membranes. *Journal of Membrane Science*, 238:83-92.

Govender, S., Jacobs, E.P., W.D. Leukes, W.D. & Pillay, V.L. 2003. A scalable membrane gradostat reactor for enzyme production using *Phanerochaete chrysosporium*. *Biotechnology Letters*, 25:127-131.

Harder, W. & Dijkhuizen, L. 1982. Strategies of mixed substrate utilisation in microorganisms. *Philosophical Transactions of the Royal Society of London*, 297:459-480.

Hai, F.I., Yamamoto, K. & Fukushi, K. 2006. Development of a submerged membrane fungi reactor for textile wastewater treatment. *Desalination*, 192:315-322.

Han, M., Kane, R., Goto, M. & Belfort, G. 2003. Discriminate surface molecular recognition sites on a macroporous substrate: A new approach. *Macromolecules*, 36:4472-4477.

Hibiya, K., Nagai, J., Tsuneda, S. & Hirata, A. 2003. Simple prediction of oxygen penetration depths in biofilms for wastewater treatment. *Biochemical Engineering Journal*, 19(1):61-68.

Ho, L.S., Ju, L.-K. & Baddour, R.F. 1990. Enhancing penicillin fermentations by increased oxygen solubility through the addition of *n*-hexadecane. *Biotechnology and Bioengineering*, 36:1110-1118.

Hobbs, G., Frazer, C.M., Gardner, C.J., Cullum, J.A. & Oliver, S.G. 1989. Dispersed growth of *Streptomyces* in liquid culture. *Applied Microbiology and Biotechnology*, 31:272-277.

Hobbs, G., Frazer, C.M., Gardner, D.C.J., Flett, F. & Oliver, S.G. 1990. Pigmented antibiotic production by *Streptomyces coelicolor* A3(2): kinetics and the influence of nutrients. *Journal of General Microbiology*, 136:2291-2296.

Hopwood, D.A., Bibb, M.J., Chater, K.F., Kieser, T., Burton, C.J., Kieser, H.M., Lydiate, D.J., Smith, C.P., Ward, J.M. & Schrempe, H. 1985. Genetic Manipulation of Streptomyces coelicolor: *A Laboratory Manual*. Norwich:John Innes Foundation. pp 365.

Hopwood, D.A., Chater, K.F. & Bibb, M.J. 1995. Genetics of antibiotic production in *Streptomyces coelicolor* A3(2), a model Streptomycete. *Biotechnology*, 28:65-102.

Horn, H. & Hempel, D.C. 1998. Modeling mass transfer and substrate utilization in the boundary layer of biofilm systems. *Water Science Technology.* 37:139-147.

Horn, H. & Hempel, D.C. 1997. Substrate utilization and mass transfer in an autotrophic biofilm system: Experimental results and simulation. *Biotechnology and Bioengineering,* 53:363-371.

Horn, H. 2000. Microsensors and tube reactors in biofilm research. In: Flemming, H-C., Szewzyk, U. and Griebe, T. (eds). *Biofilms: Investigative methods and applications.* Technomic: Lancaster.

Howell, J.A. & Atkinson, B. 1976. Influence of oxygen and substrate concentrations on the ideal film thickness and the maximum overall substrate uptake rate in microbial film fermenters. *Biotechnology and Bioengineering,* 18:15-35.

Ikasari, L. & Mitchell, D.A. 2000. Two-phase model of the kinetics of growth of *Rhizopus oligosporus* in membrane culture. *Biotechnology and Bioengineering,* 69:619-627.

Jacobs, E.P. & Leukes, W.D. 1996. Formation of an externally unskinned polysulphone capillary membrane. *Journal of Membrane Science,* 12:149-157.

Jeffries, T. W., Choi, S. & Kirk, T. K. 1981. Nutritional regulation of lignin degradation by *P.chrysosporium. Applied and Environmental Microbiology,* 42:290-296.

Judd, S. 2006. *The MBR Book: Principles and Applications of Membrane Bioreactors in Water and Wastewater Treatment.* Elsevier: Amsterdam.

Karandikara, A., Sharples, G.P. & Hobbs, G. 1997. Differentiation of *Streptomyces coelicolor* A3(2) under nitrate-limited conditions. *Microbiology,* 143(11):3581-3590.

Kieser, T., Bibb, M.J., Buttner, M.J., Chater, K.F. & Hopwood, D.A. 2000. Practical *Streptomyces* Genetics. Norwich: The John Innes Foundation.

Kim, Y-M. & Kim, J. 2004. Formation and dispersion of mycelial pellets of *Streptomyces coelicolor* A3(2). *The Journal of Microbiology,* 42:64-67.

Kodama, T., Shimada, K. and Mori, T. 1969. Studies on anaerobic biphasic growth of a denitrifying bacterium, *Pseudomonas stutzeri. Plant and Cell Physiology,* 10:855-865.

Kuenen, J.G., Jørgensen, B.B. & Revsbech, N.P. 1986. Oxygen microprofiles of trickling filter biofilms. *Water Research,* 20:1589-1598.

Leisola, M., Ulmer, D. C. & Fiechter, A. 1984. Factors affecting lignin degradation in lignocelluloses by *P. chrysosporium. Archives of Microbiology,* 137:171-175.

Leukes, W.D. 1999. Development and characterisation of a membrane gradostat bioreactor for the bioremediation of aromatic pollutants using white rot fungi, PhD thesis, Rhodes University, Grahamstown, South Africa.

Leukes, W.D., Jacobs, E.P., Rose, P.D., Sanderson, R.D. & Burton, S.G. 1999. *Secondary metabolite production.* USA patent 5945002.

Lewandowski, Z. 1994. Dissolved oxygen gradients near microbially colonised surfaces. In: Geesey, G.G., Lewandowski, Z. and Flemming, H.C. (eds). *Biofouling and biocorrosion in*

industrial water systems. Florida: Lewis Publishers. pp. 175-188.

Lewandowski, Z. & Beyenal, H. 2003a. Mass transport in heterogeneous biofilms. In: Wuertz, S., Bishop, P.L. & Wilderer, P.A. (eds). *Biofilms in wastewater treatment: An interdisciplinary approach.* London: IWA Publishing.

Lewandowski, Z. & Beyenal, H. 2003b. Use of microsensors to study biofilms. In: Lens, P., O'Flaherty, V., Moran, A., Stoodley, P. & Mahony, T. (eds). *Biofilms in Medicine, Industry and Environmental Biotechnology-Characteristics, Analysis and Control.* London: IWA Publishing. pp. 375-412.

Lobry, J.R., Flandrous, J.P., Carret, J. & Pave, A. 1992. Monod's bacterial growth model revisited. *Bulletin of Mathematical Biology,* 54(1):117-122.

MacLean, G.T. 1977. Oxygen transfer in aerated systems with two liquid phases. *Process Biochemistry,* 12:22-24.

Magnolo, S.K., Leenutaphong, D.L., DeModena, J.A., Curtis, J.E., Bailey, J.E., Galazzo, J.L. & Hughes, D.E. 1991. Actinorhodin production by *Streptomyces coelicolor* and growth of *Streptomyces lividans* are improved by the expression of bacterial haemoglobin. *Biotechnology,* 19:473-476.

Mallia, H. & Till, S. 2001. Membrane bioreactors: Wastewater treatment applications to achieve high quality effluent. *Water Industry Group,* 8:1-2.

Martin, J.F. & Demain, A.L. 1980. Control of antibiotic synthesis. *Microbiological Reviews,* 44: 230-251.

Melzoch K., Teixeira De Mattos, M.J. & Neijssel, O.M. 1997. Production of actinorhodin by *Streptomyces coelicolor* A3(2) grown in chemostat culture. *Biotechnology and Bioengineering,* 54:577-582.

Meunier, J.-R. & Choder, M. 1999. *Saccharomyces cerevisiae* colony growth and ageing: biphasic growth accompanied by changes in gene expression. *Yeast,* 15:1159-1169.

Miller, G.L. 1959. Use of dinitrosalicylic acid reagent for determination of reducing sugar. *Analytical Chemistry,* 31:426-428.

Mitchell, D.A., Do, D.D., Greenfield, P.F. & Doelle, H.W. 1991. A semi-mechanistic mathematical model for the growth of *Rhizopus oligosporus* in a model solid-state fermentation system. Biotechnology and Bioengineering, 38:353-362.

Mitchell, D.A., Von Meien, O.F. & Krieger, N. 2003. Recent developments in modelling of solid-state fermentation: Heat and mass transfer in bioreactors. *Biochemical Engineering Journal,* 13:137-147.

Mitchell, D.A., Von Meien, O.F., Krieger, N. & Dalsenter, F.C.H. 2004. A review of recent developments in modelling microbial growth kinetics and intraparticle phenomena in solid-state fermentation. *Biochemical Engineering Journal,* 17:15-26.

Monod J. 1942. *Reserches sur la Croissance des cultures bacteriennes.* Paris: Hermann and Ci.e..

Monod J. 1949. The growth of bacterial cultures. *Annual Review of Microbiology,* 3 :371-394.

Naeimpoor, F. & Mavituna, F. 2000. Metabolic flux analysis in *Streptomyces coelicolor* under various nutrient limitations. *Metabolic Engineering,* 2:140-148.

Nishidome, K., Kusuda, T., Watanabe, Y., Yamauchi, M. & Mihara, M. 1994. Determination of oxygen transfer rate to a rotating contactor by microsensor measurement. *Water Science and Technology,* 29:471-477.

Ntwampe, S.K.O. 2005. Multi-capillary membrane bioreactor design. Unpublished MTech. Thesis, Cape Peninsula University of Technology, Cape Town, South Africa.

Ntwampe, S.K.O. & Sheldon, M.S. 2006. Quantifying growth kinetics of *Phanerochaete chrysosporium* immobilised on a vertically orientated polysulphone capillary membrane: Biofilm development and substrate consumption. *Biochemical Engineering Journal,* 30:147-151.

Ntwampe, S.K.O., Sheldon, M.S. & Volschenk, H. 2008. Oxygen mass transfer for an immobilised biofilm of *Phanerochaete chrysosporium* in a membrane gradostat bioreactor. *Brazilian Journal of Chemical Engineering,* 25(4):649-664.

Ntwampe, S.K.O., Sheldon, M.S. & Volshenk, H. 2007. The Membrane Gradostat Reactor: Secondary metabolite production, bioremediation and commercial potential. *African Journal of Biotechnology,* 6(10):1164-1170.

Okamoto, S., Lezhava, T.H., Okamoto-Hosoya, Y & Ochi, K. 2003. Enhanced Expression of S-Adenosylmethionine Synthetase Causes Overproduction of Actinorhodin in *Streptomyces coelicolor* A3(2). *Journal of Bacteriology,* 185(2):601-609.

Okpokwasili, G.C. & Nweke, C.O. 2006. Microbial growth and substrate utilisation kinetics. *African Journal of Biotechnology,* 5:305-317.

Onken, U. & Liefke, E. 1989. Effect of total and partial pressure (oxygen and carbon dioxide) on aerobic microbial processes. *Advances in Biochemical Engineering/Biotechnology.* 40:137-169.

Ooijkaas, L.P., Buitelaar, R.M., Tramper, J. & Rinzema, A. 2000. Growth and sporulation stoichiometry and kinetics of *Coniothyrium minitnas* on agar media. *Biotechnology and Bioengineering,* 69:292-300.

Owens, J.D. & Legan, J.D. 1987. Determination of the Monod substrate saturation constant for microbial growth. *FEMS Microbiology Letters,* 46:419-432.

Ozergin-Ulgen, K. & Mavituna, F. 1993. Actinorhodin production by *Streptomyces coelicolor* A3(2): kinetic parameters related to growth, substrate uptake and production. *Applied Microbiology and Biotechnology,* 40:457-462.

Ozergin-Ulgen, K. & Mavituna, F. 1994. Comparison of the activity of immobilised and freely suspended *Streptomyces coelicolor* A3(2). *Applied Microbiology and Biotechnology,* 41:197-202.

Ozergin-Ulgen, K. & Mavituna, F. 1998. Oxygen transfer and uptake in *Streptomyces coelicolor* A3(2) culture in a batch bioreactor. *Journal of Chemical Technolgy and Biotechnology,* 73:240-250.

Pavasant, P., Pistikopoulos, E.N. & Livingston, A.G. 1997. Prediction of axial concentration profiles in an extractive membrane bioreactor and experimental verification. *Journal of Membrane Science,* 130:85-98.

Plisova, E.Y., Balabanova, L.A., Ivanova, E.P., Kozhemyako, V.V., Agafonova, E.V. & Rasskazov, V.A. 2005. A highly active alkaline phosphatase from the marine bacterium *Cobetia. Marine Biotechnology,* 7:173-178.

Rasmussen, K. & Lewandowski, Z. 1998. Microsensor measurements of local mass transport rates in heterogeneous biofilms. *Biotechnology and Bioengineering,* 59:304-309.

Revsbech, N.P. 1989. Diffusion characteristics of microbial communities determined by use of oxygen microsensors. *Microbial Methods,* 9:111-122.

Rudd, B.A. & Hopwood, D.A. 1979. Genetics of actinorhodin biosynthesis by *Streptomyces coelicolor* A3(2). *Journal of General Microbiology,* 114:309-313.

Schmidt, S.K., Scow, K.M. & Alexander, M. 1987. Kinetics of *p*-Nitrophenol mineralization by *Pseudomonas sp.*: Effects of second substrates. *Applied and Environmental Microbiology,* 53: 2617-2623.

Shahab, N., Flett, F., Oliver, S. G., & Butler, P. 1996. Growth rate control of protein and nucleic acid content in *Streptomyces coelicolor* A3(2) and *Escherichia coli B/r. Microbiology,* 142:1927-1935.

Shapiro, S. 1989. Nitrogen assimilation in actinomycetes and the influence of nitrogen nutrition on actinomycete secondary metabolism. In: Shapiro, S. 2003. (eds). *Regulation of Secondary Metabolism in Actinomycetes.* Florida: CRC Press. pp. 135-213.

Sheldon, M.S. & Small, H.J. 2005. Immobilisation and biofilm development of *Phanerochaete chrysosporium* on polysulphone and ceramic membranes. *Journal of Membrane Science,* 263:30-37.

Sheldon, M.S., Mohammed, K. & Ntwampe, S.K.O. 2008. An investigation of biphasic growth kinetics for *Phanerochaete chrysosporium* (BKMF-1767) immobilised in membrane gradostat reactor using flow cells. *Enzyme and Microbial Technology,* 42:353-361.

Shirling, E.B. & Gottlieb, D. 1966. Methods of characterisation of *Streptomyces* species. *International Journal of Systematic Bacteriology,* 16:313-340.

Shuler, M.L. & Kargi, F. 2002. *Bioprocess engineering: basic concepts.* 2ND ed. New Jersey: Prentice Hall.

Sinclair, C.G. & Kristiansen, B. 1987. *Fermentation kinetics and modelling.* Milton Keynes: Open University Press.

Sinnott, R.K. 1999. *Coulson & Richardson's Chemical Engineering, Volume 6: Chemical Engineering Design.* 3RD ed. Great Britain: Elsevier Butterworth-Heinemann.

Solomon, M.S. & F.W. Petersen, F.W. 2002. Membrane bioreactor production of *Lignin* and *Manganese Peroxiodase.* An International Newsletter: *Membrane Technology*, 144:6-8.

Stamatialis, D.F., Papenburg, B.J., Gironés, M., Saiful, S., Bettahalli, S.N.M, Schmitmeier, S. & Wessling, M. 2008. Medical applications of membranes: drug delivery, artificial organs and tissue engineering. *Journal of Membrane Science,* 308:1-34.

Stanojević, M., Lazarević, B. & Radić, D. 2003. Review of membrane contactors designs and applications of different modules in industry. *FME Transactions,* 31:91-98.

Takeshi, G., Gaku, M. & Ken-Ichi, K. 2001. A novel carbon fermentor having a wetted-wall of perfluorocarbon as an oxygen carrier. *Biochemical Engineering Journal,* 8:165-169.

Thibault, J., Pouliot, K., Agosin, E. & Pérez-Correa, R. 2000. Reassessment of the estimation of dissolved oxygen concentration profile and K_La in solid-state fermentation. *Process Biochemistry,* 36:9-18.

Thompson, C.J., Fink, D. & Nguyen, L.D. 2002. Principles of microbial alchemy: insights from the *Streptomyces coelicolor* genome sequence. *Genome Biology,* 3(7):1020.1-1020.4.

Tijhuis, L., Van Loosdrecht, M.C.M. & Heijnen, J.J. 1994. Formation and growth of heterotrophic aerobic biofilms on small suspended particles in airlift reactors. *Biotechnology and Bioengineering,* 44:595-608.

Tremper, K.K. & Anderson, S.T. 1985. Perfluorocarbon emulsion oxygen transport fluids; a clinical review. *Annual Review of Medicine,* 36:309-313.

Van de Lagemaat, J. & Pyle, D.L. 2005. Modelling the uptake and growth kinetics of *Penecillium glabrum* in tannic acid-containing solid-state fermentation for tannase production. *Process Biochemistry,* 40: 1773-1782.

Van der Roest, H.F., Lawrence, D.P. & Van Bentem, A.G.N. 2002. *Membrane Bioreactors for Municipal Wastewater Treatment.* London: IWA .

Venkatadri, R. and Irvine, R.L. 1993. Cultivation of *Phanerochaete chrysosporium* and production of lignin peroxidase in novel biofilm reactor systems: hollow fibre reactor and silicone membrane reactor. *Water Research,* 27:591-596.

Viniegra-Gonzalez, G., Saucedo-Castaneda, G., Lopez-Isunza, F. & Favela-Torres, E. 1992. Symmetric branching model for the kinetics of microbial growth. *Biotechnology and Bioengineering,* 42:1-10.

Voight, I., Stahn, M., Wöhner, St., Junghans, A., Rost, J. & Voight, W. 2001. Integrated cleaning of coloured waste water by ceramic NF membranes. *Separation and Purification Technology,* 25:509-512.

Wagner, Jørgen. 2001. *Membrane Filtration Handbook: Practical Tips and Hints.* 2nd ed. Minnetonka: Osmonics Inc.

Wasche, S., Horn, H. & Hempel, D.C. 2002. Influence of growth conditions on biofilm development and mass transfer at the bulk biofilm interface. *Water Research,* 36:4775-4784.

Wright, F. & Hopwood, D. 1976. Actinorhodin is a chromosomally-determined antibiotic in *Streptomyces coelicolor* A3(2). *Journal of General Micobiology,* 96:289-297.

Xu, N., Xing, W., Xu, N. & Shi, J. 2003. Study on ceramic membrane bioreactor with turbulence promoter. *Separation and Purification Technology,* 32:403-410.

Yang, N.W. & J. Ilg, J. 2006. State-of-the-art of membrane bioreactors: world wide research and commercial applications in North America. *Journal of Membrane Science,* 270:201-211.

Yang, S. &Lewandowski, Z. 1995. Measurement of local mass transfer in biofilms. *Biotechnology and Bioengineering,* 48:737-744.

Yul-Min, K. & Jae-hoen, K. 2004. Formation and dispersion of mycelial pellets of *Streptomyces coelicolor* A3(2). *The Journal of Microbiology,* 42:64-67.

Yurt, N., Beyenal, H., Sears, J. & Lewandowski, Z. 2003. Quantifying selected growth parameters of *Leptothrix discophora* SP-6 in biofilms from oxygen concentration profiles. *Chemical Engineering Science,* 58:4557-4566.

Zhang, H., Zhan, J., Su, K. & Zhang, Y. 2006. A kind of potential food additive produced by *Streptomyces coelicolor*: Characteristics of blue pigment and identification of a novel compound, λ-actinorhodin. *Food Chemistry,* 95:186-192.

Zhang, T.C. & Bishop, L.P. 1994. Experimental determination of the dissolved oxygen boundary layer and mass transfer resistance near the fluid biofilm interface. *Water Science and Technology,* 11:47-58.

Internet sources

Google, n.d. Inhomogeneous differential equations. http://mathworld.wolfram.com [3 August 2009].

Hyflux Ceparation, n.d. Hollow fibre ceramic membranes and modules. http://www.ceparation.com/ceramic-membranes-3.html [6 May 2008].

Unisense, n.d. Products. http://www.unisense.com [12 January 2009].

Unisense, n.d. Sensors. http://www.unisense.com [12 January 2009].

Unisense, n.d. Electrodes. http://www.unisense.com [12 January 2009].

Unisense, n.d. Oxygen sensors. http://www.unisense.com [12 January 2009].

APPENDICES

APPENDIX A: Actinorhodin assay

Reagents required:

ISP2 liquid medium

2 M NaOH

Procedure:

1. Transfer 1 ml of the permeate sample to a 1.5 ml eppendorf tube.
2. Centrifuge at 1000 rpm for 2 minutes.
3. Transfer 500 µl of the supernatant into a clean 1.5 ml eppendorf tube.
4. Transfer 500 µl of the ISP2 liquid medium into a clean 1.5 ml eppendorf tube (Serves as the blank sample for the assay).
5. Add 500 µl 2 M NaOH to each 1.5 ml eppendorf tube (i.e. Dilution to 1 M NaOH; pH ~ 12).
6. Mix contents of 1.5 ml eppendorf tubes vigorously by vortexing.
7. Aliquot 300 µl of the mixture in triplicate into a 96-well microtitre plate.
8. Measure absorbance at 640 nm.

To calculate actinorhodin concentration (units, mg/L) refer to Equations A.1 to A.3. E1% is the mass extinction coefficient. E1% is the absorbance of a 1% solution by mass and has the units $g^{-1}L\ cm^{-1}$. For actinorhodin E1% = 355 $g^{-1}.L.cm^{-1}$.

From Beer's Law: $A_{bs} = EC_{actino}l$ **A.1**

Therefore $C_{actino} = \frac{A_{bs}}{El}$ **A.2**

C_{actino} (1%) solution is 1g/100 ml; therefore multiply by 10 to get g/L. C_{actino} is further multiplied by 1000 to get mg/L.

$$C_{actino} = \frac{A_{bs}}{El} \times 10000 \quad \textbf{A.3}$$

Note: For a microtitre plate reader 300 µl volume gives a 0.8 cm pathlength.

APPENDIX B: Glucose assay

Reagents required:

1% DINITROSALICYLIC ACID REAGENT SOLUTION	
33, 5-Dinitrosalicylic acid (DNS)	10 g
Phenol	2 g
Sodium sulphite	0.5 g
Sodium hydroxide	10 g
Add distilled water to make 1 litre	

40% POTASSIUM SODIUM TARTRATE SOLUTION	
Potassium sodium tartrate	40g
Add 100 ml distilled water	

Procedure:

Prepare a standard glucose solution with a concentration of 5 g/L. Prepare dilutions as stated in Table B.1.

Table B.1: Dilutions for the glucose standard curve

Glucose solution (ml)	H_2O (ml)	Glucose concentration (mg/ml)
0	1.0	0
0.1	0.9	0.1
0.2	0.8	0.2
0.4	0.6	0.4
0.6	0.4	0.6
0.8	0.2	0.8
0.9	0.1	0.9
1.0	0	1.0

Note that the dilutions prepared for the standard curve will undergo the same procedure as described below.

1. Add equal volumes of DNS reagent (500 µl) and sample (500 µl) to an eppendorf tube. Mix by vortexing.
2. Heat contents of eppendorf tubes to 90ºC in a waterbath for 10 minutes. The mixture in the eppendorf tubes will become a red brown colour.
3. Cool the contents of the eppendorf tubes as it comes out to room temperature in order to stop the reaction.

4. Add 167 µl of the 40% potassium sodium tartrate solution to maintain the colour. Mix by vortexing.
5. Read in triplicate on a plate reader at 590 nm.

APPENDIX C: Phosphate assay

Reagents required:

ASCORBIC ACID (store at 4℃ for up to 3 days)

Ascorbic acid	18 g
Make up to 200 ml with dH_2O	

AMMONIUM MOLYBDATE

Ammonium heptomolybdate (dissolve first in 100 ml H_2O)	2.5 g
Add H_2SO_4 to above solution	13 ml
Make up to 200 ml with dH_2O	

Use same phosphate salt (See Table C.1) found in nutrient medium being assessed in the preparation of the standard solution. The molecular weight (Mw) of phosphate (PO_4) is 94.97.

Table C.1: Phosphate salts standard solution preparation

To prepare standard solution containing 1 mg/ml PO_4		
K_2HPO_4	Mw 174.17	183 mg per 100 ml distilled water
KH_2PO_4	Mw 136.08	143 mg per 100 ml distilled water
NaH_2PO_4	Mw 119.98	126 mg per 100 ml distilled water
NH_4PO_4	Mw 113.01	119 mg per 100 ml distilled water

Procedure:

To prepare the standard solution curve add 50 µl standard to 950 µl distilled water. Prepare dilutions as stated in Table C.2.

Table C.2: Dilutions for the phosphate standard curve

PO_4 Solution (ml)	H_2O (ml)	PO_4 Concentration (mg/ml)
0	1.0	0
0.1	0.9	0.1
0.2	0.8	0.2
0.4	0.6	0.4
0.6	0.4	0.6
0.8	0.2	0.8
0.9	0.1	0.9
1.0	0	1.0

1. Aliquot 500 µl of each standard dilution into a clean test tube.
2. Add 500 µl ammonium molybdate to each test tube, mix by vortexing.
3. Add 500 µl ascorbic acid to each test tube, mix by vortexing.
4. Stand for 30 minutes at room temperature.
5. Aliquot 300 µl of the well mixed standard dilutions into triplicate wells in clean 96-well microtitre plate and read at 650 nm on BMG Fluostar Optima.

Assay procedure for permeate samples:

1. Add 50 µl of a sample to 950 µl distilled water, mix by vortexing.
2. Aliquot 500 µl of the diluted sample into a clean test tube.
3. Add 500 µl ammonium molybdate, mix by vortexing.
4. Add 500 µl ascorbic acid to each test tube, mix by vortexing.
5. Stand for 30 minutes at room temperature.
6. Aliquot 300 µl well mixed sample into triplicate wells in clean 96-well microtitre plate and read at 650 nm on BMG Fluostar Optima.

APPENDIX D: Design templates of bioreactor glass housing with oxygen measuring ports

Figures D.1, D.2 and D.3 are design templates utilised in the manufacturing of bioreactor glass housings with ports located at various positions on the side of the glass housing. These bottm, middle and top located ports were for the attachment of an oxygen microsensor to determine the dissolved oxygen (DO) concentrations within the biofilm immobilised within the bioreactor.

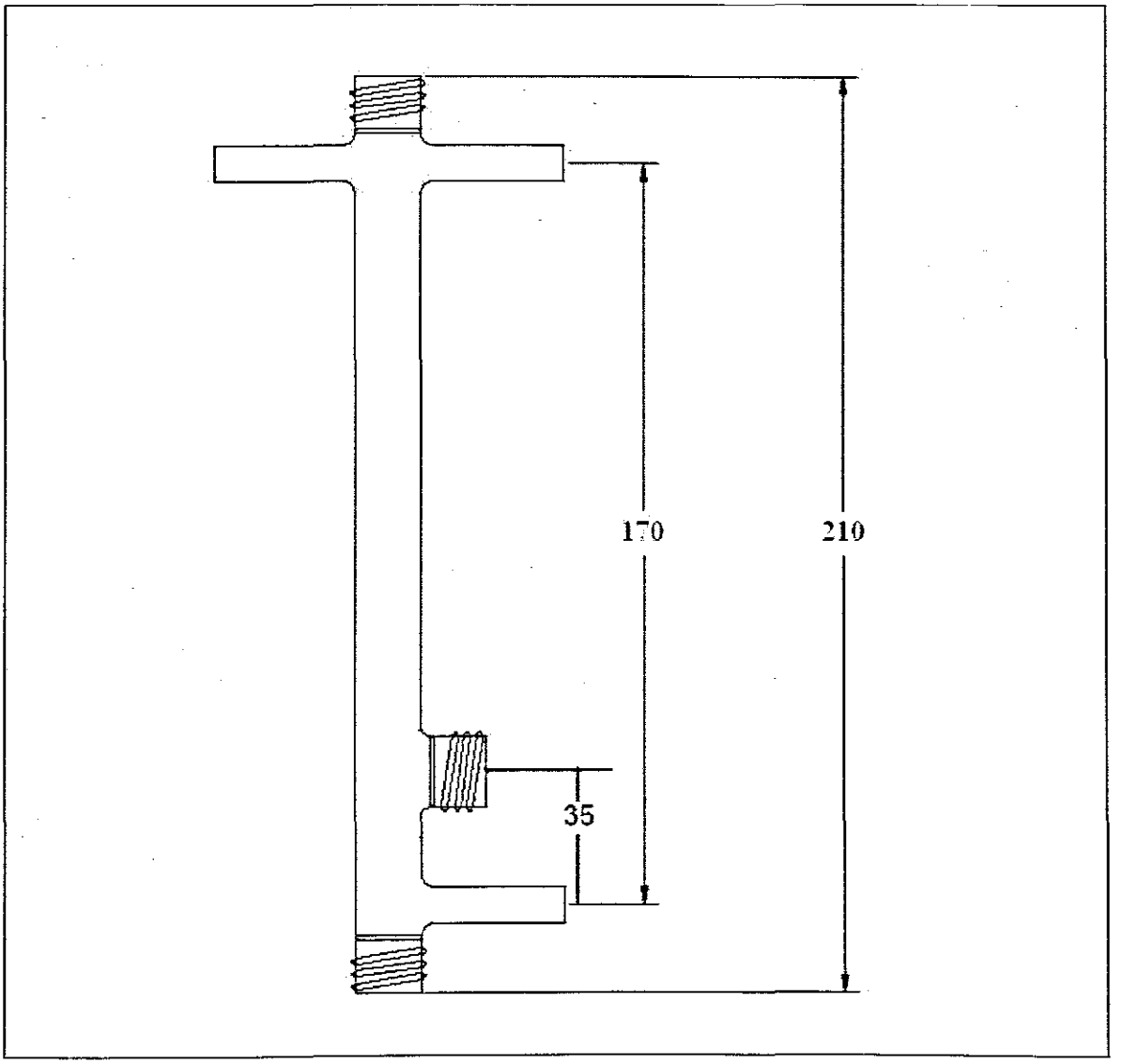

Figure D.1: Design template of a bioreactor glass housing with an oxygen measuring port located at the bottom

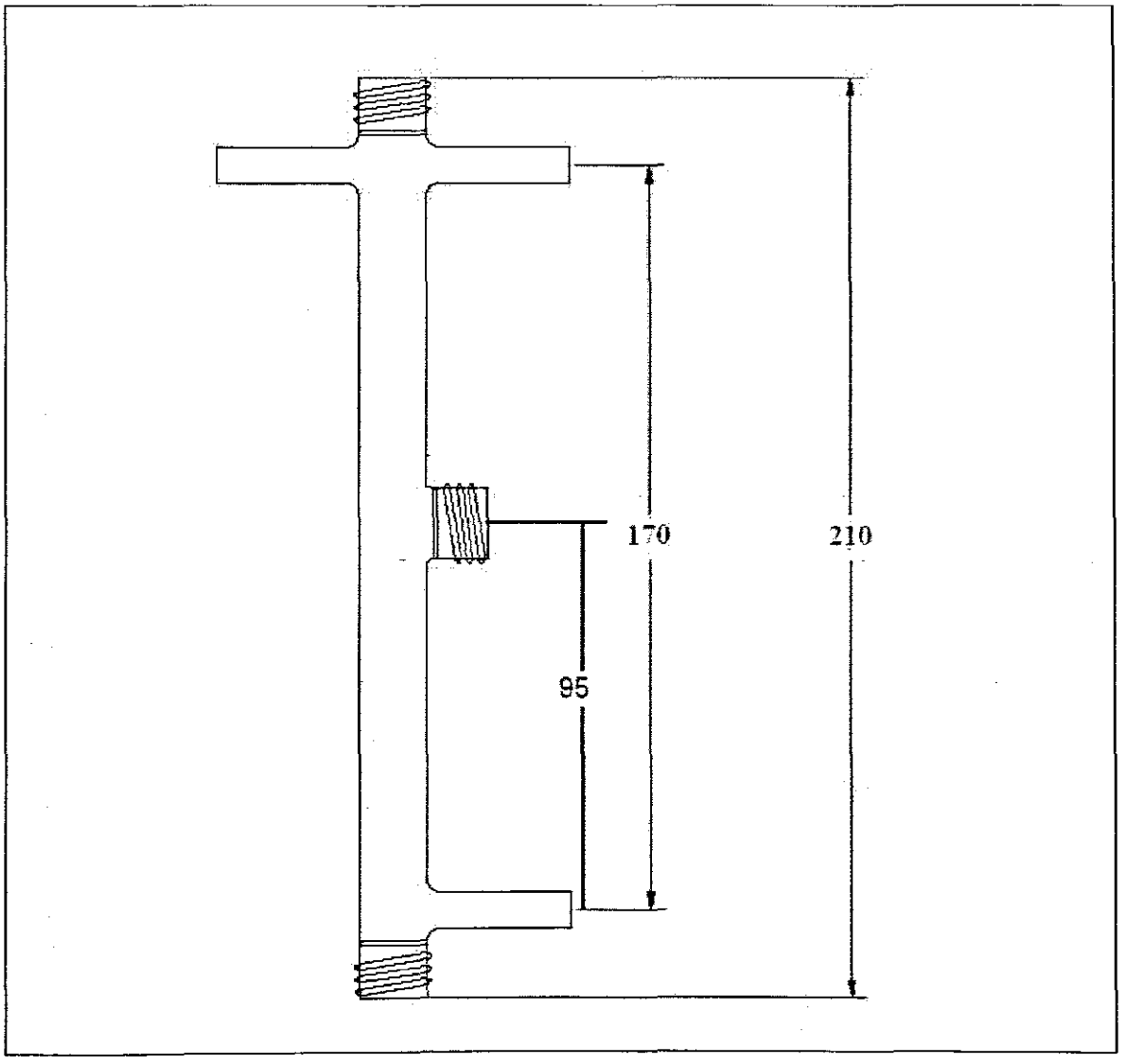

Figure D.2: Design template of a bioreactor glass housing with an oxygen measuring port located in the middle

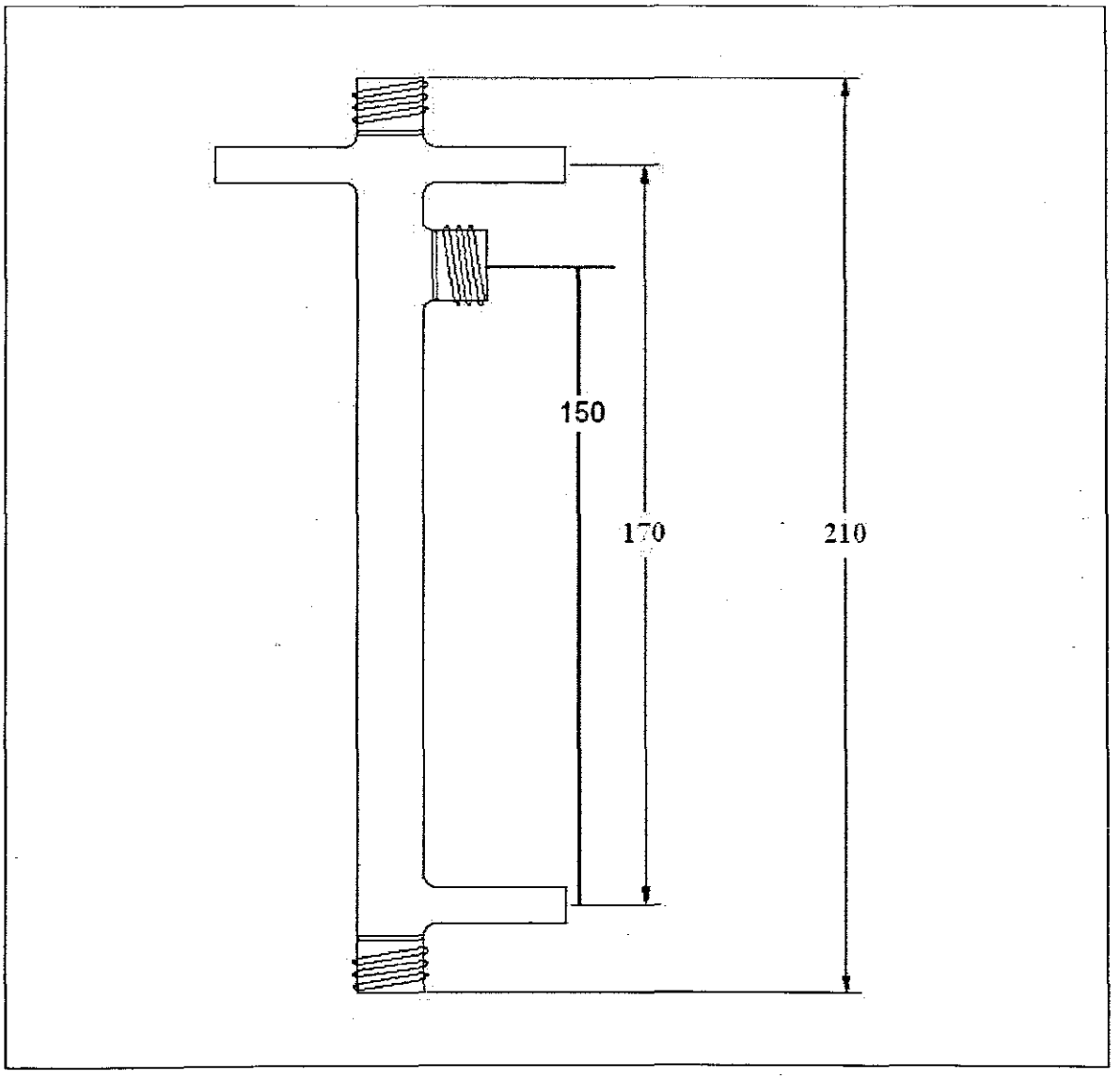

Figure D.3: Design template of a bioreactor glass housing with an oxygen measuring port located at the top

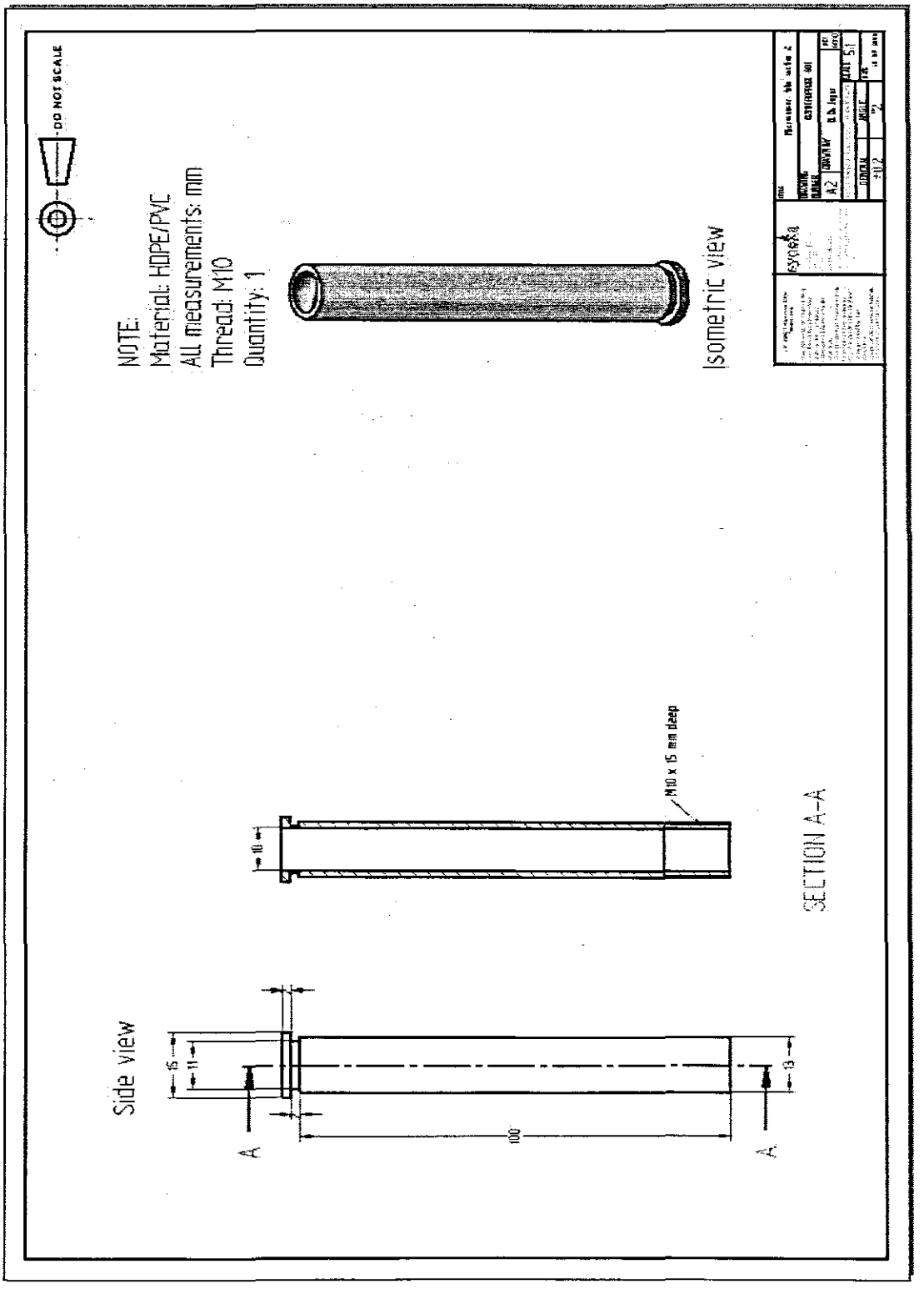

Figure E.2: Microsensor tube section 2

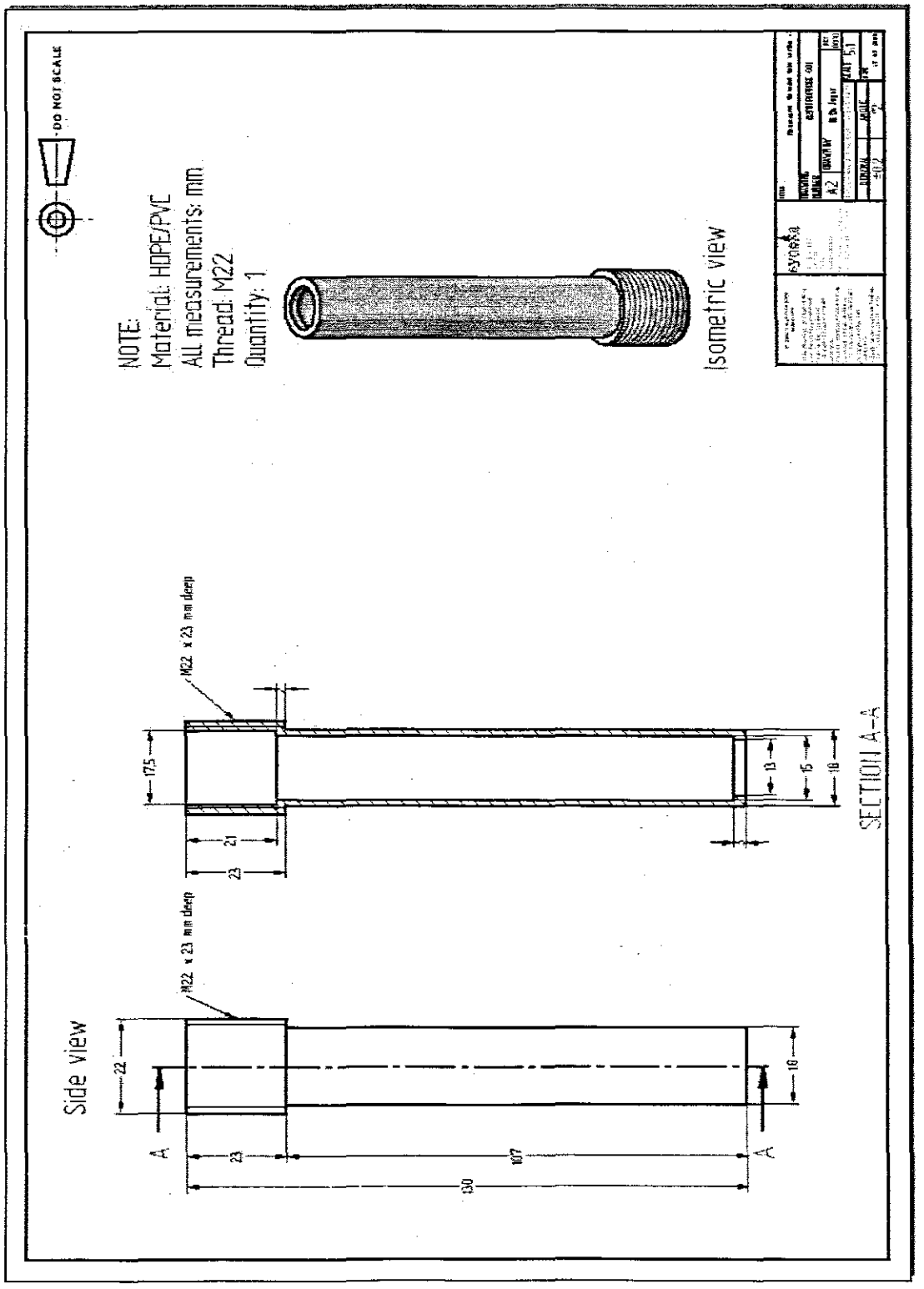

Figure E.3: Microsensor threaded tube section 1

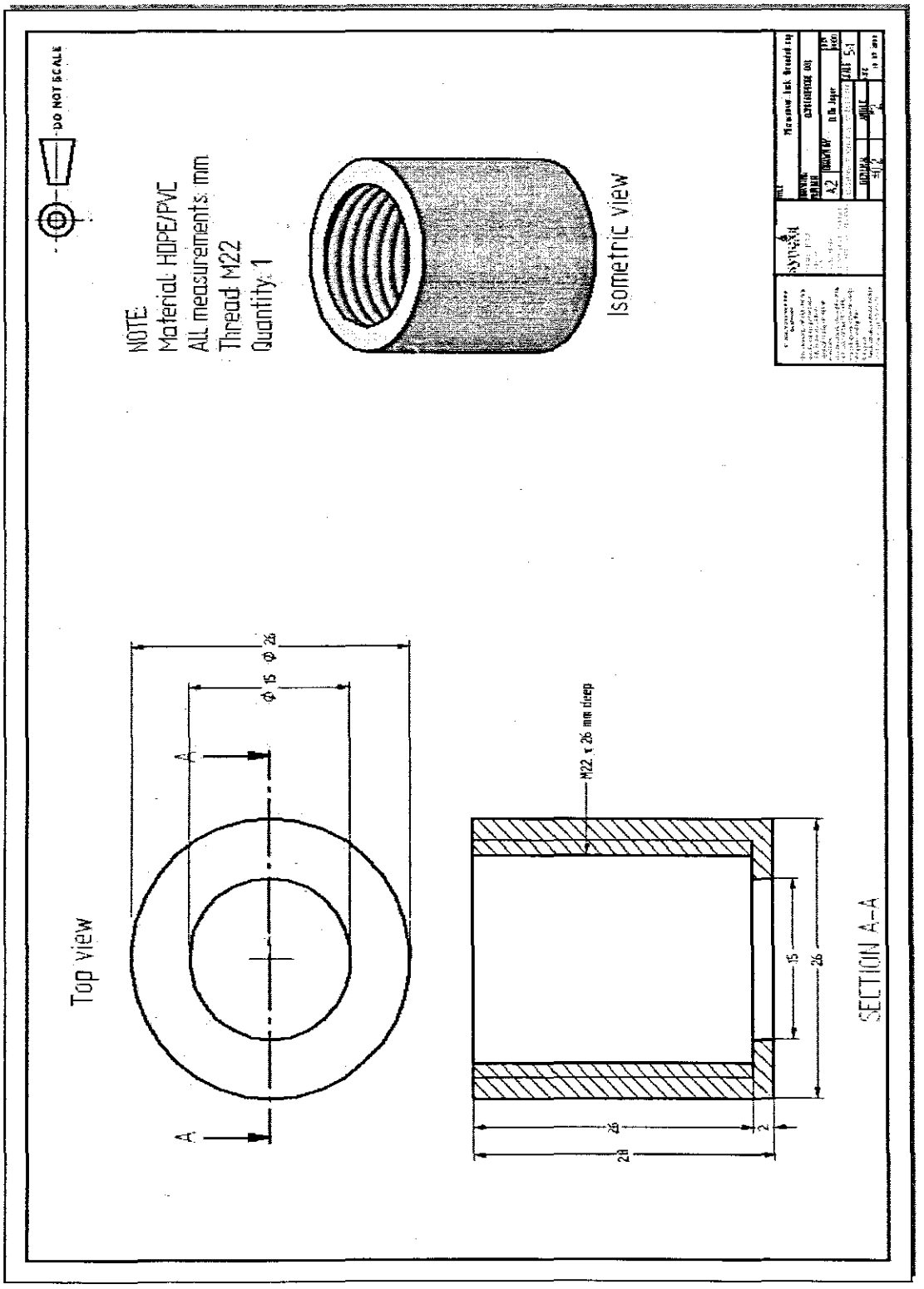

Figure E.4: Microsensor back threaded cap

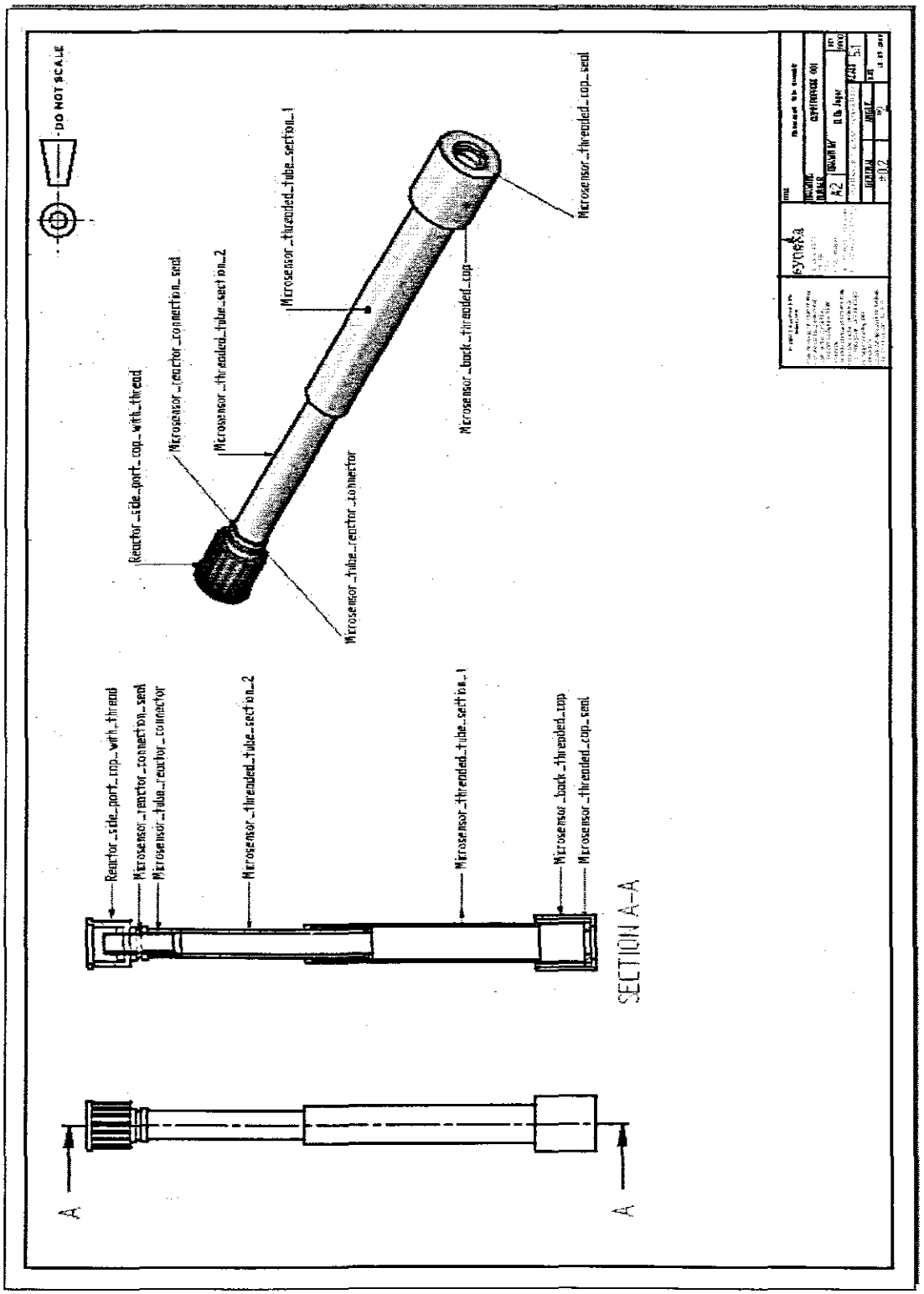

Figure E.5: Microsensro tube assembly

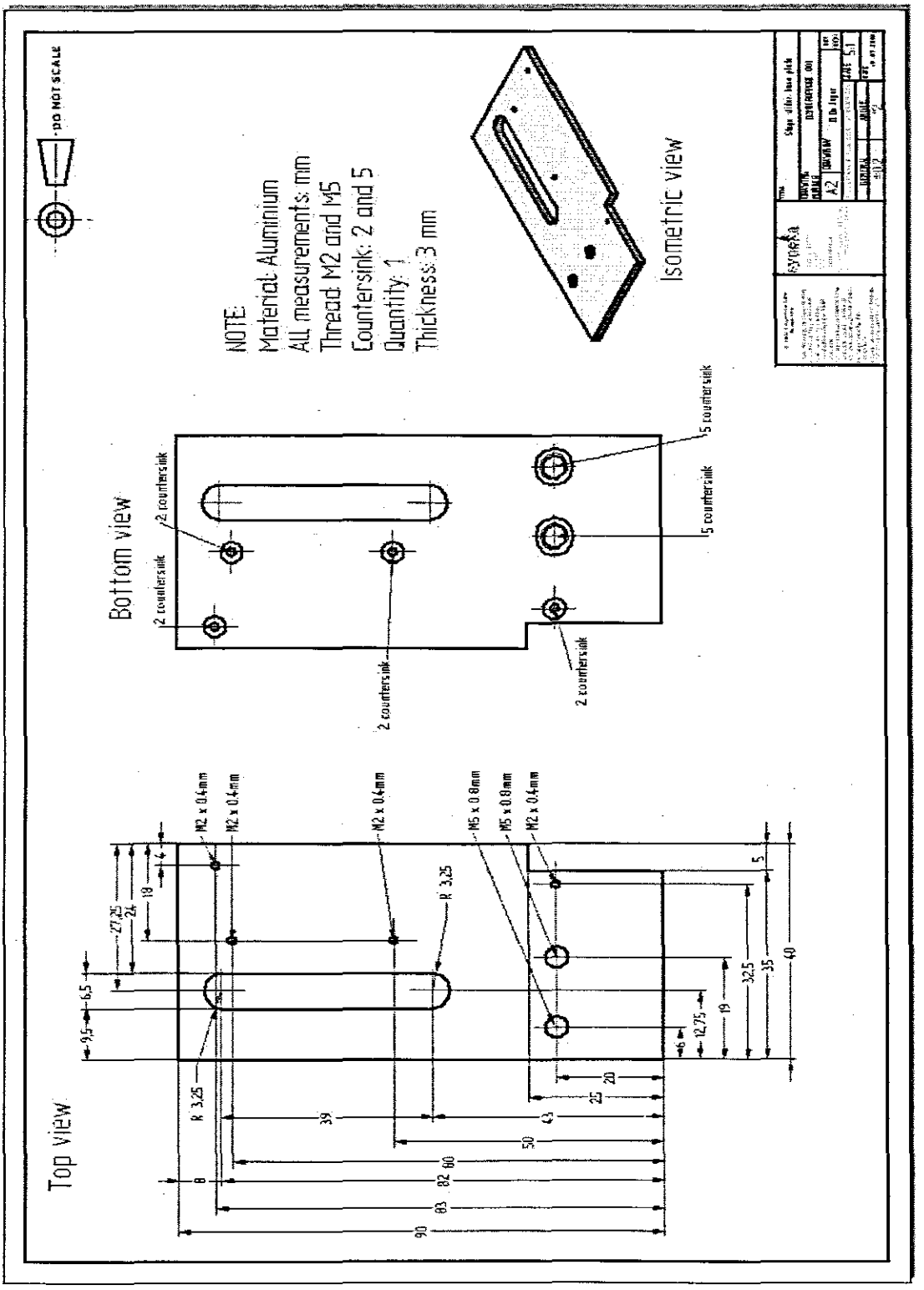

Figure E.6: Stage slider base plate

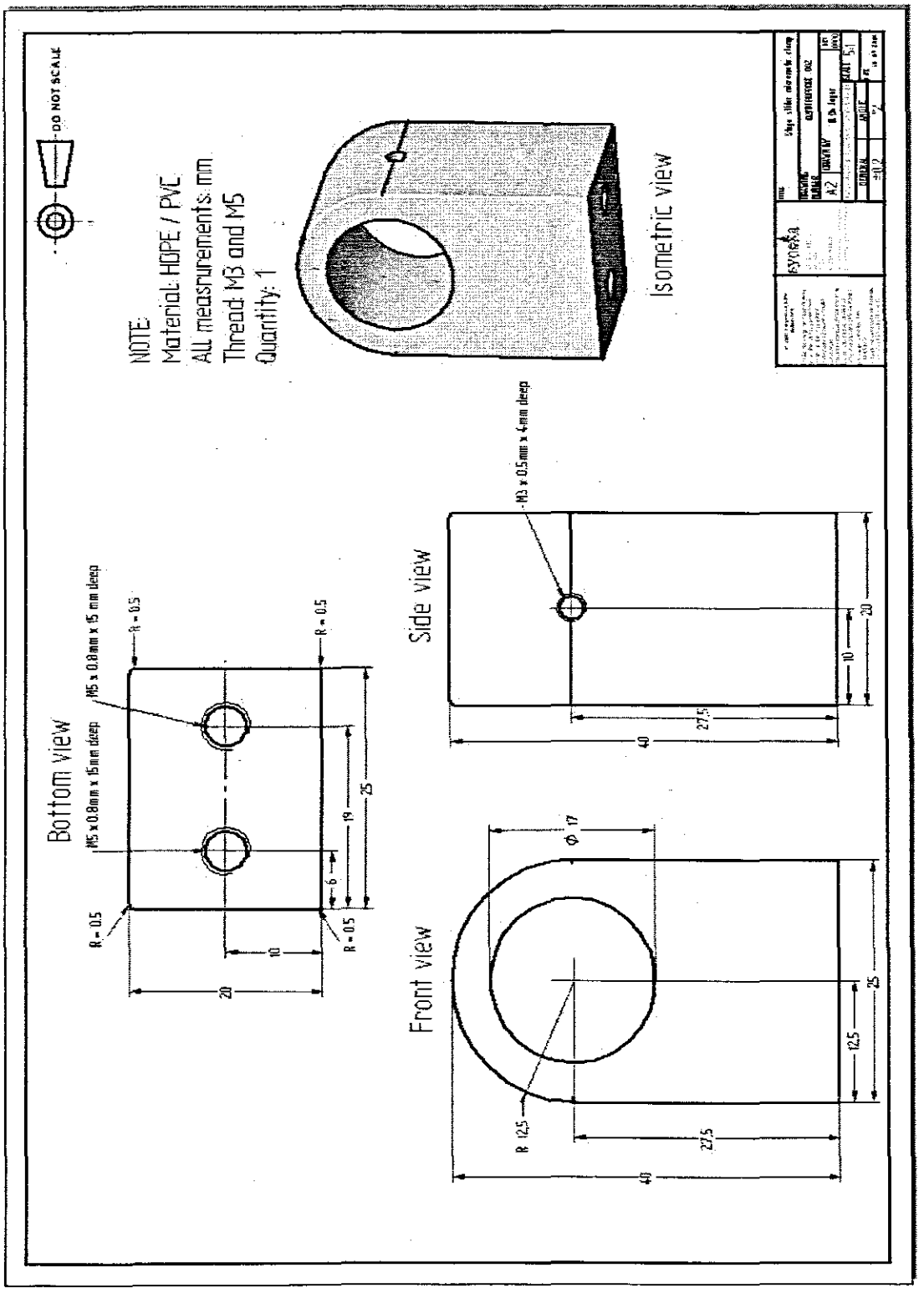

Figure E.7: Stage slider micrometer clamp

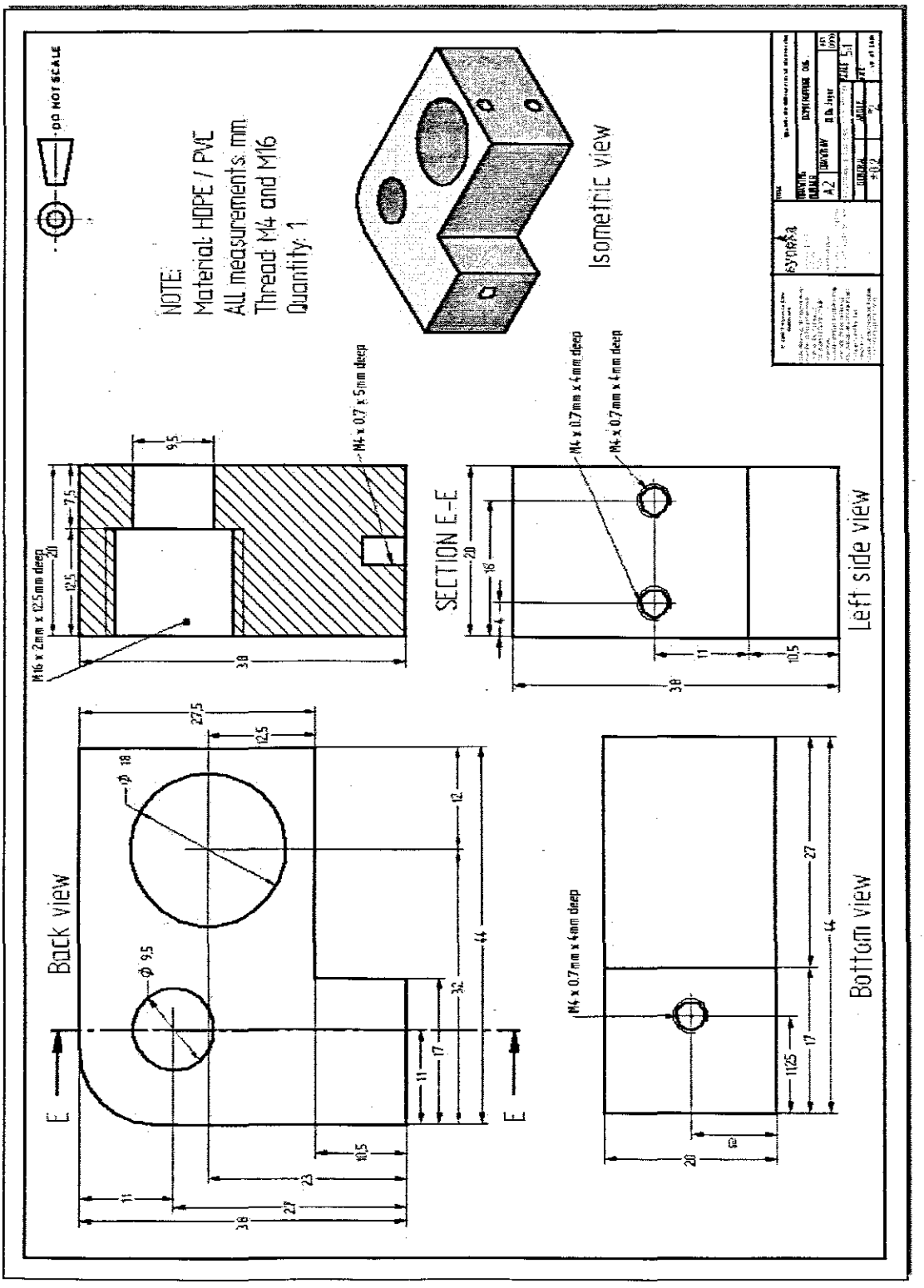

Figure E.8: Micrometer stem stationary cover and microsensor clamp

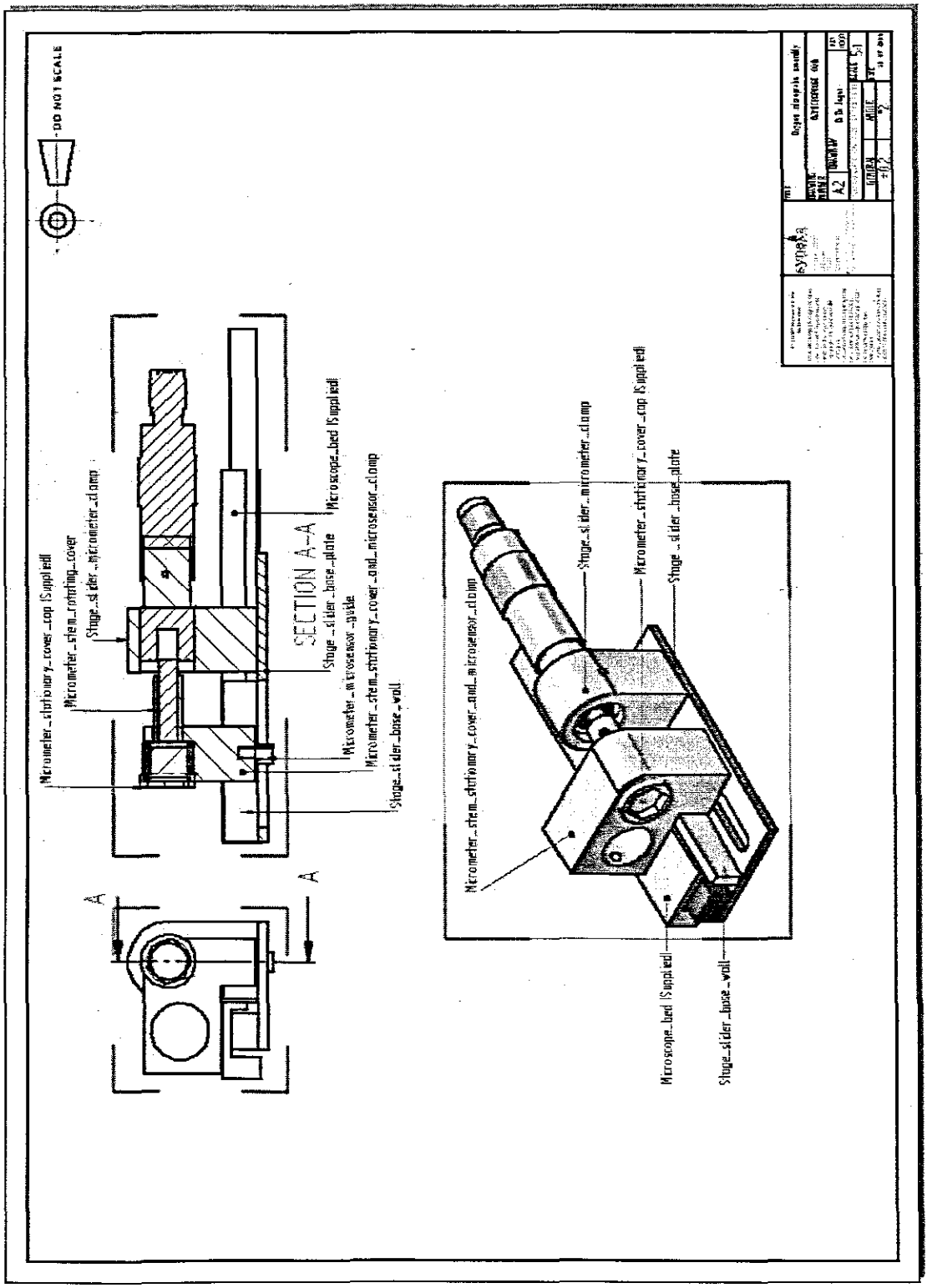

Figure E.9: Three dimensional final assembly cross section

APPENDIX F: Profile 1.0 input and output files

- **Profile 1.0 INPUT FILE**

R2 118cm no 1 Atmospheric D47

0	Depth at top of calculation domain
0.000080	Depth at bottom of calculation domain
4	Max number of equally spaced zones in interpretation (1 to 12)
4	Type of boundary conditions(1:t=C b=C, 2:t=C t=F, 3:b=C b=F, 4:t=C b=F 5:t=F b=C)
5.91	First boundary condition
0	Second boundary condition
1.161e-05	Diffusivity of water at 37C
1	Expression for sediment diffusivity (Ds)(1: Ds=Fl*D, 2: Ds=Fl**2*D, 3: Ds=D/(1+3*(1-Fl))
5.91	Concentration at x = start
-1.0e20	Minimum for consumption rate
0	Maximum for consumption rate
0.0001	Maximum deviation (in %) when accepting a calculated minimum
0.001	Level of significance in the F statistics

X	Fl	DB	ALFA	C
0	0.3	0	0	5.91
0.000020	0.3	0	0	5.22
0.000040	0.3	0	0	3.83
0.000060	0.3	0	0	2.19
0.000080	0.3	0	0	0.26

- **Profile 1.0 OUTPUT FILE**

Name of input file: 118R2D47.1.txt

Name of output file: 118R2D47.1 RESULTS

Input read from file - the calculation begins.

Zones SSE R**2 Zones: 2 3 4

1 .4610E+01 .7814 ---- .291 .470 .737
2 .2984E+01 .8585 ---------- .477 .772
3 .2167E+01 .8973 ---------- .722
4 .1780E+01 .9156

The F statistics suggest 1 zones. Choose the number of zones for further calculations: 1

ones SSE R^2 Zones:
1 .4610E+01 .7814

The F statistics have no suggestion. Choose the number of zones in final result: 1

The calculation is done: 1224 steady state profiles are tested.

Calculated concentration at top:	0.5910E+01
Calculated concentration at bottom:	0.1732E+01
Calculated flux at top:	0.1091E+00
Calculated flux at bottom:	0.0000E+00
Depth integration of production:	-0.1091E+00
Depth integration of irrigation:	0.0000E+00

Depth integration of production and irrigation in each zone:

Zones	Production	Irrigation
1	-0.1091E+00	0.0000E+00